DYNAMIC MODELLING OF THE OPERATION

OF CURRENT-LIMITING FUSES

A thesis submitted to

THE COUNCIL FOR NATIONAL ACADEMIC AWARDS

for

THE DEGREE OF DOCTOR OF PHILOSOPHY

by

SIVAGURUNATHAR GNANALINGAM,   B.Sc.(Eng)(Hons), M.Sc., C.Eng.,

M.I.E.E., M.I.Mech.E.

Department of Electrical and Control Engineering

Liverpool Polytechnic, Liverpool, Great Britain

October 1979

To Rajes, Vaani, Kanna and

Muhuntha

Abstract

The thesis is concerned with the interruption of short circuit currents by current limiting fuses with notched silver elements surrounded by silica granules and the development of dynamic simulation methods for the the arcing phenomena which occur in such fuses. The new models were added to an existing computer program developed in Liverpool Polytechnic to simulate the prearcing performance.

The method used to model dynamic arcing involved the identification of a set of state variables which characterise the system and then to develop odes connecting these variables. The state variables chosen were the current, arc length and the arc cross section.

The crowbar method was used to study the variation of arc length by arresting the arc in the fuse at any known instant of time during arcing. Subsequent X-ray photography of the fuse link enabled the arc length at that instant to be determined. By analysing the results obtained by a series of these tests the model for the rate of burnback was developed and it was shown to be a function of $i^{1.6}$.

Static models for the column gradient and the rate of increase of area of the arc were obtained by theoretical analysis supported by tests in-situ on 1 cm long arcs.

Models were also established for other parameters like initial arc voltage, electrode fall voltages and disruption time to facilitate the simulation.

Results of the computer simulation were compared with tests in the Polytechnic laboratory and a High Power (ASTA) test laboratory and good correlation was obtained.

Simulation of the arcing period permits among other things the estimation of i^2t let through and arc energy which are important in the field of fuse design, testing and application, especially in semi-conductor protecting fuses.

CONTENTS

Principal Symbols

K_e — Thermal conductivity of element

s — Cross sectional area of element

σ_e — Electrical conductivity of element

U_a — Anode voltage drop

U_k — Cathode voltage drop

j_a — Anode current density

j_k — Cathode current density

U_o — Initial voltage

i_o — Current at disruption

U_{arc} — Arc voltage

U_B — Electrode fall voltages

x_o — Initial length of the arc

n_s — Number of notches in series per element

n_p — Number of elements in parallel

ϕ — Phase angle

θ — Closing angle

μ_o — Magnetic permea bility of vacuum

σ — Electrical conductivity (generally used)

ρ_f — Density of filler

C_f — Specific heat of filler

L_f — Latent heat of fusion of filler

σ_f — Electrical conductivity of filler

t_1 — Pre-arcing period

t_2 — Total operating time

CHAPTER I

INTRODUCTION

1.1   General

The project is concerned with the study of the interruption of short circuit currents by current limiting fuses with notched silver elements surrounded by silica granules and to develop dynamic simulation methods for the arcing phenomena which occur in such fuses. The new models will be added to existing computer program that was developed in Liverpool Polytechnic to simulate the prearcing performance. The study also includes the application of the complete program to problems of practical interest.

The current limiting action of these fuses is particularly useful in protecting networks which have a high short circuit level. This property is absent in customary circuit breakers, so that current limiting fuses are often incorporated in such circuits to provide back up protection, the fuse operating above a certain value of current while the breaker operates at lower currents. By limiting the current, the mechanical and thermal stresses of the circuit, which are proportional to the square of the current, are reduced to small proportions (57). The current limiting effect also greatly reduces both damage at the point where short circuit takes place and disturbances to the system.

A typical interruption is illustrated in Fig.1.1. The short circuit current heats up the element by Joulean heating and after a certain interval of time (called the prearcing period, t_1), the notches attain melting temperature and immediately disrupt due to factors such as pinch

pressure and surface tension. Disruption introduces arcs at the notches which elongate by burning back the element, thus tending to increase the arc voltage, U_{arc}. The current limiting action of this fuse (normally called an h.r.c. fuse) depends upon the appearance of the arcs. Introduction of the arc voltage into the circuit causes rapid reduction of the current to zero.
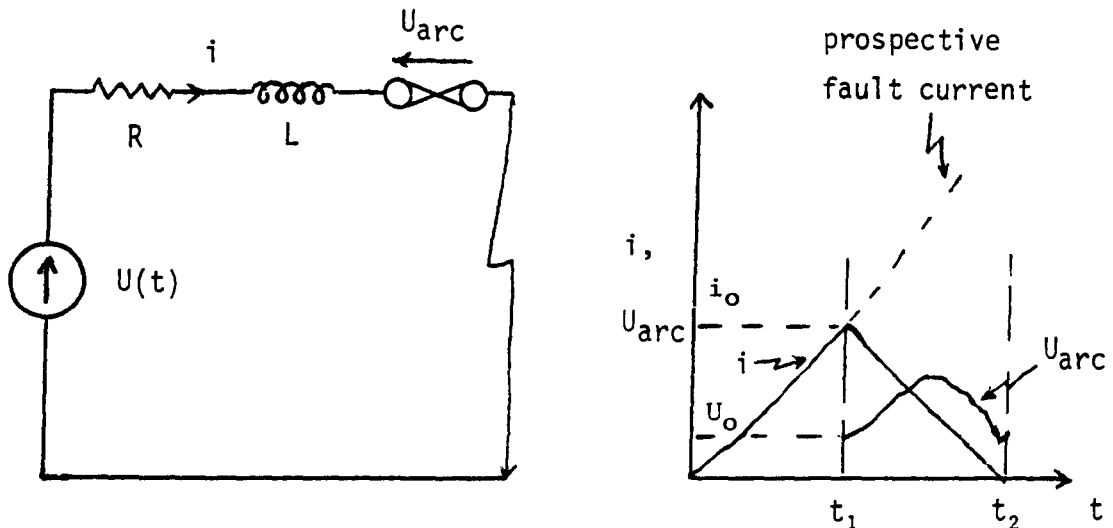
FIG. 1.1

If wire or strip elements are used in the fuse link which is subjected to a short circuit, multiple arcing is produced which can lead to excessively high arc voltage. Too high an arc voltage can cause insulation failure in the circuits that are fed from the same busbar as the faulty circuit (i.e. effectively in parallel with the fuse). Hence multiple arcing should be avoided and in practice, the fuse designer uses elements with constrictions (called notches) to control the number of arcs in industrial fuses and hence the arc voltage. The current rating of the element which is dependent on the notch cross section is reduced by the introduction of the constrictions. The

current rating of the fuse link can however be increased by providing a number of elements in parallel each having the same number of notches.

Simulation of the arcing period will permit, among other things, the estimation of the following two integrals:

(i) $\int_{0}^{t_2} i^2\,dt$ (ii) $\int_{t_1}^{t_2} U_{arc}\,i\,dt$

The first of these is very important in connection with the i^2t withstand of the device which the fuse is protecting, while the second, which is the total energy dissipated in the fuse link during arcing, has an important influence upon fuse design.

The energy dissipated depends on the prospective current and the characteristic which gives the variation of the energy has two peaks, one near the minimum fusing current and the other in the short circuit range. Knowledge of the severity of the energy let through at the second peak and the prospective current at which it takes place is important in the design of the fuse. The simulation studies will therefore be of help in the fields of fuse design, testing and applications, especially in the field of semiconductor protection fuses, where unusual waveforms are commonly encountered and past experience obtained from tests in d.c. and a.c. circuits is of doubtful value.

For the circuit of Fig.1.1,

$$\frac{di}{dt} = \frac{U(t) - iR - U_{arc}}{L}$$

3

This equation can be solved to obtain the complete current transient, provided that the arc voltage U_{arc} can be represented in some way.

Clearly the integrals (i) and (ii) above are dependent upon the variation of U_{arc} over the period from t_1 to t_2. The disruption and extinction processes at t_1 and t_2 contribute little to these integrals, but the disruption process is important in determining the initial value of arc voltage, U_0.

Since the method of representing U_{arc} is the key to this problem, a brief review of the methods which have been used in the past to model U_{arc} and other variables will be given in the next Section.

1.2   Review of Previous Work

Many previous analyses of arcing in fuses have approximated the arc voltage waveform as a fixed geometric shape, or assumed that the arc properties varied in a fixed manner with time (58) - (61). The most commonly used approximation has been to use a constant arc voltage. These methods do not give true dynamic representations, since the interaction between the circuit conditions and the arc voltage is neglected.

The remaining methods (2) - (5), (7), (9), (62) may be compared in the way that the arc voltage, length and column gradient were represented. The arc voltage of a single notched element may be written as:

$$U_{arc} = U_B + Ex$$

where x is the arc length and E the average column gradient of the arc column.

All the workers assumed a constant electrode fall voltage except Dolegowski (9) whose experimental work indicates that U_B increases significantly with i and who has given equations for the dependence of U_B upon i for silver elements.

During arcing the arc length x increases due to burning-back of the element and most authors have assumed that the erosion rate is proportional to i, which corresponds to a constant electrode fall voltage. However it is well known that a higher power of i is involved(1).

5

As far as representation of the column gradient is concerned, Oliver (4), Kroemer (2) and Ossowicki (7) assumed that the column gradient was constant.

Details of the previous work are covered in the subsequent Chapters.

Gibson (57) is one of the pioneering workers in the analysis of h.r.c. fuses with special reference to its short circuit performance. He emphasised the use of h.r.c. fuses in limiting currents in circuits and supported it by analytical and experimental results.

Wright and Beaumont (5) made a number of simplifying assumptions to develop a simulation model for the arcing phenomena of h.r.c. fuses and obtained satisfactory correlation between their model and some limited experimental results.

Wilkins (1) introduced the concept of modelling a dynamic system by identifying the set of variables for the system and developing the same number of first order differential equations connecting these variables and successfully used the principle to simulate arcing in current limiting fuses. The advantage in the principle is that further variables as necessary may be brought in as a result of further analysis to widen the scope of the application.

6

1.3 Proposed Experimental Work

From Section 1.2 it is seen that the arc voltage depends on the electrode fall voltage, arc length and the column gradient. Arc length can be determined if the rate of burnback is modelled. From Wheeler's work (19), (20) column gradient can be shown to be dependent on the current and the arc section, which in practice varies axially. Thus the expression for the column gradient incorporates the structure for the arc sectional area. The following experimental work has been carried out to determine the models for the variables involved.

(1) Burnback rate

The technique used is to short circuit the fuse during arcing by means of a 'crowbar' thyristor, thus arresting the arc elongation, the instantaneous current being simultaneously recorded. Subsequent X-ray photography of the fuse link enables the arc length at the corresponding instant of time to be measured. From the results of a large number of tests covering different element sizes and prospective currents, the variation of the rate of burnback with current has been obtained.

(2) Fixed arc length experiments

Using an electrode system designed to give a fixed arc length within a quartz filled cartridge the column gradient can be directly obtained. Analysis of the oscillograms of the arc current and voltage enabled the study of the variation of column gradient and factors which influence it.

(3) Other experiments

Experiments were also carried out to determine semi-empirical models for other parameters like initial arc voltage, electrode fall voltage and the disruption time.

7

1.4 Conclusions

Experimental work as outlined above has been carried out and semi-empirical models obtained for the variables involved.

The burnback rate in the short circuit current range has been shown to be a function of a higher power of i contrary to the findings of previous studies according to which it varies directly with i. The model has been developed by analysing the results of a wide range of tests, supported by theory as described in Chapter II. It is similar to the Turners' model in that both contain a term in $i^{1.6}$ although the Turners' coefficient is lower(8).

From the studies of Maecker(17) and Wheeler (19), (20), the stored arc energy was neglected. The tests in-situ on 1 cm long arc experiments helped to establish a static model for the column gradient which is related to the current and the arc section. The arc section changes axially and the rate of increase of arc section also has been modelled, based on these tests as given in Chapter III.

In Chapter IV, models have been developed for the initial arc voltage electrode fall voltages, the initial area of section at the electrode ends and the disruption time, based on some experiments carried out and the work of Hibner (21), Arai (30) and Dolegowski (9).

A model for the simulation of arcing behaviour of the fuse was then developed based on the differential equations established for the current, arc length and area of arc section. The program has been tested for validation of various facilities provided, such as the merging

8

of arcs, burning up to the end caps of the fuse link, etc and also used
to simulate one of the fuse tests in the laboratory with good accuracy
as covered in Chapter V.

In Chapter VI, the comparison between the simulated results of the short
circuit test on a number of typical industrial fuses and the actual High
Power (ASTA) test reports is made with good accuracy. Compared with the
'constant arc voltage' model, which is a first order model and has been
extensively used in the past, the third order model developed has
contributed highly to the field of fuse arc simulation under short
circuit conditions, thereby benefiting the fuse designer and the fuse
user. The program has the added advantage of being easily extended to
include other parameters such as the arc pressure if they are proved
by further research to be important for achieving added refinements in
the simulation.

CHAPTER II

BURNBACK RATE

2.1   Review of Previous Work

Burnback laws are generally known to be only approximate and would probably be true for a limited range of application. Some authors (2) - (6) proposed that the burnback rate of current limiting fuses is proportional to the instantaneous value of the current i, whilst others (7) - (9) considered that a higher power of i is involved.

(a) Kroemer (2) conducted experiments using a 1000V DC generator to supply currents ranging from 10 to 1000A for a fuse test circuit that is schematically shown in Fig.2.1. A contactor was connected across the branch of the circuit containing the test fuse and the measuring shunt in series as in the Figure. The contactor was initially in the closed position so as to let the current   by pass the test fuse. After the current in the circuit reached a steady value, it was opened to let the entire test current   flow through the fuse. Four equally spaced probes were provided in the fuse body along the element to monitor the potential with respect to one of the electrodes. When the element burned off, the probes came into contact with the arc successively and monitored the arc voltage at the respective locations. The distances from the centre of the elements to the probes were known. The time taken for the arc to reach each of the probes was obtained from the oscillogram of the respective probe. The distance from the centre of the element to any one probe divided by the time taken for the arc to reach the probe gave the average velocity of burnback corresponding to the average current through the fuse in the time

INDUCTOR

TEST FUSE

TO OSCILLOGRAPH

P1
P2
P3
P4
PROBES

G CONTACTOR

DC
GENERATOR

SHUNT
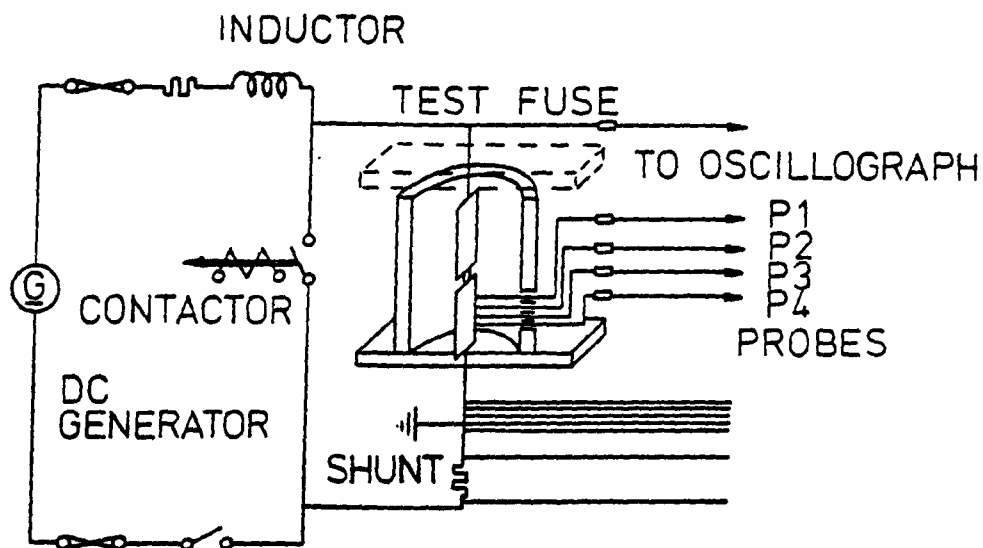
FIG. 2.1. KROEMER'S EXPERIMENT
- SCHEMATIC DIAGRAM

R L

G

T

Z2

B2

Z1 B1 S

B1 : TEST FUSE
S : SHUNT

U_{arc} i
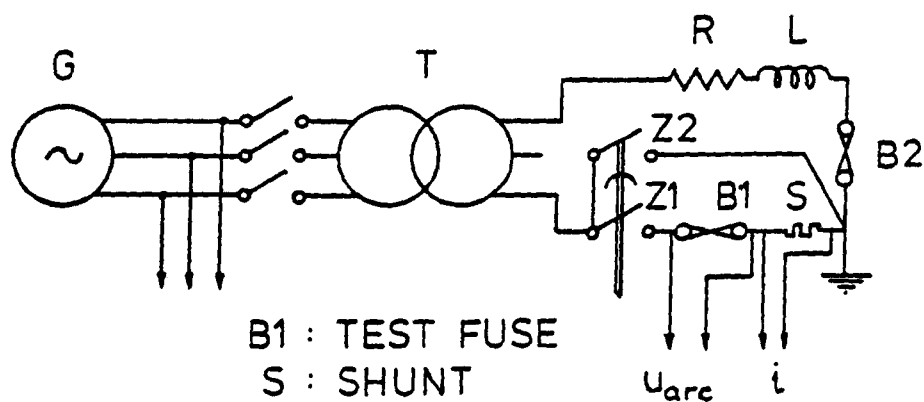
FIG. 2.2. DOLEGOWSKI'S EXPERIMENT
- SCHEMATIC DIAGRAM

interval. As there were four probes, four different velocities could be obtained from the same test. The test was repeated with different test currents.

Error was introduced by the erosion of the probe points caused by the arc, particularly in the values of the voltages measured.

Kroemer arrived at a linear relationship for the rate of burnback. The maximum deviation of the experimental values of the rate of burnback from the straight line graph was stated to be 30% and the possible error in the value of the constant C, Kroemer reckoned to be ± 20%.

$$\frac{dx}{dt} = Cj \qquad (cm.s^{-1}) \qquad\qquad (2.1)$$

where C = specific 'burn off' rate

= 0.0023 $cm^3.A^{-1}.s^{-1}$

j = current density $(A.cm^{-2})$

= i/s

i = instantaneous value of current (A)

s = cross sectional area of element (cm^2)

The maximum value of current density covered in the experimental work was around 1.2 $kA.mm^{-2}$.

(b) Schonholzer (3), Oliver (4), Wright and Beaumont (5) and Danders (6) assumed that the burnback velocity is proportional to the instantaneous value of current in their studies, on the strength of Kroemer's work. However the values of the constant C used in some of

11

these cases were different from that used by Kroemer as summarised in Section 2.6 later.

(c) Ossowicki (7), based on some experiments performed by him on low voltage silver and copper fuse elements with DC over currents, arrived at the following empirical relationship:

$$x_2 = \frac{C_1}{s} \int_{t_1}^{t_p} i \, dt + \frac{C_2}{sI_n} \int_{t_p}^{t_2} i^2 \, dt \qquad (2.2)$$

where x_2 = final arc length

t_1 = instant at which arc commenced

t_p = instant at which i^2 term influenced the arc length

I_n = rated current of fuse

i = instantaneous value of current

s = cross sectional area of fuse element

C_1, C_2 = constants

$\frac{dx}{dt}$ may therefore be considered to be a function of a higher power of i than one. However Ossowicki gave no physical justification for the above relationship.

(d) Turner and Turner (8) did extensive work on erosion of silver and copper contacts and established that the erosion loss of metal from a pair of arcing contacts is given by the following law:

$$\frac{dw}{dt} = \gamma \, i^{1.6} \qquad (2.3)$$

12

where $\frac{dw}{dt}$ = rate of loss in $\mu g.s^{-1}$

i = instantaneous value of current (A)

γ = a constant for the material and in the case of silver has a value of 2.4 for erosion in the 'evaporation mode' corresponding to relatively low current flow of up to about 1kA and a value of 40 for erosion in the 'droplet mode' for current flow higher than 1kA. At $i \simeq 1kA$, erosion takes place in the 'discontinuous mode' when γ takes a value between 2.4 and 40.

Similarity between the phenomena of erosion of contacts and the burnback of fuse elements during arcing was suggested and it was also suggested that the latter followed the same law as in Eqn (2.3) with a value of γ corresponding to the 'droplet mode'.

With erosion of contacts, a large part of the electrode power density is absorbed in heating the contacts, while in the case of a uniformly eroding fuse element the heat required to raise the metal from room temperature to its melting point would not be required. The authors estimated that there would be an increase in length of the fuse likely to be melted by a factor of approximately 3 and hence arrived at the following relationship for the burnback:

$$\frac{dx}{dt} \simeq 11.9 \times 10^{-6} \ \frac{i^{1.6}}{s} \qquad cm.s^{-1} \qquad (2.4)$$

(e) Dolegowski (9) tested fuses with notched silver fuse elements and with prospective currents ranging from 0.3 to 60 kA AC and power

factor from 0.1 to 0.35 using a circuit schematically shown in Fig.2.2. Operation of the test fuse B1 was initiated by closing switch Z_1. At a given moment after the appearance of the arc, the crowbar switch Z_2 was closed thereby stopping the arcing process. The length of the arc, x was measured from the fuse. The experiment was repeated using identical fuses, but with different time delays for the closure of switch Z_2.

The arc voltage U_{arc}, which was also measured each time, was plotted against x. The graph when extrapolated to x = o gave the value of U_B, the electrode fall voltage. U_B was found to have the following empirical relationships:

(i) For $o \leqslant j \leqslant 8$ kA.mm^{-2}

$$U_B = \Delta U_1 + k_1 i^\alpha \qquad\qquad (2.5(a))$$

where $\Delta U_1 = (20 \pm 5)$ V

$k_1 = 1.5$

$\alpha = 0.39$

(ii) For $8 < j \leqslant 20$ kA.mm^{-2}

$$U_B = \Delta U_2 + \frac{k_2 i}{s} \qquad\qquad (2.5(b))$$

where $\Delta U_2 = (30 \pm 5)$ V

$k_2 = (4.18 \pm 0.25) 10^{-5}$

$\Omega.cm^2$

The power balance at the electrodes was developed as follows:

Electric power input at the electrodes $= U_B i$

Power expended in melting and burning off the silver at the electrodes

$$= \frac{dx}{dt} \cdot s \cdot [C_V \, \Delta T + h + h']$$

where $\frac{dx}{dt}$ = rate of burnback $(cm.s^{-1})$

s = cross sectional area of element (cm^2)

C_V = specific heat of metal in solid state per unit volume $(W.s.cm^{-3})$

h = latent heat of fusion of metal per unit volume $(W.s.cm^{-3})$

h' = empirically determined quantity taking into account the energy of vaporisation of the metal and that of transformation of the thermal energy into the kinetic energy of metal vapour $(W.s. \, cm^{-3})$

$\Delta T = T_1 - T_2$

T_1 = Melting Point of the metal

T_2 = temperature of unburnt part of the element

Equating the electric power input at the electrodes to the power expended in burning back:

$$\frac{dx}{dt} \cdot s \cdot [C_V \, \Delta T + h + h'] = C_2 . U_B . i$$

where C_2 = proportionality factor

hence $\frac{dx}{dt} = [\frac{C_2}{s(C_V . \Delta T + h + h')}] \cdot U_B . i$ (2.6)

15

Substituting for U_B from the above Eqns in Eqn (2.6) it could be seen that $\frac{dx}{dt}$ has a power law dependence on i of a possible form:

$$C_1 i + C_3 i^x$$

where x lies in the range 1.39 - 2.00

Summary

The use of fixed probes inside the fuse body to monitor the burnback process in Kroemer's experiments is considered to be subject to inaccuracies as the probe points themselves were eroding in the presence of the fuse arc. The presence of probes in the fuse body may also alter arc behaviour as there could be heat transfer from the arc to the probes and it will be difficult to correct for such effects. Further only a small number of experiments with current densities not exceeding 1.2 $kA.mm^{-2}$ had been conducted. Hence the application of the findings in any case may not cover a broader range of current or current densities.

Turner and Turner made a proposal for the burnback rate of fuses basing on tests done on contacts and tested for agreement in fuses for a limited number of cases only. They conclude by suggesting further work on many more sizes of fuse elements to confirm if the same power law expression covers a broader range of elements and currents.

Dolegowski had used one switch to initiate the fuse operation and another to operate as a crowbar switch to arrest the arc in the fuse. The switches particularly the crowbar switch should be fast acting if accurate results are to be obtained and it is not clear how fast the

switches had been in his experiments. His formula relating the rate of burnback in Eqn (2.6) was not verified experimentally.

Digital-computer simulation of the complete interruption process including interactions between the arc and the circuit required more precise data on the factors which govern the burnback velocity (1). Hence a crowbar method using two fast acting thyristors, one to initiate the current through the fuse and the other as a crowbar switch to extinguish the arc after a pre-determined time from the commencement of the arc was adopted to determine the velocity of burnback in a large range of fuse element sizes and covering a broad range of prospective currents. The principle of the crowbar method as used for the experiment is briefly described in the next Section.

2.2   Crowbar Method

The arrangement for the crowbar method is schematically shown in Fig.2.3 A current i_1 would flow in the main circuit when the main thyristor is fired with a single pulse at an instant of time denoted by H in Fig.2.3(b), provided there is adequate driving voltage across the thyristor. If the crowbar thyristor is not fired, then the branch AFD will be on open circuit making i_2 = o. Hence the current through the fuse would be $(i_1 - i_2)$ = i_1 as shown in Fig.2.3(b). If the fuse did not operate, then the waveform of current could be of the form HSVN. On the other hand if the fuse melted and interruped the circuit, the waveform could be of the form HSWM, of which HS corresponds to the prearcing period and SWM to the arcing period of the operation of the fuse. During the arcing period the fuse provides an arc voltage which opposes the flow of current through the fuse and which can be considered to be due to an increasing arc resistance well above the equivalent resistance (-on state slope resistance) of a fired thyristor.

On the other hand if the crowbar thyristor is fired with another single pulse while the fuse is arcing at an instant of time denoted by K, in Fig.2.3(c), (-HK is t_c say) the arc voltage would be acting on this thyristor which will therefore immediately conduct a current i_2. $(i_1 - i_2)/i_2$, which is equal to the ratio of the resistance of the branch AFD to that of ABD would therefore be very small. Hence i_2 will be the same as i_1 and the fuse current will collapse as in Fig.2.3(c). Thus by firing the crowbar thyristor during the arcing process, the arc can be arrested instantaneously. An X-ray photograph of the fuse subsequently would provide the value for the length of the arc, x at the instant of chopping. From the oscillogram of the current waveform, the

18

INDUCTOR

MAIN
THYRISTOR

i_1 A $(i_1 - i_2)$

B

245 V,
50 HZ
AC
SOURCE

CROWBAR
THYRISTOR

i_2

TEST
FUSE

SHUNT

F

D

(a)

$(i_1 - i_2)$

S

V

W

H

J   M   N

$(i_1 - i_2)$

H

J   K   M   N

t_c

(i_2)

(b)

$(i_2)_H$

(c)   K   M
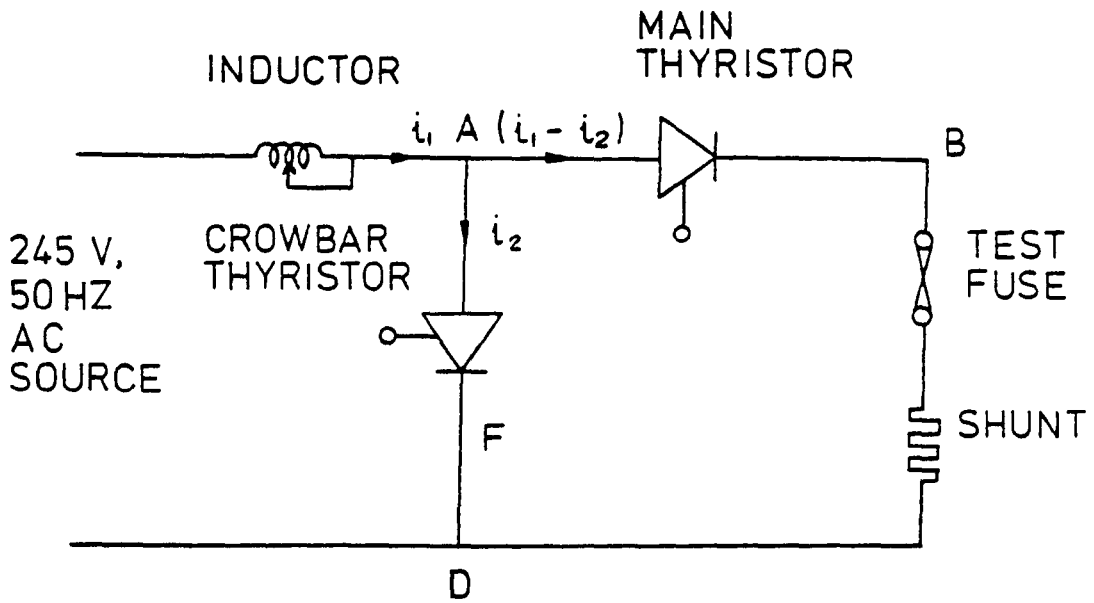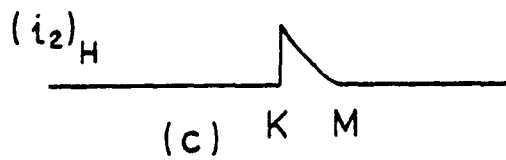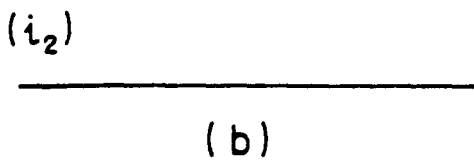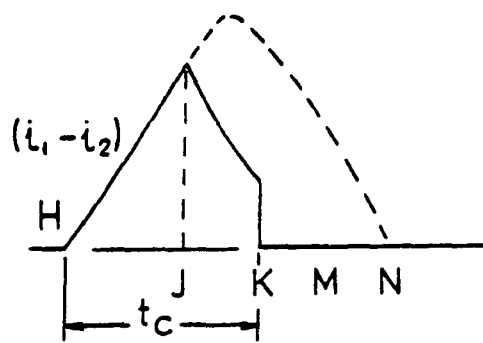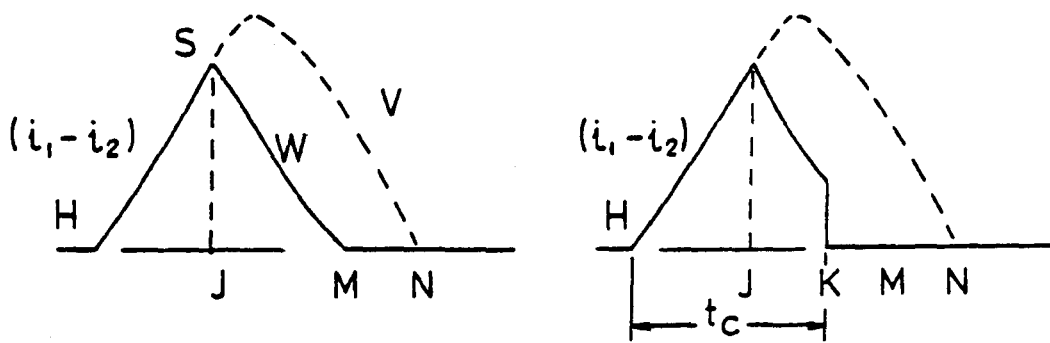
FIG. 2. 3. THE CROWBAR METHOD

instantaneous value of the current, i at the moment of chopping could be determined.

Similar fuses could be made and the above method repeated with the same circuit conditions but with different delay time t_c. x vs t_c could then be drawn and will provide the history of the arc development for the same circuit conditions.

2.3   Experimental Method

2.3.1 Test Circuit

The circuit diagram for the test arrangement is shown in Fig.2.4. The
245 V 50 Hz AC supply for the circuit was obtained directly from the MV
distribution busbars of the Energy Conversion Laboratory between the
Red phase and Neutral and protected by a 100A HRC fuse. Brief details
of the elements of the circuit are given below whilst the design
details and essential specifications of some of them are given in
Appendix 2.1.

(a) Inductor: It is a variable air cored inductor. The common end of
the inductor was marked 12 and the following two tappings were made use
of to obtain two different prospective currents:

Tap No.	Inductance (m H)	D C Resistance (ohm)	Approximate peak value of prospective current (A)
12 - 6	0.3730	0.232	1270
12 - 1	0.0483	0.083	2900

The highest peak value of prospective current approximately amounting
to 11,000A was obtained with the variable inductor removed from the
circuit.

(b) Thyristors: Both thyristors of the circuit were identical and of
High Power Thyristor YST-01S Converter Type manufactured by ASEA. The
relevant design details are given in Appendix 2.1.

(c) Co-axial shunt: 1 milliohm resistance. Design details are given

INDUCTOR   MAIN THYRISTOR

245 V,
50 HZ
SUPPLY

CROWBAR
THYRISTOR

FIRE

DELAY

AUX
FUSE

SHUNT

TEST
FUSE

TRANSIENT
RECORDER
(SLAVE)

Y2

CRO

Y1

TRANSIENT
RECORDER
(MASTER)

POW 1

POW 2

DELAY
CONTROL
UNIT
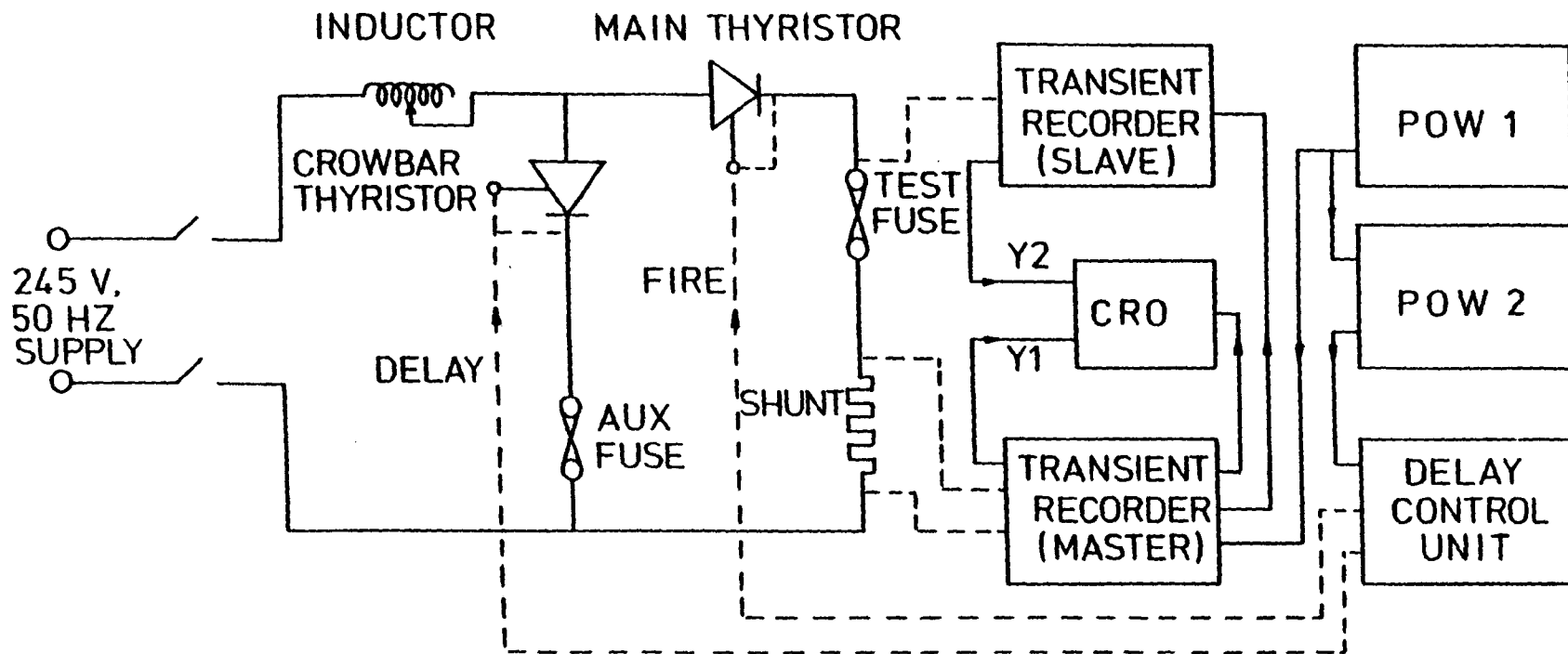
FIG. 2. 4.   CIRCUIT   DIAGRAM

(d) Auxiliary fuse: A HRC fuse of type TC 80A. This was incorporated in the crowbar limb of the circuit to give graded protection, with the main fuse in the control panel giving back up protection.

(e) Test fuse: Standard industrial cartridges of bore diameter 2.3cm and length 7.8cm were used with attachments specially turned to enable the silver fuse elements to be mounted axially within and soldered to the ends as shown in Fig.2.5. One 4.5mm thick aluminium disc with a 15mm wide slot cut radially along the disc and a 15mm x 2mm slit at the centre was fixed to one end of the cartridge with two screws. The slit facilitated the axial mounting and soldering of the fuse element. Another disc similar to the above but in addition having a 8mm dia hole in the slotted section was provided at the other end. The hole was used to fill the cartridge through with quartz. Aluminium solder was used for soldering the element to the end pieces. Care was taken to mount the element taut with the (single) notch at the centre of the cartridge. The quartz was introduced into the cartridge through a funnel fitted to the hole in the disc, while at the same time the cartridge was vibrated with a vibrator to ensure uniform packing of quartz. The type of quartz used is given in Appendix 1.1. As pointed out later in the chapter (Section 2.3.3) many fuses of identical construction were required for the studies and one of the factors to be taken care of was constant degree of 'compactness' of the quartz in the fuses made. This was achieved by vibrating the fuses while introducing the filler, for approximately the same time.

3.0

1.8   0.2   NOTCH   QUARTZ   X

4.2

0.8 d

0.9

0.2

15.2

SECTION XX   **HALF SECTIONAL ELEVATION**

1.5   ELEMENT SOLDERED

0.6 d   0.5 d

1.2

Y   ELEMENT   3.9   0.25

3.8 d   2.3 d

1.2   Y   4.0 d

0.45   FULL SCALE DIMENSIONS IN CM

SECTION YY   **HALF SECTIONAL PLAN**
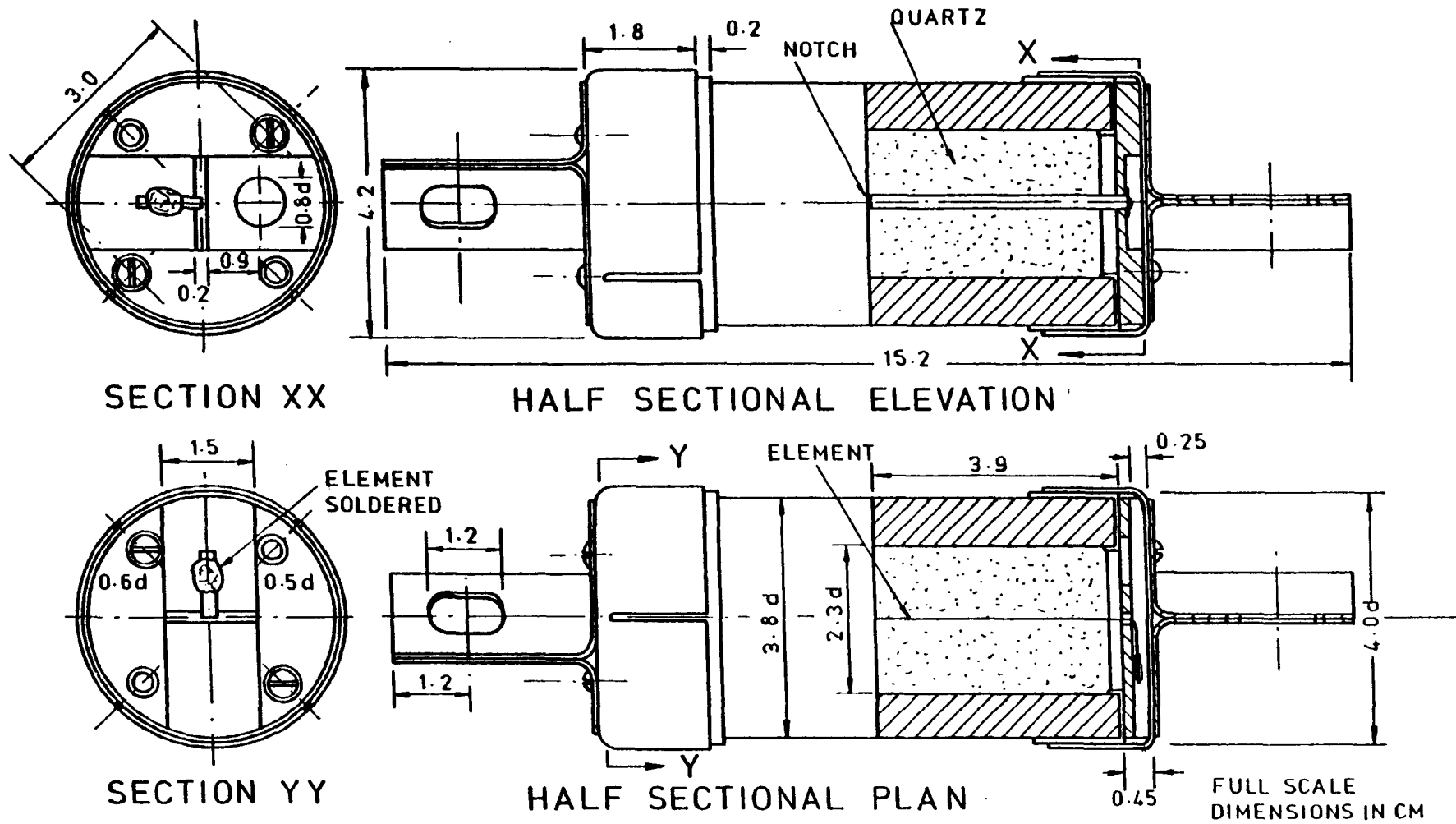
FIG. 2.5. TEST FUSE ASSEMBLY

Finally the two slotted portions of the discs were closed with insulation tape to prevent leakage of quartz and the ends fitted with the two end caps using screws.

2.3.2 Control and Display Equipment

The two Point On Wave Units named as POW1 and POW2 and the Delay Control Unit named as DC Unit controlled the operation of the circuit. The two Transient Recorders namely the Transient Recorder (Master) and the Transient Recorder (Slave) and the Cathode Ray Oscilloscope (CRO) provided the storage and display facilities for the experiment. The connection between the test circuit and these units is schematically shown in Fig.2.4.

(a) Point On Wave Units: POW1 was set to an angle α_1 and POW2 to an angle α_2. After resetting both the POW's, POW1 was fired by pressing the 'FIRE' button of the unit. POW1 gave a DC output of approximately 17V, α_1^o (or $\alpha_1/18$ ms) after the first zero crossing of the source voltage from the instant of firing. The 17V output of POW1 triggered POW2, the Transient Recorders and the CRO. POW2 produced a DC output of approximately 17V, α_2^o (or $\alpha_2/18$ ms) after the same zero crossing of the source voltage, provided $\alpha_2 \geqslant \alpha_1$. If $\alpha_2 < \alpha_1$ then the 17V output of POW2 appeared $(20 + \alpha_2/18)$ ms after the same zero crossing. In the experiment α_2 was kept higher than α_1.

(b) Delay Control Unit: The 17V output of POW2 triggered the Delay Control Unit (DC Unit) which produced two short duration pulses, one immediately on actuation and the other at time t_c later. t_c, which was more than the prearcing time t_1 was preset in the DC Unit. A brief

description of the DC Unit complete with a circuit diagram is given in Appendix 2.2. The first pulse produced, fired the main thyristor thereby initiating the operation of the fuse, and the second pulse fired the crowbar thyristor (after $t_c > t_1$) which enabled the test fuse to be short circuited and the arc development to be arrested. Arcing would have commenced in the fuse after a time t_1 from the initiation of the current through the fuse.

A typical timing sequence of the operation of the control equipment is shown in Fig.2.6.

POW1 was used in the control circuit particularly to trigger the Transient Recorders and the CRO $(\alpha_2 - \alpha_1)/18$ ms before the initiation of the fuse current so that the fuse current and voltage could be faithfully recorded in the Recorders and displayed in the CRO, as otherwise depending on the level of the trigger pulse, a certain part initially might have been lost.

(c) Transient Recorders and Cathode Ray Oscilloscope: The fuse current wave was stored in digital form in the Transient Recorder (Master) and the fuse voltage in the Transient Recorder (Slave). A 10:1 probe was used to step down the fuse voltage before inputting the Transient Recorder. The stored information was output to channels Y1 and Y2 respectively of the CRO and the two waveforms were displayed continuously in the 'Repetitive' mode. Trigger and display synchronisation facilities were available between the two Recorders. A brief description of the Transient Recorders together with some design details and calibration for typical settings of the units are given in Appendix 2.2.

SOURCE
VOLTAGE

17 V

α_1

POW 1

17 V

α_2

POW 2

t_c

DC UNIT

i_0

t_1

t_2

FUSE
CURRENT

t_1

t_c
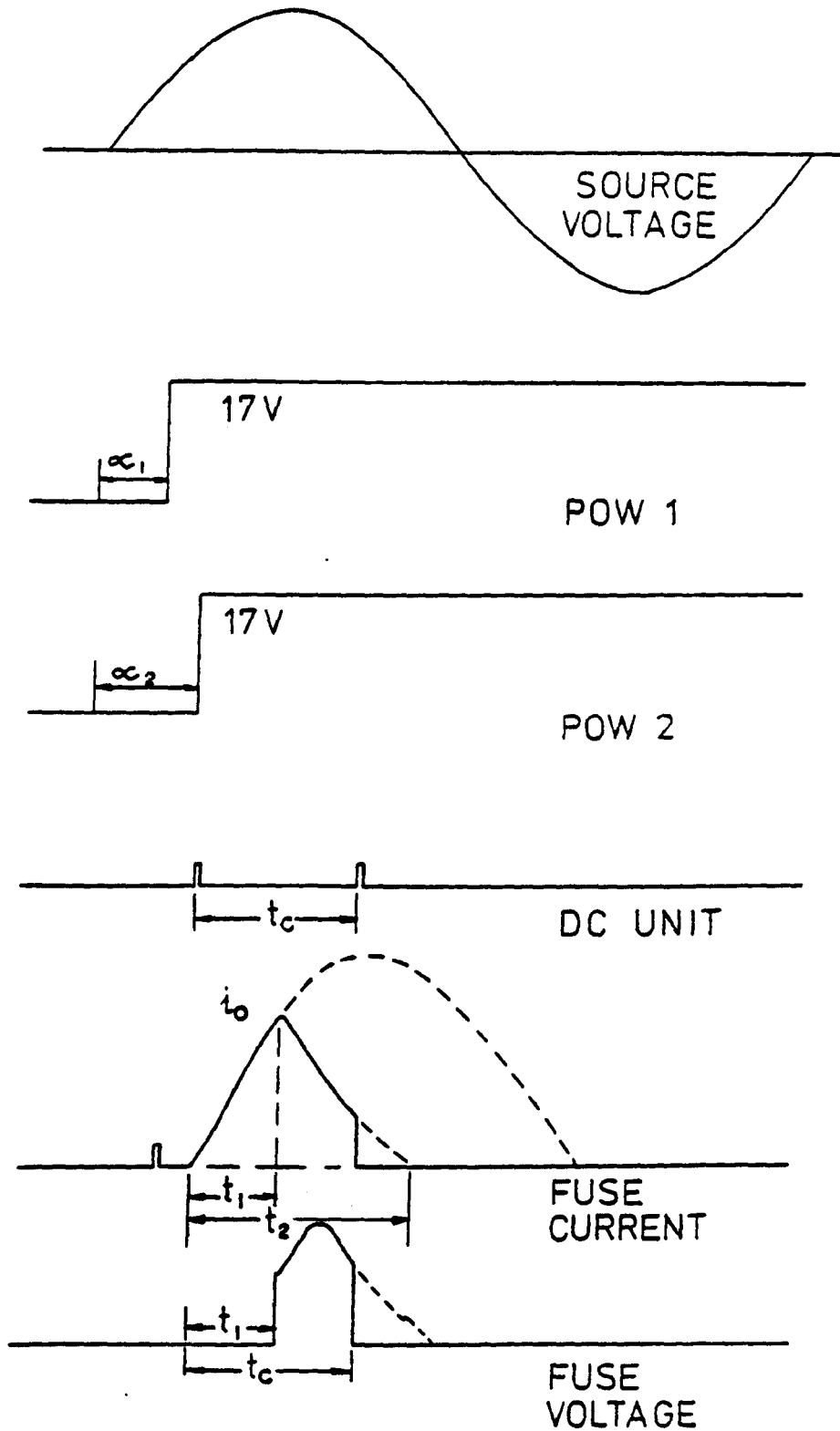
FUSE
VOLTAGE

FIG. 2.6. TIMING SEQUENCE

2.3.3 Conduct of Experiment

The fuse link was mounted horizontally in the test rig, a photograph of which is given in Fig.2.7 (a)/(b). A suitable delay time t_c was set in the DC Unit and the operation of the test fuse was initiated by firing POW1. An oscillogram of the fuse current was taken off the CRO, from which the current at the instant of chopping was obtained. A typical oscillogram is shown in Fig.2.8. Subsequent X-ray photography of the fuse enabled the corresponding value of the arc length, x to be determined with the help of a vernier microscope. The total burnback x was produced by the erosion at the arc cathode x_c and the anode x_a which were separately measured.

$$\text{i.e.} \qquad x = x_c + x_a \qquad\qquad (2.7)$$

The test was repeated for fuses with identical elements and for the same prospective current, except with different chopping time t_c, achieved by varying the DC Unit setting, thus enabling the history of the arc development to be reconstructed. An average of 9 fuses were used for each complete series of tests involving one element size and one prospective current.

Series of tests as described above were carried out for 6 different fuse elements as in Table 2.1 and three different prospective currents enumerated in Section 2.3.1(a).

24
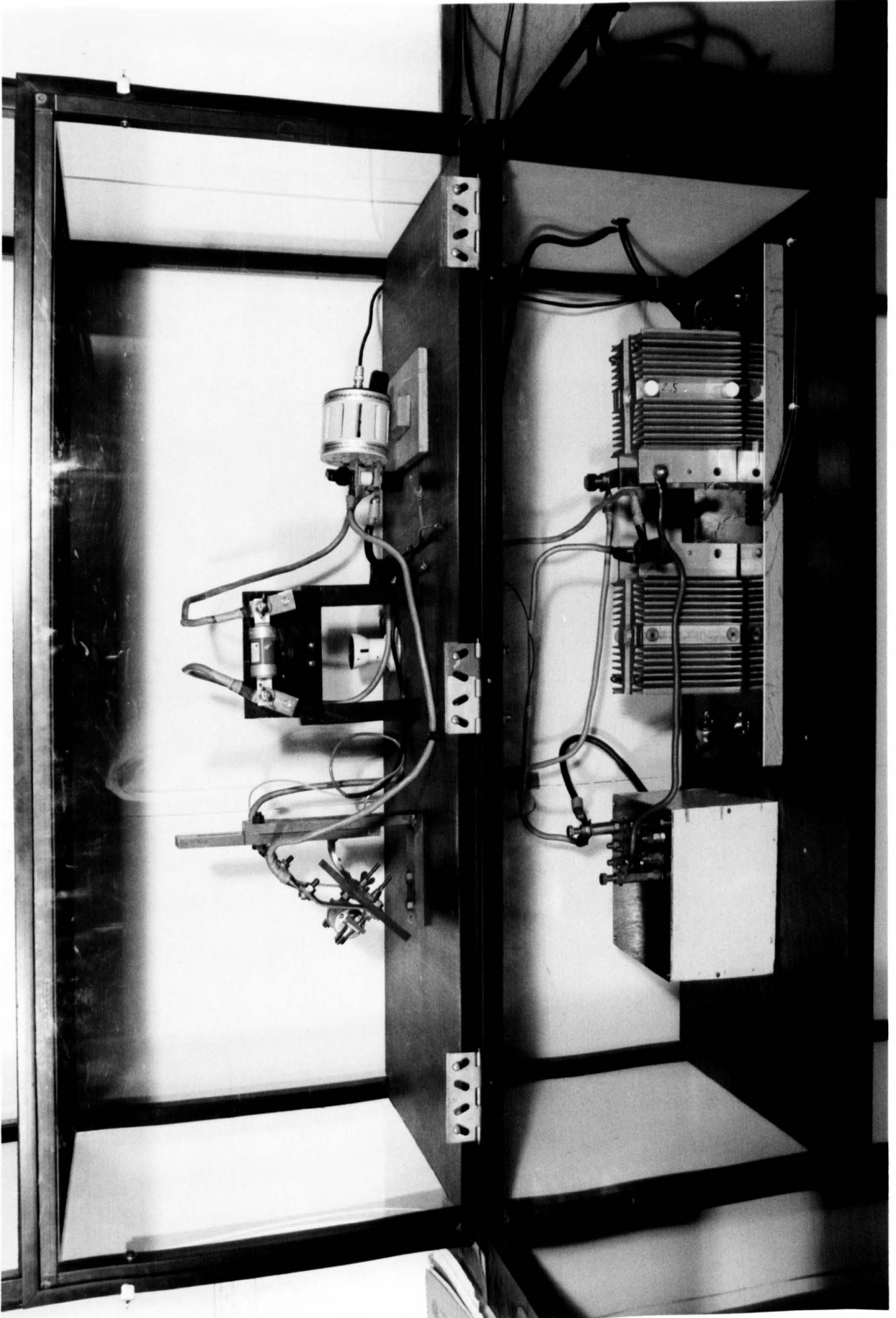
FIG. 2.7(a)   TEST RIG
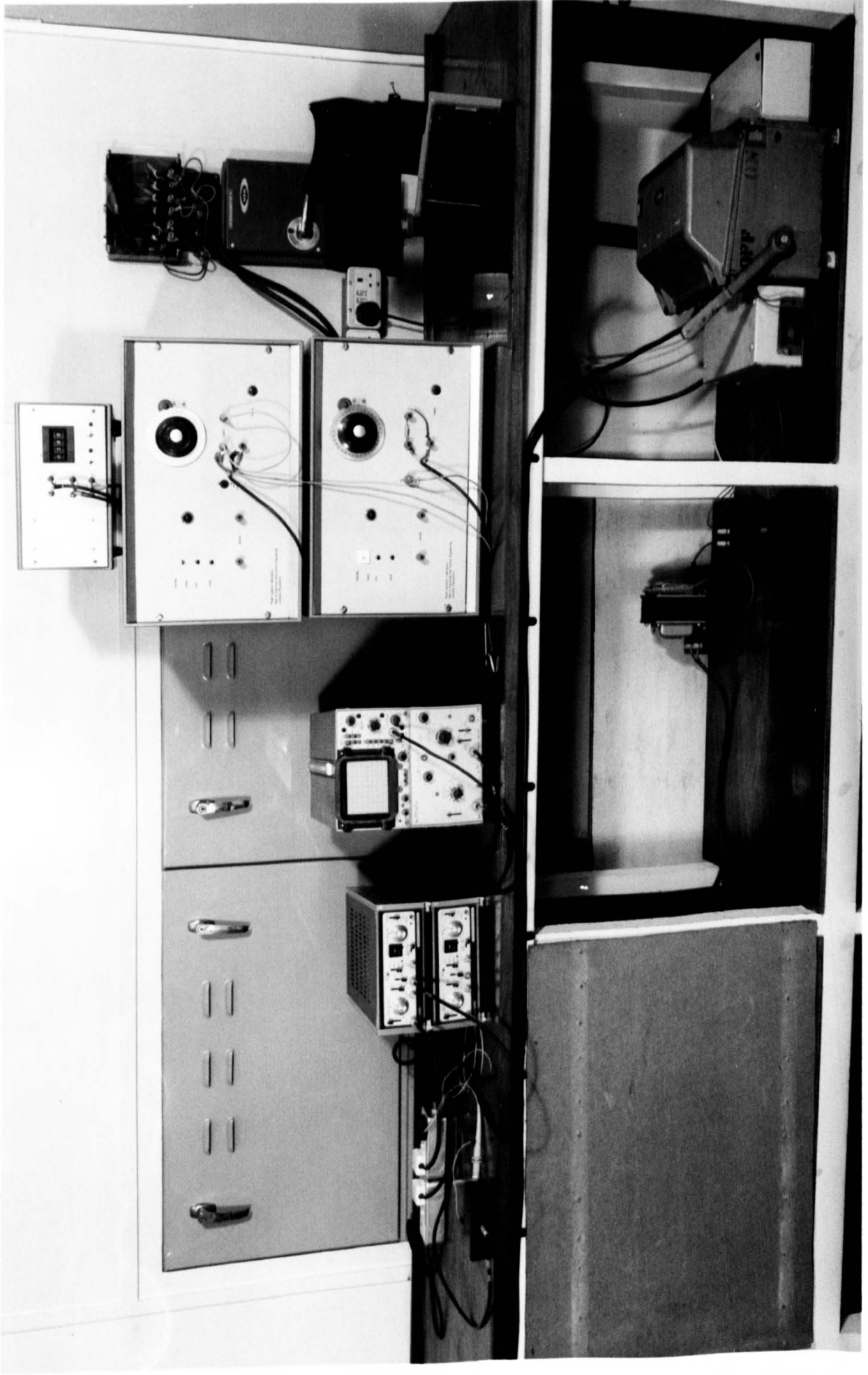
FIG. 2.7(b) CONTROL EQUIPMENT FOR THE TEST

(a)   ELEMENT   : $\frac{1}{8}$" x 0.003"
      CURRENT SENSITIVITY : 417 A/cm
      TIME SENSITIVITY   : 1 ms/cm
      t_c : 2.0 ms.   :
      PROSPECTIVE CURRENT : 7,700 A
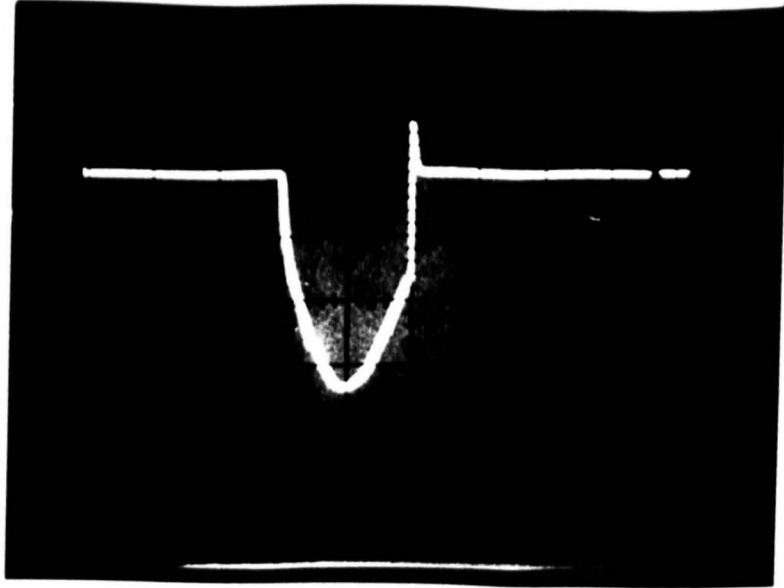
(b)   ELEMENT   : $\frac{1}{2}$" x 0.003"
      CURRENT SENSITIVITY : 208 A/cm
      TIME SENSITIVITY   : 1 ms/cm
      t_c : 7.0 ms
      PROSPECTIVE CURRENT : 2,040 A.
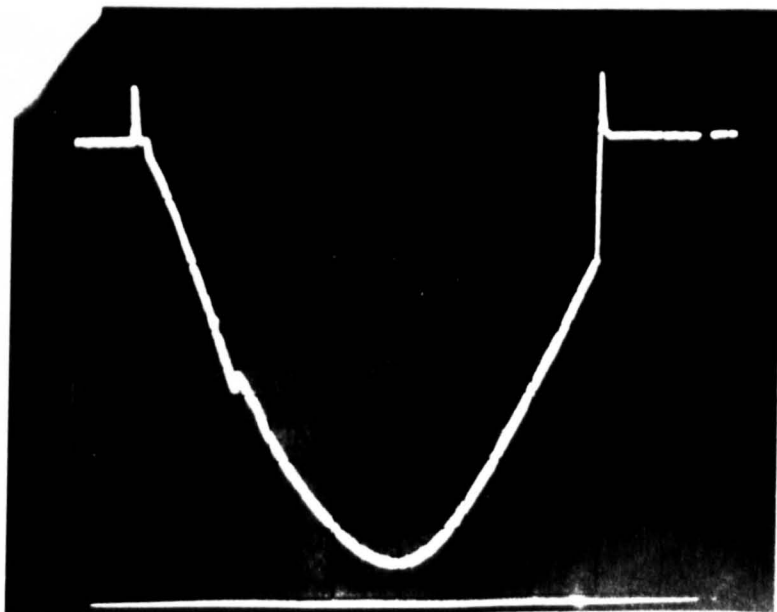
FIG.2.8. TYPICAL OSCILLOGRAMS OF CURRENT WAVE

Table 2.1   :   Fuse Elements

Symbol for Element	Width x Thickness (inch x inch)	Area of cross section (cm²)
RL2	$\frac{1}{8}$ x 0.003	0.00242
RL2	$\frac{1}{8}$ x 0.006	0.00484
RL2	$\frac{1}{8}$ x 0.010	0.00806
RL1	$\frac{1}{16}$ x 0.003	0.00121
RL4	$\frac{1}{4}$ x 0.003	0.00484
RL5	$\frac{1}{2}$ x 0.003	0.00968

The notch in all the fuses had a length and width each of 0.030 inch.

Fig.2.9(a) shows the X-ray picture of the fuses used for one series of tests with the same prospective current and (typical) element size $\frac{1}{8}$" x 0.003", whereas Fig.2.9(b) shows the X-ray picture for another series of tests with the widest element size $\frac{1}{2}$" x 0.003".

Some tests were also carried out with the test fuse mounted in the test rig in the vertical position to examine any possible gravitational effect in the ratio of the cathode/anode burnback.
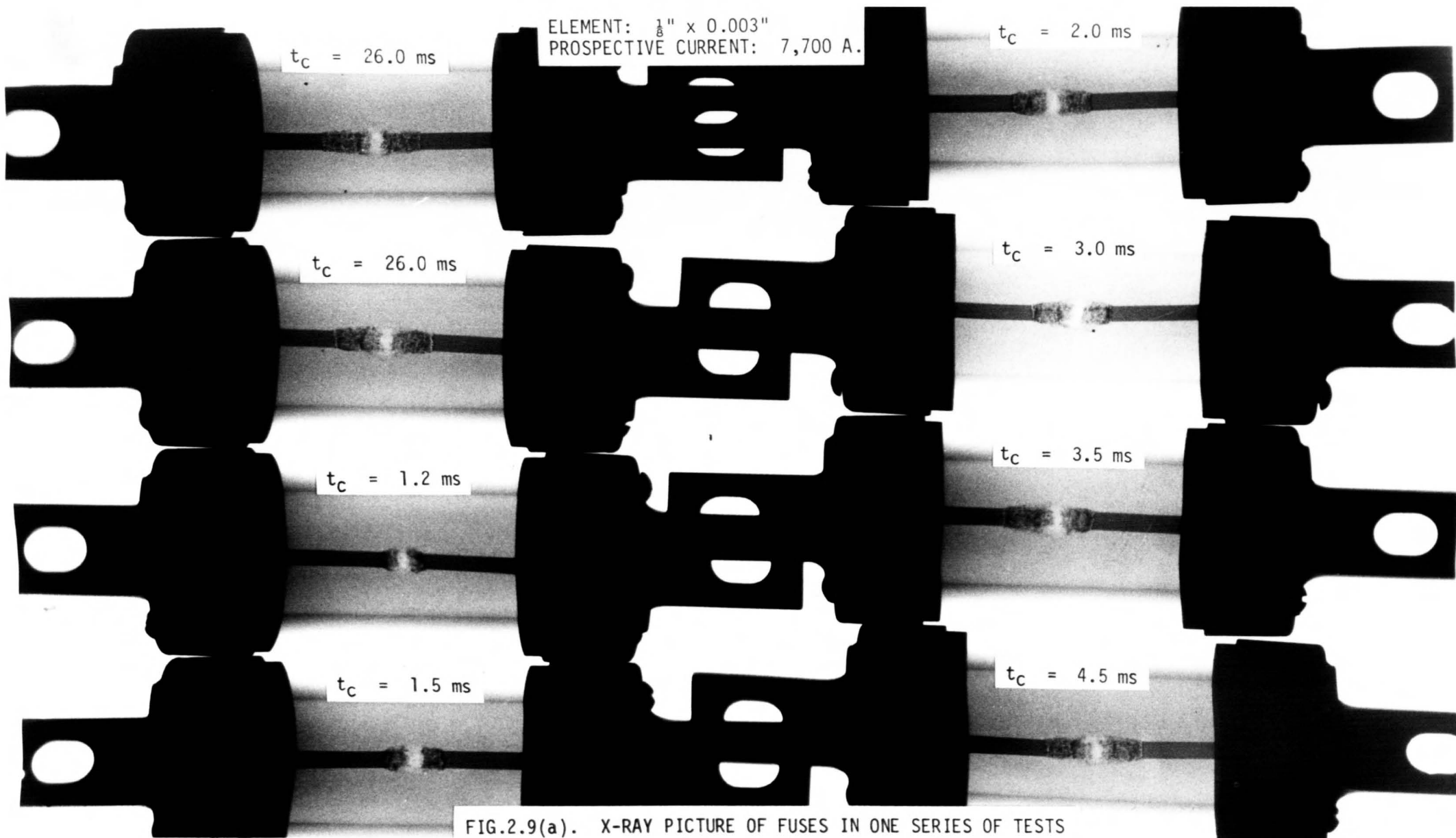
ELEMENT: $\frac{1}{8}$" x 0.003"
PROSPECTIVE CURRENT: 7,700 A.

t_c = 26.0 ms

t_c = 26.0 ms

t_c = 1.2 ms

t_c = 1.5 ms

t_c = 2.0 ms

t_c = 3.0 ms

t_c = 3.5 ms

t_c = 4.5 ms

FIG.2.9(a).   X-RAY PICTURE OF FUSES IN ONE SERIES OF TESTS

FIG.2.9(b). X-RAY PICTURE OF FUSES IN ONE SERIES OF TESTS

ELEMENT: $\frac{1}{2}$" x 0.003"
PROSPECTIVE CURRENT: 890 A.

t_c = 2.8 ms

t_c = 3.0 ms

t_c = 4.0 ms

t_c = 5.0 ms

t_c = 9.5 ms

t_c = 9.0 ms

t_c = 8.0 ms

t_c = 7.0 ms
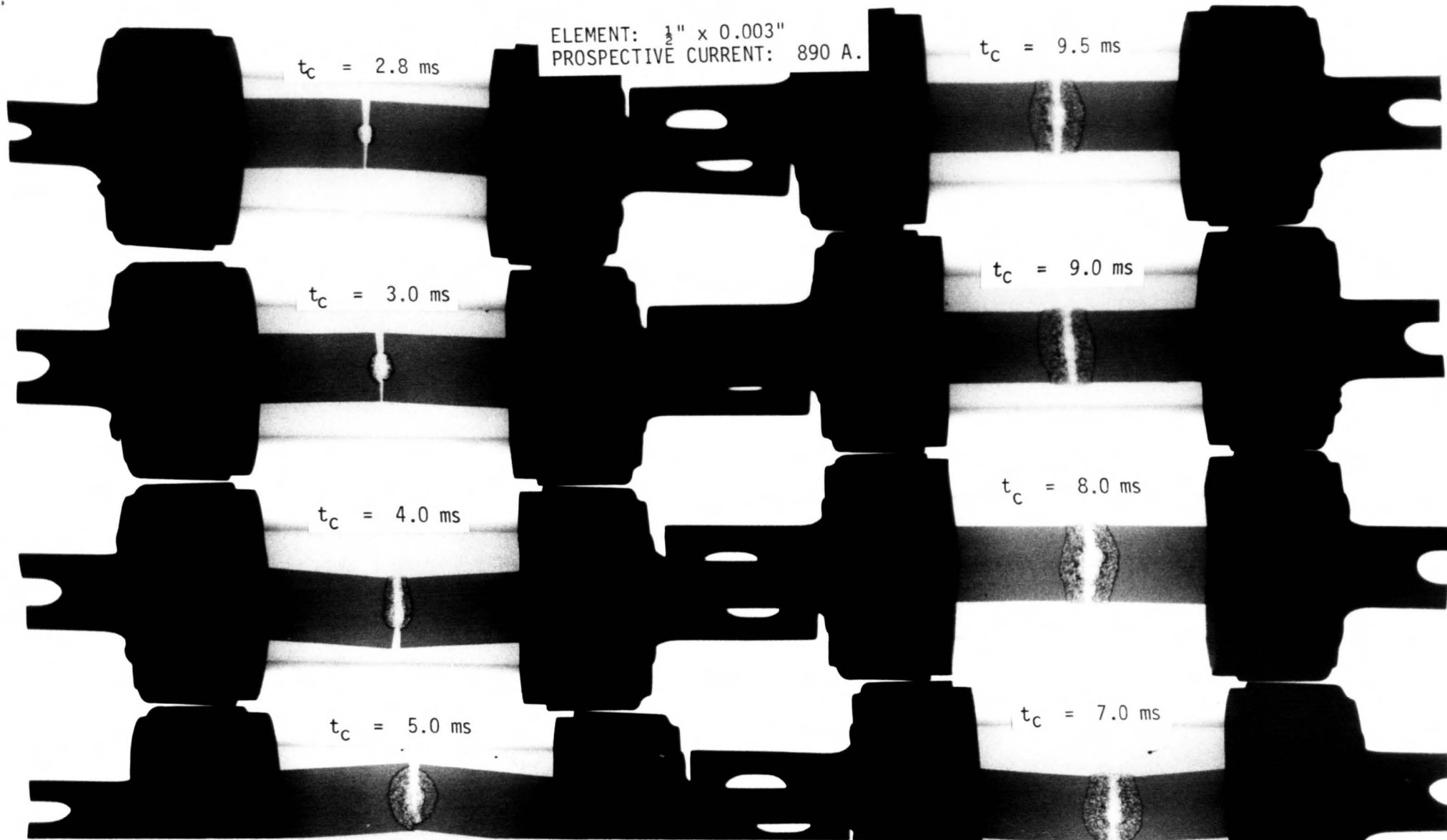
2.4   Results

2.4.1 Treatment of Results

The arc length x was plotted against the chopping time t_c for the 22 series of tests carried out, as referred to above. Tangents to the curves were drawn at selected points on the curves. These tangents gave the rates of burnback dx/dt corresponding to the instantaneous values of current obtained from the oscillograms for the respective chopping times. Velocities determined in this way could only be determined with confidence over the central part of the x : t_c graphs. Values of velocity corresponding to the initial part of the arcing period were inaccurate, since the erosion was concentrated near the element central axis and hence the burnback values had to be estimated by taking simple average values which procedure could effect inaccuracies. This tendency however disappeared as erosion progressed. The error was relatively high for wider elements. Two of these plots are shown to illustrate typically the shapes of the characteristics:

(a) Fig.2.10(a): x vs t_c for element size ⅛" x 0.003".
Plots of instantaneous values of current, i vs t_c and dx/dt (as determined from x : t_c graph) vs i are shown.

(b) Fig.2.10(b): x vs t_c for element size ½" x 0.003" and other plots as above.

Schedules 1 to 22 in Appendix 2.3 give the values of t_c, i, x_c, x_a, x, dx/dt and dv/dt, the last being the volumetric erosion obtained by multiplying dx/dt by the element cross sectional area s. Graphs of dx/dt vs i were then drawn, one for each element size (Fig.2.11(a) to Fig.2.11(f)) which showed that dx/dt was not a linear function of i,

ELEMENT : $\frac{1}{8}" \times 0.003"$

PEAK VALUE OF PROSPECTIVE CURRENT ~ 2900 A
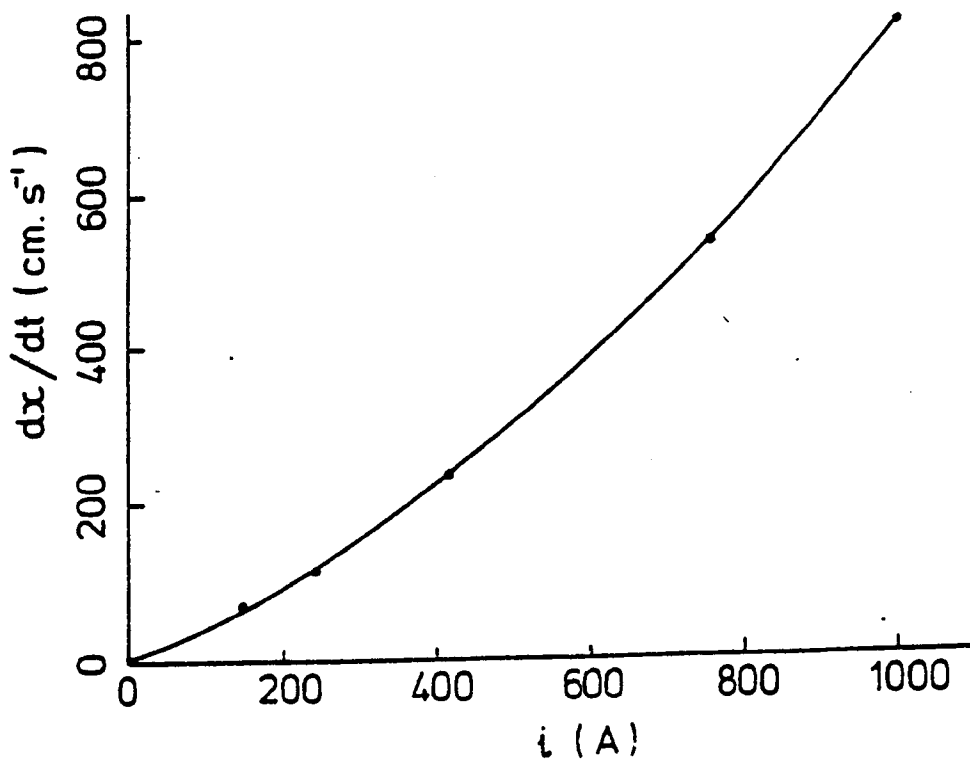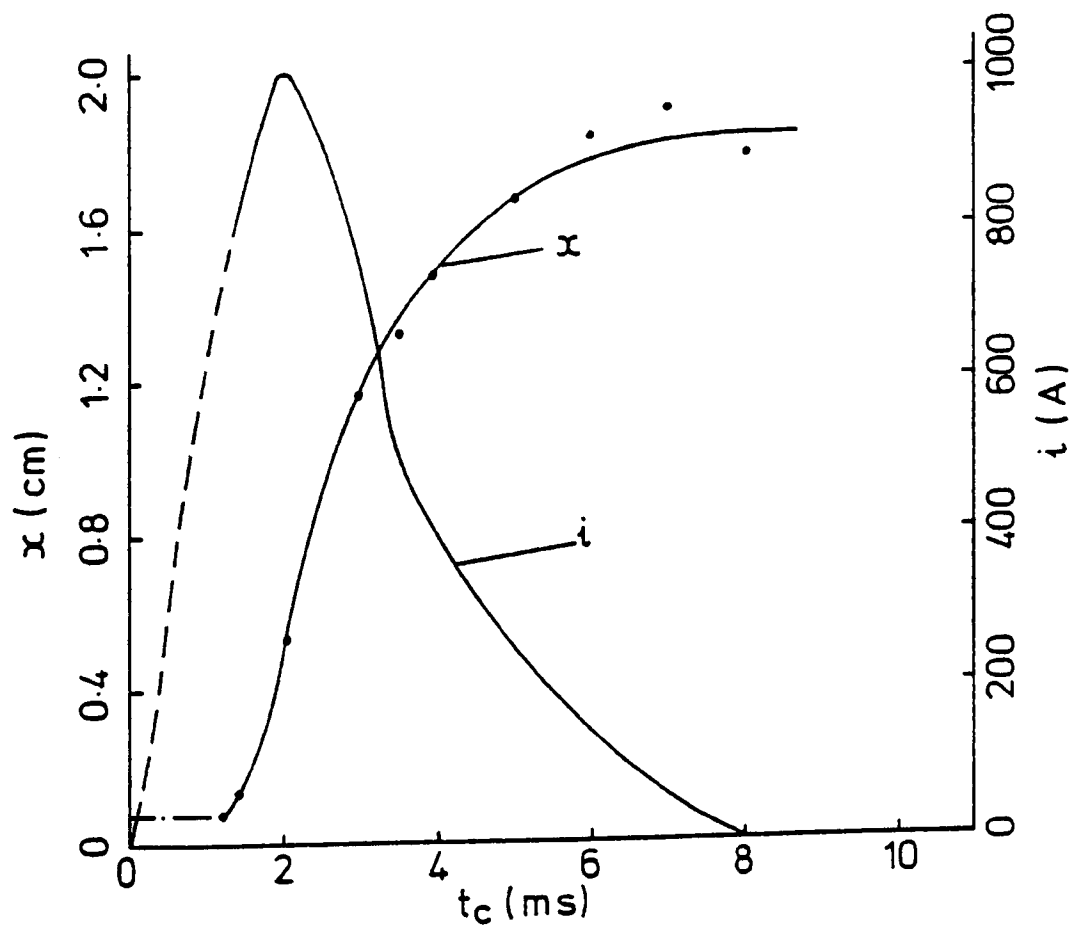
FIG. 2.10(a). RATE OF BURNBACK vs CURRENT
(FOR 1 SERIES OF TESTS)

ELEMENT : $\frac{1}{2}'' \times 0.003''$
PEAK VALUE OF PROSPECTIVE CURRENT ~ 2900 A
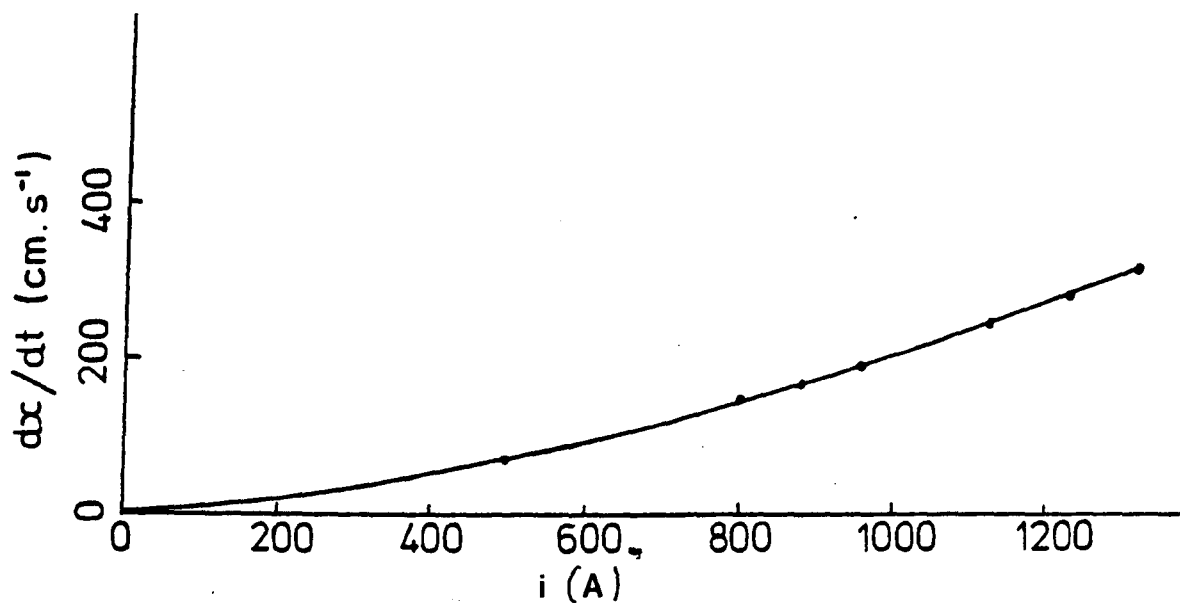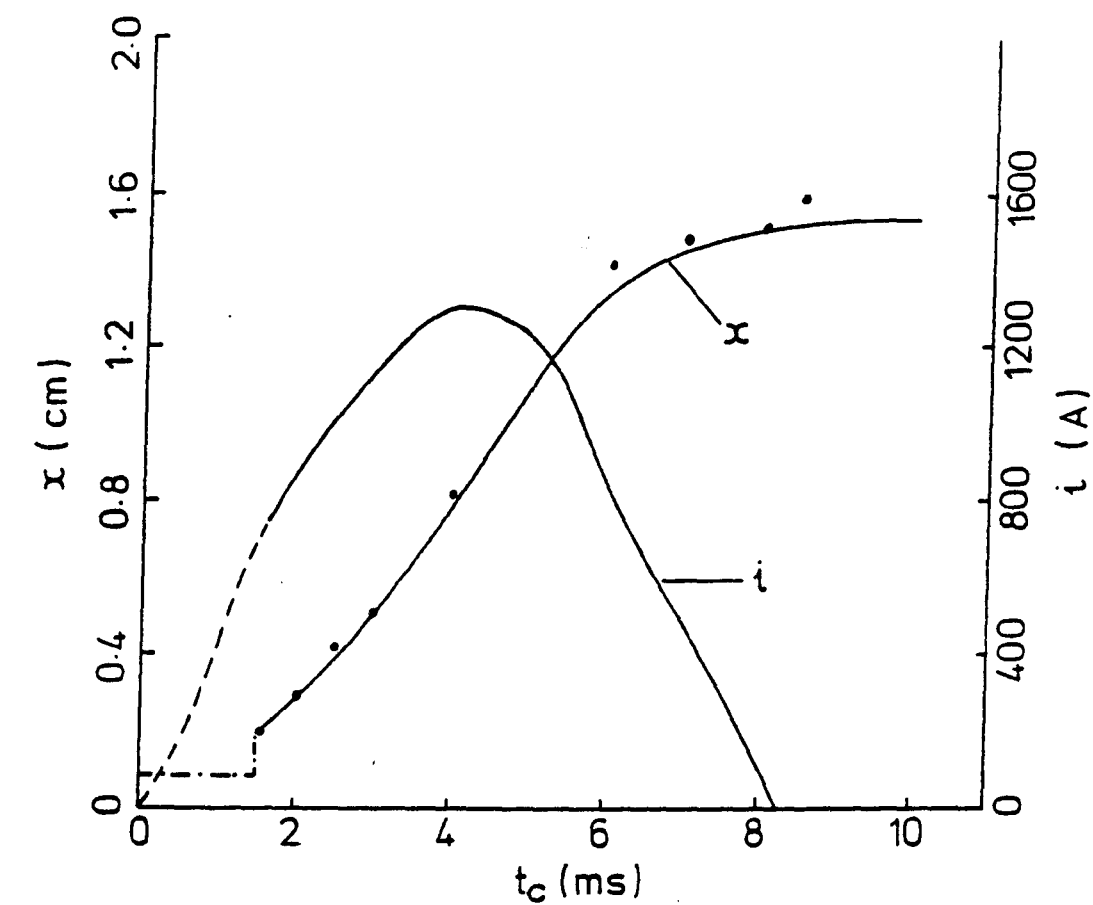
FIG. 2.10(b). RATE OF BURNBACK vs CURRENT
(FOR 1 SERIES OF TESTS)

but obeyed some power law. A study of the effect of element width and thickness revealed that these were only important in so far as they determined the current density. It was found that for any value of the instantaneous current, the ratio $\frac{dx}{dt} / \frac{i}{s}$ was constant. Thus we have:

$$\frac{(dx/dt)}{(i/s)} = f(i) \tag{2.8}$$

Analysis of all the test results showed that $f(i)$ could be fitted as $(a + bi^\gamma)$. $\frac{(dx/dt)}{(i/s)}$ vs i was drawn (Fig.2.12) and when extrapolated to $i = 0$ gave a value

$$a = 4.6 \times 10^{-4} \qquad cm^3.A^{-1}.s^{-1}$$

$$Log [\frac{(dx/dt)}{(i/s)} - a] \qquad vs \log i$$

was found to be linear (Fig.2.13) and:

$$the\ gradient,\ \gamma = 0.6$$
$$b = 0.219 \times 10^{-4}$$

Hence $\quad \frac{dx}{dt} = 10^{-4}(4.6 + 0.219\ i^{0.6})\ \frac{i}{s} \tag{2.9}$

$$\frac{dV}{dt} = 10^{-4}(4.6 + 0.219\ i^{0.6})\ i \tag{2.10}$$

Eqn (2.9) gives the velocity of burnback in $cm.s^{-1}$ and Eqn (2.10) gives the volumetric rate of erosion in $cm^3.s^{-1}$ with i in A and s in cm^2. In Fig.2.14, experimentally determined values of the volumetric rate of erosion and those predicted by Eqn (2.10) have been plotted against the current. There are 128 points on the figure and the correlation coefficient between the measured and predicted values is 98%. Eqn (2.9) is valid for instantaneous current densities up to 11 $kA.mm^{-2}$.

ELEMENT : $\frac{1}{8}'' \times 0.003''$
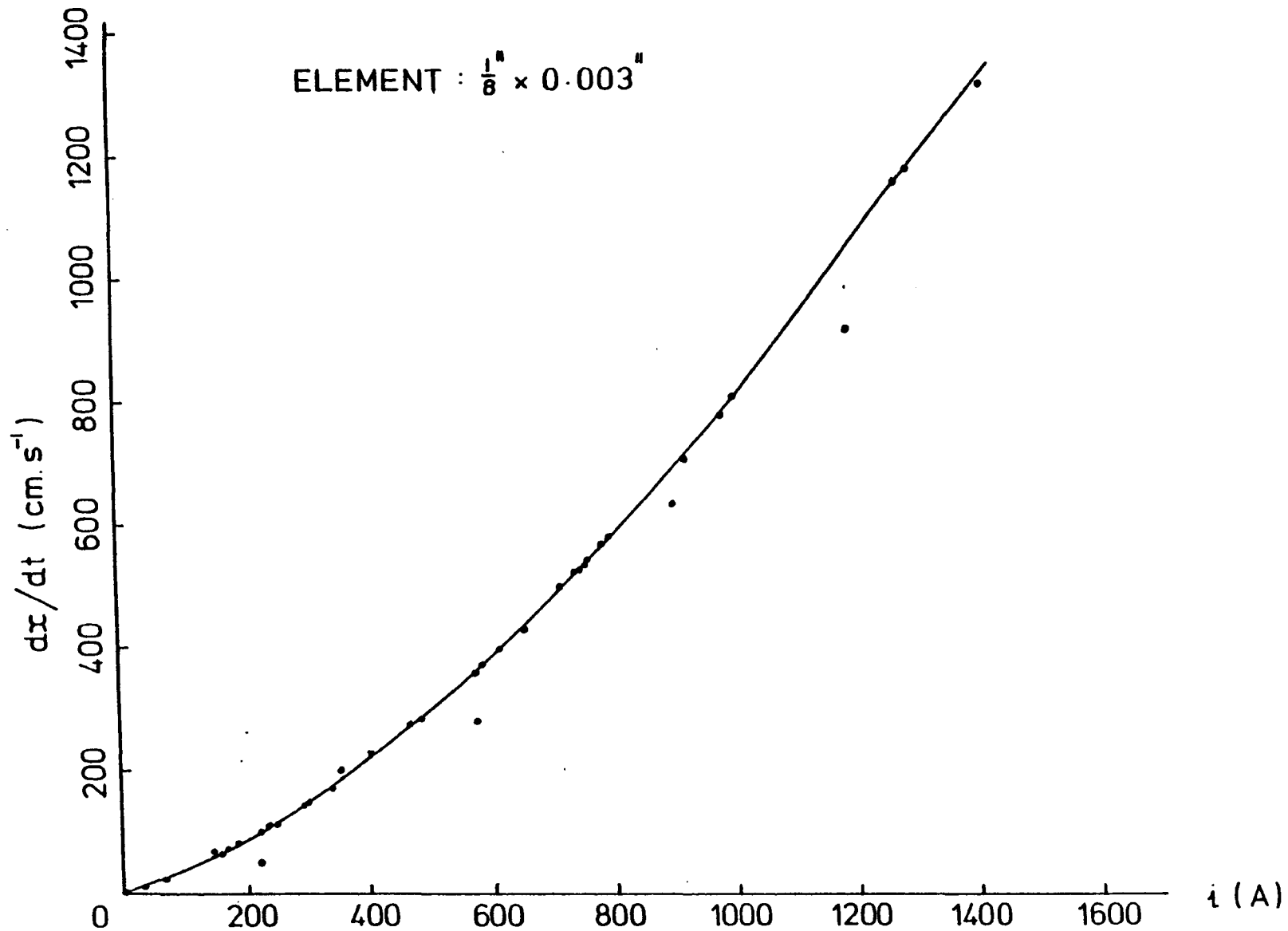
FIG. 2.11(a). RATE OF BURNBACK vs CURRENT

ELEMENT : $\frac{1}{8}'' \times 0.006''$
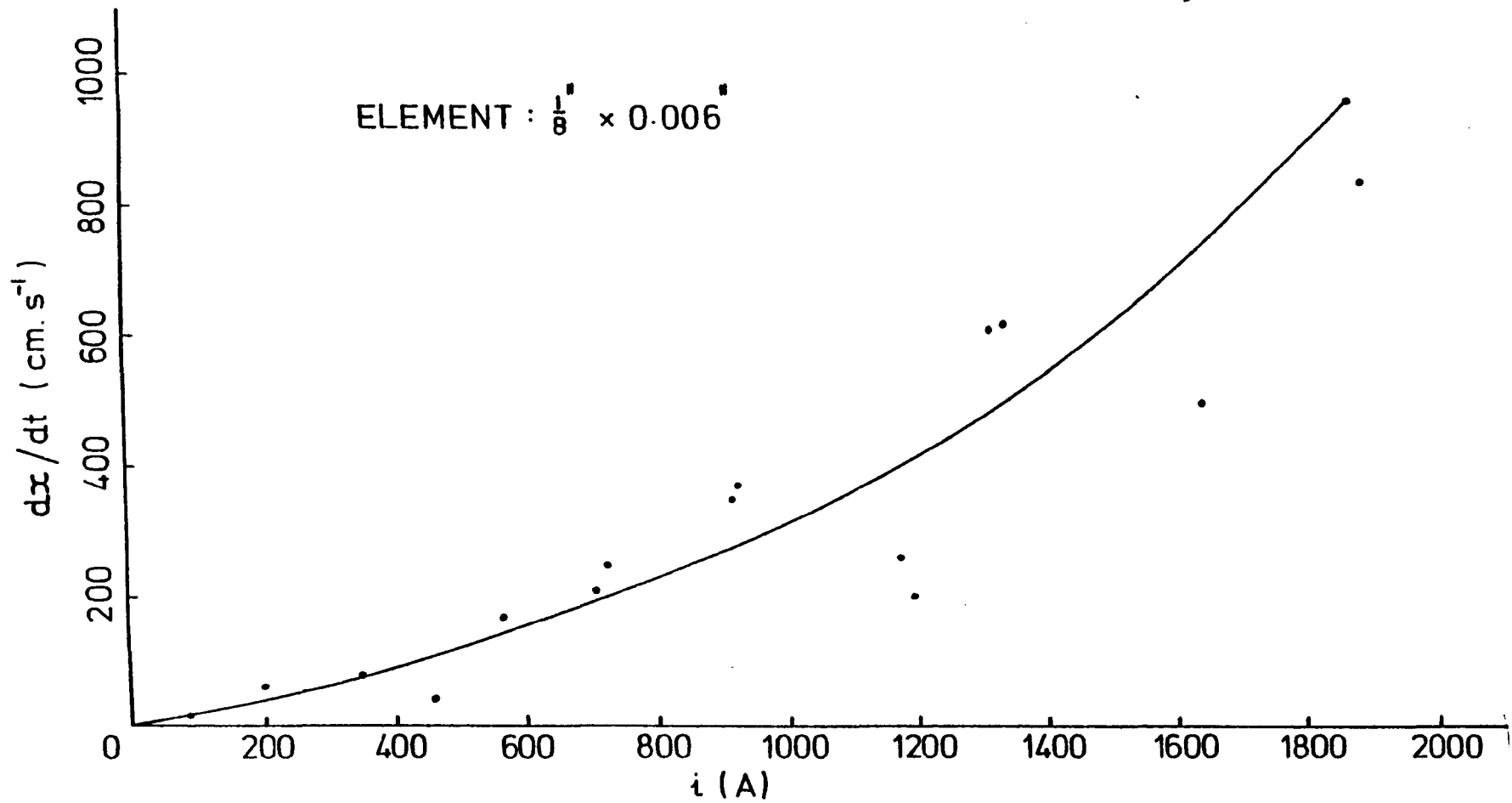
FIG. 2.11(b). RATE OF BURNBACK vs CURRENT
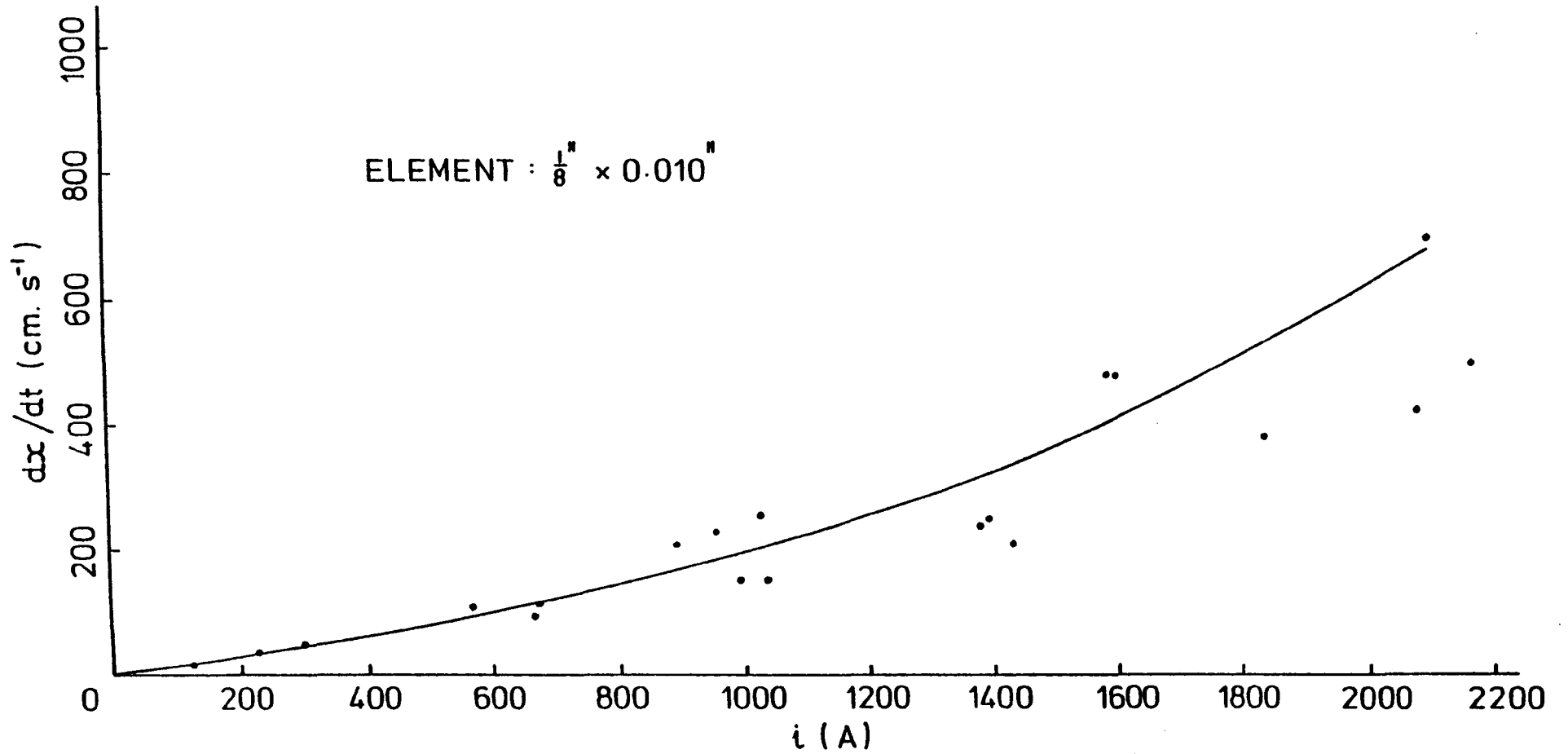
FIG. 2. 11(c). RATE OF BURNBACK vs CURRENT

ELEMENT: $\frac{1}{i_6} \times 0.003$
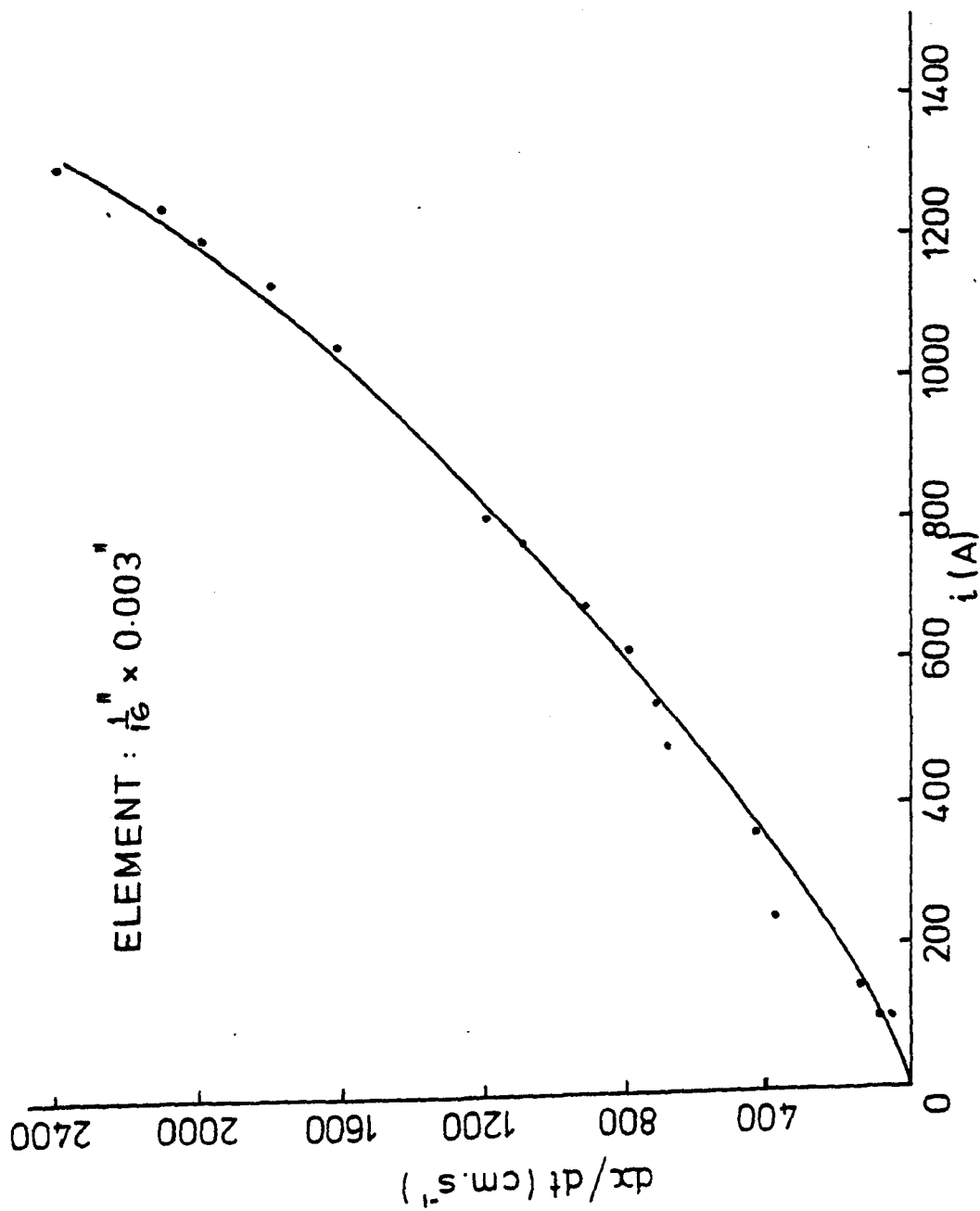
FIG. 2. 11(d) RATE OF BURNBACK vs CURRENT

i (A)

dx/dt (cm.s⁻¹)

ELEMENT : $\frac{i^n}{4} \times 0.003$
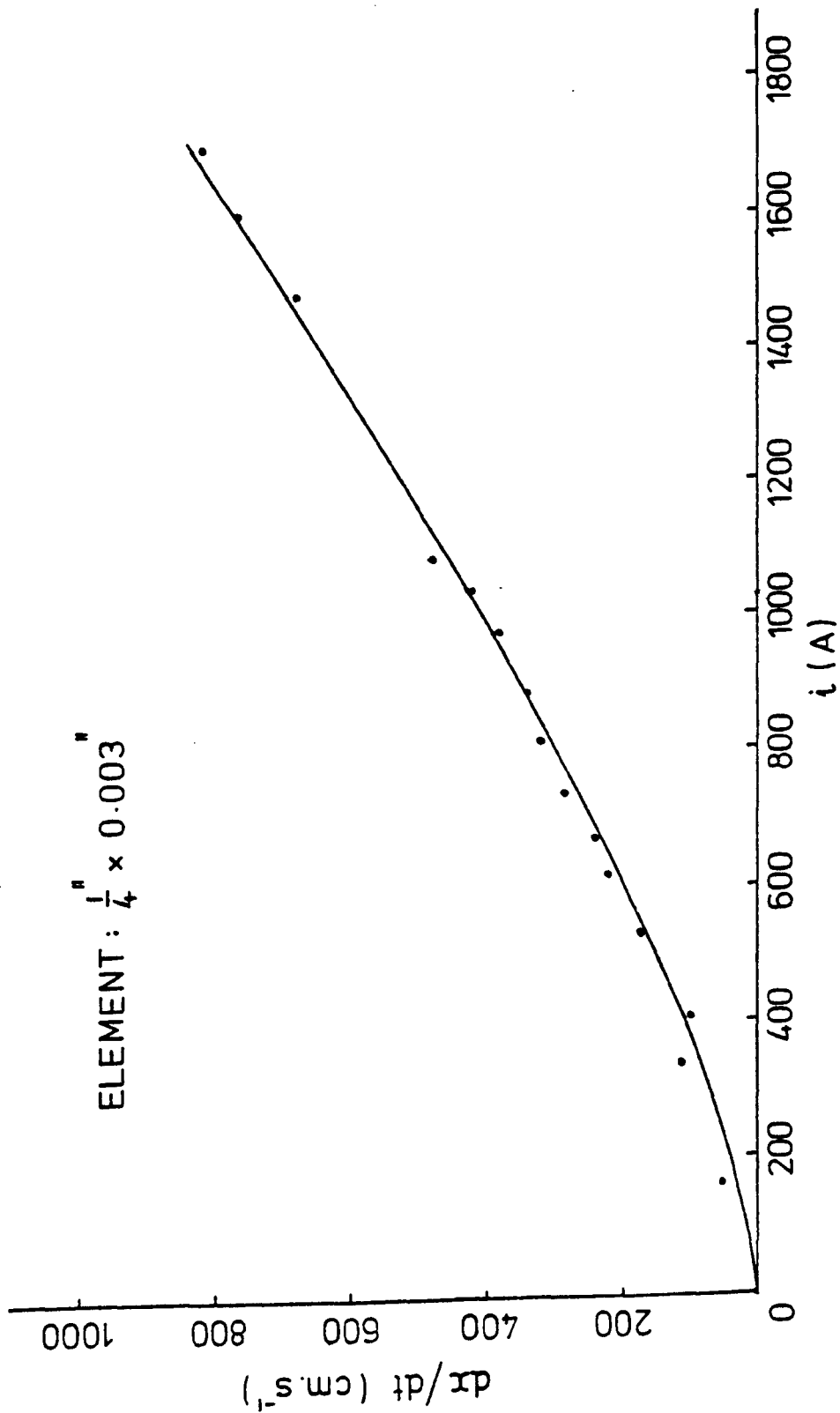
FIG. 2.11(e). RATE OF BURNBACK vs CURRENT

$\frac{dx}{dt}$ (cm.s^{-1})

i (A)
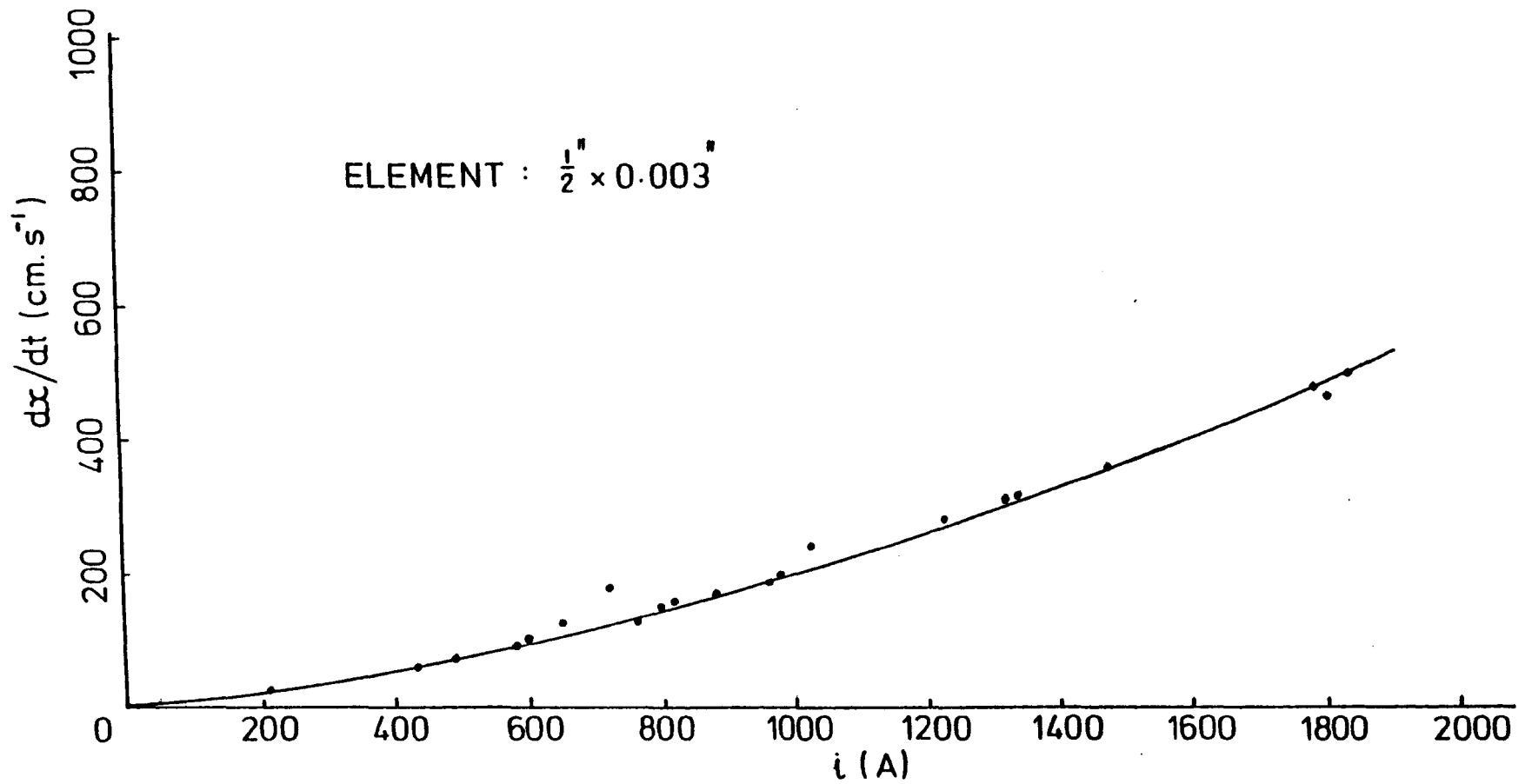
FIG. 2.11(f). RATE OF BURNBACK vs CURRENT
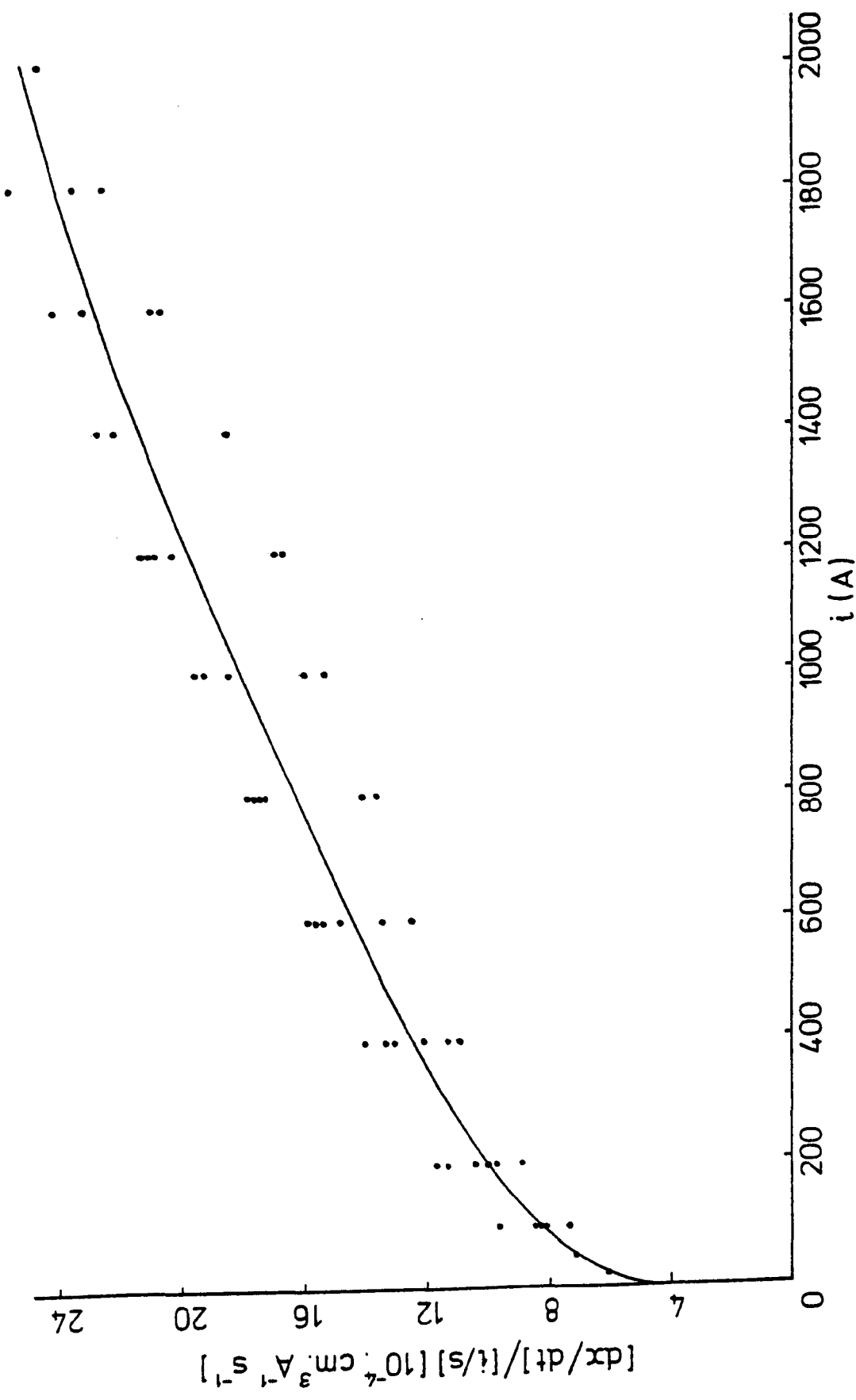
FIG. 2.12. (RATE OF BURNBACK / CURRENT DENSITY) vs CURRENT
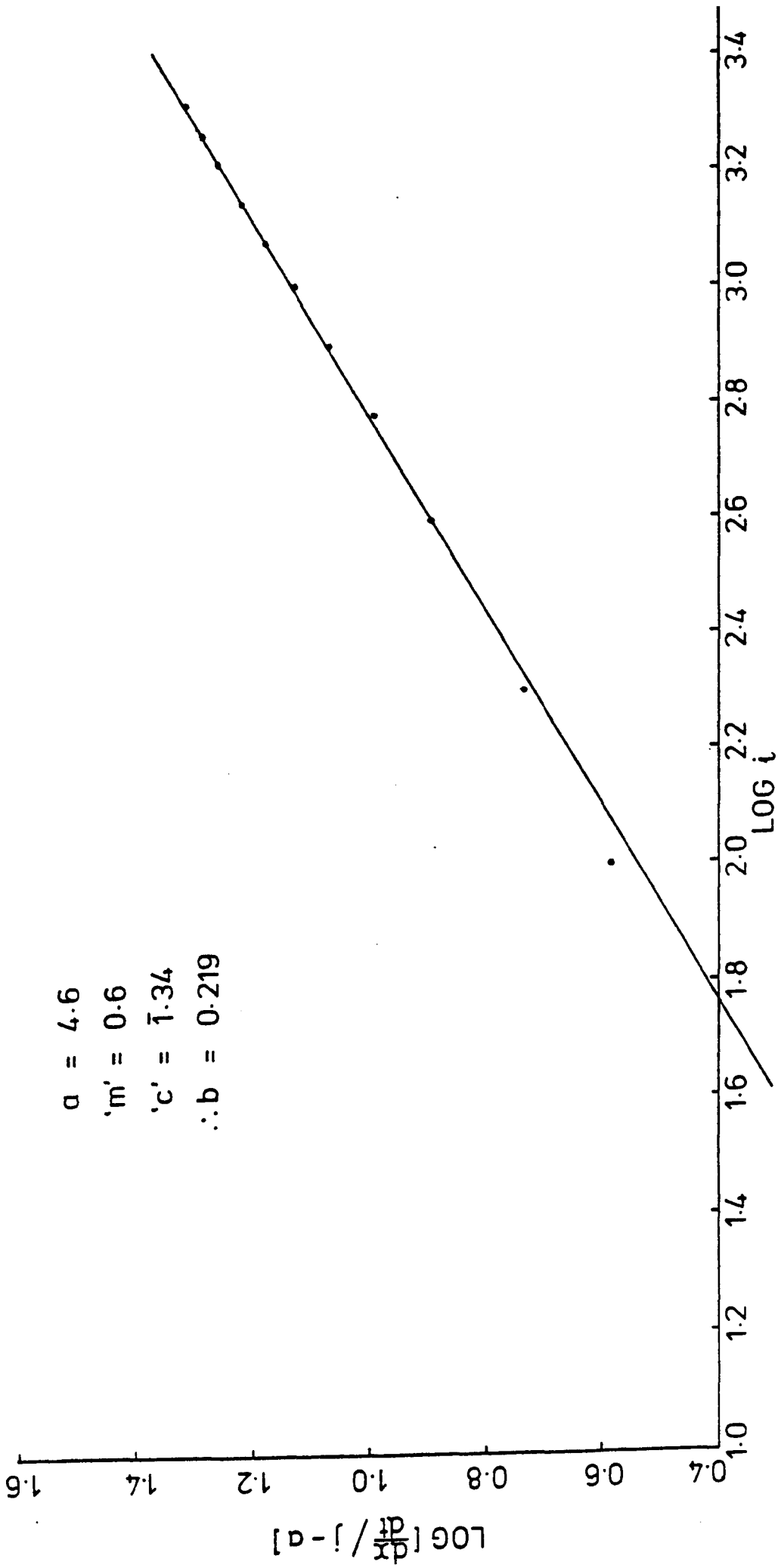
FIG. 2.13. LOG $\left[\frac{dx}{dt} / j-a\right]$ vs LOG i

$a = 4.6$

'm' $= 0.6$

'c' $= \bar{1}.34$

$\therefore b = 0.219$

LOG $\left[\frac{dx}{dt} / j-a\right]$

2.4.2 Cathode/Anode Burnback Ratio

In Eqn (2.9), x is the total arc length which is produced by erosion at the arc cathode, x_c and at the anode, x_a.

Hence
$$\frac{dx}{dt} = \frac{dx_c}{dt} + \frac{dx_a}{dt} \qquad (2.11)$$

The burnback at disruption is small and the rate of burnback at the cathode and anode should be proportional respectively to the length of burnback at the cathode and at the anode, since i is same.

Measurements of x_c and x_a (average values) taken from 214 X-rays of fuses showed that the ratio x_c/x_a was equal to 1.008 ± 0.12. We may conclude that the erosion rates at the cathode and anode are equal.

2.4.3 Effect on Vertical Mounting of Fuse

A few tests were carried out with the test fuse mounted in the test rig in the vertical position with the anode on top. Measurements of x_c, x_a and x showed that the average velocity of burnback and the ratio of cathode/anode burnbacks were not affected much by mounting the fuse vertically. The results are given in Appendix 2.4.
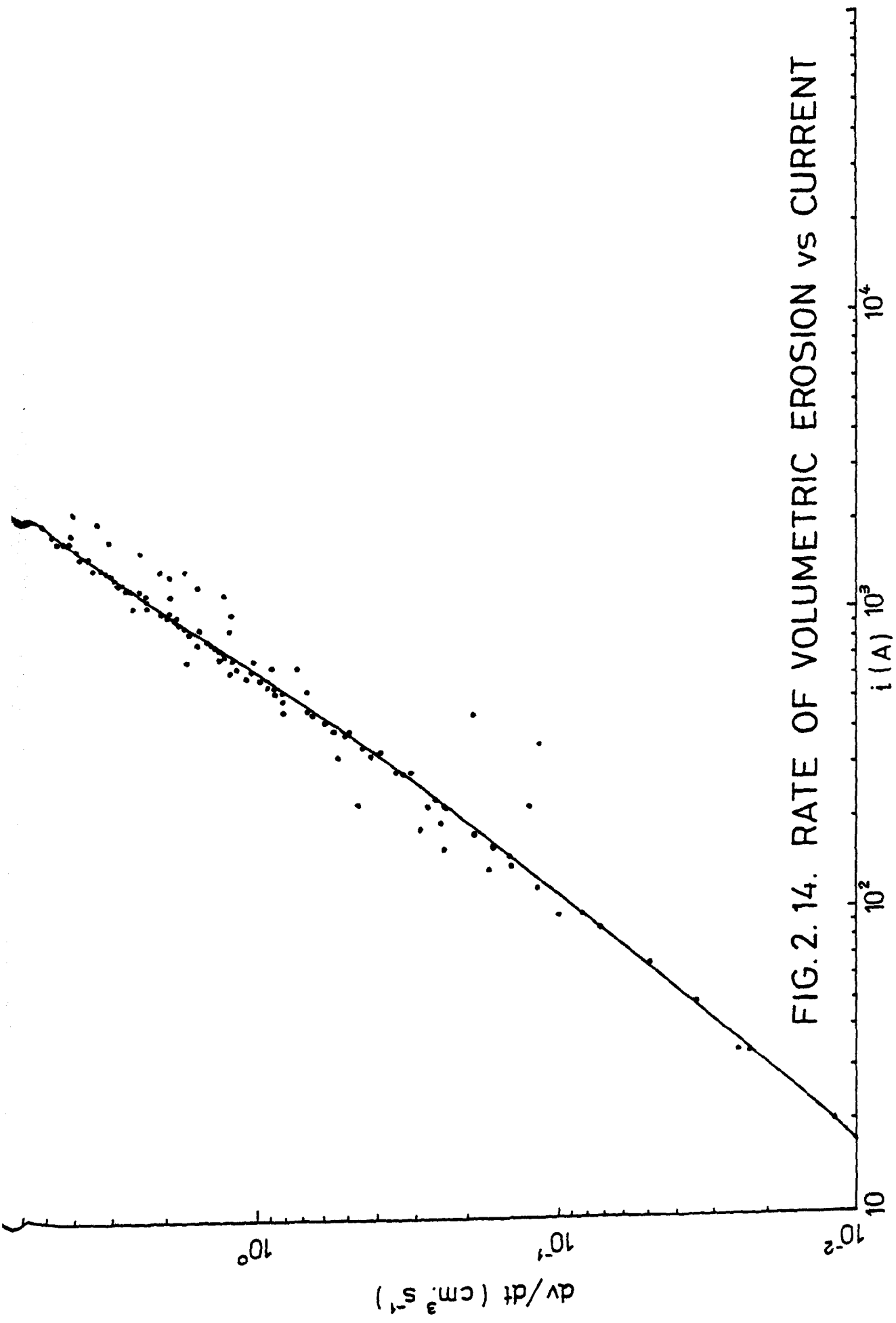
FIG. 2.14. RATE OF VOLUMETRIC EROSION vs CURRENT

2.5   Discussion

2.5.1 Power Balance at the Electrodes

When a solid is heated by constant heat flux F at its surface any

melted material being removed in the liquid state, the rate of erosion

would be given by (14):

$$\frac{dx}{dt} = \frac{F}{\rho(L + C.\Delta T)} \qquad (2.12)$$

where ρ = specific weight,

           L = latent heat of fusion,

           C = specific heat,

          ΔT = (Melting Point - bulk temperature),

                 of the material

If the solid is heated to the liquid stage and the liquid partly

vaporised, then the term $\rho(L + C\Delta T)$ in the above Eqn should be modified

to include the additional energy required per unit volume. If the

fraction of the material vaporised is β, then the energy per unit

volume of removed material would be:

$$\gamma = \rho_1 \{L_1 + C_1 (T_m - T_A)\} + \beta\rho_2 \{L_2 + C_2 (T_v - T_m)\}$$

where ρ_1, ρ_2 = specific weights of solid and liquid

          L_1, L_2 = latent heats of fusion and vaporisation

          C_1, C_2 = specific heats of solid and liquid

             T_m = M.P. of the material

             T_v = B.P. of the material

             T_A = bulk temperature

Hence in general we could write:

$$\frac{dx}{dt} = \lambda F \qquad (2.14)$$

$$\text{where} \quad \lambda = \frac{1}{\gamma}$$

$$= \text{erosion parameter}$$

In the case of a uniformly eroding fuse element under short circuit conditions, no energy is required for electrode heating, after the initial small time delay required for erosion to commence has elapsed, the initial input energy being thereafter stored in the metal behind the retreating interface (14). Eqn (2.14) is applicable as it has been shown (1), (25), that the removal of silver is partly in the liquid state and partly in the vapour state. If we assume a bulk temperature of $200^{\circ}C$ and the arc root to be at the B.P. of silver with removal of the metal entirely in the vapour state then $\beta = 1$ and λ can be shown to be approximately $0.03cm^3$. kJ^{-1} using thermophysical data for silver as furnished in Appendix 1.1. However some of the silver will flow away in the liquid form $\underset{\wedge}{\text{with great force}}$ through the interstices between the quartz particles which will give a larger value of λ in practice (1). F is variable and comprises two components F_c and F_a causing erosion respectively at the cathode and anode ends of the eroding element (5), (6).

$$F_c = (1 - f)(U_k + U_i - U_e)j_k \qquad (2.15)$$

$$F_a = (U_a + U_e)j_a \qquad (2.16)$$

$$\text{where} \quad U_e' = \text{electronic work function voltage,}$$
$$(4V \text{ was assumed})$$

and U_i = ionisation potential (assumed to be about 17V),

for silver

f = fraction of cathode current carried by electrons (in the range 0.4 - 0.5)

Erosions at the cathode and anode would then be:

$$\frac{dx_c}{dt} = \lambda_c (1 - f) (U_k + U_i - U_e) j_k \qquad (2.17)$$

$$\frac{dx_a}{dt} = \lambda_a (U_a + U_k) j_a \qquad (2.18)$$

where λ_c, λ_a are erosion parameters for cathode and anode which depend upon the properties of the element material and the relative proportion of silver vapour and liquid silver in the eroded material (1).

Hence the most important power balances at the cathode and anode under steady state erosion conditions give:

$$\frac{dx}{dt} = \lambda_a (U_a + U_e) j_a + \lambda_c(1 - f)(U_k + U_i - U_e) j_k \qquad (2.19)$$

In order to explain the observed equality of erosion rates at anode and cathode it is necessary that the two terms on the r.h.s. of Eqn (2.19) are equal. For arcs between massive electrodes erosion at the cathode greatly exceeds that at the anode because $j_c >> j_a$. j_c is typically greater than $10kA.mm^{-2}$, j_a is less than $1kA.mm^{-2}$ and the current density in the positive column is of the order of $0.01 kA.mm^{-2}$ (10). However, in fuse arcs under short circuit conditions the arc column is constricted by the surrounding filler and current densities of several $kA.mm^{-2}$ are obtained. Thus j_a is constrained to be of the same order

31

as j_c. Nevertheless under low over current conditions these arguments relating to the constriction of the arc channel would not apply because the channel current density would be much lower. j_c could be higher than j_a which would explain Oliver's (4) observation of a higher erosion rate at the cathode for small DC over currents (-cathode erosion approximately 1.6 times the anode erosion).

Danders has shown that it is quite feasible for $(U_a + U_e)$ to be equal to $(1 - f)(U_k + U_i - U_e)$ making reasonable assumptions for the value of the parameters (6). Finally, there is no reason why the individual erosion parameters λ_a and λ_c should differ appreciably from a value around 0.03 cm^3. kJ^{-1} (1) and so the two terms on the r.h.s. of Eqn (2.19) should be approximately equal and $\frac{dx}{dt}$ can be obtained by doubling either term. As an approximate relationship $\frac{dx}{dt}$ can be rewritten as:

$$\frac{dx}{dt} = \lambda j \left[(U_a + U_e) + (1 - f)(U_k + U_i - U_e) \right] \qquad (2.20)$$

where $j = i/s$, is the current density in the element

λ = erosion parameter, is generally not a constant

f is also a variable

Dolegowski's results (9) suggest that the total electrode-fall voltage increases with current according to:

$$U_a + U_k = C_1 + C_2 \, i^n$$

where n is roughly between 0.39 and 1 as analysed in Section 2.1(e)

Hence it could be seen that the r.h.s. of Eqn (2.20) will not be a linear function of i, but rather a higher power function of i, as empirically obtained in Eqn (2.9). Thus Dolegowski's experimental results are in close agreement with the findings of this study.

Onuphrienko (11) explained the equality of anode and cathode erosion rates by assuming that electrode processes play no part in the erosion, which was considered to be due solely to radiation from the plasma column.

Wheeler (12) and Lowke (13) have made similar suggestions. However the electrode power densities predicted by Eqn (2.20) are quite sufficient to explain the observed erosion rates.

2.5.2 Initial Burnback of Wider Elements

In the wider elements there was an initial tendency for the erosion to be concentrated near the element central axis as can be seen in Fig.2.9 (b) for ($\frac{1}{2}$" x 0.003") element. The current density and hence the power density were relatively small for these elements since the cross sectional area was high.

During the initial stage of arcing the plasma was confined to the neck of the element in the centre. The rate of burnback, which is dependent on the heat flux emitted by the plasma would be high at the neck and low at parts of the element cross section remote from the central axis. Hence the erosion would be concentrated near the element central axis initially.

As the arc elongates plasma would have caused the surrounding silica to

melt and would spread across a larger cross section of the element, eventually filling up the entire section. At that stage the heat flux became reasonably uniform across the cross section of the element, tending to make the burnback too uniform across the element as shown in Fig.2.9(b).

2.5.3 Effect on Vertical Mounting of Fuse

From the results shown in Appendix 2.4, it can be seen that in the case of fuse operation under short circuit conditions, gravity does not influence the burnback as neither the total burnback of the bottom electrode was lower than that of the other nor was the total burnback of the element substantially different from the corresponding one for horizontal mounting.

Due to gravitational effect more of the molten silver would be removed from the upper electrode than the other. However experimentally this effect was shown to be negligible probably because the burnback was under short circuit conditions and the time involved for the whole process was so small that the rate of burnback was not affected by the gravitational pull.

2.5.4 Effect of Filler Grain Size

Variation of filler grain size would be expected to produce some changes in the velocity of burnback predicted by Eqn (2.9).

The type and mean grain size of sand and the initial setting of the sand influence the initiation of arc, the rate of growth and final volume and length of the arc column (15). Experiments performed on h.r.c.

fuses with silver fuse elements for DC low over current conditions (15) showed that the average rate of burnback was virtually independent of the mean grain size during the early half of the arcing period, but decreased by about 40% when the mean grain size of the filler was increased from 0.48mm to 1.06mm for the same "compactness".

With larger mean grain size, the inter-spacial volume between grains would be larger and hence the lumen area would tend to be larger when substantial burnback had taken place. Larger lumen section could indicate a smaller voltage gradient (as shown in Section 3.2.3) and consequently less power input, which would probably explain why the rate of burnback during the latter part of the arcing period was less than for smaller mean grain size filler. More experimental work and theoretical analysis would be required to quantify this effect. However in the case of eroding silver fuse elements under short circuit conditions, the influence of mean grain size may be small and any changes in the equation for rate of burnback would most probably be accommodated by a constant multiplying factor, rather than by changes to the fundamental power law.

2.5.5 Arc Length vs Time

The burnback reached a maximum when the arc current was extinguished. It was observed that the length of burnback was a maximum when the arc current was chopped with the crowbar thyristor at the instant of extinction. There was a tendency for the arc length to be reduced by up to 10 per cent when the chopping was effected a few milliseconds after the current zero. The reasons for this effect are still unclear.

2.6   Comparison with Previous Work

From a review of previous work done as analysed in Section 2.1, it would be seen that most previous published data has assumed a linear dependence of erosion rate on current, the volumetric erosion rate being given by

$$\frac{dv}{dt} = C\,i \tag{2.21}$$

Kroemer (2) gave a value of 0.0023 cm³. A^{-1}. s^{-1} for C basing on experimental results with current densities not exceeding some 1.2 kA. mm^{-2}. Wright and Beaumont (5) made assumptions corresponding to C ~ 0.0048 cm³. A^{-1}. s^{-1}. Danders (6) took C = 0.00144 cm³. A^{-1}. s^{-1} and Onuphrienko (11) indicated that C lies between 0.0025 and 0.0050 cm³. A^{-1}. s^{-1}, depending on the length of arc. The extremes of these values of C are indicated on Fig.2.15, together with the volumetric erosion rate predicted by the present work as given by Eqn (2.10). Fig. 2.15 shows a marked difference between this characteristic and the 'linear erosion' formulae but since the characteristic crosses all the 'linear erosion' characteristics the values of C quoted above will give correct results for certain values of current.

Turner and Turner found that erosion of silver contacts follows the law

$$\frac{dw}{dt} = 40\,i^{1.6} \quad \mu g.s^{-1}$$

This was shown in Section 2.1 to give the following volumetric rate for silver fuse elements:
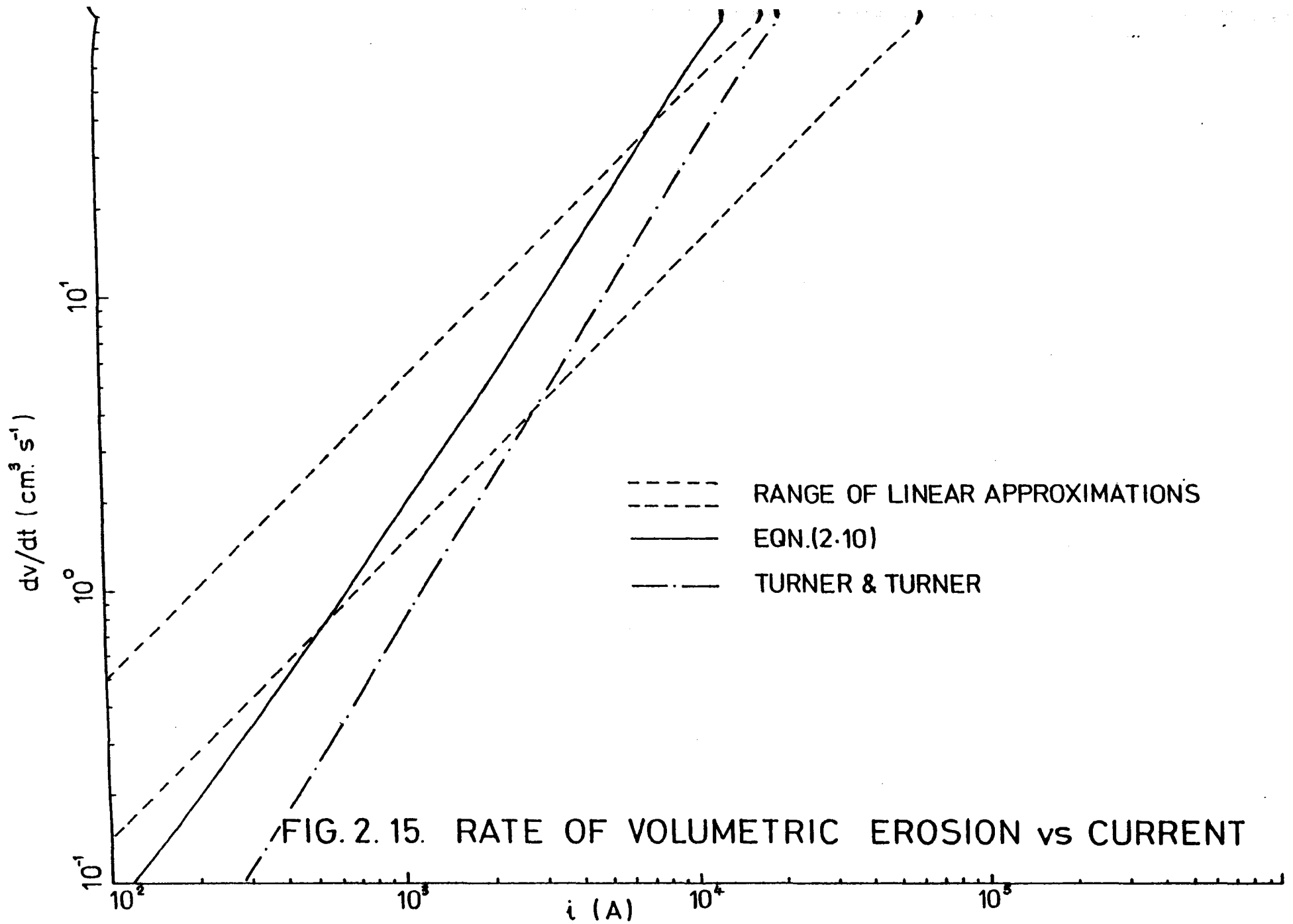
FIG. 2.15. RATE OF VOLUMETRIC EROSION vs CURRENT

- - - - - RANGE OF LINEAR APPROXIMATIONS

———— EQN.(2·10)

—·—·— TURNER & TURNER

y-axis: dv/dt ($cm^3. s^{-1}$)

x-axis: i (A)

$$\frac{dv}{dt} \sim 11.9 \times 10^{-6} \; i^{1.6} \; cm^3.s^{-1}$$

which characteristic is also shown in Fig.2.15. Although a similar
power law dependence is evident it will be seen that the volumetric
erosion rate suggested by the authors is low.

2.7 Conclusions

The experiments showed that the velocity of burnback depends upon the fuse element current according to a power law and that there is no appreciable difference between anode and cathode burnbacks. These results have been interpreted in terms of power balances at the arc roots.

The expression for the rate of burnback will be used later for the simulation of the arc.

CHAPTER III

COLUMN GRADIENT

3.1   Review of Previous Work

Determination of the column gradient of arcs in current limiting fuses

operating under short circuit conditions is quite difficult as it

involves length, area of cross section and voltage of the arc which

vary with time and the circuit conditions and are not precisely

determinable. A limited amount of work has been done in this field and

is reviewed below. It showed that the fuse arc behaviour could be

represented by a static characteristic. Some work has also been done

generally in high power constricted arcs and in particular the wall

stabilised cylindrical arc. This is considered to give an insight into

the more complex phenomena prevailing in the fuse arc and hence is also

included in the review.

(a) Kroemer (2) used the same experimental arrangement as that described

in Section 2.1(a) to examine the variation of arc voltage with arc

current. For a certain value of arc current (which was kept constant

for the test), the arc voltage of a fixed length of arc as monitored by

a particular probe was obtained. This procedure was repeated for

different arc currents and graphs of arc voltage vs arc current drawn

for a number of different current sizes as shown in Fig.3.1.

From the graphs one could observe a large gradient of 4 ohm/4.8 cm

approximately as the arc current increased from low values up to about

100 A and then the gradient decreased to 0.4 ohm/4.8 cm. There had

39

FROM KROEMER'S STUDIES
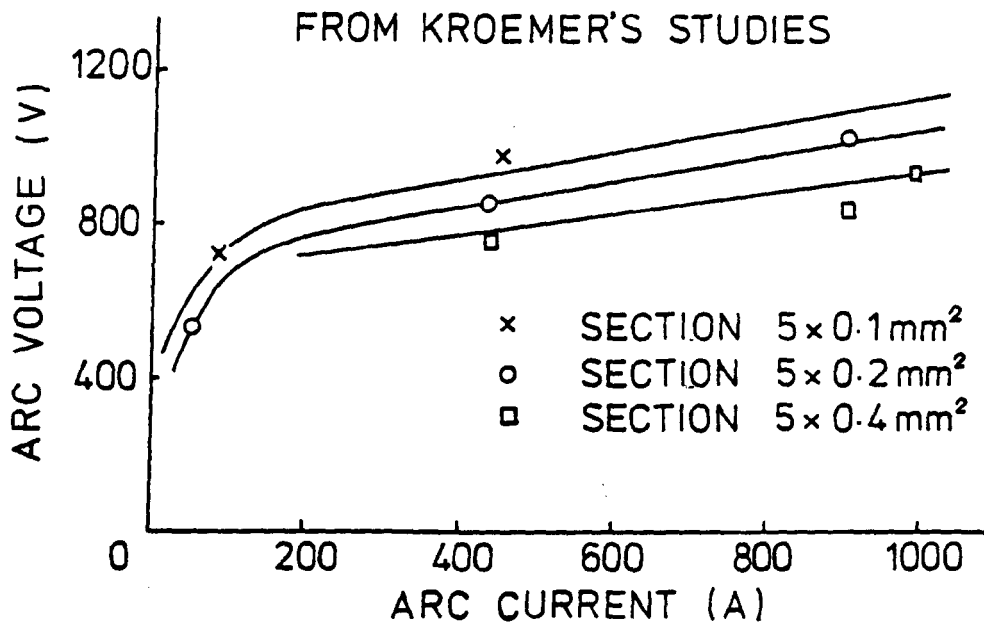
FIG. 3.1. ARC VOLTAGE vs ARC CURRENT
ARC LENGTH : 4·8 cm

FROM HUHN'S STUDIES
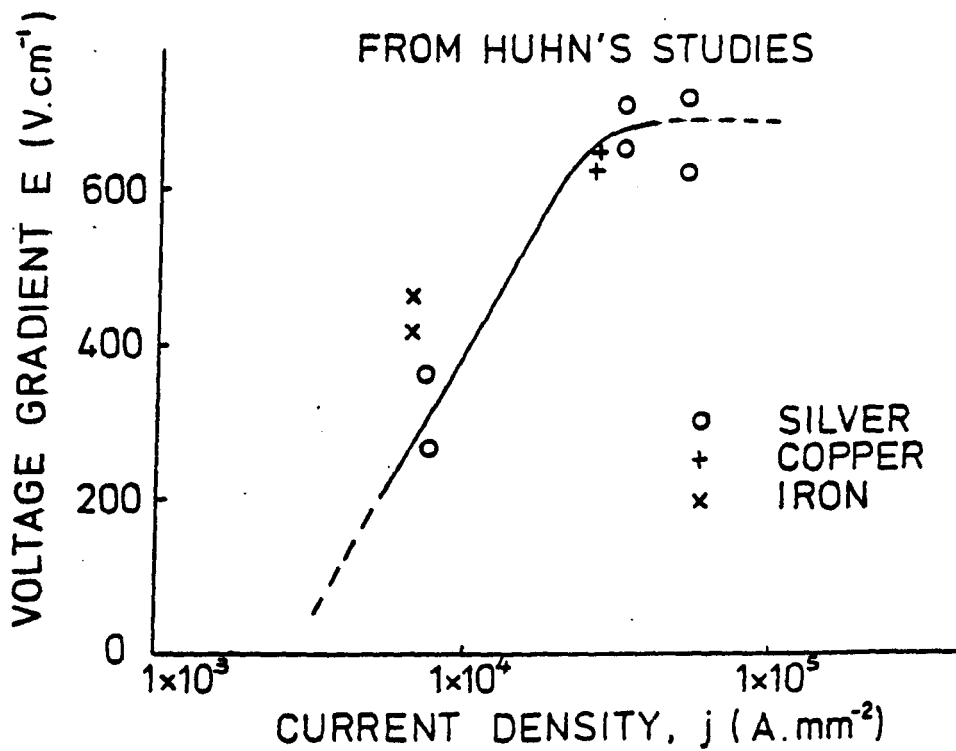
FIG. 3.2. VOLTAGE GRADIENT vs
CURRENT DENSITY

been some scatter in the experimental points away from the graph drawn. However the shape of the graph indicates that the arc voltage could be a function of arc current to a power between zero and one.

(b) Huhn (16) examined the behaviour of exploding wires in a granular medium and showed experimentally that the voltage gradient E increased with current density j as shown in Fig.3.2. He used wires of various metals including silver, copper, iron and tungsten, and quartz sand of average granular diameter 0.2 to 0.3mm as filler. There is a considerable scatter in the experimental points with respect to the graph drawn. However no theoretical analysis was given to substantiate the shape of the graph.

The fuse element was 175mm long and there was multiple arcing when the element fused. There could have been errors introduced in the determination of E because of multiple arcing.

Copper behaved similar to silver and iron gave higher values of E. However the scatter in the experimental points is so high for the various materials considered that the difference between their characteristics do not fit a definite trend.

(c) Onuphrienko (11) based on some experimental and theoretical studies that he made of the arcing process in sand filled fuses showed that the voltage gradient E increased linearly with j as follows:

$$E = C_1 j + C_2 \quad (V.cm^{-1}) \qquad\qquad (3.1)$$

where $C_1 = 3.75 \times 10^{-1}$

$C_2 = 200$

j = current density in the element in $A.mm^{-2}$

The maximum value of the current density covered in the experimental study appears to be about 3500 $A.mm^{-2}$. The graph of E vs j is shown in Fig.3.3.

However he concluded that refinements may be necessary to the above expression for E which therefore required further studies to be made. The element used is also shown in the same figure.

(d) Danders (6) examined the variation of arc voltage with current density j in a wide range of fuses with silver fuse elements and having rated voltages from 600 to 1000 volts and rated currents from 80 to 630 A.

As indicated in Section 2.1(b), Danders assumed that the rate of burnback is proportional to the current density j. The following relationship was therefore obtained for the arc voltage $U_{arc}(t)$:

$$U_{arc}(t) = n_s (U_a + U_k) + n_s E (j) \{x_0 + \int_o^t \alpha.j.dt\}(V) \qquad (3.2)$$

where E (j) = gradient of arc column

$\alpha = \dfrac{U_x}{V_{Ag}}$ $(mm^3.A^{-1}.s^{-1})$

= specific burn off rate

U_x = total voltage which when multiplied by the

41

THICKNESS
0.2 - 1 mm

16 mm
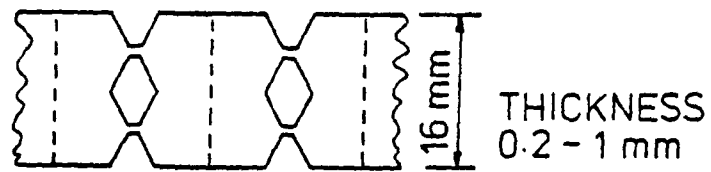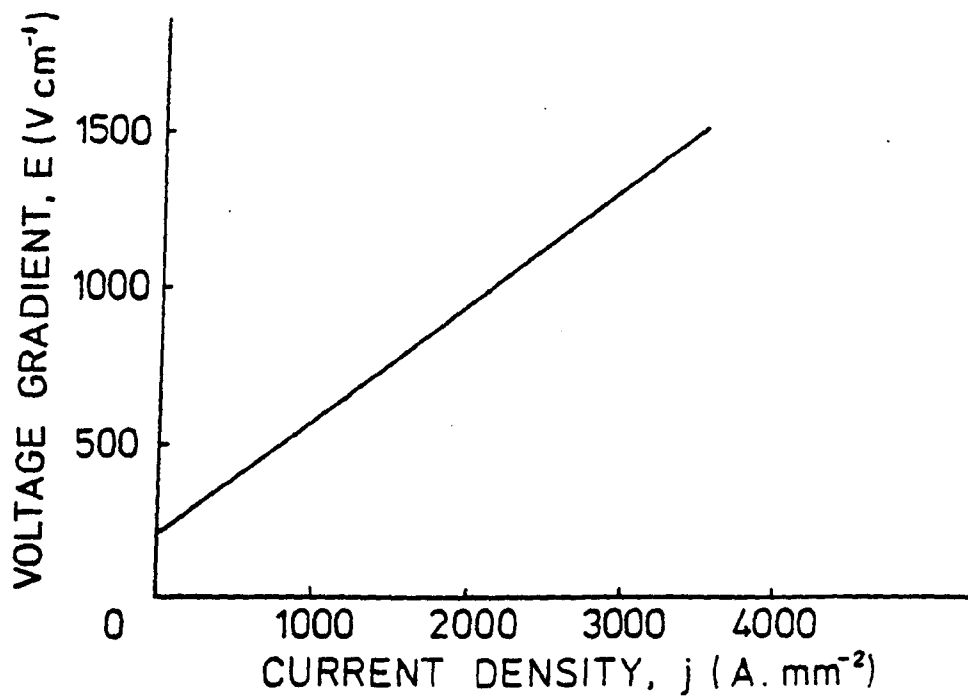
FUSE ELEMENT

FIG. 3.3. VOLTAGE GRADIENT vs
CURRENT DENSITY

FROM DANDERS'S STUDIES

FUSE ELEMENT
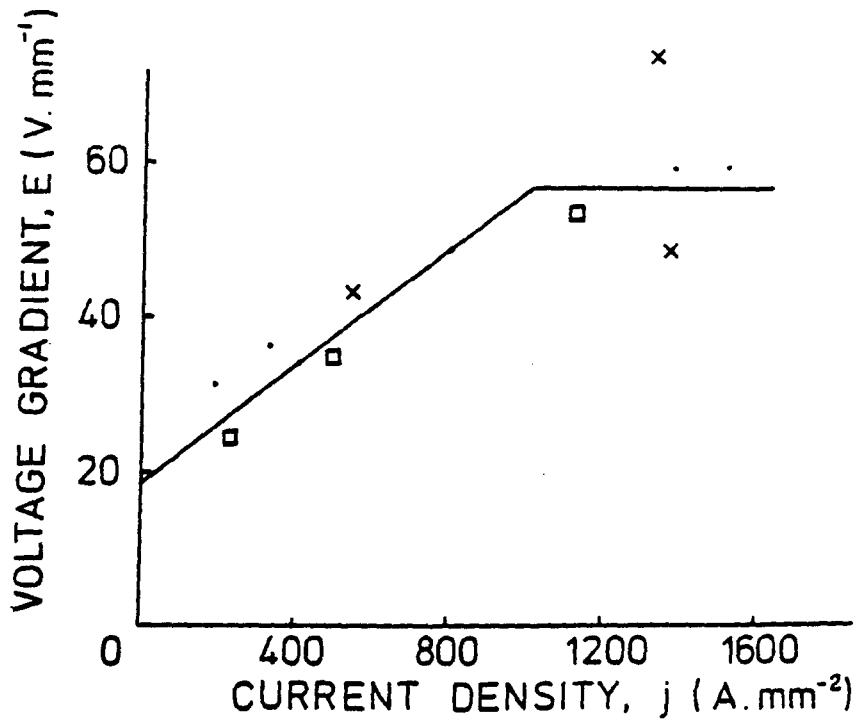
FIG. 3. 4. VOLTAGE GRADIENT vs
CURRENT DENSITY (CASE 1)

current density gave the anode and cathode loss energy per unit area

V_{Ag} = the heat energy required for melting, raising the temperature of the smelt to Boiling Point and evaporating unit volume of silver $(J.mm^{-3})$

j = instantaneous value of current density in the element

= i/s $(A.mm^{-2})$

$U_{arc}(t)$ and j were obtained from the oscillograms taken during arcing of the fuse voltage and current. As for U_B, he used an expression based on Dolegowski's work (9):

$$U_B = U_a + U_k$$
$$= 20 + \kappa \ (i(t)^{.39}) \qquad (V) \qquad\qquad (3.3)$$

κ was 1.5 in Dolegowski's work; but Danders considered two cases separately:

Case I   : $\kappa = 0$

Case II : $\kappa = 1.5$

Certain assumptions were made for the parameters involved in the expression for U_x and using a computer programme, Eqns (3.2), (3.3) were solved to determine $E(j)$ for various values of j. Both cases gave similar results:

Case I : In the range $0 \leqslant j \leqslant 1000$ A.mm^{-2}

$$E(j) = 18.75 + 3.78 \times 10^{-2}j \quad (V.mm^{-1}) \qquad (3.4)$$

with a mean deviation of $m = \pm 3.9$ $(V.mm^{-1})$

In the range $1000 \leqslant j \leqslant 1600$ A.mm^{-2}

$$E(j) = 56.6 \quad V.mm^{-1} \qquad (3.5)$$

with a mean deviation of $m = \pm 7.2$ V.mm^{-1}

Case II : In the range $0 \leqslant j \leqslant 1600$ A.mm^{-2}

$$E(j) = 25.0 + 1.87 \times 10^{-2}j \quad (V.mm^{-1}) \qquad (3.6)$$

with a mean deviation of $m = \pm 5.9$ V.mm^{-1}

Danders preferred the results obtained from Case I and the corresponding E (j) vs j graph is shown in Fig.3.4. The type of fuse element used is also shown in the same figure.

(e) Maecker (17) analysed thermal plasma and its application to observed phenomena extensively. He considered a cylindrical arc with a fixed wall temperature. Assuming that the energy supplied by the electric current to unit volume of the plasma is balanced by a divergence of the heat flow, he arrived at the Elenbaas Heller form of the energy balance:

$$\sigma E^2 + \frac{1}{r} \frac{d}{dr} \left(r K \frac{dT}{dr} \right) = 0 \qquad (3.7)$$

where   K = thermal conductivity,

T = temperature at radius r, of the plasma

Solution of Eqn (3.7) gives the temperature distribution in the plasma with the field strength, $\sigma(T)$ and $K(T)$ as parameters.

The current i is given by: $\quad i = 2\pi E \int_{0}^{R} \sigma \, r \, dr \qquad (3.8)$

43

where R = radius of plasma column

to be drawn

It enables a plot of E vs $\frac{i}{A}$ and this characteristic shows that at low

currents E (i) has a tendency to fall with increasing i due to the

rapid increase of the degree of ionisation with temperature and partly

due to the expansion of the conducting diameter. At the higher

currents the characteristic passes a minimum and increases again

because the ionisation is nearly completed and the tube is almost

filled with conducting plasma.

Maecker showed that the solution of Eqn (3.7) was simplified by

replacing T by the 'heat flow potential'

$$S = \int_0^T K(T)dt \qquad (3.9)$$

i.e.   dS = K dT.

σ and K were considered as functions of S rather than of T.

The following relationships were assumed for fully ionised gas (i.e.

very high currents):

$$\sigma \propto T^{3/2}$$

$$K \propto T^{5/2}$$

$$S \propto T^{7/2}$$

$$\sigma \propto S^{3/7}$$

$$K \propto S^{5/7}$$

Eqns (3.7) and (3.8) were solved using the above relationships and the following solution obtained for high currents:

$$E \propto i^{4/10} \tag{3.10}$$

The graph of E vs i for a monatomic gas at atmospheric pressure as calculated is given in Fig.3.5.

(f) Fraser (18) conducted experiments using sealed glass (Pyrex 7740) capillaries of 100 to 600 microns diameter ($-$ 1 micron $= 1\mu m$) with tungsten electrodes sealed into the ends. An exponentially decaying discharge current waveform was employed and tests were performed over a range of time constants of the order 80 to 500 μ sec.

E vs j characteristics of such discharges are given in Fig.3.6, from which it may be noted that the initial conditions of all the discharges lie close to a common characteristic of the form:

$$E = K j^{0.4} \tag{3.11}$$

where K = a constant

and it holds until the current decreases to approximately 0.2 kA.mm^{-2}.

Fraser also obtained estimates of the temperature of the channel as a function of time and showed that the magnitude of the heat storage term ρC_p (dT/dt) was generally less than 1 per cent of the instantaneous power input to the discharge.

(g) Wheeler (19) analysed theoretically a high power constricted plasma

FROM MAECKER'S STUDIES

VOLTAGE GRADIENT, E (V.cm⁻¹)

ARC CURRENT i (A)
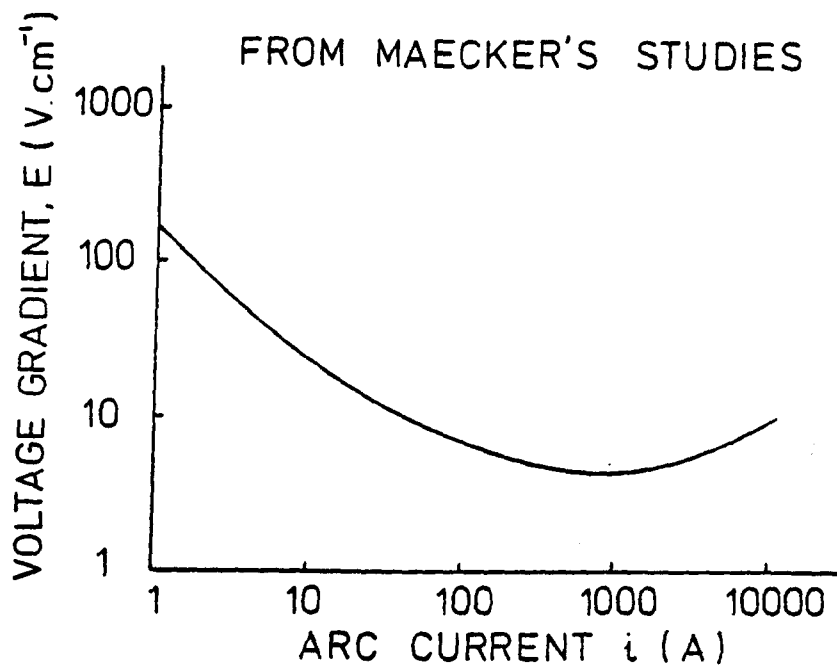
FIG. 3. 5. VOLTAGE GRADIENT vs CURRENT
FOR MONATOMIC GAS AT
ATMOSPHERIC PRESSURE

FROM FRASER'S STUDIES

VOLTAGE GRADIENT, E (V.cm⁻¹)

10^3

2/400   2/100

4/600

10^2

$E = kj^{0.4}$

10^1 10^2 10^3 10^4 10^5 10^6

CURRENT DENSITY, j (A.cm⁻²)
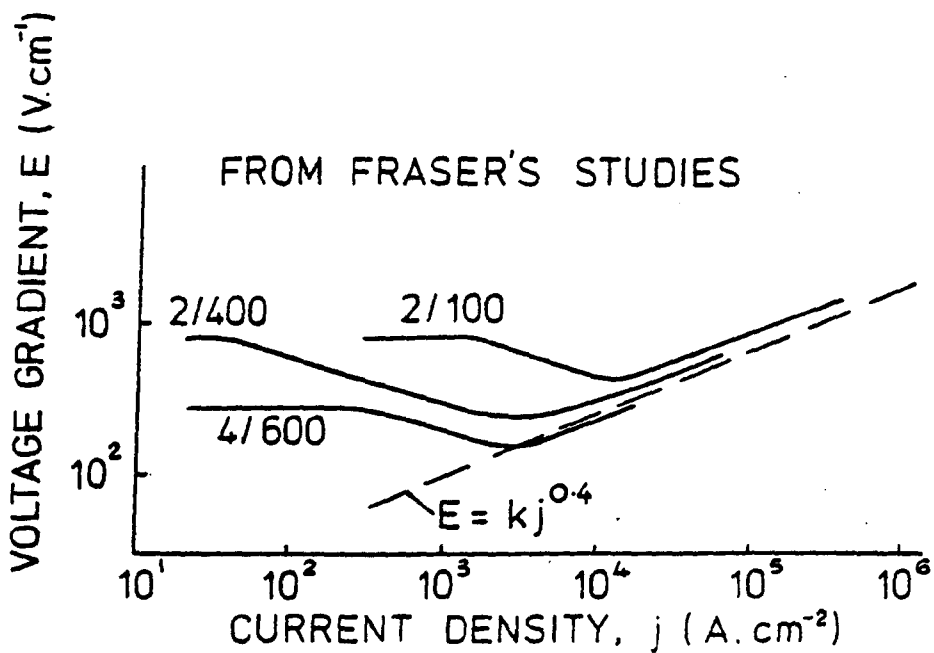
FIG. 3. 6. E - J CHARACTERISTICS OF
TRANSIENT ARCS IN CAPILLARIES
T=190 μs   2/100 INDICATES TUBE LENGTH = 2cm
TUBE BORE = 100 × 10⁻⁶ m

discharge column (cylindrical), assuming that such plasma behaved as a Lorentz gas i.e. a plasma in which the ions are infinitely massive. For a Lorentz gas the thermal and electrical conductivities at a temperature T are given by:

$$K = K_0 T^{5/2} \tag{3.12}$$

$$G = G_0 T^{3/2} \tag{3.13}$$

where $K_0 = \dfrac{7.81 \times 10^{-12}}{Z \ln \Lambda}$ $(Js^{-1}K^{-1}cm^{-1})$

and $G_0 = \dfrac{2.63 \times 10^{-4}}{Z \ln \Lambda}$ $(\Omega^{-1}cm^{-1})$,

are considered very weak functions of temperature T, electron density N- and the charge Z of the ions present in the plasma and hence as an approximation were assumed constant.

Λ = Coulomb cut off

Maecker (17) also assumed expressions for K and G similar to the above, in his analysis.

Energy losses by radiation were not considered and the storage energy component was neglected. The energy balance between the electrical power generation and the power lost by thermal conduction can be put in the general form:

$$- \text{div} (K \text{ grad } T) = GE^2 \tag{3.14}$$

For a cylindrical plasma column it reduces to:

$$-\frac{1}{r} \frac{d}{dr} \left(r K \frac{dT}{dr} \right) = GE^2 \qquad (3.15)$$

Eqns (3.12), (3.13) and (3.15) were solved using suitable transformations and the following solutions obtained:

$$T(o) = 5.04 \times 10^3 \ RE \qquad (3.16)$$

$T(o)$ was the temperature at $r = o$

$$T(o)^{5/2} = 9.00 \times 10^6 \ Z(1n\Lambda)R^{-1}i \qquad (3.17)$$

where i = plasma current (A)

The temperature profile was also obtained and shown to be flat in the vicinity of the axis. For example

$$T(r) > 0.9 \ T(o) \ for \ r < 0.5R.$$

Elimination of $T(o)$ between Eqns (3.16) and (3.17) gave:

$$E = 0.120 \ (Z1n\Lambda)^{2/5} \ R^{-7/5} \ i^{2/5} \qquad (3.18)$$

This Eqn showed :

$$E \ \alpha \ \frac{i^{0.4}}{A^{0.7}} \qquad (3.19)$$

where $A = \pi R^2$

= area of cross section of the plasma column (cm^2)

Wheeler [20] carried out measurements of the electrical parameters of

high current discharge in capillaries and compared the results with the theoretical studies made by him in (19). There was very good agreement between the theoretical analysis and experimental results and he confirmed :

$$E \; \alpha \; i^{0.4}$$

(h) Tslaf (34) carried out investigations on the variations of the current density j and mean temperature T of an electric arc in a narrow insulating channel.

He assumed that the electrical conductivity σ was a linear function of the temperature and the voltage gradient was independent of the current and showed that the current density can be put in the form:

$$j \; = \; K \, \frac{i^{0.5}}{\delta^{0.75}} \qquad\qquad (3.20)$$

where i = arc current (A)

δ = channel width or arc thickness

K = a constant

Based on work by Kukekov (32) Tslaf showed that the voltage gradient is a function of δ:

$$E \; = \; 190 \, / \, \sqrt{\delta} \qquad (V.m^{-1}) \qquad\qquad (3.21)$$

He considered the energy balance equation of a long static arc:

$$\sigma E^2 = -\lambda \frac{\partial^2 T}{\partial x^2} \tag{3.22}$$

where λ = thermal conductivity of the arc

x = distance in the direction of the arc movement

Solving Eqn (3.22), he showed:

$$T = 5800 + 36 \frac{i^{0.5}}{\delta^{0.25}} \tag{3.23}$$

The mean temperature can be seen to increase with rise in current and with the reduction of the arc thickness, and has been estimated in the range of 12,000 - 10,000°K for a thickness 1 - 4 mm.

From Eqns (3.20) and (3.21)

$$\sigma = \frac{j}{E}$$

$$= \frac{K}{190} \frac{i^{0.5}}{\delta^{0.25}}$$

$$= 25 \ i^{0.5}/\delta^{0.25} \tag{3.24}$$

(i) Dynamic Arc Model

Thy dynamic arc model of Cassie or Mayr can be briefly put in the following form:

$$G = \frac{1}{R}$$

$$= f(Q) \tag{3.25}$$

$$R \frac{d}{dt} \left(\frac{1}{R}\right) = \frac{d}{dt} \left(\ln \frac{1}{R}\right)$$

$$= \frac{f'(Q)}{f(Q)} (W - N) \tag{3.26}$$

where G = conductance,

          R = arc resistance,

          W = E i

              = electric power input,

          N = power dissipation

                (due to all causes),

          Q = energy content,

                per unit length of the arc

The dynamic arc model is particularly useful for circuit breaker arcs wherein the thermal energy and time constant (of the order of a few µs (47))are comparatively high. The behaviour of the circuit breaker arcs during the current zero period has been analysed by various workers in some details (48), (49), (50), (51), (52). Some referred to the time constant of these arcs in the mathematical sense, i.e. the time required for the arc conductance to fall by $\frac{1}{e}$; others interpreted it as the time between the passage of the current through zero and the conductance of the circuit breaker becoming substantially zero. Time constant was considered to vary with time throughout the zero period with the magnitude of the current being interrupted and with the wave shape of the early part of the transient recovery voltage (53). The time constant of the arc is comparable with the current zero period in which the arc behaviour is analysed to determine variation of arc parameters such as conductance, etc.

It is shown in Section 3.4.5 that the internal energy of the fuse arc is a small per cent of the total column input energy and that the time constant is very small (- fraction of a μs). Any change in the power input to the arc will result in an equal change in the power dissipation immediately as the time constant is small.

Unlike in the case of the circuit breaker arc during the zero period, the time constant of the fuse arc is very small compared to the total arcing period considered in the study (approximately 2 - 6 ms) so that its dynamic behaviour will be minimal. The dynamic arc model of Eqn (3.26) is therefore considered unnecessary for simulating fuse arc behaviour.

However when the arcing period is too low (- say a fraction of a ms) as to be of the same order as the time constant of the arc, it could be shown that the internal energy of the lumen would be comparatively high and that the dynamic behaviour of the arc becomes important.

Summary

From the various static models enumerated above, it could be seen that the voltage gradient of the arc column, E increased with the instantaneous value of the current, i for high currents.

The findings of Danders (6) and Onuphrienko (11) are similar in that both showed that E increased linearly with j (or i) as in Figs.3.3 and 3.4. The values of E are approximately the same up to $j = 1 \text{ kA.mm}^{-2}$. However there was a substantial scatter in the experimental points of Danders. Danders obtained the values of E(j) from Eqn (3.2) using a

computer program. But Eqn (3.2) was time dependent and hence E would have been governed by the circuit conditions as well e.g. power input to the arc, cross section of lumen,[*] etc. Factors such as area of lumen section have not been accounted for in the computations and hence the empirical relationship between E and j as determined in the studies may not be accurate. Onuphrienko has used a V - type of taper from shoulder to neck in his elements which could cause inaccuracies in the measurements of burnback, E, etc. It is not clear how E was obtained experimentally.

Maecker (17) analysed a cylindrical arc with fixed wall temperature and showed for a fully ionised gas:

$$E \alpha \ i^{0.4}$$

Fraser (18) experimentally showed for exponentially decaying currents (- high currents) in capillary tubes:

$$E \alpha \ j^{0.4}$$

Wheeler (19), (20) showed theoretically and verified experimentally for a high-power constricted cylindrical plasma discharge:

$$E \alpha \ \frac{i^{0.4}}{A^{0.7}}$$

Tslaf (34) analysed the electric arc in a narrow insulating channel and showed:

* Lumen is the arc canal.

52

$$E \; \alpha \; \frac{1}{\sqrt{\delta}}$$

i.e. $E \; \alpha \; \frac{1}{A^{0.5}}$ if unit width of arc is considered

One of his assumptions that E is independent of current is questionable in the light of work by most other previous workers, which might explain the contrast between his model for E and the other models considered.

The dynamic arc model has been shown to be unnecessary for fuse arc simulation in (i) above and a 'static model' is therefore considered for E vs i. However the model would have to be 'quasi-dynamic' as it should accommodate variations of the arc characteristics caused by arc elongation due to burnback and increase of lumen section, during the arcing process.

The findings of Maecker, Fraser and Wheeler as above could appropriately be applied to the arcing process in current limiting fuses operating under short-circuit conditions. The present study is for arcs in these fuses with notched silver elements (rectangular section). Hence the theoretical study made by these workers particularly that of Wheeler who brought out the effect of the area of arc section, has to be modified to take account of the shape of arc section - this is done in Section 3.2.3. At the same time a more accurate experimental determination of E is necessary so that its relationship with variables like i and its control by circuit conditions can be established. Voltage gradient involves column voltage and column length. Inaccuracies may be minimised by choosing one of these variables fixed in the experimental procedure. Accordingly the length of the arc was fixed at 1 cm and voltage gradient

computed from the voltage measurements as in Section 3.4.

3.2   Voltage Gradient of Plasma Discharge Columns

3.2.1 Cylindrical Column

In Section 3.1, based on Wheeler's work (19), it is pointed out that the voltage gradient of a high power constricted plasma discharge column could be put into the form:

$$E = 0.120 \ (Z \ln \Lambda)^{2/5} \ R^{-7/5} \ i^{2/5} \qquad (V.cm^{-1})$$

Area of section of plasma, $A = \pi R^2$, so that the above expression becomes

$$E = 0.267 \ (Z \ln \Lambda)^{2/5} \ (\frac{i^{0.4}}{A^{0.7}}) \qquad (V.cm^{-1}) \tag{3.27}$$

where   Z = charge of the ions present in the plasma

   Λ = Coulomb cut off

3.2.2 Thin Column of Rectangular Section

If we consider unit width of a column of rectangular section having thickness 2R and infinite width and solve the equation expressing energy balance between Joule heating and thermal conduction, assuming that the plasma behaves as Lorenz gas as in Appendix 3.1, we get:

$$E = a_1 \ (Z \ln \Lambda)^{2/5} \ R^{-1} \ i^{2/5} \qquad (V.cm^{-1}) \tag{3.28}$$

where $a_1 \simeq 0.109$

If A is the area of unit width of the column, then A = 2R and Eqn (3.28) becomes:

55

$$E = 2a_1(Zln\Lambda)^{2/5} \ (\frac{i^{0.4}}{A}) \qquad (V.cm^{-1}) \qquad (3.29)$$

The expressions for the voltage gradient in the above two cases are similar except that (i) in the cylindrical column $E \propto \frac{1}{A^{.7}}$

whilst, (ii) in the thin infinitely wide column $E \propto \frac{1}{A}$.

A in the latter case is area of unit width of section.

3.2.3 Fuse Arc Column

From the foregoing, we would expect the voltage gradient of the fuse arc column to be a function of the shape of the lumen section amongst other variables. The shape of the section is complex but the factors that govern it can be looked into, with a view to determining its trend. Mean grain size of quartz, its compactness and packing density, shape of the element section and pinch pressure due to current flow are some of the factors involved.

Pinch pressure which varies with the direction in general is analysed for different discrete sections below:

(a) The pinch pressure in a cylindrical column is uniform all round (and radially inwards) (24)

$$P_r = i \ j \times 10^{-7} \qquad (N.m^{-2})$$

where i = current (A)

j = current density $(A.m^{-2})$

as shown in Fig.3.7(a).

(b) The pinch pressure in a column of rectangular section is variable

(a) CIRCULAR SECTION

$$P_r = i\,j \times 10^{-7}\ \mathrm{N.m^{-2}}$$

(b) RECTANGULAR SECTION

$a > b$

$P_R > P_x > P_y$

EXPRESSIONS FOR THESE ARE GIVEN IN APPENDIX 3.2.
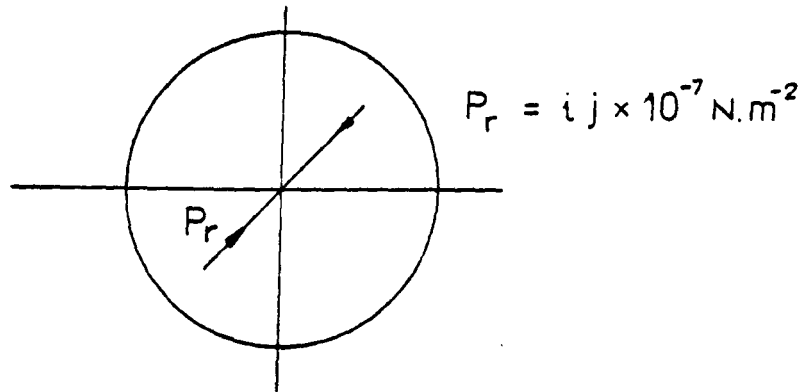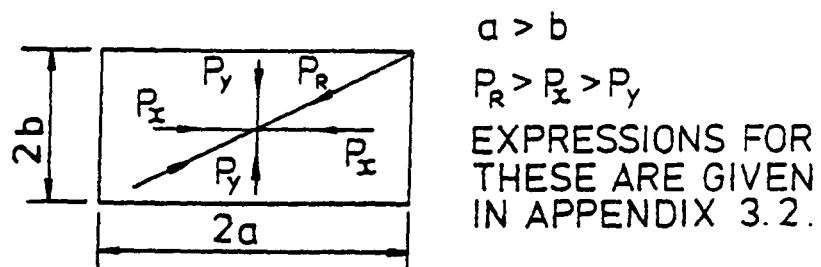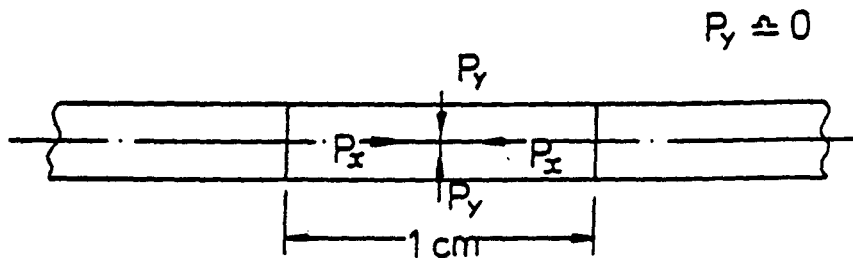
(c) THIN RECTANGULAR SECTION

$P_y \simeq 0$

FIG. 3.7. PINCH PRESSURE IN COLUMNS OF VARIOUS SECTIONS

and depends on the direction with respect to one of the axes.

P_x is greater than P_y and

P_y is the minimum,

as shown in Fig.3.7(b).

Expressions for P_x, P_y and P_d (along the diagonal directions) are given in Appendix 3.2.

(c) The pinch pressure in a thin column of rectangular section column (with infinite width) is mainly along the X axis and negligible along the Y axis as shown in Fig.3.7(c).

(d) The fuse arc originates from an element of rectangular section having a thickness/width ratio relatively small (~ 0.024 for the $\frac{1}{8}$" x 0.003" element). From (b) above, it could be seen that the pinch pressure along a direction parallel to the width is larger than that in the perpendicular direction. The arc pressure is the same in all directions and tends to make the lumen section larger whilst the pinch pressure tends to make the section smaller. During the arcing period, there is expansion of the arc as the arc pressure is generally higher than the pinch pressure. It could therefore be seen that the directional variation of the pinch pressure tends to make the thickness/width of the lumen section larger and the section itself more or less elliptical during the arcing period.

The behaviour of the fuse arc may therefore be considered as that of an arc between a cylindrical type and a thin rectangular type. Hence from Eqns (3.27) and (3.29), taking the mean of the indices of A

57

and of the coefficients, we could write the following for the fuse arc:

$$E = a_2 \ (Z\ln\Lambda)^{2/5} \ (\frac{i^{0.4}}{A^{0.85}}) \qquad (V.cm^{-1}) \qquad\qquad (3.30)$$

where $a_2 \simeq 0.242$

Wheeler (20) quoted the following values for Z and $\ln\Lambda$ from his experimental investigations of the high power constricted plasma discharge:

$$Z \simeq 2.8$$

$$\ln\Lambda \ : \ 5 \ to \ 10$$

If these values are substituted in Eqn (3.30) it becomes:

$$For \ \ln\Lambda = 5 \ : \ E = 0.695 \ \frac{i^{0.4}}{A^{0.85}} \qquad (V.cm^{-1}) \qquad (3.31(a))$$

$$For \ \ln\Lambda = 10 \ : \ E = 0.918 \ \frac{i^{0.4}}{A^{0.85}} \qquad (V.cm^{-1}) \qquad (3.31(b))$$

The values of the coefficient in the above Eqns reflect the possible order of value of the coefficient. However the correct value of the coefficient should be determined empirically from experimental results, as it depends on the average values of Z, $\ln\Lambda$, etc. which would be only characteristic of the plasma considered.

The models for E of a column having a circular section (Wheeler - Eqn (3.27)), a column having a rectangular section with infinite width (Eqn (3.29)) and the fuse arc column (Eqn (3.30)) are compared in Fig.3.8.

$\beta = 0.267; \quad n = 0.7$
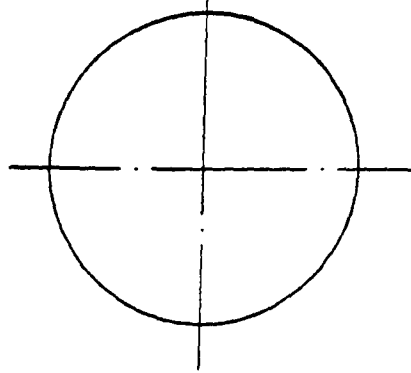
(a) CIRCULAR SECTION

$\beta = 0.218; \quad n = 1.0$
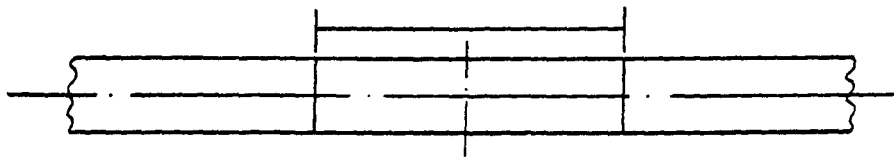
(b) THIN RECTANGULAR SECTION

$\beta = 0.242; \quad n = 0.85$
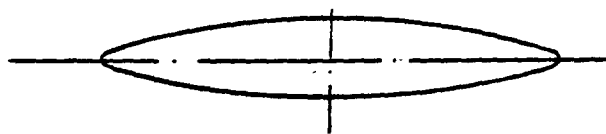
(c) FUSE ARC SECTION (ELLIPTICAL)

$$E = \beta \, (Z \ln \Lambda)^{0.4} \, (i^{0.4}/A^n)$$

FIG. 3. 8. MODELS FOR VOLTAGE GRADIENT
OF COLUMNS OF VARIOUS SECTIONS

The model in Eqn (3.31) requires some modification to accommodate low current conditions since E infact does not reduce to zero when i tends to zero. In Maecker's analysis when the current was reduced below a certain value (1000A), E instead of steadily decreasing began to increase from a minimum value. This part of the characteristic is similar to the Mayr's static model (E i = N) which could be incorporated in the general model for a fuse arc to simulate the increasing trend of E when the current is reduced below a certain value. The general expression for the voltage gradient of a fuse arc then becomes:

$$ E = \gamma \frac{i^{0.4}}{A^{0.85}} + \frac{N}{i} \quad (V.cm^{-1}) \quad (3.32) $$

where γ and N are constants and N should be such that $\frac{N}{i}$ has little effect for relatively high values of current. The $\frac{N}{i}$ component causes a negligible change in the i^2t or energy component of the arc and does not affect the general shape of the characteristics except in the low current range (approaching arc extinction), when it preponderates and changes the gradient of the E vs i characteristics from positive to negative when the current is reduced.

In general there would be a voltage across the fuse at arc extinction due to the source voltage and point on wave switching, which (arc voltage) gives a non zero voltage gradient at zero current. The $\frac{N}{i}$ component is included for computational convenience so that it simulates the required finite arc voltage at the end of the arcing period when the current is small and also helps to provide the necessary transition to the actual voltage appearing near current zero.

The condition i tending to zero in the above equation is not admissible as then E would tend to infinity. Hence the model in Eqn (3.32) is applicable subject to the condition that i takes a certain specified minimum value (say of 1 A).

The model incorporates the variable A, the area of lumen section which also requires some study. The rate of expansion of lumen $\frac{dA}{dt}$ is examined in the next Section.

3.3 Rate of Expansion $(\frac{dA}{dt})$ of Fuse Arc

In a fuse having a single notched silver element, at the end of the pre-arcing period, an arc is struck as the notch disrupts which (arc) then elongates with a rate of burnback given by Eqn (2.9) in Section 2.4.1. At the same time, the arc expands transversely at a certain rate. Analysis of the latter while elongation also is taking place would be complicated. To simplify the study of expansion, a uniform arc of constant length is considered. The theoretical analysis of such an arc is taken up in this Section and the experimental investigation is covered in the next.

The basic model for the one centimetre long fuse arc surrounded by partially melting silica is depicted in Fig.3.9.

Time for the Silica Surface to Reach Melting Point

The incident heat flux, F from the lumen heats the surrounding silica. The time taken from the commencement of the arc to raise the surface temperature of the adjoining silica to its melting point can be determined from the following formula (14):

$$ T = \frac{2F}{K_f} \left(\frac{\alpha_f \ t}{\pi} \right)^{\frac{1}{2}} \qquad (^{\circ}C) $$

where K_f = thermal conductivity,

α_f = thermal diffusivity,

of the filler

t = time taken to raise the surface temperature
to $T^{\circ}C$.
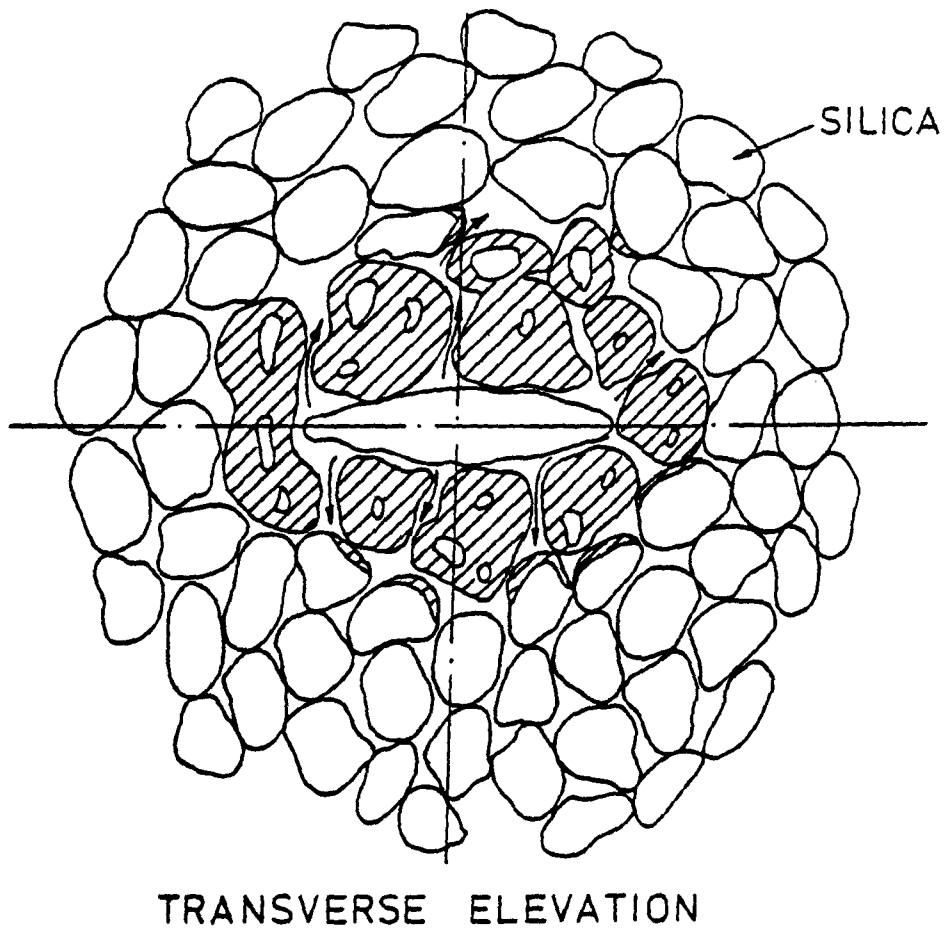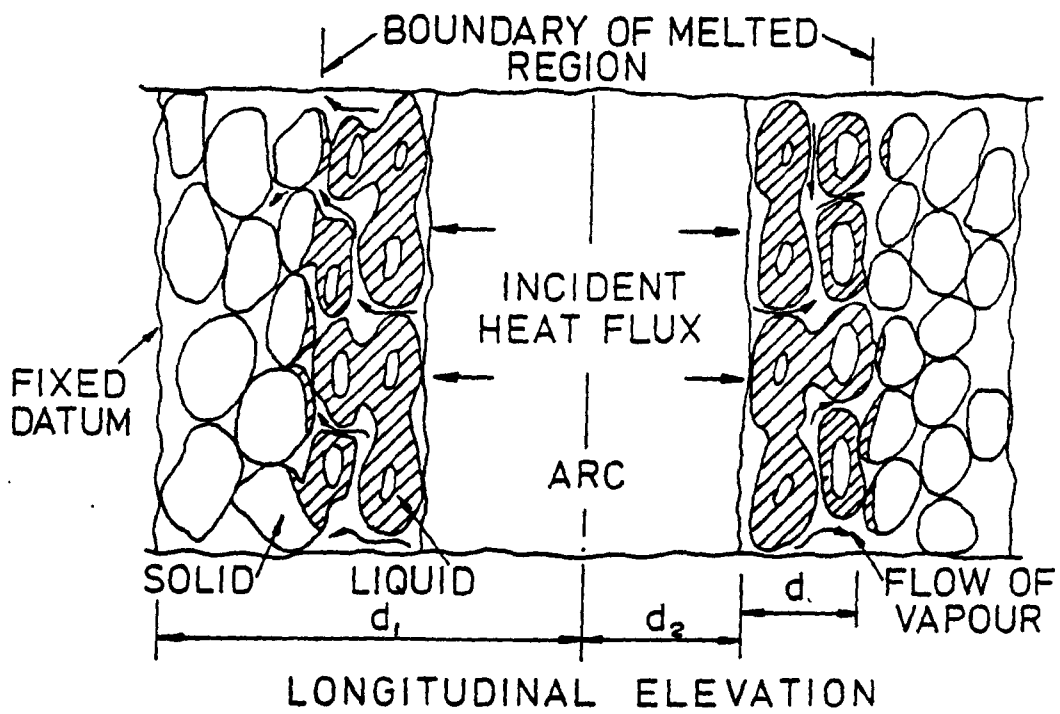
FIG. 3.9. BASIC MODEL FOR CONSTANT
LENGTH FUSE ARC

For a typical element size ($\frac{1}{8}$" x 0.003") and instantaneous value of current of 1000 A and voltage gradient of 300 $V.cm^{-1}$, the time for the silica surface to reach melting point would be approximately 0.1 μs, which is very small.

The time taken for the surface to boil is approximately 0.3 μs. It shows that the time lag involved in the melting or boiling of the silica surface is negligibly small. However there is an appreciable time lag involved for the heat to be conducted to the interior of the silica granules.

At a time t from the commencement of arc, let:

area of lumen section	$= A \ (cm^2)$
column gradient	$= E \ (V.cm^{-1})$
instantaneous value of current	$= i \ (A)$
average thickness of fusion of silica (fulgurite)	$= d \ (cm)$

The incident heat flux from the lumen at an estimated temperature of over $10,000^o$ K (25) produces the following effects:

(i)   boiling off silica vapour from surface layers

(ii)   melting of deeper layers of silica below its surface

(iii)   fusion of silica particles together - reducing the air spaces and thus retreating the fulgurite wall

(iv)   condensation of silica vapour and release of its latent heat of condensation on the surfaces of the particles located in the outer side of the region of fusion

(v)   condensation of silver vapour in the fulgurite thereby

            exchanging its latent heat to the silica.

In an interval δt (in a quasi steady state):

(a) input energy to the column

$$= E \; i \; \delta t \qquad (\text{J.cm}^{-1})$$

(b) assuming a volume of silica δV_1 is melted in each cm

length of arc, energy absorbed by fusion of silica

$$= \rho_f \; (C_f \; \Delta T + L_f) \; \delta V_1$$

$$\simeq 3800 \; \delta V_1 \qquad (\text{J.cm}^{-1})$$

(using standard thermo-physical data as

given in Appendix 1.1)

where ΔT = (Melting Point - ambient termperature) of

the silica

Hence considering energy balance of the arc,

$$E \; i \; \delta t = 3800 \; \delta V_1 + \delta W_s \qquad\qquad (3.33)$$

where δW_s = internal energy of lumen per cm (J.cm^{-1})

The internal energy of the lumen W_s is estimated in the next Section to be a very small per cent of the total column input energy and hence neglected in Eqn (3.33) as a first approximation, so that it can be written as:

$$E \; i \; \delta t = 3800 \; \delta V_1 \qquad\qquad (3.34)$$

Due to melting and fusion of silica, the lumen area will increase by δA and the corresponding increase, in its volume would be $1 \times \delta A = \delta A$ cm³ per cm length of lumen. The increase in the lumen size can therefore be considered to be dependent on the volume of silica melted. If the ratio of the increase in volume of lumen to the volume of silica melted at any instant during arcing is $\alpha(t)$, then:

$$\alpha(t) = \frac{\delta A}{\delta V_1} \qquad (3.35)$$

$\alpha(t)$ is time dependent and would start with a small value (α_1) at the instant of arc initiation and increase with time due to increase in fusion. The structure of α is analysed later in this Section.

Substituting for δV_1 from Eqn (3.35) in Eqn (3.34) and taking limits,

$$\frac{dA}{dt} = \frac{\alpha(t)\ Ei}{3800} \qquad (cm^2.s^{-1}) \qquad (3.36)$$

Maximum value of α

From Eqn (3.35) we would expect $\alpha(t)$ to have a maximum value when maximum melting and fusion of silica take place as in an over current condition.

Let δV be the initial volume per unit length of arc occupied by silica up to the outer barrier of the region of fusion. Due to 'compactness' of the silica, only about 60% would have been occupied by solid silica and the rest by air (5): However the percentage could differ depending on the mean grain size of the silica used and the technique used in packing the silica.

Hence $\qquad \delta V_1 = 0.6 \; \delta V$ $\qquad\qquad\qquad\qquad$ (3.37)

Silica when completely melted increases in volume by 7%. For the case considered assuming the entire volume δV_1 melted and fused, the volume of fused silica would be:

$$\delta V_1 \times 1.07 = 1.07 \; \delta V_1$$

Hence from Eqn (3.37)

$$\text{Volume of fused silica} = (1.07 \times 0.6)\delta V$$
$$= 0.64 \; \delta V \qquad\qquad\qquad (3.38)$$

Thus $\qquad \delta A = \delta V - 0.64 \; \delta V$
$$= 0.36 \; \delta V \qquad\qquad\qquad (3.39)$$

and the maximum value of α will be

$$\alpha_m = \frac{\delta A}{\delta V_1} = 0.6 \qquad\qquad\qquad (3.40)$$

However the correct value of α_m would depend on the actual packing density.

Expression for α

At the commencement of the arc in the fuse α is assumed to have a constant value α_1 which would possibly depend on the size and packing density of silica and the shape of the notch section. Melting and boiling of the silica vapour would initially be confined to the silica in the vicinity of the element. As arcing progressed, the silica vapour

would flow radially outwards to points further away from the axis and melt more of silica. At the same time due to lumen pressure a greater proportion of the melted silica would fuse and occupy the air space. Hence for the same volume of silica melted, the more would be the retreating of the fulgurite inner wall, indicating that lumen area would increase. Thus α would increase with arcing; it is assumed that α has an exponential lag variation with a fixed time constant, τ.

Since the initial value of α is α_1 and the maximum value α_m, the expression for α becomes:

$$\alpha(t) = \alpha_1 + (\alpha_m - \alpha_1)\ (1 - e^{-t/\tau}) \qquad (3.41)$$

Correct values of α_1 τ and α_m (which is of the order of 0.6) were determined from a series of experiments with fuse arc of 1 cm long to give the best 'fit'.

Substituting for α from Eqn (3.41) in Eqn (3.36), the rate of expansion of the lumen section becomes:

$$\frac{dA}{dt} = \{\alpha_1 + (\alpha_m - \alpha_1)(1 - e^{-t/\tau})\}\ \frac{Ei}{3800} \qquad (cm^2.s^{-1}) \qquad (3.42)$$

3.4 Constant Length Fuse Arc Experiments

3.4.1 General

Experiments with constant length fuse arc helped to verify the theory in Sections 3.2 and 3.3, and establish the models for:

(i) voltage gradient for the arc column

(ii) rate of expansion of the arc column.

The same ceramic cartridges as used for the 'burnback' experiments in Chapter II were used for the fuse assembly in this case too to ensure the same conditions. But instead of the notched element, 1 cm long strip silver element had to be used to produce the required 1 cm long arc. Two aluminium attachments specially made for the tests were connected on to the two end discs of the fuse assembly as in Fig.3.10. 1 cm long strip element was clamped to the inner ends of the aluminium attachments which served as thick electrodes for the 1 cm arc produced by passing a fault current through the fuse. The element assembly comprising the element and the two aluminium attachments was introduced into the cartridge centrally and connected to one of the end discs by a screw and soldering arrangement and to the other by soldering. Finally silica was introduced to fill the inner empty space of the cartridge and packed by adopting the same procedure as for the burnback experiments.

3.4.2 Conduct of the Experiment

The same circuit arrangement as in Fig.2.4 was used for these experiments. The test fuses were mounted horizontally in the rig. The auxiliary fuse was removed and the time delay for the chopping of the

SECTION XX

HALF SECTIONAL ELEVATION

QUARTZ

ELEMENT CLAMPED TO ELECTRODE

SECTION YY

SOLDERED

ALUMINIUM ELECTRODE

HALF SECTIONAL PLAN

FULL SCALE DIMENSIONS IN CM
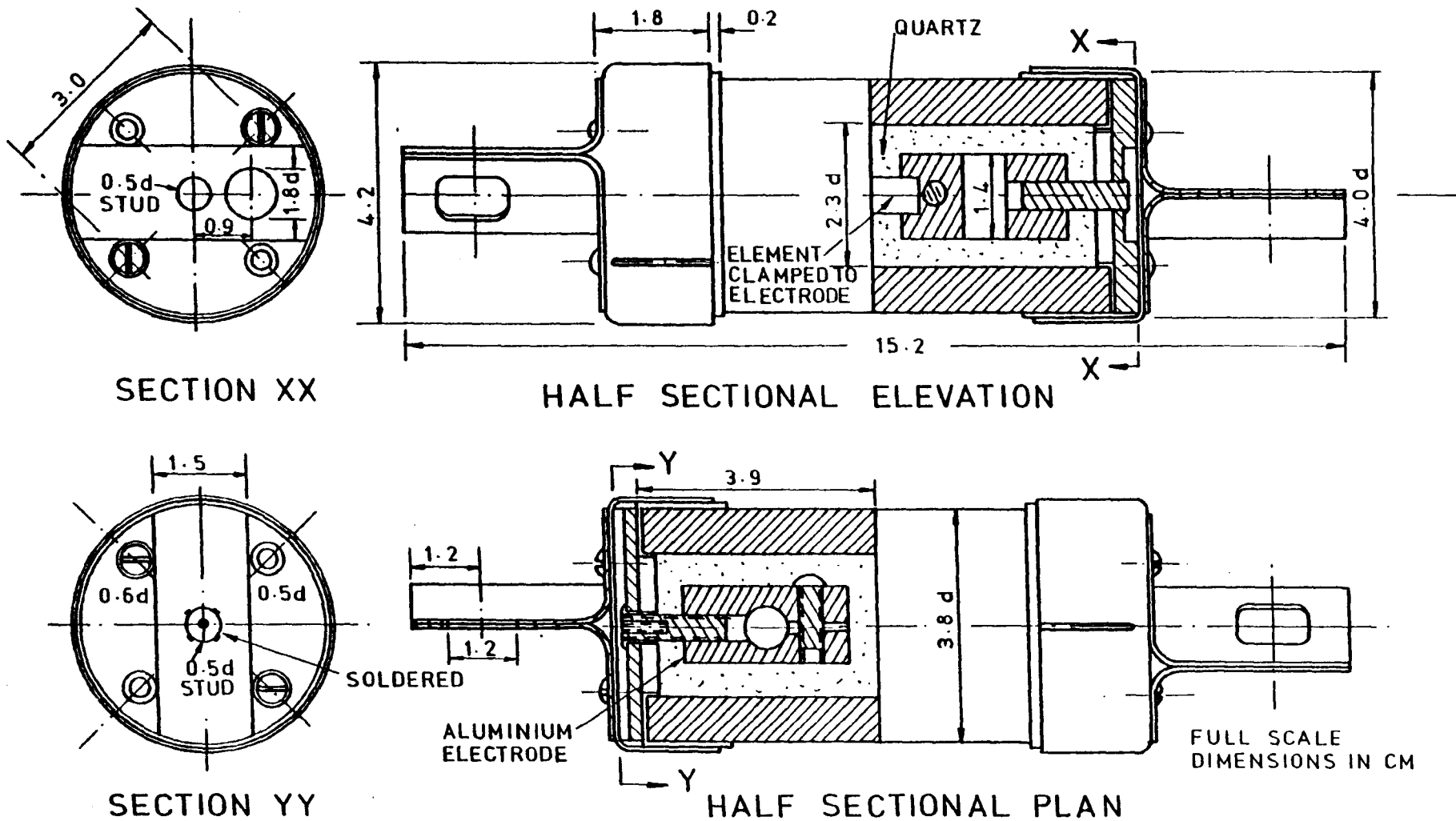
FIG. 3.10. TEST FUSE ASSEMBLY

arc as set on the DC Unit was made relatively large (- around 14 ms), so that the fuse arc was effectively not chopped during the test. An oscillogram of the fuse current and voltage was taken in each test - typical ones are shown in Fig.3.11.

Thirteen tests were carried out in all using the following element sizes and with various prospective currents and fault currents initiated at different points on wave:

$\frac{1}{16}$" x 0.003" (RL1)

$\frac{1}{8}$" x 0.003" (RL2)

$\frac{1}{8}$" x 0.006" (RL2)

$\frac{1}{4}$" x 0.003" (RL4)

3.4.3 Analysis of Results

From the oscillogram taken in each test, the instantaneous values of fuse current i and the fuse voltage V at various times from the commencement of arcing were obtained.

As there were no notches in the element and the current density at the end of the prearcing period would have been possibly more than 1 $kA.mm^{-2}$ (the minimum current density to cause multiple arcing (22)), the arc struck initially was of the multiple arc type. The number of arcs depended on the width of the element and could be estimated (26). The number of arcs estimated agreed with that shown in the X-ray photograph of the fuse taken after the test. A typical X-ray photograph is shown in Fig.3.12. The arcs merged in a relatively short time of 0.1 to 0.2 ms, at the end of which time, a single arc of 1 cm length was formed

(a) ELEMENT   : $\frac{1}{8}$" x 0.003"
     CURRENT SENSITIVITY : 260 A/cm
     VOLTAGE SENSITIVITY : 104 V/cm
     TIME SENSITIVITY   : 2 ms/cm
     PROSPECTIVE CURRENT : 2,040 A
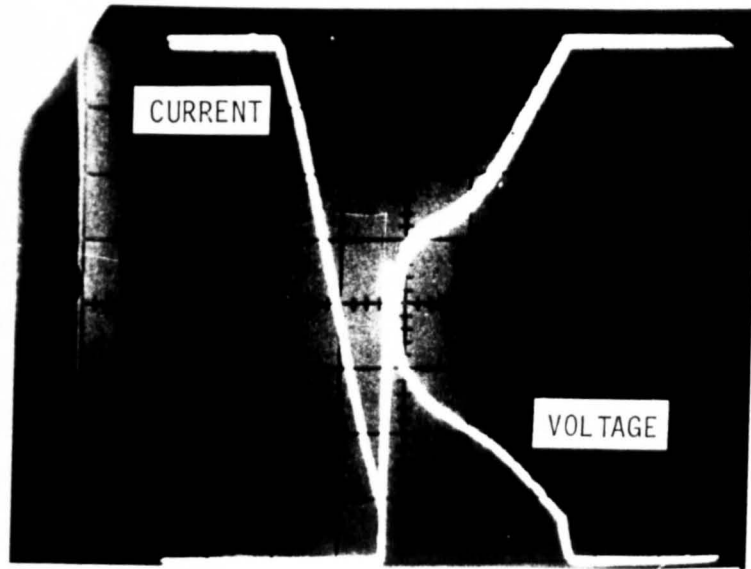
CURRENT

VOLTAGE

(b) ELEMENT   : $\frac{1}{4}$" x 0.003"
     CURRENT SENSITIVITY : 521 A/cm
     VOLTAGE SENSITIVITY : 104 V/cm
     TIME SENSITIVITY   : 1 ms/cm
     PROSPECTIVE CURRENT : 7,700 A.
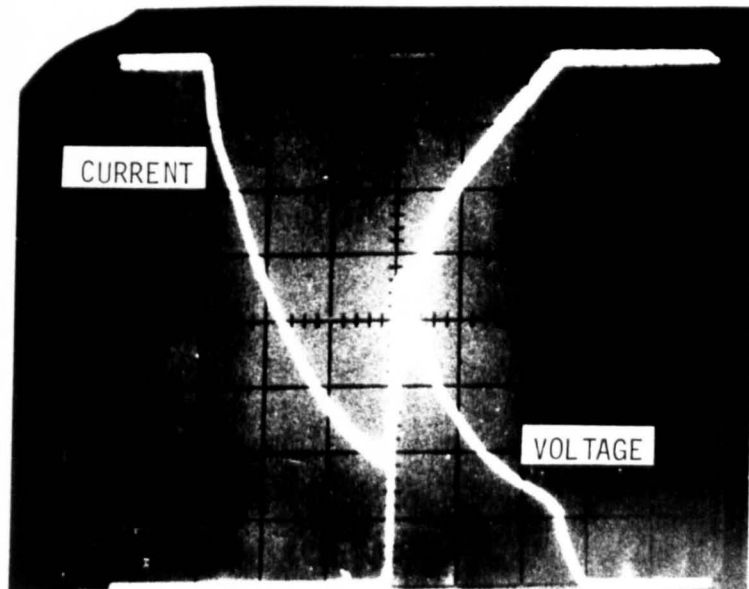
CURRENT

VOLTAGE

FIG.3.11. TYPICAL OSCILLOGRAMS OF CURRENT & VOLTAGE WAVES.

(TESTS WITH 1 CM LONG ARC)

FIG. 3.12. X'RAY PICTURE OF FUSES WITH $\frac{1}{8}'' \times 0.003''$ ELEMENT (1cm LONG ARC) (DIFFERENT PROSPECTIVE CURRENTS USED)
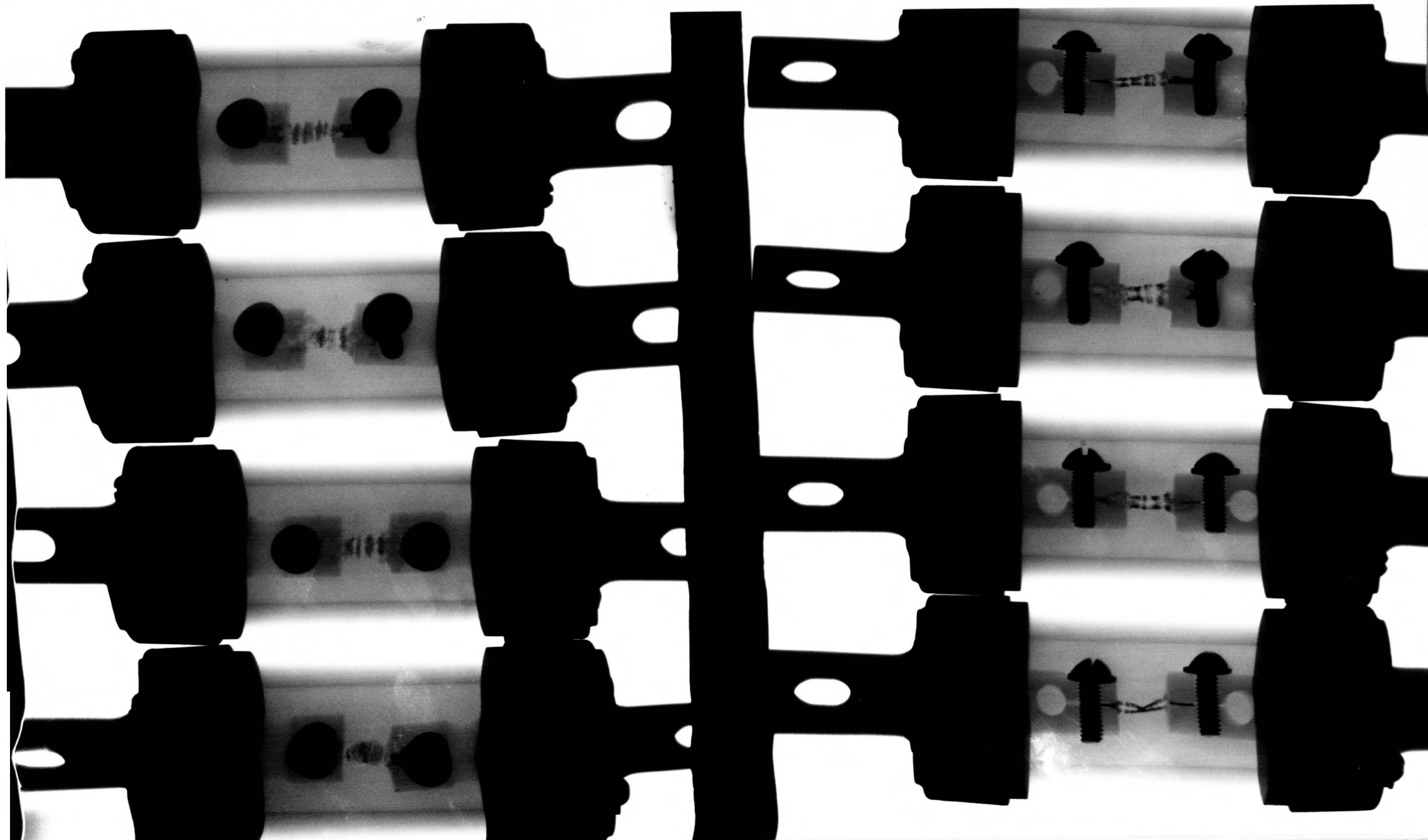
having an average lumen sectional area $A_o{}'$ cm^2.

The area of lumen section increased during the arcing period and the voltage gradient too changed as a result. The voltage gradient was obtained from the experimental results, by subtracting the electrode fall voltage (which was taken constant at 20 V for aluminium) from the fuse voltage, U_{arc} since the arc length was 1 cm.

The appropriate areas of lumen section were estimated by taking measurements of the tunnel of some of the fulgurites in these tests. During the period between the time of the test and the examination of the fulgurite, however, the molten mass could have moved while cooling and solidified into forms different to those existing at the time of the incident. But as solidification was in general quite rapid, the error involved is small. An allowance was given for the reduction in the area of section of the tunnel while estimating the lumen area and obtaining its order.

Instantaneous values of the current and voltage gradient obtained from the oscillogram together with the order of magnitude of the final area of lumen section helped to confirm the structure of the expressions for the voltage gradient E (- Eqn (3.32)) and the rate of expansion of lumen section $\frac{dA}{dt}$ (- Eqn (3.42)) and also to determine the correct values for the coefficients involved in the expressions so as to provide the best 'fit'. For this analysis, Mayr component N/i in the expression for E which was substantial only for low values of current (say less than 10 A) was ignored to simplify the calculations involved. The best 'fit' was as follows:

69

$$E = 0.914 \frac{i^{0.4}}{A^{0.85}} \qquad (V.cm^{-1}) \qquad (3.43)$$

(excluding the Mayr component for the present)

i.e.
$$A = 0.9 \frac{i^{0.47}}{E^{1.18}} \qquad (cm^2) \qquad (3.44)$$

$$\frac{dA}{dt} = \frac{\alpha E i}{3800} \qquad (cm^2.s^{-1}) \qquad (3.45)$$

where $\alpha = 0.08 + 0.55 (1 - e^{-t/10})$ $\qquad (3.46)$

t = time in ms from the commencement of arc.

The coefficient of 0.914 established in Eqn (3.43) above is of the same order as that in the theoretical analysis in Eqn (3.31). α_m established is 0.63 which again is of the same order as estimated (0.6) in Eqn (3.40).

Values of t' (the time from the initiation of fault current), E and i as obtained from the oscillogram (except for the initial value of E corresponding to 1 cm arc at the instant of arc disruption - E_0' which was separately obtained as indicated below), $\frac{dA}{dt}$ as obtained from Eqns (3.45) and (3.46), A_{obs} as obtained from Eqn (3.44) and A_{calc} are scheduled in Appendix 3.3 for each of the tests. A_{obs} gives the observed values and A_{calc}, the calculated values of area of lumen section.

Initially A_{calc} was made equal to A_{obs} corresponding to the instant of

arc disruption and then A_{calc} was assumed to increase discretely at a rate equal to the corresponding calculated value of $\frac{dA}{dt}$:

$$A_{calc} (t' + \Delta t_1) = A_{calc} (t') + \frac{dA}{dt} (t') \times \Delta t_1 \quad (cm^2)$$

Graphs of A_{calc} and A_{obs} against t' for two of the tests are given in Figs.3.13 (a) and (b) which show good correlation.

Voltage gradient E_0' of equivalent 1 cm arc column at the instant of arc disruption

In Eqn (3.46), t is the time from the commencement of arcing, and the model considered for analysis is a fixed length (one cm) arc. In the experiments performed, the fixed length arc was formed after a small but definite interval of time from the instant of (multiple) arcing. Hence to analyse the results of these experiments, it was considered appropriate to determine the 'equivalent' value of the voltage gradient, E_0' at the time of disruption by extrapolation. The procedure is briefly stated below.

The current and voltage waveforms are depicted in Figs.3.14 (a) and (b) respectively.

t' = time from the initiation of fault current

t_1 = prearcing period

t_1' = instant of multiple arcing

t_1'' = instant of arcs merging

For $t' \geqslant t_1''$, $E = (U_{arc} - 20)$ $(V.cm^{-1})$

71

TEST 1.
ELEMENT : $\frac{1}{16}$" × 0.003" (RLI)

Area of lumen section (cm²) plotted against time, t' (ms), ranging from 2 to 8 ms.

—— A_{obs} vs t'
× × A_{calc} vs t'

(a)

TEST 8.
ELEMENT : $\frac{1}{8}$" × 0.003" (RL2)

Area of lumen section (cm²) plotted against time, t' (ms), ranging from 3 to 9 ms.

—— A_{obs} vs t'
× × A_{calc} vs t'

(b)
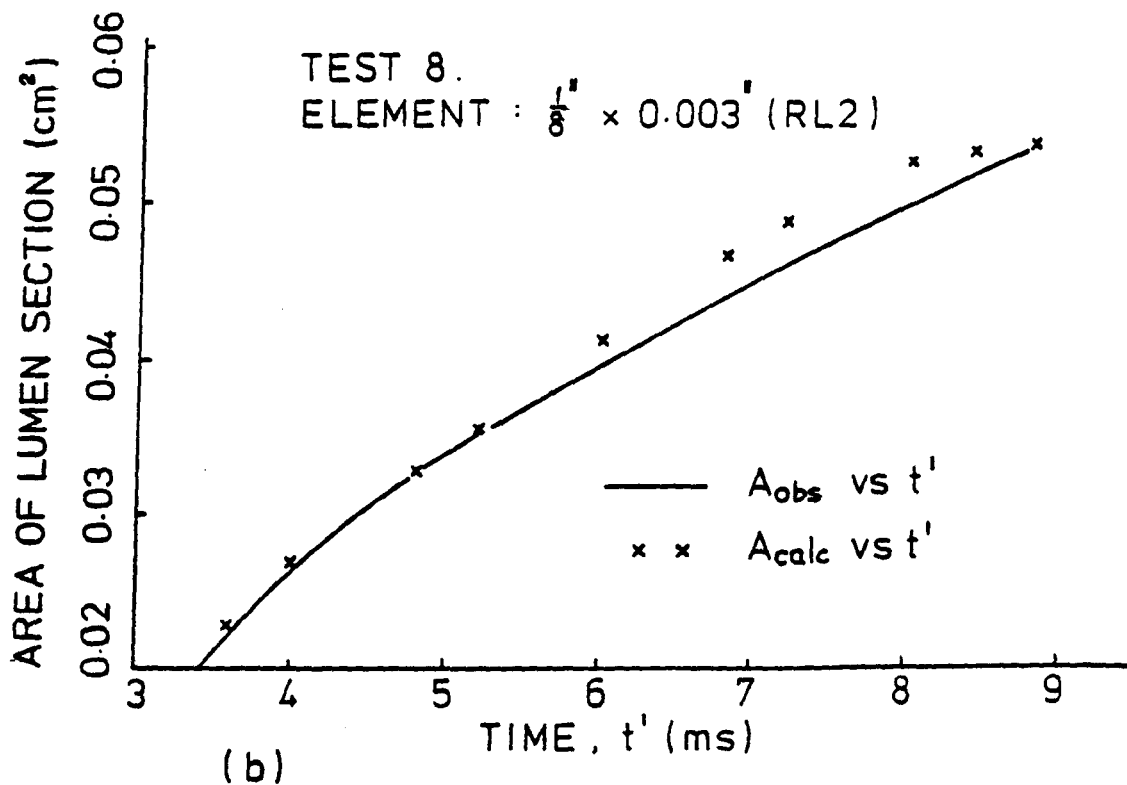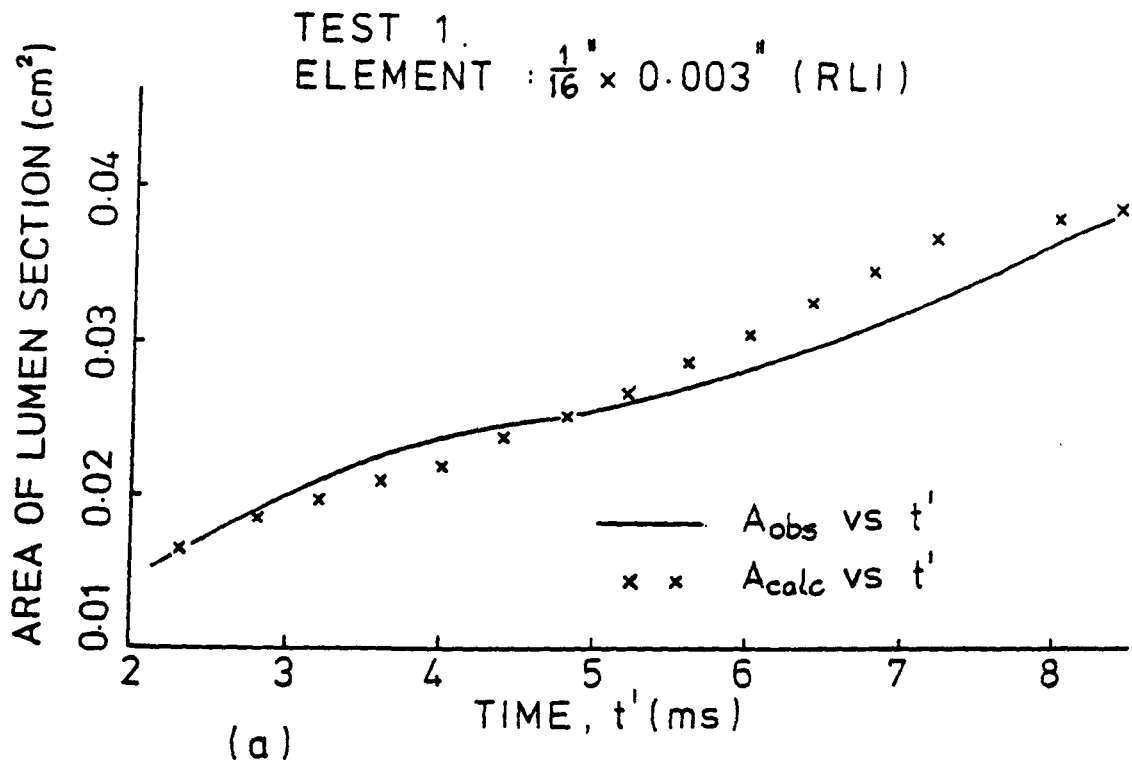
FIG. 3. 13. AREA OF LUMEN SECTION
vs INSTANT OF ARCING
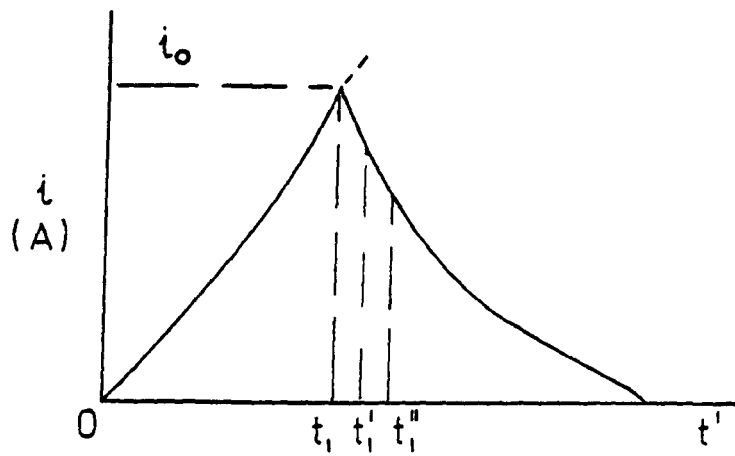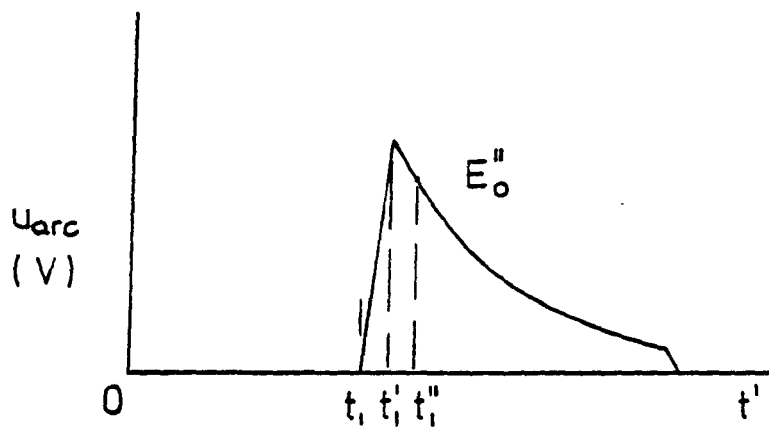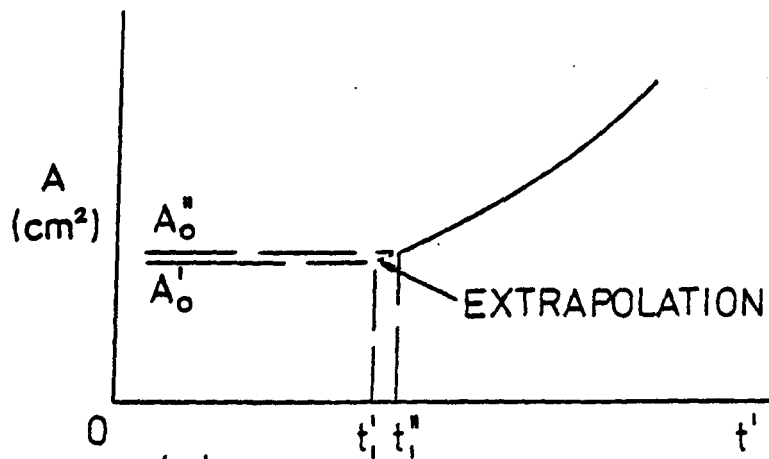
FIG. 3.14. DETERMINATION OF AREA OF
SECTION A_o' OF (EQUIVALENT) I
cm ARC AT INSTANT OF ARC DISRUPTION

(PLEASE SEE SECTION 3.4.3.)

where U_{arc} = fuse voltage

Also the instantaneous value of current, i was known from the oscillogram, so that A_{obs} could be calculated from Eqn (3.44)

A_{obs} vs t' was drawn for the arcing period commencing from $t = t_1"$ (as in Fig.3.14(c)) and then extrapolated backwards to $t = t_1'$ and the area of lumen section A_0' obtained corresponding to this instant. From Eqn (3.43) the corresponding value E_0' was obtained by substituting the value of A_0'.

3.4.4 Voltage Gradient vs Current

The characteristics of voltage gradient (E) vs current (i) for two of the constant length arc experiments carried out are given in Figs.3.15 (a) and (b). In each figure the variation of the 'observed' value (E_{obs}) and the 'calculated' value (E_{calc}) against i (i_{obs}) is given for comparison. The values of E_{obs} and i_{obs} were obtained from the oscillograms taken. The initial value of E_{calc} was assumed to be the same as the initial value of E_{obs}. The initial value of A_{calc} was obtained from the model in Eqn (3.44) and then it was assumed to increase discretely at a rate equal to the corresponding value of dA/dt calculated from Eqns (3.45) and (3.46):

$$A_{calc} (t' + \Delta t_1) = A_{calc} (t') + \frac{dA}{dt} (t') \times \Delta t_1 \quad (cm^2)$$

E_{calc} was then calculated by substituting the value of A_{calc} in Eqn (3.43) The results for the two tests are tabulated in Appendix 3.4. There is good agreement between E_{obs} and E_{calc} vs i_{obs} characteristics as seen from the graphs.

72

TEST 1
ELEMENT : $\frac{1}{16}" \times 0.003"$

— E_{obs} vs i_{obs}

× × E_{calc} vs i_{obs}
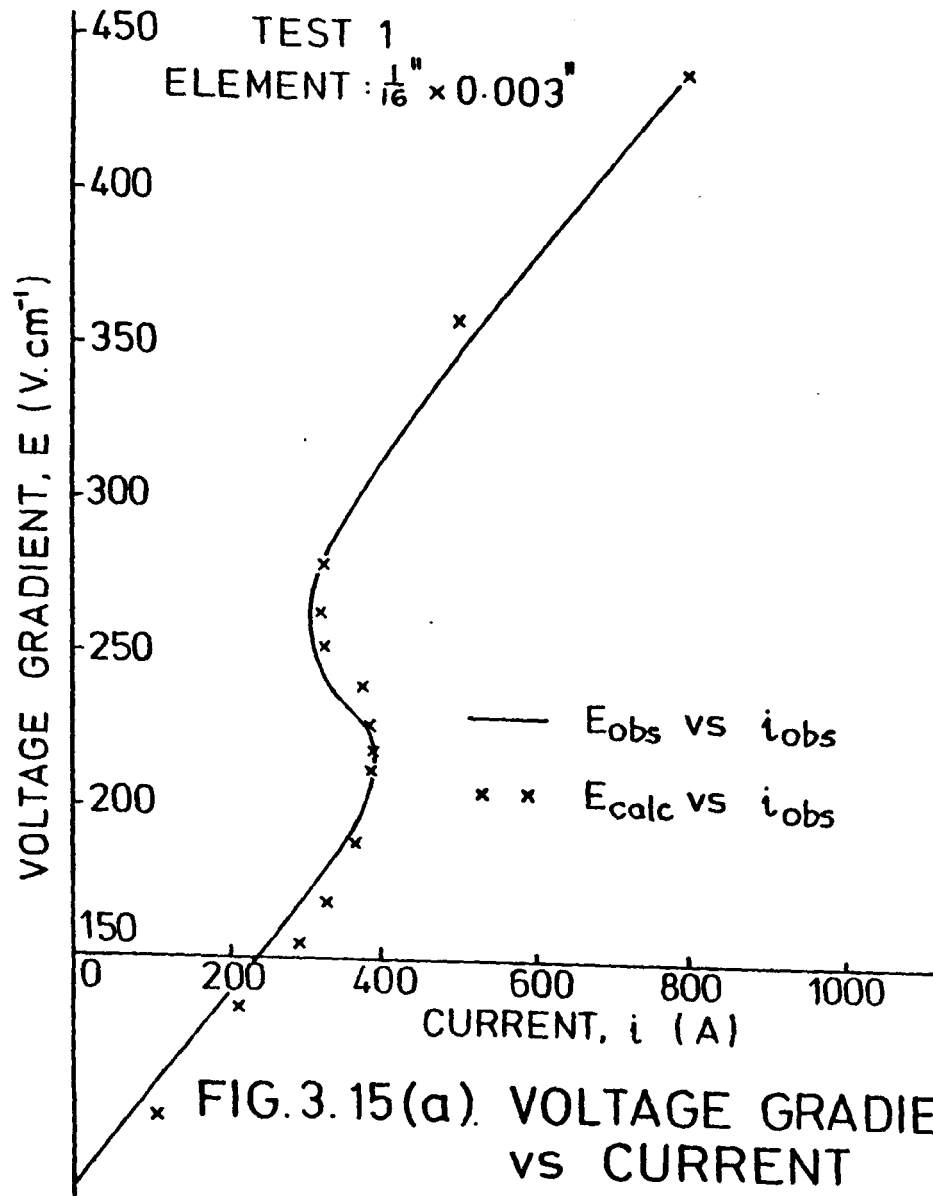
FIG. 3.15(a). VOLTAGE GRADIENT vs CURRENT

- - - - FUSE ARC CHARACTERISTICS

—— $E = \delta \dfrac{i^{0.4}}{A^{0.85}}$

A TAKES FIXED VALUES OF A1, A2, A3, A4 etc.
A1 < A2 < A3 < A4

FIG. 3.15(a)

A = A1

A = A2

A = A3

A = A4

A = A5

A = A6
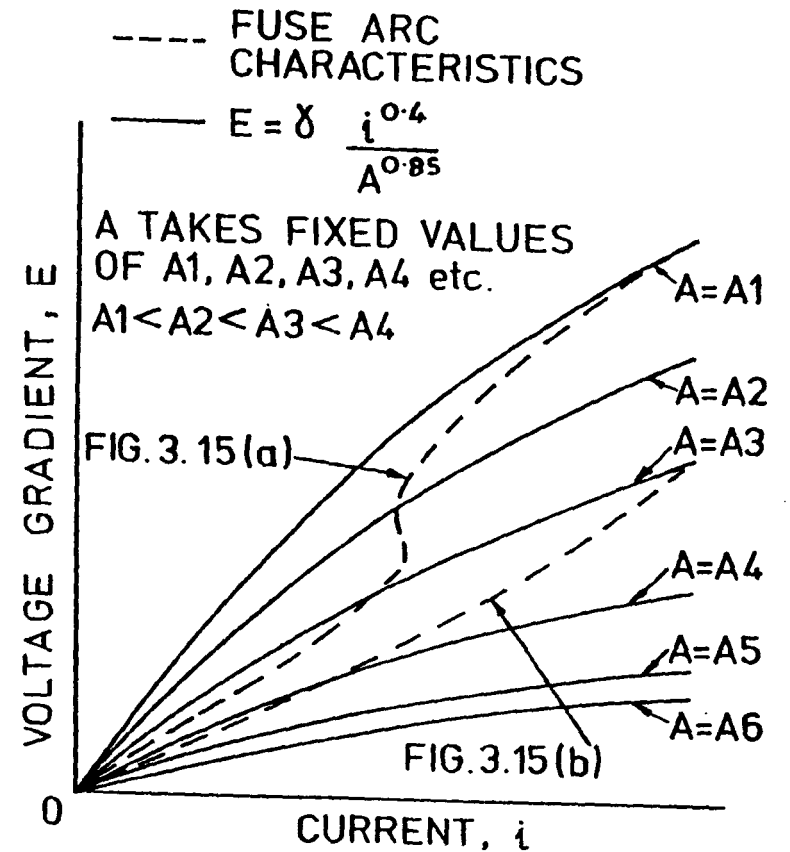
FIG. 3.15(b)

FIG. 3.15(c). ILLUSTRATION OF E vs i CHARACTERISTICS OF FUSE ARC
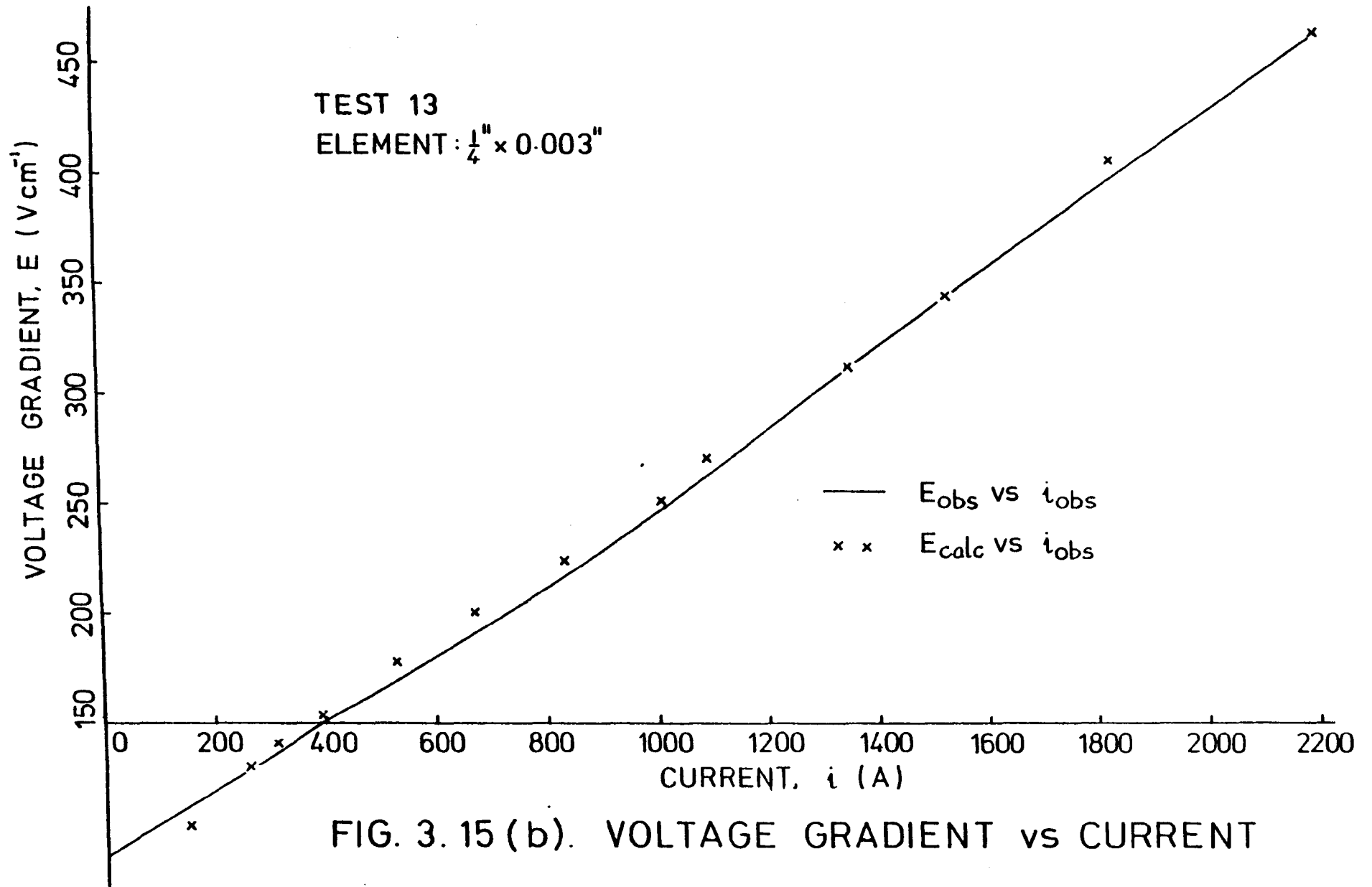
FIG. 3.15 (b). VOLTAGE GRADIENT vs CURRENT

(a) Fig.3.15(a) :   Element $-\frac{1}{16}$" x 0.003" (RL1)

Inductor Tap No.1 was connected in the power circuit (Fig.2.4) and the fuse current initiated at '18° phase' on the voltage wave (POW2 : 18°)

(b) Fig.3.15(b) :   Element - $\frac{1}{4}$" x 0.003" (RL4)

No inductor was used in the power circuit (Fig.2.4) and the fuse current was initiated at '80° phase' on the voltage wave (POW2 : 80°).

There is some dissimilarity between the characteristics shown and those of the previous workers given in the review in Section 3.1. It is also observed that a single E vs i characteristic does not represent the general fuse arc behaviour as the shapes in Figs.3.15 (a) and (b) themselves are different. The variation of the area of lumen section during the whole arcing period is the factor that explains the difference in the shapes of the characteristics obtained.

(1) In the first test considered the circuit conditions were such that during arcing, the current instead of steadily decreasing from the cut off value to zero, increased at a certain stage and finally dropped down to zero. During the period when the current increased the column input power also correspondingly increased, causing a rapid increase in the area of lumen section which explains the point of inflexion in the characteristic. The concept is illustrated in Fig.3.15(c).

(2) The second characteristic is typical and is for a test in which the current dropped steadily to zero during the arcing period. The column input power also decreased during the whole period and there was no rapid increase in the area of lumen section unlike in the first case. The characteristic is also illustrated in Fig.3.15(c).

3.4.5 Internal Energy and Time Constant of Fuse Arc

(a) The internal energy of the fuse arc lumen of one of the tests carried out with 1 cm arc is estimated in Appendix 3.5:

$$\text{Internal energy} = 0.054 \text{ J} \quad \text{for 1 cm arc}$$

$$\text{Total column input energy} = 915 \text{ J} \quad \text{for 1 cm arc}$$

Internal energy is 0.006% of the total column input energy and hence is negligibly small.

Fraser (18) corroborated this/by showing experimentally that the magnitude of the heat storage term $\rho \, C_p \, (\frac{dT}{dt})$ of the plasma was generally less than one per cent of the instantaneous power input to the plasma.

Frind (35) carried out some work in fuse arcs and expressed the/opinion that the internal energy of the fuse arc plasma is a very small per cent-age/of the column input energy and hence could be neglected when considering energy balance.

(b) The arcing period in the test = 5.4 ms

$$\text{Hence the average power input} = \frac{915}{5.4 \times 10^{-3}} \text{ W.cm}^{-1}$$

$$= 0.169 \text{ MW.cm}^{-1}$$

Average power loss, $N_0 \simeq$ Average power input.

74

An approximate value of the time constant of the arc can be obtained
by using Mayr's value: $\dfrac{Q_0}{N_0}$

where Q_0 = stored energy per unit length of the arc

Time constant $\simeq \dfrac{0.054}{0.169}$ μs

$= 0.32$ μs

which is very small.

3.5   Conclusion

Models have been established for the voltage gradient E and the rate of expansion $\frac{dA}{dt}$ of the lumen section of a fuse arc by theoretical analysis and experimental verification. They will be used for the simulation of fuse arc in later Chapters.

The structure of E includes A, the area of lumen section which varies during the arcing period. As the expression for $\frac{dA}{dt}$ is known, A could be determined if a model for A_0, the area of lumen section at the instant of arc disruption is established.

The analysis of A_0 is dealt with in the next Chapter along with that of other essential parameters for the arc simulation.

DISRUPTION AND ARC ELECTRODE PROCESSES

4.1   Review of Previous Work

A limited amount of work has been done so far in the analysis of the disruption and arc electrode processes of notched silver elements. Hibner (22), (23) studied the variation of ignition voltage, U_0 in strip and notched elements in a granular medium. Dolegowski (9) and Onuphrienko (11) experimentally analysed the electrode fall voltages of fuses with notched elements.

Extensive work was carried out on the disruption phenomenon of silver wires when subject to large over-currents, some of the contributors being Nairne (54), Plateau (31), Baxter (28), Kleen (27), Carne (40), Lipski and Furdal (29), Vermij (25), (37) Nasilowski (36), Hibner (41), Huhn (16), Turner (38) and Arai (30). A brief review of these studies is also given as some of them are considered useful for the analysis of the behaviour of notched elements.

A discussion of the review is given in the next Section.

(a)   Wire Elements

(1)   A series of swellings is often observed on the surface of a wire subjected to a large over-current. The formation of these unduloids was first observed by Nairne (54) in 1773. It is virtually certain he did not visualise the wires potential in protecting circuits against damage by excessive current, though he used wires to safely discharge

batteries during which process he observed multiple meltings in both iron and silver wires.

(2) One hundred years later in 1873, Plateau (31) observed that such unduloids appeared in the intermediate transformation phase of a long thin horizontal cylindrical mercury column placed in a certain manner inside a liquid with a much smaller density. Before the column finally became broken up, it first changed into an unduloid i.e. a body formed by a turn of a wavy line around a straight line parallel to the longitudinal axis of symmetry of the wave.

(3) The formation of unduloids on burnt wires, has been used as a basis for theoretical explanation of many properties of fuses investigated by Baxter (28). He attributed the step-wise voltage build up across the terminals of a fuse to the formation of series of arcs at the nodes of the unduloids.

(4) The unduloid phenomenon was studied by Kleen (27), who explained it by the surface tension acting on the molten surface of the wire. He showed that the pitch of the unduloids, h_{mean} was proportional to the wire diameter, d_0 :

$$h_{mean} = k \, d_0 \qquad\qquad (4.1)$$

where k = Kleen's ratio

(5) Carne (40) gave a theoretical analysis of unduloids and attributed the transformation of the wire just before arc ignition into unduloids to a 'mix' of two contradictory effects :

78

(i) the radial temperature gradient connected with heat
     conduction from the centre towards the external layers

(ii) the radial temperature gradient of melting temperature
     according to Claudius Clapeyron's equation due to
     'pinch pressure'.

If the wire was only affected by (i) above it would begin to melt from
its axis where the temperature is the highest. In practice the melting
commences at the surface and hence (i) is not an acceptable theory for
the unduloid formation.

The 'pinch pressure' is the highest at the axis and the lowest at the
surface. The melting temperature increases with pressure and hence the
Melting Point is lower at the surface than at the axis, which indicates
that melting would commence at the surface. However this 'skin effect
heating' of the wire was criticised by Lipski (46) who considered that
the theory is doubtful and fails in many experimental cases.

(6) Lipski (29) quoted an approximate formula for silver and copper in
silica filler grain to melt at the outer side and form unduloids, that
immediately before arcing the current density should exceed a certain
value :

$$j > k. \frac{1}{r} \hspace{4cm} (4.2)$$

where j = current density $(A.mm^{-2})$

        r = radius of wire (mm)

$$k = \text{material constant (for copper, } k = 10^2 A.mm^{-1} \text{ and for}$$

$$\text{silver, } k = 1.9 \times 10^2 \; A.mm^{-1})$$

He presented results of his investigation of unduloid formation on hard-drawn and soft silver wires with diameters between 0.16 and 1.0 mm and suggested that unduloids form only on hard-drawn wires and not on soft wires. This raised a controversy and Turner (38) showed by experiment that hardness should not be a criterion for unduloid formation. Lipski (46) subsequently agreed with the above and proposed that unduloid formation may be attributed to the existence of oxide or similar layers on the surface at the time of disruption.

(7) Vermij (25) studied the disruption and electrode processes of fuses with silver wire elements surrounded by granular medium as well as air and showed that during the disruption process, there was superheating of the liquid silver (at the point of disruption) and that the evaporation process may start at temperatures of the order of 3800° C, well above the Boiling Point at atmospheric pressure (2075° C). He proposed that the electrical behaviour of the fuse element can be characterised virtually by a step increase of the fuse resistance at the instant of evaporation (disruption). During and immediately after the evaporation process, the metal vapour was partly or fully ionised (thermal ionisation) and the specific resistance of the silver vapour could become 10^2 to 10^4 times the specific resistance of silver in the liquid state at the actual evaporation temperature. During the evaporation process a rapid transition takes place from metallic to gaseous conduction.

Vermij (37) analysed theoretically the voltage gradient at disruption, E_0 and compared it with some of his experimental results:

He proposed that E_0 was effected by a number of short arcs per unit length connected in series, each having an arc voltage e_0. Because these arcs were very short, e_0 was mainly determined by anode and cathode processes and was therefore as a first approximation a constant so that:

$$E_0 = n \ e_0 \qquad (4.3)$$

where n = number of short arcs in series per unit length

If h_{mean} is the distance between successive globules, then

$$n = \frac{1}{h_{mean}} \qquad (4.4)$$

Using Kleen's result,

$$h_{mean} = k \ d_0 \qquad (4.5)$$

where d_0 = diameter of the wire

k = Kleen's constant

(Nasilowski (36) quoted a value of $\frac{16}{3}$ for k)

Hence from Eqns (4.3), (4.4) and (4.5)

$$E_0 = \frac{k_1}{d_0} \qquad (4.6)$$

where $k_1 = \frac{e_0}{k}$

= a constant

His experimental results however showed that E_0 was inversely proportional to the square of d_0 :

$$E_0 = \frac{k_2 \ i_0}{d_0{}^2} \qquad (4.7)$$

Vermij explained the difference between the structure of his empirical formula as given above and the theoretical expression as derived in Eqn (4.6) by attributing the former to 'striated disintegration', and the other to 'unduloid disintegration'. It was pointed out that 'unduloid disintegration' was replaced by 'striated mechanism', when the current density was above a certain value (of the order of 20 kA.mm^{-2}) and he was working with current densities above that. This aspect was also confirmed by Lipski (39).

(8)   Hibner (41) proposed the concept of resistance gradient method to determine the ignition voltage U_0 of wire element fuses. The resistance gradient, g_r was defined as the resistance of a unit length of the disintegrated fuse element so that :

$$U_0 = i_0 \ 1 \ g_r \qquad (4.8)$$

where 1 = total length of arcs in series

Using the principle of the resistance method (42), (43), (44), he (21) showed that the ignition voltage of a wire element is given by :

$$U_0 = \rho_0 \ 1 \ \sqrt{\frac{i_0}{s}} \qquad (V) \qquad (4.9)$$

where ρ_0 = fuse-wire element disintegration resistivity at

instant of disruption

$$= 0.505 \, \Omega \, A^{0.5}$$

1 = length of element between the end rings (total length of arc)   (cm)

The above expression is valid provided :

$$\varepsilon = \frac{L \, i_0^2}{2 \, 1 \, s} \geq 25 \times 10^3 \qquad W.s.cm^{-3} \qquad (4.10)$$

and $i_0 \geq 50 \, I_n$ (A)   (4.11)

where ε = magnetic field energy per unit volume of arc
$(W.s.cm^{-3})$

L = circuit inductance (H)

I_n = rated current (A)

There appears to be no physical basis for the expression in Eqn (4.9) which is considered to be empirical.

(9) Huhn (16) considered the effect of the mean grain size of the filler on the initial voltage gradient in silver wire elements of diameter 0.22 mm and showed experimentally that E_0 was a constant at around 600 V.cm^{-1} when the mean grain size of the filler was increased from lower values up to about 0.2 mm and then it decreased steadily to about 200 V.cm^{-1} with further increase of filler size up to about 2 mm. The mean grain size of 2 mm used by him in the experiments is too large to be found in practical fuses.

(10) Arai (30) studied the disruption of silver wires having diameters of
0.1, 0.2, 0.3, 0.4 and 0.5 mm and length 5 cm, which were stretched in
air or embedded in sand and subjected to very large currents. He
observed some deformations on the flash X-ray photograph which were
different from unduloids. The deformations took place after complete
liquifaction of the wires - a model for the deformation is shown in
Fig.4.1, in which r_0 is the wire radius, r_1 the radius of the neck and
r_2 that of the swell. The sharply squarish shapes of necks and swells
were observed under conditions of very high current density and wires
of large diameter. The necks and swells in this case were attributed
to the pinch effect. The rounded necks and swells were observed on the
wire of small diameter or moderate currents and these deformations were
attributed to pinch effect and surface tension.
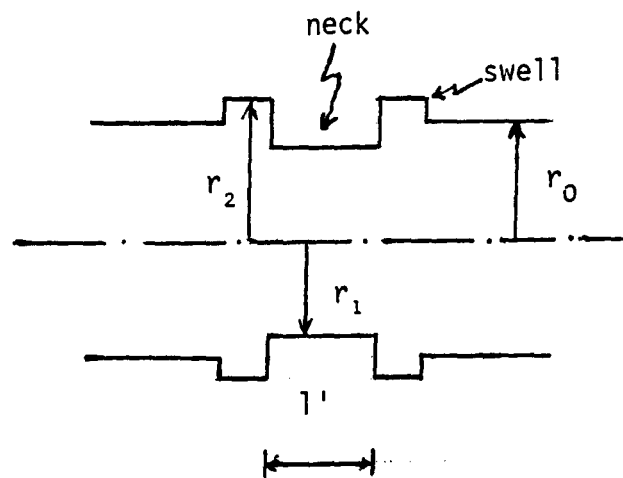
FIG.4.1. ARAI'S MODEL FOR DEFORMATION

The surface tension, electromagnetic force and thermal stress give rise to the surface wave on the cylindrical liquid. The wires being affected by the electromagnetic pinch deform into a series of swells and necks in accordance with the surface wave. Pinch pressure can be shown to be:

$$P = \frac{1}{4} \mu_0 \, j^2 \, r_0^2 \, [1 - (\frac{r}{r_0})^2] \qquad (N.m^{-2}) \qquad (4.12)$$

where j = current density

r_0 = wire radius

r = lateral distance from the axis at which pressure is considered

The maximum pressure occurs at the axis and is proportional to the square of the current density. The very small irregularities due to the surface wave give rise to a longitudinal force difference acting in the direction from the smaller to the larger cross section (24). This longitudinal differential force gives rise to a flow in the liquid cylinder, making the neck smaller and smaller and the swell larger and larger. Considering the flowing liquid as incompressible, the time from the start of the deformation to the instant of disintegration was worked out as:

$$t_d = \frac{7.4}{\varepsilon \, \alpha} \, (\frac{\rho}{\mu_0})^{\frac{1}{2}} \, \frac{s}{i_0} \qquad (s) \qquad (4.13)$$

where ε = ratio of length of neck to r_0 (of the order of 3-5)

α = flow coefficient (of the order of 0.6)

ρ = density of silver (g.cm^{-3})

μ_0 = $4\pi \times 10^{-2}$ (dyne.A^{-2})

85

$$s \ = \ \text{area of cross section of wire (cm}^2)$$

$$i_0 \ = \ \text{current at disruption (A)}$$

If ε and α can be assigned some fixed average values for a range of prospective currents, wire sizes and mean grain size of filler then Eqn (4.13) can be re-written as:

$$t_d \ = \ \lambda \ \frac{s}{i_0} \qquad \text{(s)} \qquad\qquad (4.14)$$

$$\text{where} \quad \lambda \ = \ \frac{7.4}{\varepsilon \, \alpha} \ (\frac{\rho}{\mu_0})^{\frac{1}{2}}$$

$$= \ \text{a constant}$$

If $\varepsilon = 4$, $\alpha = 0.6$ $\rho = 9.3 \ \text{g.cm}^{-3}$ (liquid silver)

then $\lambda = 27$ so that:

$$t_d \ = \ 27 \ (\frac{s}{i_0}) \qquad \text{(s)} \qquad\qquad (4.15)$$

Arai obtained a good agreement between his experimental results and the model he developed above.

He recognised that the stepwise voltage rise corresponded to successive arc initiations at some of the necks.

(b) Strip Elements

Hilbner (26) showed for a 60 mm long copper strip element that the disruption time, t_d has the following empirical relationship:

$$t_d \ = \ 19 + 0.31 \ b \qquad (\mu s) \qquad\qquad (4.16)$$

86

where b = width of the strip (mm)

The above expression is current independent and hence differs in structure from Arai's model for t_d of wire elements which is a function of the current at disruption (Eqn (4.14)).

Hibner's expression for t_d was not supported by theoretical analysis unlike Arai's model which was based on theoretical analysis and experimental verification. Hence the former is not considered for the present study.

(c)   Notched Elements

(1)   Dolegowski (45) conducted experiments using single notched elements and obtained an empirical relationship for U_0 as follows:

$$U_0 = 11 + bj_0 \qquad (V) \qquad\qquad (4.17)$$

where j_0 = current density at ignition $(kA.mm^{-2})$

b = 4.18 for copper

It is apparent from the expression that when the current density was small, U_0 approached 11V.

In Chapter II (Section 2.1 (e)) later models established by Dolegowski (9) for U_B, basing on his experiments with notched silver fuse elements in granular medium (0.2 to 0.4 mm grain size) are given. There were two models, one for current densities up to 8 $kA.mm^{-2}$ and the other between 8 and 20 $kA.mm^{-2}$. The first model covers broadly the range of current densities of this study and is given below:

87

$$0 \leqslant j \leqslant 8 \ kA.mm^{-2}$$

$$U_B = \Delta U_1 + k_1 \ i^\alpha \qquad (V) \qquad\qquad (4.18)$$

where $\Delta U_1 = (20 \pm 5)$ V

$$k_1 = 1.5$$

$$\alpha = 0.39$$

From the expression in Eqn (4.17), for low values of j, U_B can be shown to be less than 11V, whereas from Eqn (4.18), the corresponding value would be (20 ± 5) V. Dolegowski's values in this respect are therefore inconsistent.

(2) Hibner (23) examined the iginition voltage of notched silver elements in a granular medium and obtained a similar expression as for wire elements, applying the principle of the resistance gradient method:

$$U_0 = \rho_0' \ l' \ \sqrt{\frac{i_0}{s_z}} \qquad (V) \qquad\qquad (4.19)$$

where ρ_0' = fuse element disintegration resistivity at disruption time

$$= 0.60 \ \Omega \ A^{0.5}$$

l' = total length of the arc at time of disruption (cm)

$$= \sum_{1}^{n} l_{zn}$$

l_{zn} = length of any one notch (cm)

$$n \quad = \quad \text{number of notches}$$

$$s_z \quad = \quad \text{area of cross section of notch } (cm^2)$$

$$\text{(assumed same for all notches)}$$

provided :

$$\frac{s_z}{s} < 0.6 \qquad\qquad\qquad (4.20)$$

$$1 \text{ mm} < \sum_{1}^{n} l_{zn} < 0.04 \sqrt[4]{s_z} \; U_n \qquad\qquad (4.21)$$

where s = area of element cross section (cm^2)

U_n = rated voltage (V)

As in the case of the wire elements, Hibner's expression for U_0 in Eqn (4.19) is considered to be empirical and not based on any physical concept.

(3) Onuphrienko (11) examined the case of two series arcs merging and noted there was a reduction of only about 20-30 V in the arc voltage, which indicated that the average value of U_B was around 20-30 V.

(4) Wright and Beaumont (5) for their analysis of high-breaking capacity fuse link arcing phenomena assumed a constant value of 10V for the cathode fall drop. They suggested a value equal to the ionisation potential (7.56 V for silver) for the anode fall drop since field ionisation was considered to be the probable mechanism for the ion production at the anode. Thus they used a constant value of 17.56V for U_B (notched silver elements).

4.2 Discussion of the Review

The arc disruption process is complex and comprises a number of possible mechanisms. An analysis of the previous work covered in the review above provides some insight into the possible structure of the following parameters associated with the disruption and electrode processes in fuses with notched silver elements:

(1) Electrode fall voltages, U_B

(2) Initial arc voltage, U_0

(3) Disruption time, t_d

(1) Electrode fall voltages, U_B

Dolegowski (9) carried out extensive work in notched silver element fuses to determine the variation of U_B. As pointed out in Section 4.1 (c) (1) if his model for $o \leqslant j \leqslant 8$ kA.mm^{-2} is considered:

$$U_B = (20 \pm 5) + 1.5 \; i^{0.39} \qquad \text{(V)} \qquad \qquad (4.22)$$

U_B for some discrete values of i worked out using the above model for a typical element ($\frac{1}{8}$" x 0.003") is given below:

j (kA.mm^{-2})	i (A)	U_B (mean value) (V)
1	242	32.8
4	968	41.9
8	1936	48.7

The values of U_B obtained above are high compared to those proposed by other workers like Onuphrienko (11) and Wright and Beaumont (5). As the length of the fuse elements used by Dolegowski was long (about 6 cm) and the current densities too were high, it was possible that there was some multiple arcing which might have been not taken into account. This would have resulted in the higher values of U_B obtained by Dolegowski.

In Section 2.5.1 of Chapter II however it was pointed out that the general structure of Dolegowski's model conforms to the theory used for substantiating the model for the 'burnback rate'. Hence a modified form of the model is proposed and supported by experimental verification as described in Section 4.3.3.

(2) Initial arc voltage, U_0

If a fuse having a silver element with n_s identical notches in series and surrounded by silica is considered, then using Hibner's result for U_0 in Eqn (4.19) which is apparently independent of the number of notches in series, the average column voltage gradient at disruption would be given by:

$$E_0 = \frac{U_0 - n_s U_B}{l'}$$

$$= \rho_0{}' \sqrt{\frac{i_0}{s_z}} - \frac{n_s U_B}{l'} \qquad (V.cm^{-1}) \qquad (4.23)$$

$$\text{where } \rho_0{}' = 0.6 \, \Omega \, A^{0.5}$$

$$l' = \text{total length of the arcs}$$
$$= n_s \, l_z$$

91

l_z = length of each notch

U_B = electrode fall voltage per notch, assumed constant as an approximation

Assuming i_0, s_z and l' are kept constant, then from Eqn (4.23), E_0 would be a linear function of n_s, decreasing with increase of n_s. This is obviously wrong since E_0 should be a function of i_0 and the area of lumen section only, as seen from the model for E in Eqn (3.43) of Chapter III. Hence Hibner's result in Eqn (4.19) needs to be modified so as to give realistic values of U_0 for a variable n_s. The following model for E_0 rectifies the deficiency in Hibner's result and will be used for the present study:

$$E_0 = \lambda \sqrt{\frac{i_0}{s_z}} \qquad (V.cm^{-1}) \qquad (4.24)$$

where λ equals a constant (less than $0.6 \, \Omega \, A^{0.5}$) to be determined

Vermij's expression for E_0 for wire elements in Eqn (4.6) based on the formation of unduloids can be written as:

$$E_0 = \frac{k_1}{d_0}$$

$$\alpha \frac{1}{\sqrt{s}} \qquad (4.25)$$

where s = area of wire section

= area of section at the point of disruption

It would be noted that the above expression has a structure similar to that in Eqn (4.24) as far as the area of element section is concerned.

The value of U_B at disruption could be obtained from the model for U_B as indicated in (1) above.

Hence the revised model for U_0 would be:

$$U_0 = \lambda 1' \sqrt{\frac{i_0}{s_z}} + n_s U_B \qquad (4.26)$$

Some experiments as described in Section 4.3 were carried out to confirm the suitability of the model in Eqn (4.26) and to determine the correct value of λ.

(3) <u>Disruption time, t_d</u>

In a fuse with a single notched silver element, the current density is the highest at the notch which reaches the Melting Point first. Thus disruption takes place at the notch when a part of it is transformed to the liquid state. Arai's model for disruption time for wire elements is considered applicable to the notch:

$$t_d = \lambda' \frac{s_z}{i_0} \qquad (s) \qquad (4.27)$$

where λ' = a constant inversely proportional to ε as in the case of the wire elements

ε = ratio of the length of the neck to r_0 which would be the equivalent radius of the notch cross section

4.3 Experiments with Double Notched Elements

4.3.1 Principle of the Experiments

The experiments with double notched elements helped to confirm the possible dependence of U_B and U_0 on variables such as current and element dimensions.

A large overcurrent was passed through a fuse having a double notched element in silica; a typical drawing of the element is shown in Fig.4.2(a). The widths of the notches were made equal so that the areas of the notch sections were the same - s_z. At the end of the pre-arcing period disruption would take place at each of the two notches simultaneously in general and the initial length of the arc, l' would be equal to the sum of the notch lengths.

$$s_z = \text{width of notch} \times \text{thickness of element (cm}^2) \qquad (4.28)$$

$$l' = l_{z1} + l_{z2} \text{ (cm)} \qquad (4.29)$$

where l_{z1}, l_{z2} = individual notch lengths (cm)

Typical diagram showing the fuse current (ABCD) and voltage (MNPQRSX) waveforms during arcing is shown in Fig.4.2 (b), (c). Disruption took place immediately after current reached B (corresponding to i_0) over a period of t_d as shown in the voltage wave form (MK), when the ignition voltage U_0 (which was the sum of the arc voltages in the notches) appeared across the fuse. U_0 was measured from the oscillogram and corresponded to i_0. After a certain time (- time taken for the two separate arcs to extend by burning back and merge), at the instant corresponding to L, the arc voltage 'dipped' by a value U_B. At that

94

$I' = I_{Z1} + I_{Z2}$
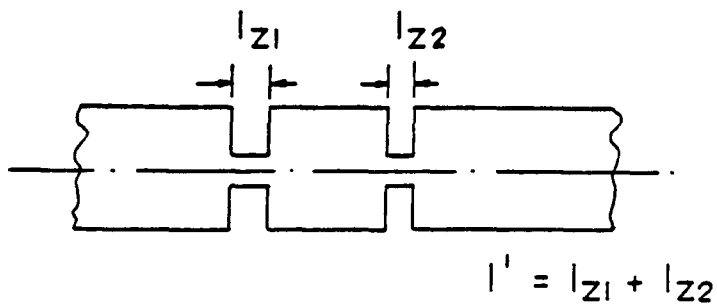
(a) DOUBLE NOTCHED ELEMENT
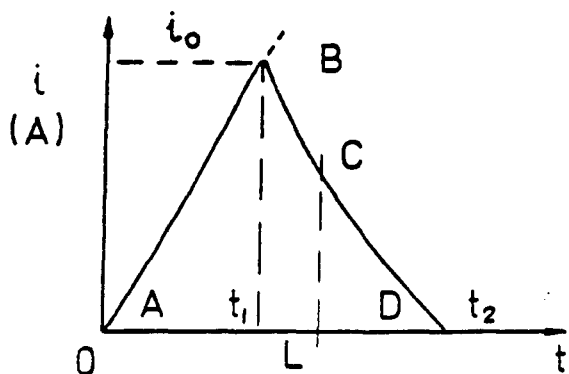
(b) FUSE CURRENT WAVEFORM
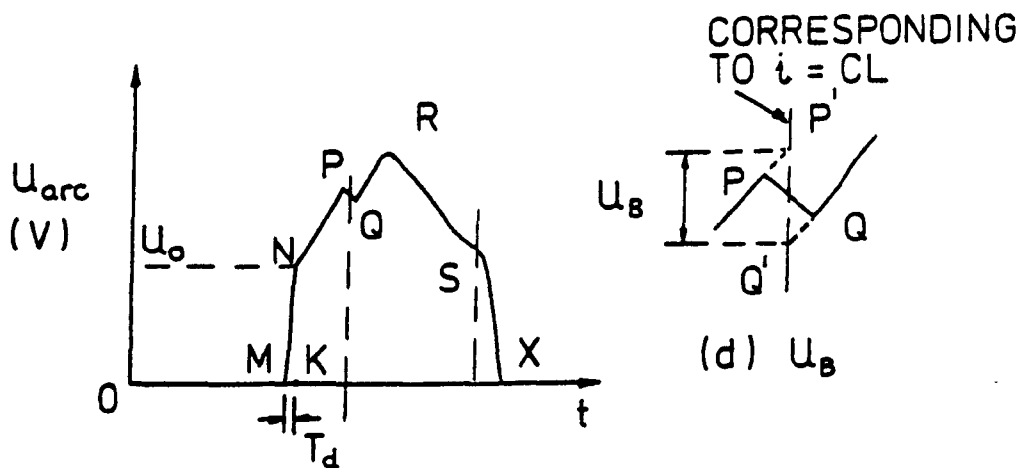
(c) FUSE VOLTAGE
WAVEFORM

(d) U_B

FIG. 4.2. EXPERIMENT WITH DOUBLE
NOTCHED ELEMENTS
(TYPICAL DIAGRAMS)

instant the two arcs became one arc having a length almost equal to the sum of the two individual lengths. Hence the 'dip' corresponded to the loss of electrode fall voltages of the 'vanished' single arc. Instead of being a vertical 'dip' in the voltage waveform, the drop of voltage extended over a small period of time (about 0.1 ms), as seen from one of the oscillograms shown in Fig.4.3. The correct value of U_B was scaled off from P' Q', obtained by extrapolation (Fig.4.2(d)) and it corresponded to the current CL which was also measured from the oscillogram.

Various values of U_0 and U_B were obtained by repeating the test with fuse elements having different s_z and l' and by subjecting to different prospective currents.

In the case of the thick elements with unequal notch lengths, there was a tendency for the disruption at the two notches not to synchronise so that U_0 measured corresponded to one of the notches (the longer of the notches) only as shown in Fig.4.3(b).

4.3.2 Conduct of the Experiment

A double notched silver fuse element was prepared by suitably punching off a strip element. The element was mounted centrally in the standard ceramic cartridge and soldered to the end discs. The rest of the procedure for the preparation of the test fuse assembly was the same as the 'burnback rate' experiments in Chapter II.

The test fuse was connected horizontally in the rig and the fuse current initiated by adopting the circuit arrangement as in Fig.2.4 in Chapter II.
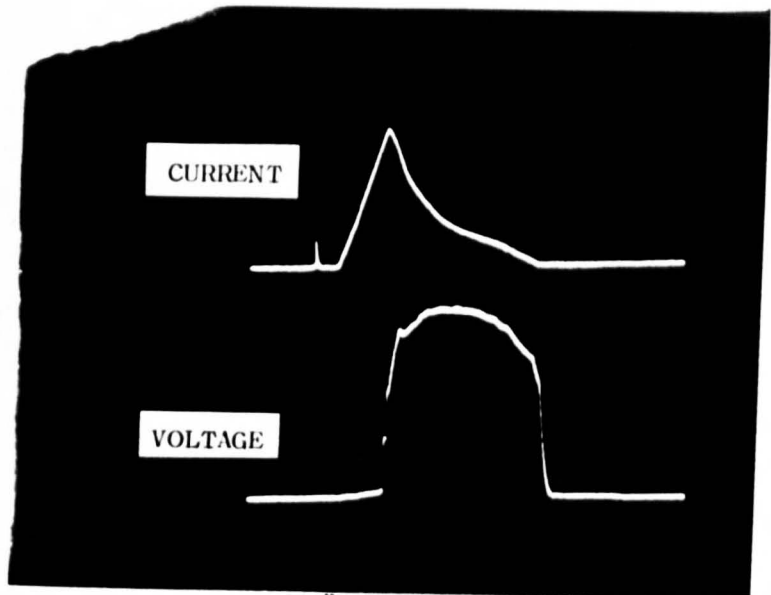
(a) ELEMENT : $\frac{1}{8}'' \times 0.003''$
     CURRENT SENSITIVITY : 417 A/cm
     VOLTAGE SENSITIVITY : 104 V/cm
     TIME SENSITIVITY   : 2 ms/cm
     PROSPECTIVE CURRENT : 2,040 A
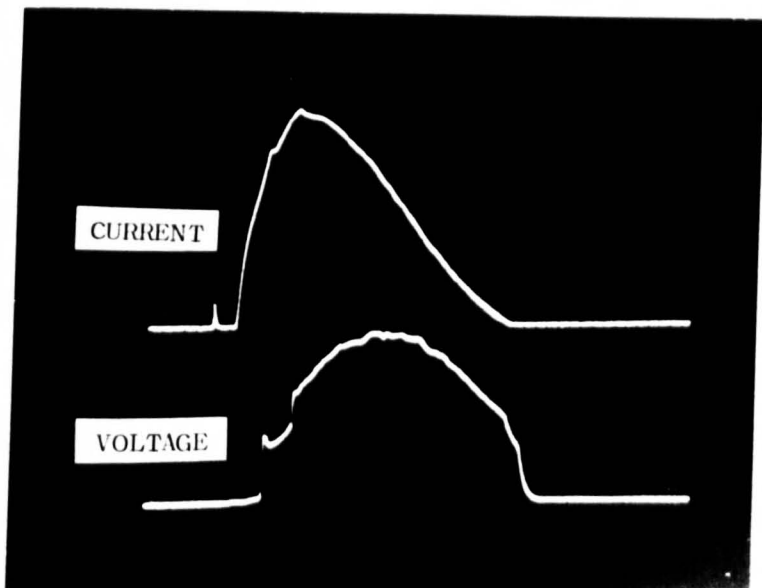
(b) ELEMENT : $\frac{1}{8}'' \times 0.006''$
     CURRENT SENSITIVITY   : 417 A/cm
     VOLTAGE SENSITIVITY   : 104 V/cm
     TIME SENSITIVITY   : 1 ms/cm
     PROSPECTIVE CURRENT : 7,700 A

FIG. 4.3. TYPICAL OSCILLOGRAMS OF CURRENT
& VOLTAGE WAVES (TESTS WITH
DOUBLE NOTCHED ELEMENTS)

The auxiliary fuse was however removed from the circuit and the chopping time set on the DC Unit was made large (about 14 ms) so that effectively the fuse arc was unchopped during the test. An oscillogram of the fuse current and voltage was taken in each test - oscillograms of two of the tests performed are shown in Fig.4.3.

Tests were carried out with different notch lengths and sections and prospective currents.

4.3.3 Analysis of Results

The area of the notch section, s_Z and the total notch length l' for each fuse element were calculated using Eqns (4.28) and (4.29). In the case of tests where U_0 corresponded distinctly to one notch only as apparent from the oscillogram taken, the length of that notch only (l_{Z_1} or l_{Z_2}) was considered in place of l'.

From the oscillogram in each test, the ignition voltage U_0 and the corresponding current i_0 and the electrode fall voltages U_B (as extrapolated) and the corresponding current i were measured. These values and the proposals made in Section 4.2 above were made use of to determine the models for U_B and U_0:

(1) Model for U_B

A modified form of Dolegowski's model for U_B (in Eqn (4.22)) as given below was shown to give good agreement with the experimental results as in Appendix 4.1 and hence adopted:

$$U_B = 15.0 + i^{0.39} \qquad (V) \qquad\qquad (4.30)$$

The constant term in the model is the same as the lower limit of the corresponding term in Dolegowski's model. The variable term containing the power component of i is basically the same except that the coefficient was reduced from 1.5 to 1.0.

(2) Model for U_o

The expression for U_B at disruption obtained from the model in (1) above, when substituted in Eqn (4.26) gives:

$$U_o = \lambda \, 1' \sqrt{\frac{i_o}{s_z}} + n_s \, (15.0 + i_o^{0.39}) \qquad (V) \qquad (4.31)$$

where n_s = number of notches in series (generally two for the experiments carried out)

U_o was calculated for various values of λ and compared with its measured value for each test. The best fit was obtained with $\lambda = 0.4$; the correlation coefficient between the experimental and calculated values of U_o (which are tabulated in Appendix 4.2) is 99%. The models for E_o and U_o would therefore be:

$$E_o = 0.4 \sqrt{\frac{i_o}{s_z}} \qquad (V.cm^{-1}) \qquad (4.32)$$

$$U_o = 0.4 \, 1' \sqrt{\frac{i_o}{s_z}} + n_s \, (15.0 + i_o^{0.39}) \qquad (V) \qquad (4.33)$$

4.4 Model for Disruption Time, t_d

In Section 4.2 above, it has been shown that t_d for fuses with notched silver elements can be expressed in the following form,on the basis of Arai's work (30):

$$t_d = \lambda' \frac{s_z}{i_0}$$

As a first approximation λ' was assumed to be the same as the average value of 27 considered by Arai for wire elements. Hence the model for notched elements becomes:

$$t_d = 27 \frac{s_z}{i_0} \qquad (s) \qquad\qquad (4.34)$$

By substituting the different values of i_0 and s_z in the studies made, it is found:

$$t_d \text{ ranged from 16 to 38 } \mu s \qquad\qquad (4.35)$$

These values agree well with those obtained from the oscillograms of arc voltage.

Arc simulation may not include any elaborate model for t_d as it has minimal influence particularly as in the present study. However the model for t_d in Eqn (4.34) is incorporated in the arc simulation as it is considered useful in a broader application.

It is not known if any work has been done so far to determine a model for A_e, the area of lumen section at the electrode ends. A_e possibly depends on a number of factors such as:

(a) element cross sectional area

(b) area available due to air spaces between filler grains. This depends upon the packing arrangements and mean grain size of the silica used.

The manner in which these factors influence the model is complex and extensive experimental analysis is required to develop a complete model. However, with a view to completing the arc simulation, an approximate model is proposed based on the experimental results available.

From Fig.4.4(a) which shows a typical element cross section in a fuse, it can be seen that the air space adjoining the element is relatively small. When the arc burns back, a part of the silver blocks this space as there will be inadequate time for the silver to percolate into the remote space. Thus as a first approximation, A_e can be taken to be the same as s, the element cross sectional area:

$$A_e = s \qquad (cm^2) \qquad (4.36)$$
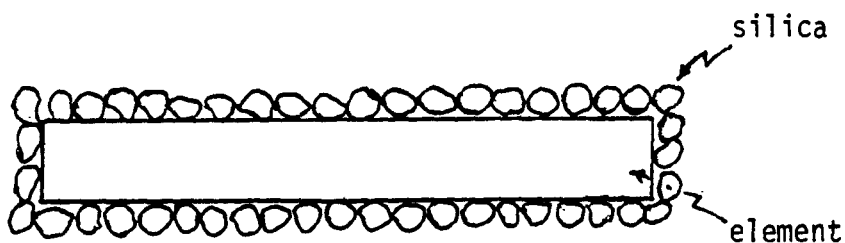
FIG.4.4(a)

However in the case of an element having a small cross sectional area, the dimension of the silica and the area available for the arc to extend transversely is much larger than the element cross sectional area as is seen in Fig.4.4(b).

The examination of the fulgurite (ends) obtained from the laboratory tests for small cross sectional area elements showed that A_e was never less than about 0.017 cm². From the results of the constant arc length experiments in Chapter III, the equivalent area of section at the commencement of arcing which is approximately the same as A_e, has an average value of about 0.017 cm² so that for elements with c.s.a. less than 0.017 cm², A_e is taken as 0.017 cm².
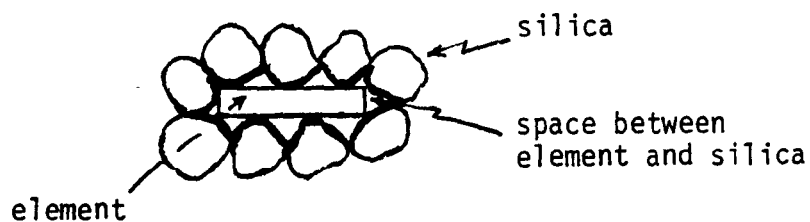
- FIG.4.4(b)

Hence the general model which has been adopted can be summarised as:

$$
\left.
\begin{array}{lll}
\text{(i)} & \text{For } s < 0.017 \text{ cm}^2, & A_e = 0.017 \text{ cm}^2 \\
\text{(ii)} & \text{For } s \geqslant 0.017 \text{ cm}^2, & A_e = s \text{ (cm}^2)
\end{array}
\right\} \qquad (4.37)
$$

4.6 Conclusions

Models have been established for the undermentioned parameters associated with the disruption and electrode processes. They are considered essential for the arc simulation in fuses with notched silver elements:

(1) Electrode fall voltages, U_B - in Section 4.3.3 (1)

(2) Initial arc voltage, U_0 - in Section 4.3.3 (2)

(3) Disruption time, t_d - in Section 4.4

(4) Area of lumen section at the electrode ends, A_e - in Section 4.5

CHAPTER V

DIGITAL COMPUTER SIMULATION

5.1   General

A standard method of modelling a dynamic system is to identify a set of n variables which characterise the system and then to develop a set of n first order differential equations connecting these variables, the jth equation of the set being:

$$\frac{dy_j}{dt} = f_j (t, y_1, \ldots y_j, \ldots y_n) \qquad (5.1)$$

If the functions f_j are known together with the initial conditions of the variables at $t = t_0$, the Eqns (5.1) can easily be solved by using standard library programmes for numerical integration, one of which is the subroutine F4 RUNK which is described later in the Chapter. There is no difficulty in including non-linearities and discontinuities in the functions.

The advantages of using this approach to the modelling of arcing in fuses is that it is possible to add new variables and new funtional relationships to the list in Eqn (5.1) as a further knowledge of the processes becomes available as a result of experimental research. Furthermore, arrangement of the equations in this simple form helps develop a clearer understanding of the physical processes which are being simulated. The use of the digital computer then simplifies matters, rather than complicates them.

The theoretical studies and experimental investigations as described in Chapters II - IV provided the required set of differential equations and the initial values of the variables.

5.2   Model for Arcing in a Fuse with Notched Elements

A fuse with n_p silver elements in parallel each having n_s notches in series when subjected to a short circuit current gets heated by Joulean heating, the highest temperature being reached at the sections through the centres of the notches. At the end of a certain time (- the prearcing period, t_1), the notches attain melting temperature. Disruption ensues immediately thereafter predominantly due to pinch pressure and an arc is struck at each notch, so that there are n_s series arcs per element initially. Each arc extends across the entire notch length during the disruption period and constitutes the first lumen segment. The arc elongates by burning back the element at its ends. The rate of burnback at any instant is the same for each arc as it is a function of the arc current only and given by Eqn (2.9) of Chapter II:

$$\frac{dx}{dt} = 10^{-4}[4.6 + 0.219 \ \{\frac{i(t)}{n_p}\}^{0.6}] \ \{\frac{i(t)/n_p}{s}\} \quad (cm.s^{-1}) \tag{5.2}$$

where $i(t)$ = circuit current (A)

This is the first member of Eqn (5.1). The initial value of x is the notch length, x_0. A discrete time step of Δt (which is fixed) is assumed and the above equation numerically integrated to produce a series of lumen segments, half of each segment being in either end of the arc. The initial arc elongates by filling up these segments step by step as arcing proceeds. The process is illustrated in the model in Fig.5.1. The model depicts the condition two time steps after the disruption. The length of each lumen segment measured along the axis is fixed whilst its area of section assumed constant along its whole

n_s NOTCHES IN SERIES

n_p ELEMENTS IN PARALLEL

XXL

FIG. (a). FUSE ELEMENT

END CAP

XL
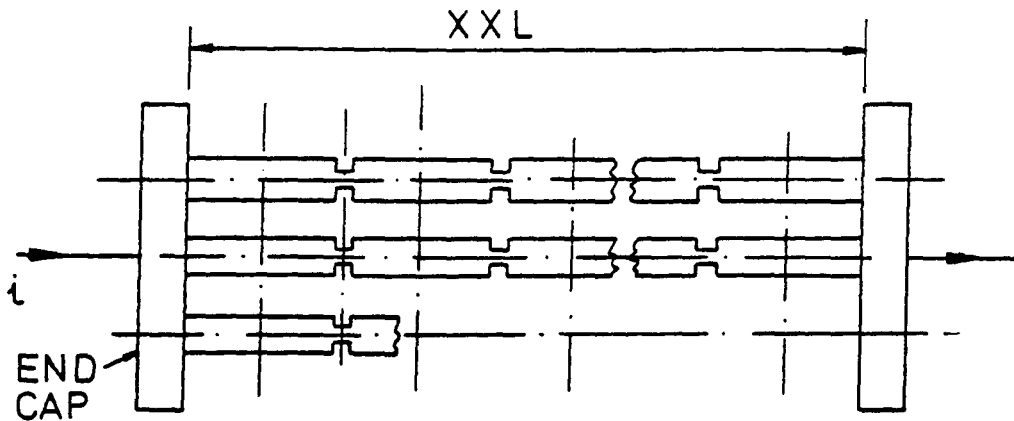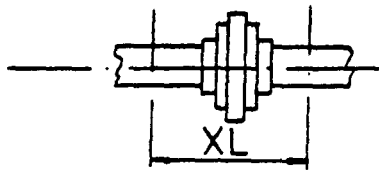
FIG. (b). INDIVIDUAL ARC (OR SERIES ARC)
COMPRISING K LUMEN SEGMENTS

FIELD : E_j
AREA : A_j

$\Delta x_j / 2$

S

j^{th} SEGMENT

$\Delta x_1 = x_0$

CENTRE
OF NOTCH
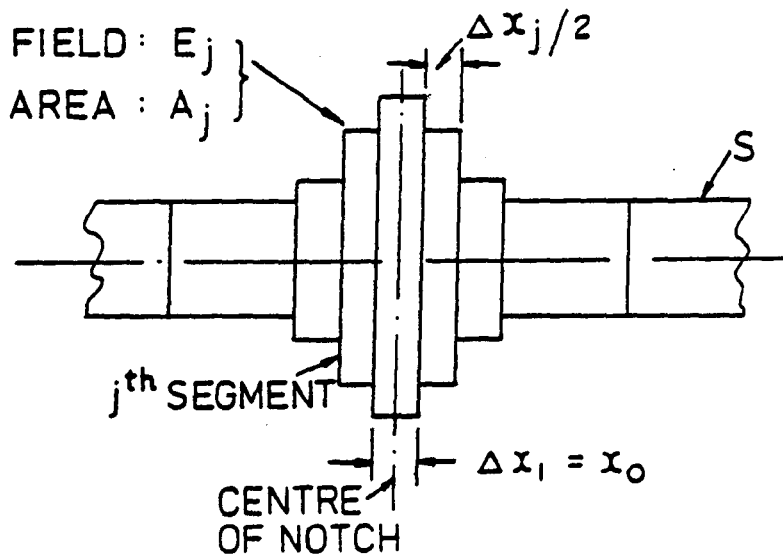
FIG. (c).   FIG. (b) TO A LARGER SCALE

FIG. 5.1. MODEL OF FUSE BEFORE THE
MERGING OF THE SERIES ARCS

length has a fixed initial value, A_e as in Eqn (4.37) and increases with a rate of expansion established in Eqns (3.45) and (3.46) of Chapter III:

$$\frac{dA_j(t)}{dt} = \{0.08 + 0.55 \ (1 - e^{-t'/10})\} \ \frac{E_j\{i(t)/n_p\}}{3800} \quad (cm^2.s^{-1}) \qquad (5.3)$$

where $A_j(t)$ = area of section,

$\quad\quad\quad E_j$ = voltage gradient, of the jth lumen segment at time t

$\quad\quad\quad t'$ = time in ms from the instant the jth segment is added to the arc

$\quad\quad\quad j$ = (1, ... , k)

$\quad\quad\quad k$ = number of lumen segments in the arc

Eqn (5.3) constitutes a set of k o.d.e.s for numerical integration, the initial area of the segments, A_e being known. The current values of the area of section, $A_j(t)$ of the segments at any time during the arcing are known by the numerical integration, so that E_j could be determined from the model in Eqn (3.43) with the Mayr component $\frac{N}{i}$ added. N is assumed to be 200, based on Maecker's E vs i characteristic for a monatomic gas at atmospheric pressure (Fig.3.5), i.e.

$$E_j = 0.914 \ \frac{[i(t)/n_p]^{0.4}}{[A_j(t)]^{0.85}} + \frac{200}{\{i(t)/n_p\}} \quad (V.cm^{-1}) \qquad (5.4)$$

The arc voltage is the sum of the voltages across the segments and the electrode fall voltages in the n_s arcs in series:

$$U_{arc} (t) = n_s \ [\ \sum_1^k E_j.\Delta x_j + U_B \ (i)] \quad (V) \qquad (5.5)$$

* However the initial area $A_1(t_d)$ of the first segment is different and given by Eqn 5.16.

105

where Δx_j = length of the jth segment

$$U_B(i) = 15.0 + [i(t)/n_p]^{0.39} \quad \text{(V)}$$

From Eqn (4.30)

The rate of change of circuit current becomes:

$$\frac{di}{dt}(t) = \frac{U(t) - i(t) \cdot R - U_{arc}(t)}{L} \quad (A.s^{-1}) \quad (5.6)$$

where $U(t)$ = instantaneous value of the source voltage

at time t

Eqn (5.6) provides the differential equation for the state variable i. The initial value of i is equal to the current at disruption ($- i_0$ approximately), so that the solution of Eqn (5.6) gives the value of i at any time t.

The o.d.e. for arcing i^2t per element is:

$$\frac{d}{dt}(i^2t) = [\frac{i(t)}{n_p}]^2 \quad (5.7)$$

The initial value of the arcing i^2t is worked out later in Section 5.3.1 (3)(e). Hence the numerical integration of the above equation gives the current value of the arcing i^2t.

The o.d.e. for arc energy per element is:

$$\frac{d(W_{arc})}{dt} = U_{arc}(t) \cdot [\frac{i(t)}{n_p}] \quad (5.8)$$

106

where W_{arc} = arc energy per element

The initial value of the arc energy is analysed later in Section 5.3.1 (3)(f). Hence the numerical integration of the above equation gives the current value of the arc energy.

When the length n of each arc of the element equals XL the distance between the adjacent notches, the arcs merge into a single arc of length n_s. XL. If the arc current is not extinct by that time, there will be further burnback which confines to the outer ends of the single arc and is at the same rate as in Eqn (5.2):

$$\frac{dx_e}{dt} = 10^{-4} \left[4.6 + 0.219 \left\{\frac{i(t)}{n_p}\right\}^{0.6}\right] \left\{\frac{i(t)/n_p}{s}\right\} \quad (cm.s^{-1}) \qquad (5.9)$$

where x_e = extension of arc length after the arcs' merging at time t and equals zero initially

Eqn (5.9) provides the o.d.e. for the variable x_e. The numerical integration of the equation gives an addition of lumen segments to the ends of the single arc (- half of each segment to either end). The model of the fuse after the arcs' merging is depicted in Fig.5.2.

x_e and $\frac{dx_e}{dt}$ are assigned zero volues until the single arc is formed so that the numerical integration of Eqn (5.9) becomes effective only after the arcs' merging.

After the arcs merge, $\frac{dx}{dt}$ is made equal to zero so that the total elongation of the arc is due to elongation of the extensions x_e only.

107

n_s NOTCHES IN SERIES
n_p ELEMENTS IN PARALLEL

XXL

FIG. (a). FUSE ELEMENT

XL
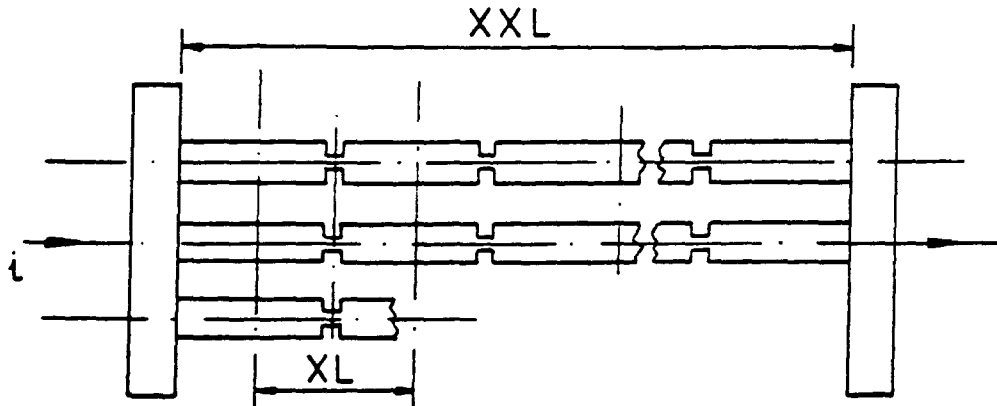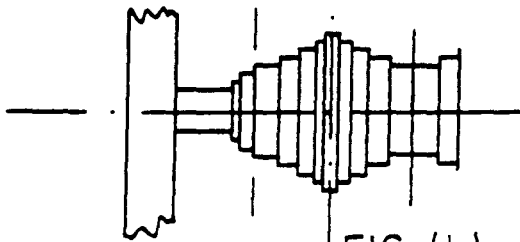
FIG. (b). MERGED ARC
(LEFT HAND END)

$\Delta x_j/2$ Δx_i TWO OF THE SERIES
ARCS MERGE HERE

$\frac{1}{2}\Delta x_{e(i)}$

$\frac{1}{2}\Delta x_{e(k_e)}$ E_j
A_j
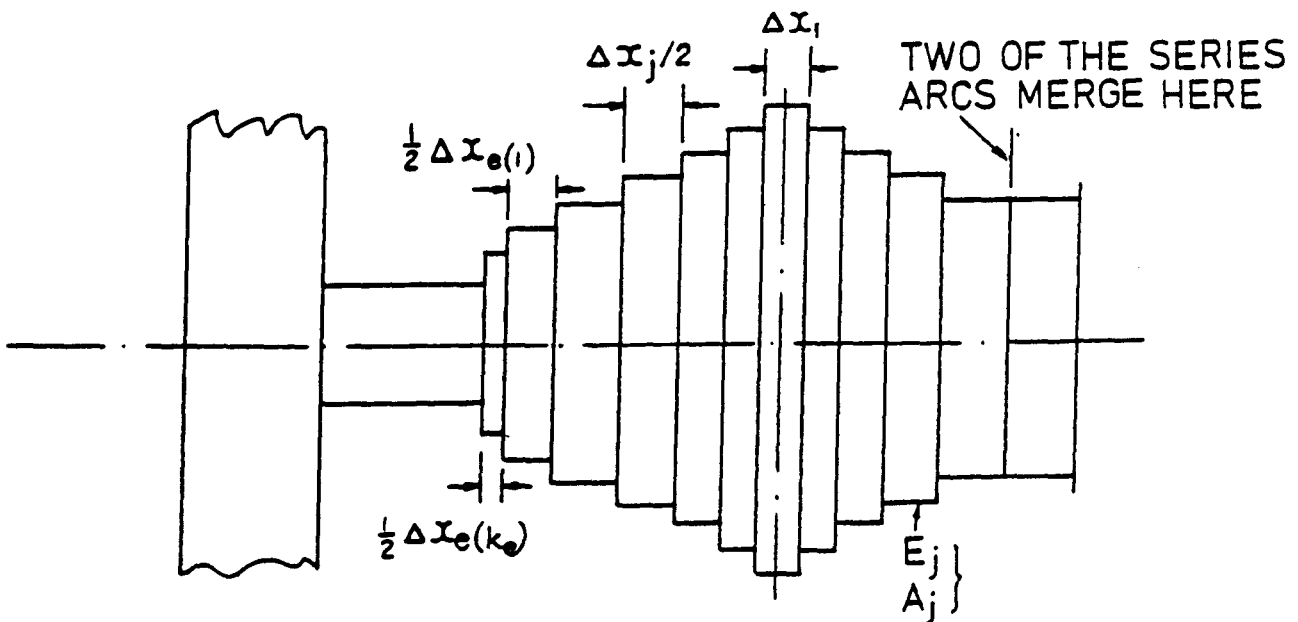
FIG.(c).   FIG.(b) TO A LARGER SCALE

FIG. 5.2.   MODEL OF FUSE AFTER THE
MERGING OF THE SERIES ARCS

The lumen segments added to the ends of the single arc each commence with the same initial area A_e as for the segments in the individual arcs, and expand with a rate having the same structure as in Eqn (5.3).

$$\frac{dA_{(jj1 + n)}(t)}{dt} = \{0.08 + 0.55 (1 - e^{-t'/10})\} \quad \frac{E_{(jj1 + n)} \{i(t)/n_p\}}{3800}$$

$$(cm^2.s^{-1}) \hspace{4cm} (5.10)$$

where $A_{(jj1 + n)}(t)$ = area of section,

$E_{(jj1 + n)}$ = voltage gradient, of the nth lumen segment in the arc extension at time t

t' = time in ms from the instant the nth segment is added to the single arc

n = $(1, \ldots, k_e)$

k_e = number of lumen segments in the arc extension

Eqn (5.10) provides another set of k_e o.d.e.s. for numerical integration $A_{(jj1 + n)}$ and $\frac{dA_{(jj1 + n)}}{dt}$ are assigned zero values until the arcs merged so that they become effective only after the single arc is formed.

The areas of section of the segments in the individual arcs continue to increase even after the arcs' merging. Values of E_j and $E_{(jj1 + n)}$ are obtained by substituting the values of $A_j(t)$ and $A_{(jj1 + n)}(t)$ in Eqn (3.43). The arc voltage after the arcs' merging is:

$$U_{arc}(t) = n_s \sum_1^k E_j \cdot \Delta x_j + \sum_1^{k_e} E_{(jj1 + n)} \cdot \Delta x_{e(n)}$$

$$+ U_B(i) \qquad (V) \qquad\qquad (5.11)$$

where $\Delta x_{e(n)}$ = length of nth lumen segment added to the single arc

The rate of change of circuit current is given by Eqn (5.6) the numerical integration of which is continued until the circuit current reaches the assigned minimum value (cs). If the total arc length reaches the end cap spacing, then $\frac{dx_e}{dt}$ is set to zero.

The rates of change of arcing $i^2 t$ and arc energy are the same as before the arcs' merging and given by Eqns (5.7) and (5.8).

5.3   Computer Program

5.3.1 Flow Diagram

The flow diagram of the program is given in Fig.5.3. The list of variables and the main symbols used in the program are given below:

y_1 = t

           = time from end of the prearcing period (s)

y_2 = current per element

           = i/n_p (A)

y_3 = x_k

           = arc length per notch (individual arc) (cm)

y_4 = $x_e(k_e)$

           = arc length at the ends of the single arc (after merging of the individual arcs)   (cm)

$y_{(j + 4)}$ = A_j

           = area of section of the jth lumen segment in each individual arc   (cm^2)

$y_{(jj1 + n + 4)}$ = $A_{(jj1 + n)}$

           = area of section of nth lumen segment at the ends of the single arc   (cm^2)

$y_{(jj3 + 5)}$ = arcing i^2t per element   (A^2s)

$y_{(jj3 + 6)}$ = arcing energy per element   (J)

j   = (1, ... , k)

k   = number of lumen segments in each individual arc at any time (k has a maximum value of jj1)

n   = (1, ... , k_e)

k_e = number of lumen segments (full) at the ends of the

110

single arc (k_e has a maximum value of jj2)

jj3	= jj1 + jj2
M	= jj3 + 6
	= order of the system + 1
x_f	= $n_s \cdot x_k + x_{e(k_e)}$
	= total arc length (cm)
Δx_j	= length of jth lumen segment in each individual arc (cm)
$\Delta x_{e(n)}$	= length of nth lumen segment at the ends of the single arc (cm)
E_j	= voltage gradient at the centre of the jth lumen segment in each individual arc ($V.cm^{-1}$)
$E_{(jj1 + n)}$	= voltage gradient at the centre of the nth lumen segment at the ends of the single arc ($V.cm^{-1}$)
U_B	= electrode fall voltages (V)
U_{arc}	= V_{arc}
	= arc voltage (V)
c	= $n_p \cdot y_2$
	= i
	= circuit current (A)
rrc	= $n_p \cdot \dfrac{dy_2}{dt}$
	= rate of rise of circuit current ($A.s^{-1}$)
A_{isqt}	= $n_p^2 \cdot y_{(jj3 + 5)}$
	= total arcing i^2t in the fuse (A^2s)
A_{engy}	= $n_p \cdot y_{(jj3 + 6)}$
	= total arcing energy in the fuse (J)
cs	= minimum value of current permitted in the circuit in the program (A)

E_{rms}	= rms value of the source voltage	(V)
Z	= circuit impedance	(Ω)
R	= circuit resistance	(Ω)
L	= EL	
	= circuit inductance	(H)
θ	= THETA	
	= closing angle	(°)
F	= frequency of supply	(Hz)
C_1	= i_0	
	= circuit current at disruption	(A)
t_1	= TI_1	
	= prearcing period	(s)
t_d	= TI_0	
	= disruption time	(s)
XL	= distance between notch centres	(cm)
XXL	= distance between end caps	(cm)
TICOR1	= correction in time to determine the instant at which the individual arcs merged	(s)
TICOR2	= correction in time to determine the instant at which the single arc reached the end caps	(s)

The manner in which the Arc Simulation Program works with reference to the subroutines used is outlined below:

(1) Subroutine INPUTS

The following parameters are input:

   (a) circuit parameters comprising the source voltage, the

112

READ DATA

$E_{rms} < 1.0?$ — YES → STOP

NO

CALL PREARC
CALCULATE t_i, i_o
$t_d, E_i, A_i(t_d)$

INITIALISE VARIABLES
$K=1, KE=1, KG=1, KH=0$
$Y_1 = t_d, Y_2 = i_o/n_p, Y_3 = x_o,$
$Y_4 = 0, Y_5 = A_i(t_d), Y_{(j+4)}\big|_{j=2,jj3} = 0$

CALL F4RUNK
$(M, 0, \Delta t, Y, DY, P, Q)$

YES

$(n_p \times Y_2) < cs?$

NO

$Y_3 > XL$ and $KE=1?$

YES → KE = KE+1

NO

$Y_3 = XL?$ — YES

NO

WRITE FINAL
VALUES OF
$Y_1, x_f,$
A_{isqt}, A_{engy}

CALL AINIT
CORRECT Y_1
TO MAKE
$Y_3 = XL$
CALCULATE
U_{arc}

CALL AINIT
CALCULATE U_{arc}

$K = K+1$

$x_f = n_s \times Y_3 + Y_4$

WRITE: $Y_1, n_p \times Y_2$
$x_f, n_p \times \frac{dY_2}{dt}, U_{arc}$
A_{isqt}, A_{engy}

CALL F4RUNK$(M, 1, \Delta t, Y, DY, P, Q)$
AND OBTAIN CURRENT VALUES
OF VARIABLES(i·e AT $Y_1 = Y_1 + \Delta t$)

$x_f > XXL$ and $KG=1?$ — YES

NO

$x_f = XXL?$

YES   NO

KE = KE+1

CALL AINIT
CALCULATE
U_{arc}

KH = KH + 1

CALL AINIT
CALCULATE
U_{arc}

KG = KG + 1
KE = KE + 1

CALL AINIT
CORRECT Y_1
TO MAKE
$x_f = XXL$
CALCULATE
U_{arc}

FIG. 5.3. FLOW DIAGRAM FOR PROGRAM
TO SIMULATE FUSE ARC

circuit impedance, the phase angle and the closing angle

(b) fuse paramters

(c) time step, Δt

(d) the maximum possible number of lumen segments in each individual arc, jj1 and the maximum possible number of lumen segments at the ends of the single arc (after the arcs' merging), jj2

(e) minimum value of current permitted for the circuit current, cs

This subroutine is called to the Arc Simulation Program.

(2) Subroutine PREARC

This subroutine was developed in the Liverpool Polytechnic to analyse the prearcing behaviour of a typical fuse with notched silver elements and hence to determine the prearcing time, t_1 and the instantaneous value of the circuit current, i_0 at the end of the disruption period. Details of the program are in (55).

The prearcing program is run as an independent main program with the circuit and fuse parameters separately input and the values of t_1 and i_0 obtained. These values are then read to the subroutine PREARC of the Arc Simulation Program. The subroutine is then called by the Arc Simulation Program.

(3) Initialisation of the state variables

The state variables are initialised corresponding to the instant when the arc is struck i.e. at the end of the disruption period.

113

(a) Time (independent variable).

Disruption takes place in time t_d which is modelled in Chapter IV:

$$t_d = 27 \frac{s_z}{(i_o/n_p)} \qquad \text{(s)} \qquad (5.12)$$

The initial value of time is made equal to t_d:

$$y_1 = t_d$$

$$= 27 \frac{s_z}{(i_o/n_p)} \qquad \text{(s)} \qquad (5.13)$$

(b) Arc length

As pointed out in Section 5.2, the arc struck at each notch extends across the entire notch length during the disruption period so that the initial arc length per individual arc is:

$$y_3 = \Delta x_1$$

$$= x_1$$

$$= x_0 \qquad \text{(cm)} \qquad (5.14)$$

(c) Area of lumen section

The initial voltage gradient at the centre of the first lumen section has been analysed in Chapter IV:

$$E_1(t_d) = 0.4 \sqrt{\frac{i_o/n_p}{s_z}} \qquad \text{(V.cm}^{-1}\text{)} \qquad (5.15)$$

114

Using the model for the area of section in Eqn (3.44) of Chapter III, the initial area of the first segment becomes:

$$y_s = A_1(t_d)$$

$$= 0.9 \; \frac{(i_0/n_p)^{0.47}}{[E_1(t_d)]^{1.18}} \qquad (cm^2) \qquad (5.16)$$

(d) Circuit current

The circuit current at the beginning of the disruption period is i_0. The initial arc voltage influences the value of the current at the end of the disruption period:

From Eqn (4.30), The electrode fall voltage is

$$U_B = 15.0 + (\frac{i_0}{n_p})^{0.39} \qquad (V) \qquad (5.17)$$

Thus the initial arc voltage becomes:

$$U_{arc}(t_d) = U_0$$

$$= n_s \; [E_1(t_d) . \; \Delta x_1 + U_B]$$

$$= n_s \; [E_1(t_d) . \; \Delta x_1 + \{15.0 + (\frac{i_0}{n_p})^{0.39}\}] \quad (V) \quad (5.18)$$

The rate of rise of circuit current during the disruption period is obtained from the circuit equation:

$$\frac{di}{dt}(t_d) = \frac{U(t_d/2) - i_0 R - \frac{1}{2} U_{arc}(t_d)}{L} \qquad (A.s^{-1}) \qquad (5.19)$$

The initial value of current per element is therefore given by:

$$y_2 = \frac{i(t_d)}{n_p}$$

$$= \frac{i_0 + \{\dfrac{di(t_d)}{dt}\} \cdot t_d}{n_p} \qquad \text{(A)} \qquad \qquad (5.20)$$

(e) Arcing i^2t

Assuming that the arc current increased linearly from zero to i_0 during the disruption period, the initial value of arcing i^2t per element becomes:

$$y_{(jj3 + 5)} = (i_0/n_p)^2 t \qquad \text{(A}^2\text{s)} \qquad \qquad (5.21)$$

(f) Arc energy

Taking the mean value of the arc voltage of $\frac{1}{2} U_{arc}(t_d)$ during the disruption period, the initial arc energy dissipated per element is:

$$y_{(jj3 + 6)} = \frac{1}{2} U_{arc}(t_d) \cdot (\frac{i_0}{n_p}) \cdot t_d \qquad \text{(J)} \qquad \qquad (5.22)$$

(g) Other state variables

The initial values of the remaining state variables are made zero:

$$y_4 = 0$$

$$y_{(j + 4)} = 0$$

where $j = (2, \ldots jj1)$

116

$$y_{(jj1 + n + 4)} = 0$$

where $n = (1, \dots jj2)$

(4) Subroutine F4 RUNK (M, INIT, Δt, Y, DY, P, Q)

The subroutine F4 RUNK is an ICL library program in the Liverpool Polytechnic computer service and provides the numerical integration of the system of o.d.e.s representing the behaviour of the fuse arc, as enumerated in Section 5.2, using the standard fourth order Runge-Kutta process and produces an approximate solution:

$$y_j \ (t + \Delta t) \qquad [j = 2, \dots (jj3 + 6)]$$

given the initial conditions of the variables.

The o.d.e.s for the state variables are provided in the subroutine DERY (M, Y, DY) which is called every time subroutine F4 RUNK is called into the Arc Simulation Program.

After the initialisation of the variables subroutine F4 RUNK is called with INIT = o. The current values of the variables and the derivatives will be the initial values which are printed out. The output values are:

(i) Time from the end of the prearcing period, y_1 (s)

(ii) Circuit current, c   (A)

(iii) Total arc length, x_f (cm)

(iv) Rate of rise of circuit current, $\frac{dc}{dt}$ $(A.s^{-1})$

(v)   Rate of elongation of individual arc, $\frac{dx}{dt}$ (cm.s^{-1})

(vi) Rate of elongation of single arc (after the arcs'

merging), $\frac{dx_e}{dt}$ (cm.s^{-1})

(vii) Arc voltage, U_{arc} (V)

(viii) Arcing i^{2}t, A_{isqt} (A^{2}s)

(ix) Arc energy, A_{engy} (J)

Upon re-entry INIT is made equal to 1 and the subroutine called. The subroutine AINIT is called to input the initial area, A_e (which has the model in Eqn (4.37) of Chapter IV) and the function vs called to provide the instantaneous value of the source voltage during the time step. The current values of the variables and derivatives printed correspond to the instant at the end of the first time step. This process is repeated keeping INIT = 1.

Provision is made in the program to check for the arcs' merging and if it happens, the correct time of merging is determined by interpolation. Appropriate corrections are made to the values of the variables and the correct values printed corresponding to the time of arcs' merging.

A similar interpolation and set of corrections are made if and when the single arc (after the arcs' merger) reached the end caps of the fuse.

For a set of circuit conditions, the program is continued until the circuit current reached a value less than the assigned minimum value (cs).

Listings of the Prearc Program and the Arc Simulation Program are annexed.

5.3.2 Results

(a) Optimum values of time step, Δt

In Appendix 5.1, the results of the program with varying Δt, XL and XXL for a certain set of test conditions using a single notched silver element, $\frac{1}{8}$" x 0.003" (RL2) are given. The time step of 0.1 ms gave values of final arc length and arcing time near to those obtained experimentally. When the time step was increased to 0.2 ms, the arcing time increased substantially although arcing i^2t and energy were only marginally affected. On the other hand reduction of the time step to 0.05 ms gave almost the same results as of 0.1 ms at the expense of a larger computer time. Hence an optimum value of 0.1 ms was taken for Δt for the studies made.

(b) Validation of the program

Tests were carried out to validate various aspects of the program. In one set of these, the notch spacing XL read in was varied for a single notched element, keeping XXL well above the actual final arc length. The results of final arc length and arcing i^2t, energy and time were not materially affected by keeping XL above or below the final arc length as could be seen in Appendix 5.1, corresponding to a time step of 0.1 ms. This is expected for a single notched element wherein there is no case of arcs' merging.

(c) Computed responses compared with experimental measurements of a typical short circuit test

A fuse with a single notched silver element was subjected to a short circuit test with a prospective current of approximately 765 A. The element parameters and the circuit conditions are given below:

Element parameters

Element: ⅛" x 0.003" (RL2)

Notch length: 0.079 cm

Notch width: 0.074 cm

Circuit conditions

RMS voltage: 245 V

Z : 0.320 Ω

ϕ : 36^0

θ : 18^0

The test circuit shown in Fig.2.4 of Chapter II was used for the test and by selecting a comparatively large time setting of 14 ms in the DC Unit, the fuse arc current was allowed to flow without being chopped during the arcing period. Oscillograms of the arc current and voltage waveforms were obtained. At the end of the test, the final arc length was determined by measuring the length of the fulgurite. The values of the current at disruption and the prearcing period as obtained from the oscillogram were input to the Arc Simulation Program. The computed responses obtained from the program and the observed values of the main parameters during the arcing process showed favourable comparison as in Fig.5.4.

(1) Arcing period

The observed value of 5.85 ms for the arcing period compares well with the computed value of 6.00 ms which is approximately only 2.5% higher than the observed value.
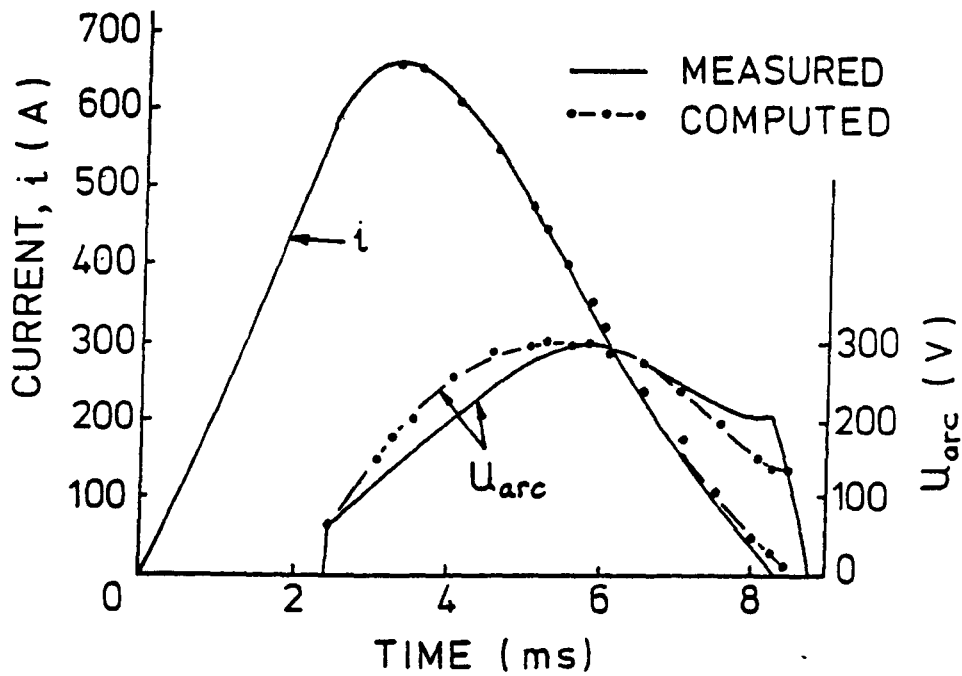
(a)
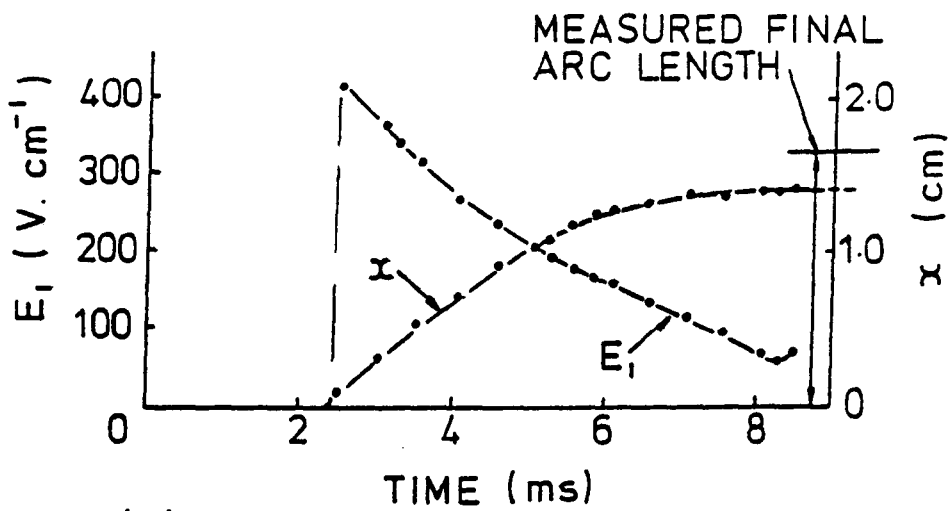
(b)
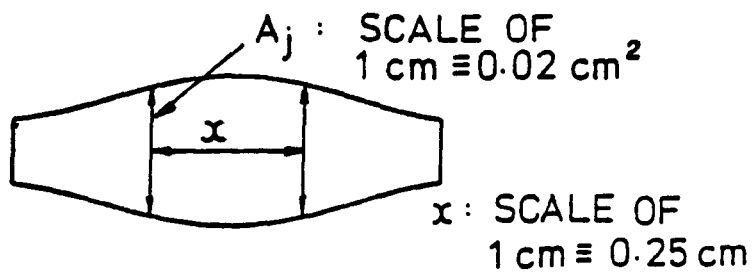
(c) INNER CAVITY OF FULGURITE
      (COMPUTED)

FIG. 5.4. SHORT CIRCUIT TEST
           WAVEFORMS ($\frac{1}{8}'' \times 0.003''$ ELEMENT)

(2) Arc current and voltage

The observed and computed values of the arc current and voltage are plotted against time in Fig.5.4(a). The computed waveform of the arc current practically coincides with its observed waveform, the maximum difference between the values at any instant of time is 10%.

The maximum value of U_{arc} computed is approximately the same as that observed (300 V) and the values of U_0 are also the same (60 V). A striking difference in the two waveforms is that the maximum value of U_{arc} computed occurs at 5.2 ms after the commencement of arc, whilst in the oscillogram there is a time lag of 0.6 ms approximately. This brings back the question of whether a dynamic arc model (say of the type of Cassie's) should also be incorporated in the modelling. However the general shape of the two waveforms is the same. During the latter part of the arcing period however there is a difference, the computed value being less than the other. An increase in the value of the constant N of the model for E (Eqn 3.32) would rectify or minimise this difference. N was taken to have an average value of 200 based on Maecker's curve of E vs i (Fig.3.5). Further investigation may be required to determine any adjustment for N.

(3) Voltage gradient at the notch centre, E_1

The plot of E_1 computed vs the instant of arcing is given in Fig.5.4(b). The characteristic is similar to that of Kroemer (2) for a notched copper element size 5 mm x 0.2 mm with an approximate current of 500 A. In Kroemer's case, the gradient dropped from a value of 300 $V.cm^{-1}$ at the commencement of arcing to about 50 $V.cm^{-1}$ at the end of the arcing period whilst in the test results, the gradient dropped from 400 $V.cm^{-1}$

to 60 V.cm^{-1}. Although the fuse and circuit parameters are different, the shapes of the E_1 vs arcing time characteristics are similar. The drop in the characterisitic is expected as during the arcing, the area of lumen section increased and the arc current eventually diminished to low values, both effects tend to reduce E as seen in the model in Eqn (3.32).

(4) Final arc length, x

The shape of the curve showing the arc length computed vs time as depicted in Fig.5.4(b) is similar to that of the characteristic obtained experimentally in Chapter II (- Fig.2.10(a)). In the latter case however the circuit conditions were different in that the prospective current was higher although the same element size was used. The final arc length computed is however lower than that measured by about 15%. Errors in the values of i_0 and t_1 in the oscillogram could cause some discrepancies in the values of x computed.

(5) Fulgurite inner profile

Variation of A_j along the axis of the lumen at the end of the arcing period is depicted in Fig.5.4(c).

The characteristic shows that the area of section is the highest at the centre and tapers towards the ends as is found in practice in a fulgurite.

122

5.4   Conclusions

A model for the arc in a fuse with notched silver elements has been proposed and digital computer simulation based on F4 RUNK library program established. Optimum values for the time step, Δt was determined for the studies. The program coupled with the prearcing program developed earlier (55) was tested to simulate the behaviour of an experimental fuse with single notched silver element under short circuit test conditions with considerable accuracy.

The complete program will be applied to simulate the behaviour of typical industrial fuses under short circuit conditions in the next Chapter.

CHAPTER VI

SIMULATION OF HIGH POWER BREAKING TESTS

6.1   General

The computer program developed in Chapter V was used to simulate high

power breaking tests of some typical industrial fuses. The fuses

considered are all rated at 1000 V and have current ratings respectively

of 600 A (for the fuse type F 600), 500 A (for the fuse type F 500) and

250 A (for the fuse type F 250); the geometric details of the fuses are

listed in Table 1.

The fuses were tested by a High Power Test Laboratory (ASTA) and the

circuit conditions for 7 selected tests are listed in Table 2. The

circuit conditions and fuse details were input to the Prearcing Program

and the values of the current at disruption (i_0) and the prearcing time

(t_1) obtained for each test. These values were than read into the Arc

Simulation Program along with the circuit and fuse details. The

following main parameters output by the two programs are given in Table

3 together with the corresponding values from the test reports as made

available by GEC Fusegear Ltd:

t_1, t_{arc}, t_2, U_0, i_0, i_0' (peak current), U_{arc} (peak arc voltage), x_f,

i^2t (let through) and energy

The short circuit waveforms computed and observed in the tests are given

in Figs.6.1 to 6.7. A comparative report on the computed responses and

the observed results is given in the next Section.

124

Table I

Details of Typical Industrial Fuses (with Notched Silver Elements)

Fuse Type	Rated Voltage (V)	Rated Current (A)	Element details
F 600	1000	600	n_p = 8 (in 2 bodies), n_s = 6 element width = (0.320 ± 0.002)", element thickness = 0.015" notch width = (0.029 ± 0.001)", notch length = (0.031 ± 0.005)" XL = ($\frac{5}{16}$ ± 0.010)", XXL = 6.9 cm
F 500	1000	500	n_p = 8 (in 2 bodies), n_s = 5 element width = (0.320 ± 0.002)," element thickness = 0.010" notch width = (0.029 ± 0.001)", notch length = (0.031 ± 0.005)" XL = (0.3123 ± 0.010)", XXL = 4.7 cm
F 250	1000	250	n_p = 4 (in 1 body), n_s = 5 element width = (0.320 ± 0.002)", element thickness = 0.010" notch width = (0.029 ± 0.001)", notch length = (0.031 ± 0.005)" XL = (0.3123 ± 0.010)", XXL = 4.7 cm

Table 2

Circuit and Test Details

Test No.	Fuse used	Applied RMS Voltage (V)	Prospective current RMS (kA)	Power Factor	Sin. θ	
I	F 600	715	91.10	0.16	0.87	
II	F 600	714	61.50	0.13	0.08	
III	F 600	740	16.60	0.14	0.05	
IV	F 500	696	106.00	0.15	0.11	
V	F 500	719	8.81	0.12	0.41	
VI	F 250	701	118.00	0.17	0.04	(before zero).
VII	F 250	693	5.36	0.14	0.15	

Table 3

Test Report Comparing the Computed Responses with Observed Results

	t_1 (ms)	t_{arc} (ms)	t_2 (ms)	U_0 (V)	i_0 (kA)	i_0' (kA)	U_{arc} (peak) (kV)	x_f (cm)	i^2t (Let through) ($10^6 A^2 s$)	Energy (kJ)
Test I										
Computed	0.79	5.46	6.25	453	29.3	35.2	1.42	5.11	2.264	87.52
Observed	1.00	4.70	5.70	580	35.0	37.3	1.08	-	*	Δ
Test II										
Computed	2.12	7.63	9.75	411	22.3	25.1	1.19	5.34	2.407	103.71
Observed	2.10	5.60	7.70	604	22.3	28.5	1.16	-	*	Δ
Test III										
Computed	4.08	7.21	11.29	373	16.9	20.1	1.19	5.05	1.866	82.33
Observed	4.30	6.50	10.80	580	18.0	23.0	1.12	-	*	Δ
Test IV										
Computed	1.28	8.00	9.28	350	18.1	19.5	1.00	4.67	1.471	77.83
Observed	1.50	5.70	7.20	440	23.0	23.0	1.10	-	**	Δ

Table 3   continued

	t_1 (ms)	t_{arc} (ms)	t_2 (ms)	U_0 (V)	i_0 (kA)	i_0' (kA)	U_{arc} (peak) (kV)	x_f (cm)	i^2t (Let through) (10^6A^2s)	Energy (kJ)
Test V										
Computed	3.68	6.99	10.77	292	10.9	13.1	0.95	4.06	0.813	45.78
Observed	4.00	6.00	10.00	440	12.0	14.4	0.93	-	**	Δ
Test VI										
Computed	1.27	8.33	9.60	369	10.5	10.5	1.01	4.70	0.391	40.56
Observed	1.20	8.30	9.50	486	12.4	12,4	0.97	-	***	+
Test VII										
Computed	3.87	7.21	11.08	296	5.6	7.00	1.02	4.16	0.230	25.92
Observed	3.60	6.20	9.80	445	5.0	6.59	1.05	-	***	+

* 4×10^6 A^2s (maximum)

** 2×10^6 A^2s (maximum)

***

Δ Body temperature : very hot

+   Body temperature : cold

6.2   Comparison between the Computed Responses and the Observed

Results

In general there is a good correlation between the computed responses and the observed results as seen in Figs.6.1 to 6.7. Salient features of the comparison are given below:

(1) Arc Voltage

Most previous workers (2) - (5) assumed a simple model of constant arc voltage for their models, whereas the general shape observed shows that it is variable with a maximum at an instant of time depending on the circuit and other conditions. The simulation also produces such a variable characteristic.

There are three aspects that are different in the computed and observed waveforms:

(a) U_0 computed is lower than that observed by about 20 to 36%. An increase of the voltage from near zero to a value approximately equal to 30 - 160 V during the prearcing period was observed in the test oscillographs. Such a rise in voltage is unusual but may be attributed to thedrop in the heated fuse element, any contact resistance and the shunt, if it was included in the voltage measuring circuit. The increase in the observed value of U_0 is partly attributed to this voltage.

The model for U_0, which is a function of the intial voltage gradient at the notch centre, E_0 and U_B, is based on Hibner (21), (23) and Dolegowski's (9) work, supported by a few experiments

129
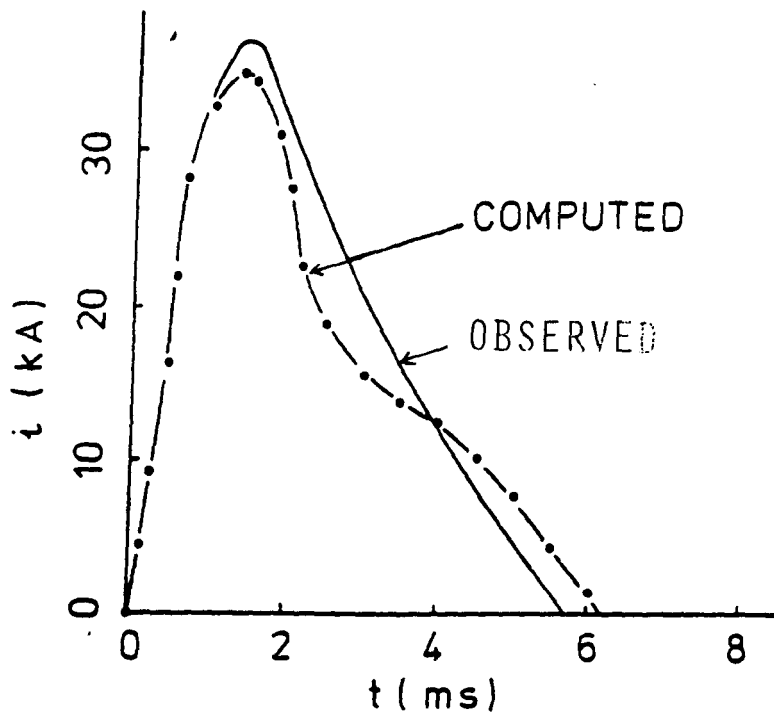
(a) FUSE CURRENT vs TIME
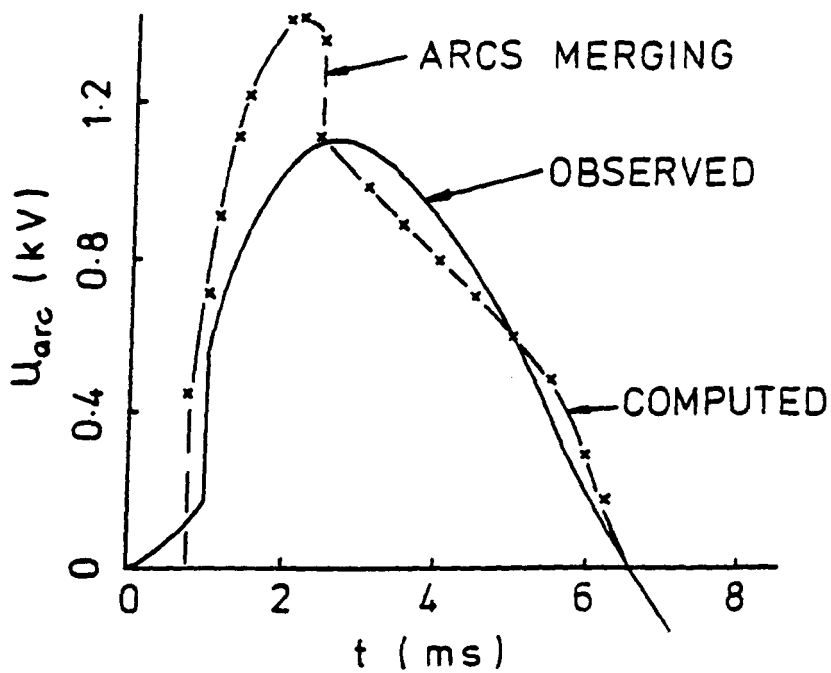
(b) ARC VOLTAGE vs TIME

FIG. 6.1. SHORT CIRCUIT WAVEFORMS
IN TEST I
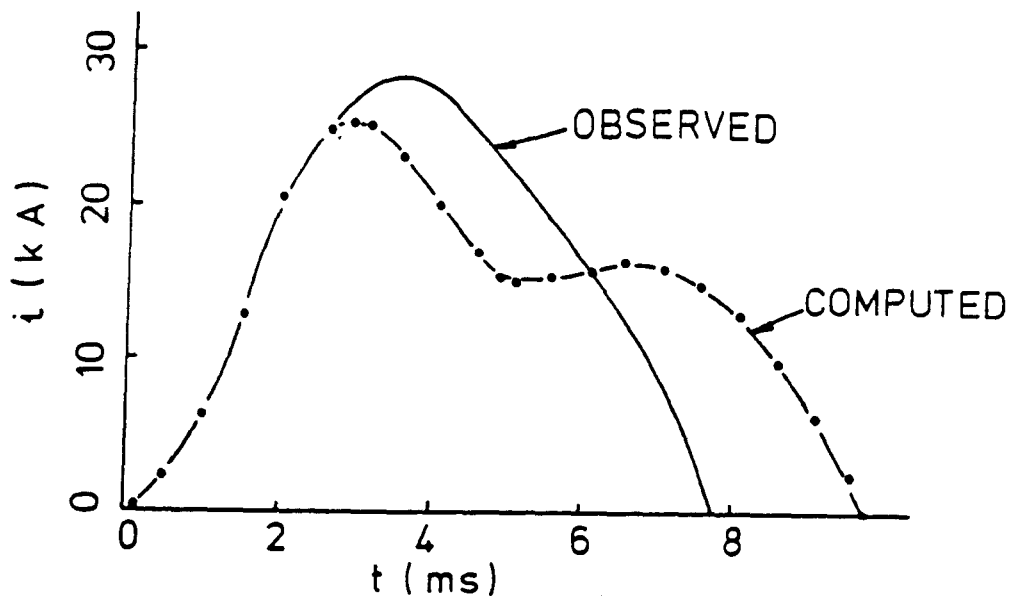
(a) FUSE CURRENT vs TIME
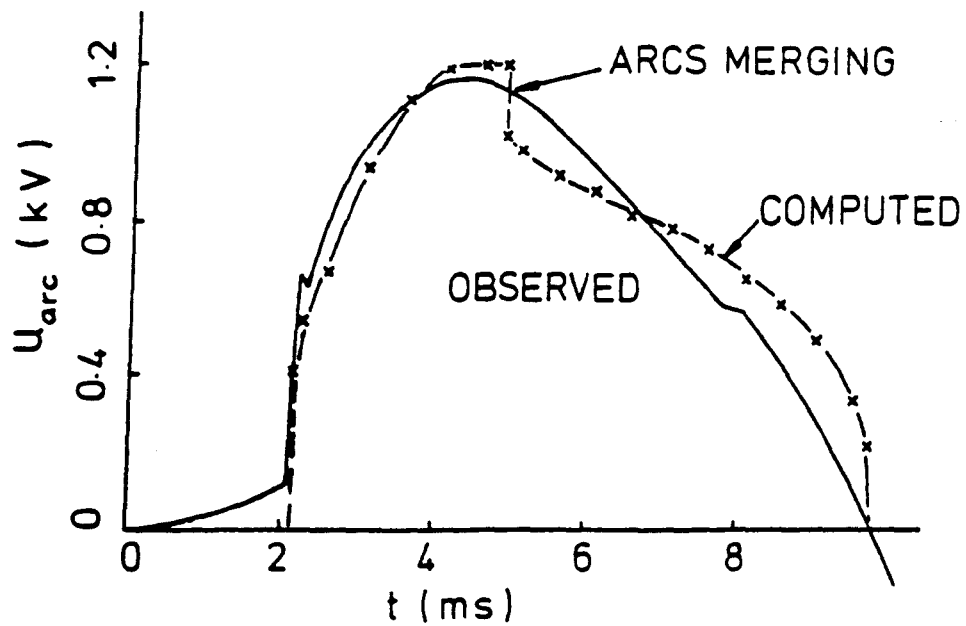
(b) ARC VOLTAGE vs TIME

FIG. 6.2. SHORT CIRCUIT WAVEFORMS
IN TEST II
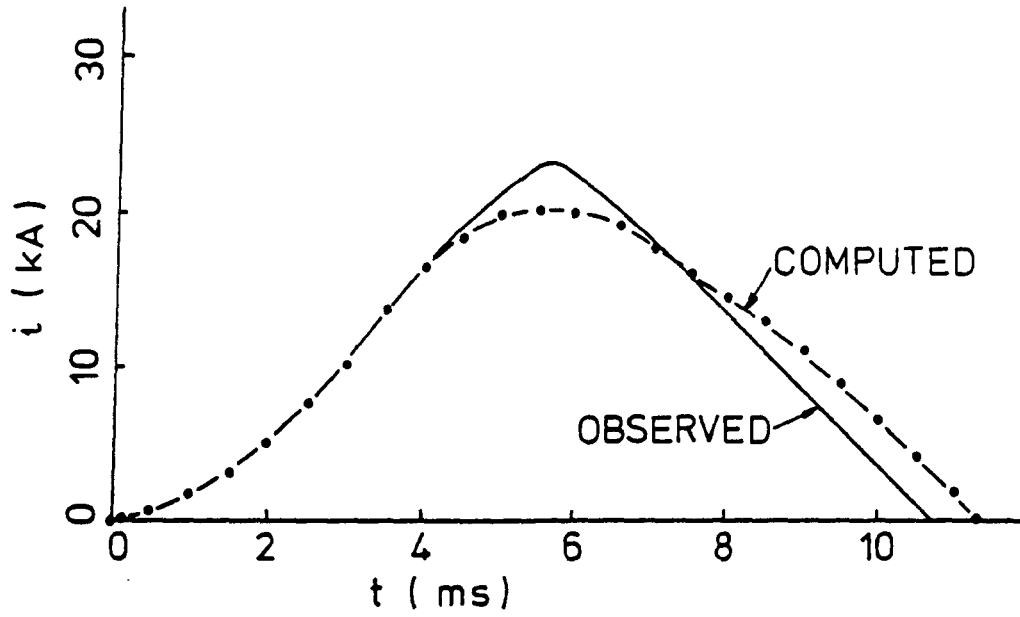
(a) FUSE CURRENT vs TIME
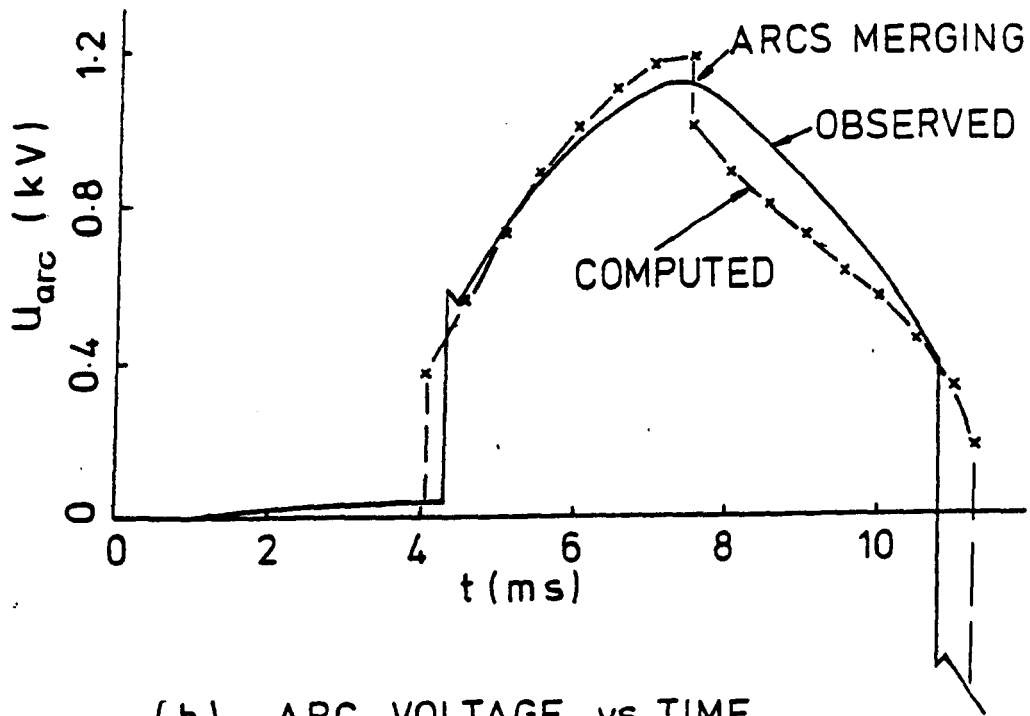
(b) ARC VOLTAGE vs TIME

FIG. 6.3. SHORT CIRCUIT WAVEFORMS
IN TEST III
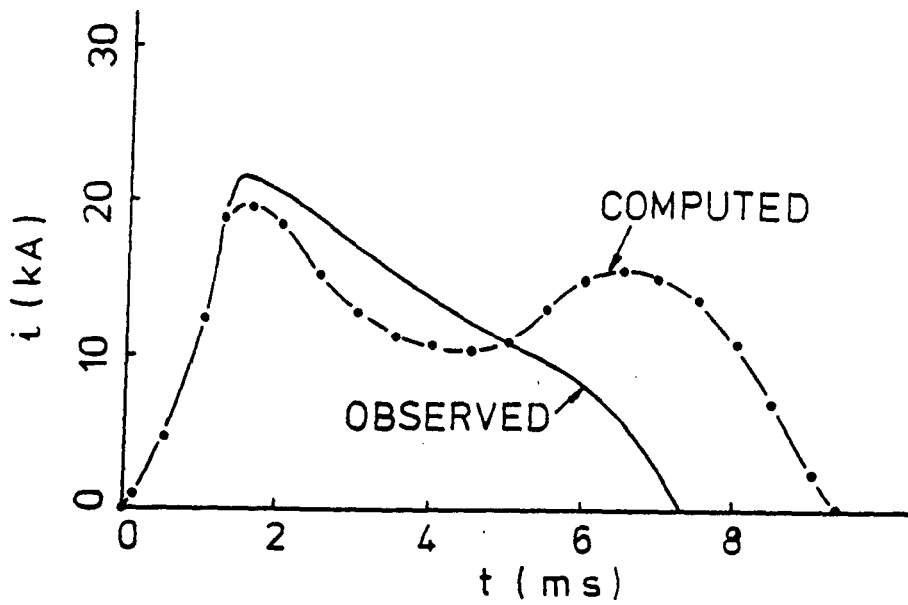
(a) FUSE CURRENT vs TIME
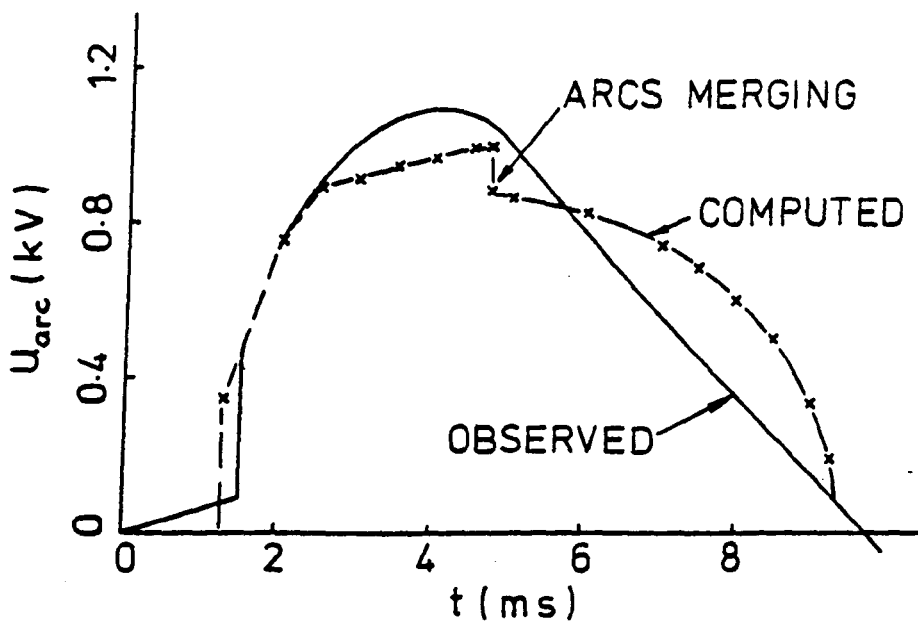
(b) ARC VOLTAGE vs TIME

FIG. 6.4. SHORT CIRCUIT WAVEFORMS
IN TEST IV
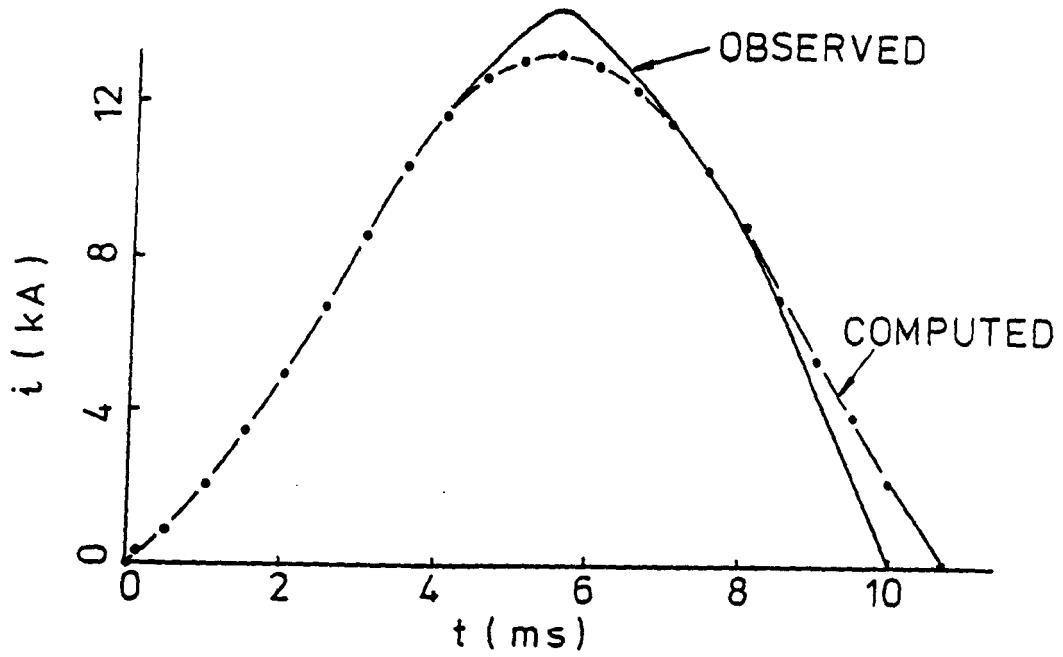
(a)   FUSE   CURRENT vs TIME
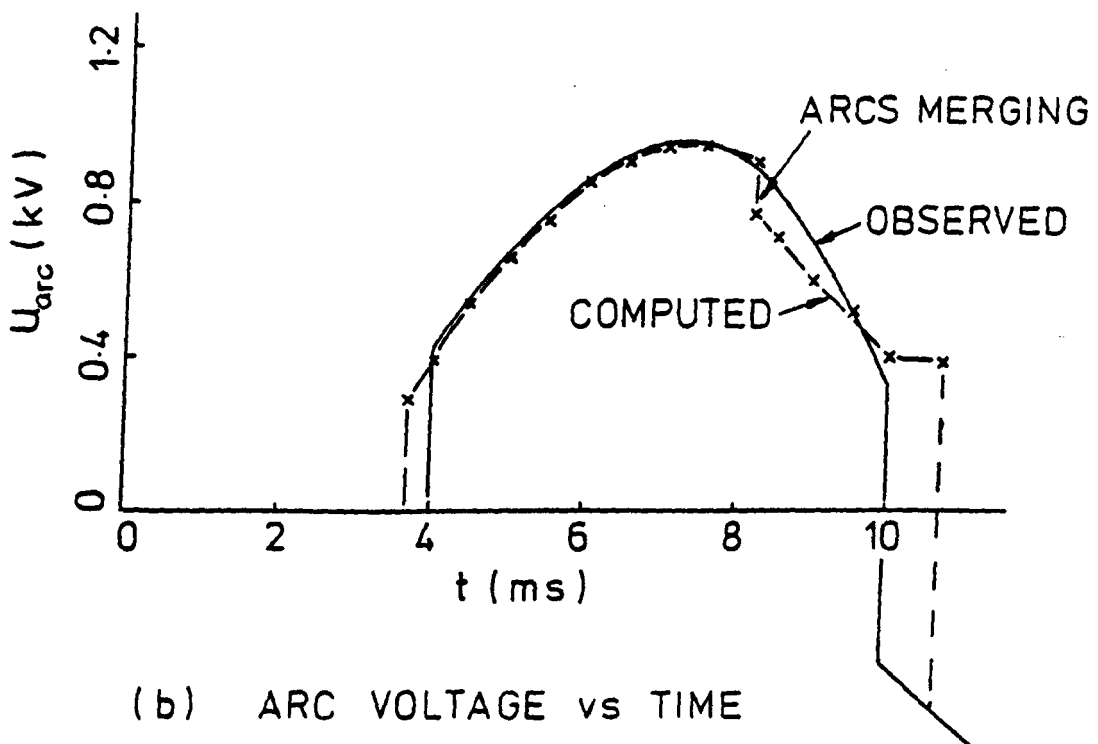
(b)   ARC VOLTAGE vs TIME

FIG. 6.5.   SHORT CIRCUIT WAVEFORMS
IN TEST V
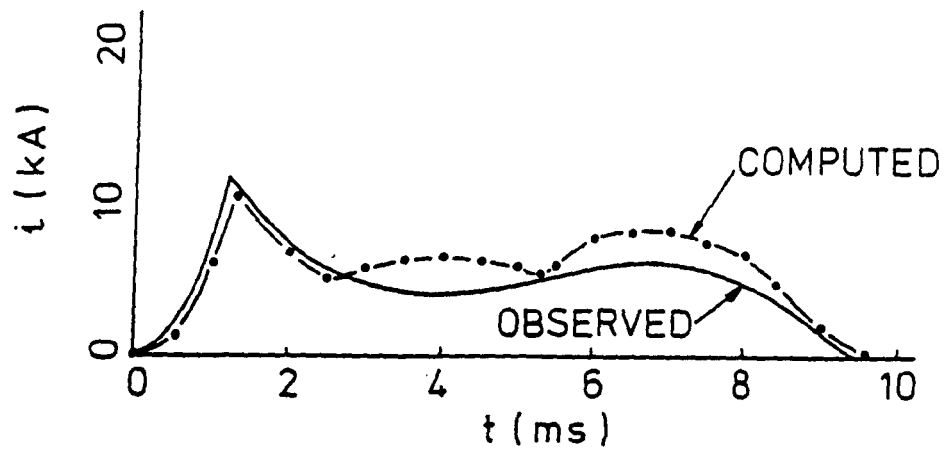
(a) FUSE CURRENT vs TIME
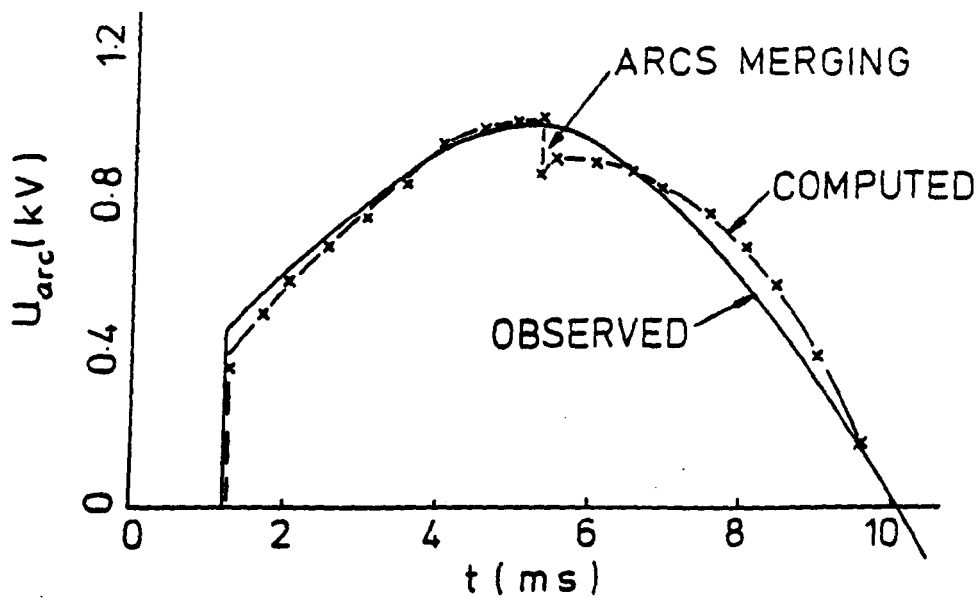
(b) ARC VOLTAGE vs TIME

FIG. 6.6. SHORT CIRCUIT WAVEFORMS
IN TEST VI
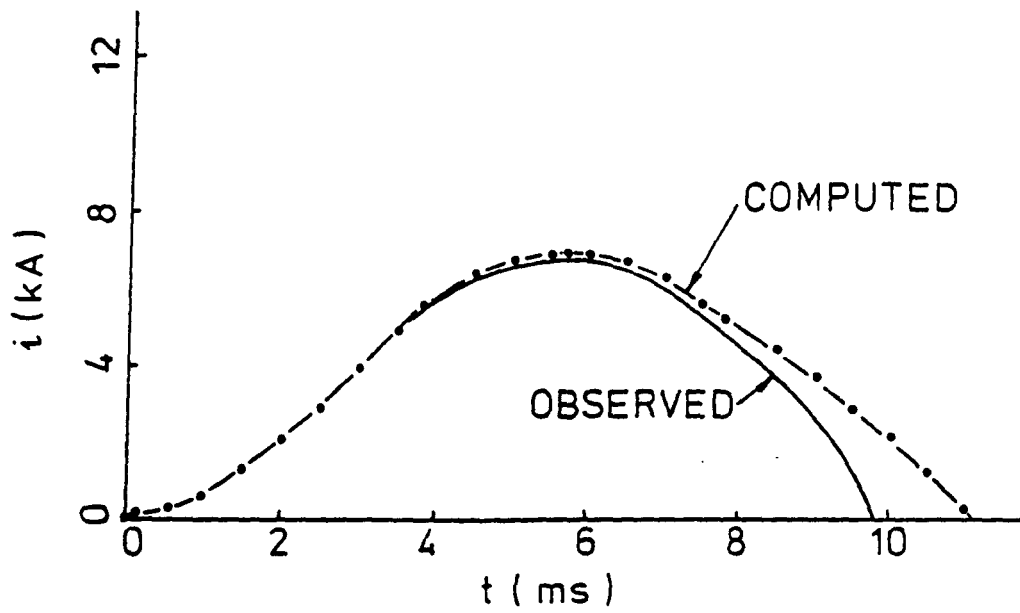
(a)   FUSE CURRENT vs TIME
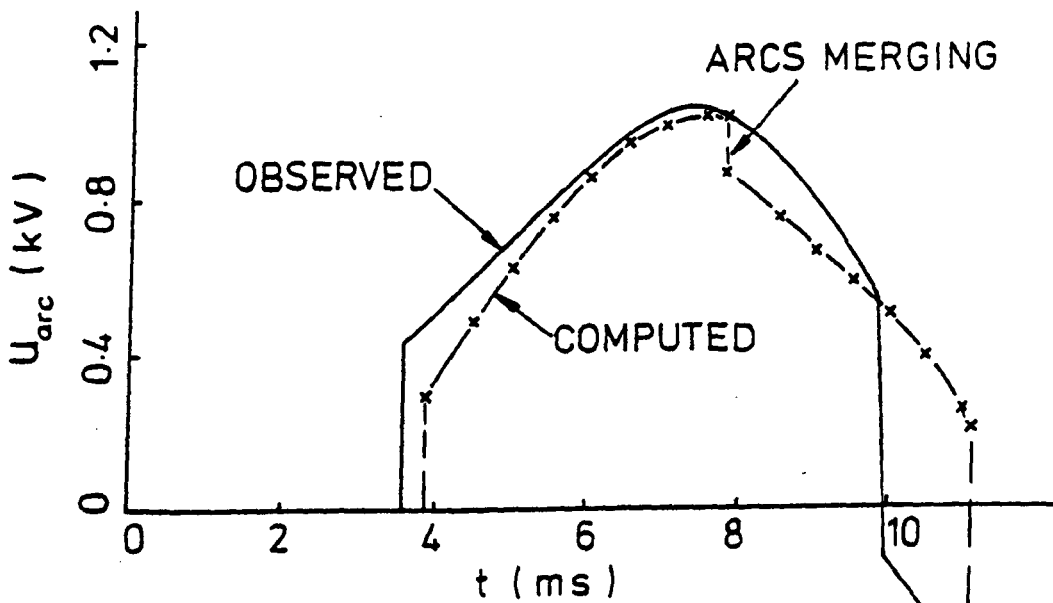
(b)   ARC VOLTAGE vs TIME

FIG. 6.7.   SHORT CIRCUIT WAVEFORMS
IN TEST VII

described in Chapter IV. The model requires some refinement so as to extend its validity to comparatively high currents as were used in these tests.

(b) A kink (drop) in the voltage waveform was observed immediately after the appearance of the initial voltage in some of the test oscillographs and not in the simulation. It was possibly due to a dynamic phenomenon taking place in the arc in-situ. There is difficulty in obtaining the time span covered by the kink with accuracy for further analysis due to the small time scale of the oscillographs. However it could be of the order of a few μs. Further study on the lines of a dynamic arc model for this period may be considered.

(c) During the arcs' merging, the simulation gave a drop in voltage due to the reduction in the total electrode fall voltages as indicated in Chapter V. The step fall in voltage depended on the number of series arcs and the value of U_B at the instant of merging and varied from about 120 V to 190 V in the tests. Such a large step fall in voltage was not noticeable in the test oscillographs. A likely reason is that the arcs did not really merge simultaneously so that the change in voltage during merging was gradual. Another aspect that requires further analysis is the structure of U_B and whether the computed values were higher than the observed values. However any refinement adopted to the model of U_B should be done in conjunction with that of U_0 in view of (a) above.

The peak arc voltage simulated is of the same order as that observed except in Test I wherein it is higher by about 30%.

(2) Arc current

While the shapes of the computed and observed waveforms were
similar, a few differences were observed in some of the tests:

(a) The prearcing times predicted by the Prearcing Program differ from
the corresponding observed values by a small margin and accordingly
the currents at disruption were different. This may be attributed
to some inaccuracies in the circuit conditions.

(b) The peak current computed is generally lower than the observed
value by a maximum of 15%, except in the case of Test VII wherein
the computed value was somewhat higher.

(c) The substantial drop in voltage at the instant of arcs' merging in
the simulation gave a tendency to increase $\frac{di}{dt}$ thereby prolonging
the arcing. This explains why generally a higher arcing time was
predicted.

In Test II the merging of arcs took place at an instant close to
the peak of the source voltage so that the step drop in arc
voltage was enough to change the current slope from a negative
value to a positive value. However the current resumed the
declining state after a short time. There was hence a hump in the
simulated wave which was not present in the observed wave.

Humps were also noticed in the simulation in Tests IV and VI for
similar reasons.

The arc current and voltage waveforms obtained from the UV recorders in the tests were generally to low scales so that there were some inaccuracies introduced in the observed values. Again there were some errors in the time scale due to the acceleration of the recorder printing paper, which accounts for some discrepancies between the observed results and predicted responses.

(3) Final arc length

The final arc length computed was of the correct order of magnitude as realised in practice. In Test VI the arcs reached the end caps and this was attributed to the sustained arcing as reflected in the humps (2) of the current waveform.

(4) i^2t let through

The i^2t let through computed is generally within the maximum value specified for the fuse type concerned. The actual value depends on the circuit conditions.

(5) Energy dissipated

From the computed values of the energy dissipated, an estimate of the increase in temperature of the fuse body was obtained using the parameters of the fuse body and contents. The estimates agree with the notes of the test report in regard to the temperature condition of the body, except in the case of Test VI. In this case there was only 1 test body and the energy dissipated of 40.56 kJ should correspond to a high temperature condition of the body whereas in the report it was shown as being cold.

The energy dissipated in the fuse in Test II was 103.71 kJ and corresponded to the peak energy value of the energy / prospective current characteristic (critical current test).

6.3   Conclusions

6.3.1   Refinements Proposed

(a)   Prearcing Program

The prearcing Program was developed in Liverpool Polytechnic and used in the past to simulate the prearcing conditions for various fuses and test conditions with good accuracy (55). However, when the program was used for the 7 tests using typical industrial fuses, some discrepancies were observed in the computation of t_1 and i_0. This may be attributed to possible errors in the circuit conditions and physical constants of the element material as mentioned earlier.

The values of t_1 and i_0 output by the Prearcing Program were read into the Arc Simulation Program so that the discrepancies in the values of t_1 and i_0 would cause corresponding errors in the output of the latter. It is expected however that such effects are minimal as the errors in the values of t_1 and i_0 were not substantial.

(b) U_0 and U_B

As pointed out in Section 6.2, the values of U_0 simulated were lower than the observed values by approximately 20 to 36%. The initial value of the current/time gradient during the arcing period depends on U_0 which is a function of E_0 and U_B (initial value) which were modelled in Chapter IV on the basis mainly of Hibner's and Dolegowski's work, supported by a few experiments in the present study. U_B was modelled to give lower values than obtained by Dolegowski for reasons enumerated in Chapter IV. The model of U_B requires modification to give still lower values so as to be in the range of values proposed by Onuphrienko (11) and Wright and Beaumont (5). This will tend to make the overall drop

during the arcs' merging to reduce. In practice the arcs will not merge simultaneously. On the other hand if they do merge simultaneously then it would mean there is a transient increase in the equivalent column gradient so that the change in overall voltage drop across the fuse is minimal.

While considering a modified form of model to provide lower values of U_B, E_0 would require refinement so as to give higher values than obtained in the simulation. The revised models should be designed to give a net increase in the value of U_0 as required in the tests.

The refinements proposed above will improve the simulation of the arc current and voltage particularly in Tests II, IV and VI.

6.3.2 Uses of the Simulation

Besides providing the simulations of the arc current and voltage waveforms with remarkable accuracy, the program also provides information of important parameters such as the peak current, peak voltage, i^2t let through and energy dissipation.

From design considerations, the prospective current of 61.50 kA used in Test II was meant to correspond to the peak energy dissipation in the short circuit range for the fuse type F 600. This was in fact confirmed by the simulation as the energy dissipated was 103.71 kJ which was higher than the relevant values in the other tests using the same type of fuse.

Large sums of money were spent for each high power breaking test.

Savings could be effected by resorting to the simulation method using the program developed as an alternative to the short circuit test at least in certain cases.

The program could also be used for purposes such as:

(a) to study the effects of change of closing angle on the performance of the fuse.

(b) to study how existing fuses can be re-designed to meet special application requirements.

(c) preliminary design studies of new fuses being developed.

CHAPTER VII

CONCLUSIONS

7.1   General

Extensive studies have been made of the interruption of short circuit currents by current limiting fuses with notched silver elements surrounded by silica granules and dynamic simulation methods developed for the arcing phenomena occurring in such fuses. The new models, which are basically semi-empirical have been incorporated in a composite program named the Arc Simulation Program. The program was added to the Prearcing Program which was previously developed in Liverpool Polytechnic to simulate the prearcing performance of the fuses, so that both programs provided a complete simulation of the fuse operation under short circuit conditions. The salient features of the models developed for the arcing phenomena are given in Sections 7.2 to 7.4 below.

7.2   Burnback Rate

From the tests on a range of elements in-situ, using the crowbar method and covering a wide range of prospective currents, a semi-empirical differential equation was derived for the rate of burnback. The rate of burnback was shown to depend on the instantaneous value of current i according to a power law, although the popular view of most past workers had been that it varied directly as i. There was a similarity between the model and that of Turners' in that both were functions of $i^{1.6}$ for higher values of the current. However the multiplying coefficients were different, Turners' being less than that in the new model.

The studies also established that the burnback at the anode end was approximately the same as that at the cathode.

The influence of the mean grain size of the filler may be marginal provided it is a practical size, and any changes in the structure of the differential equation would most probably be accommodated by a constant multiplying factor, rather than by changes to the fundamental power law. Further experiments will be required to establish the adjustment for the influence of filler size.

7.3   Column Gradient

The tests in-situ on 1 cm long arc helped to examine the factors affecting the column gradient. Based on these tests and the work of Maecker (17), Wheeler (19) and Frind (35) it was decided that the stored arc energy could be neglected for the simulation. The time constant of the arc was shown to be very small compared to the overall arcing period so that a dynamic arc model was considered unnecessary for the arc simulation and a static model was chosen for E vs i. However the model was quasi-dynamic as it had to accommodate variation of the arc characteristic caused by arc elongation due to burnback and increase of arc section due to fusion of the sand.

Variation of the area of arc section with time which was also studied in Chapter III has been shown to be due to the reduction of volume of silica due to fusion caused by the electrical power input to the arc. Using the concept of the power balance and space conservation in the surrounding medium, a model was developed for the differential equation for A.

Based on theoretical analysis and experimental verification (by 1 cm long arcs) it was shown that E varied as $i^{0.4}$ for higher currents. However for comparatively low currents (less than a few amperes), E was shown to vary inversely as i in accordance with Maecker's studies. These two aspects were embodied in the overall model for E.

139

7.4   Electrode and Disruption Processes

Based on a few experiments with double notched elements and the work of Hibner (21), (23), Arai (30) and Dolegowski (9) models were developed for the initial arc voltage, electrode fall voltages, the initial area of section at the electrode ends and the disruption time in Chapter IV.

7.5 Computer Simulation

The computer simulation was provided basically by the solution of the differential equations for the state variables i, x and A. The equations were integrated step by step using the fourth-order Runge-Kutta method. At each step, the arc length was assumed to increase by a certain amount, when another state variable - the area of the new lumen segment, was added to the list.

The program provides for the simulation of the arcing phenomena in a fuselink containing elements in parallel each with identical multiple notches. The program allowed for the change in the state of the arc when merging of the series arcs occurred. Facilities were also available in the program to stop the burnback when the total arc length equalled the distance between the end caps of the fuselink. During the integration process, $\int i^2 dt$ and $\int U_{arc} i\, dt$ were also evaluated so that at the end of the arcing process, the arcing i^2t and energy were output.

Results of the computer simulation were compared with tests in the Polytechnic laboratory and a High Power (ASTA) test laboratory and good correlation was obtained. Values of t_1, t_2, peak current, peak arc voltage, i^2t let through and energy expended were predicted with good accuracy.

However the comparison revealed certain defects in the simulation which were discussed in Chapter VI. They were in respect of the models for U_0 and U_B and the manner in which the series arcs merge in each element. Further study would be required to improve these models so as

to rectify the discrepancies in the simulation. The pressure condition in the fuse arc was not included in the simulation. This and any other parameter if found important may be incorporated as state variables to add refinements to the simulation. However on the whole the simulation is considered successful.

7.6 Conclusions

The program should prove useful for fuse design and application. Tests in the High Power short circuit laboratory are expensive. Although certain specific short circuit tests by ASTA are essential to meet statutory requirements, it should be possible to substitute preliminary tests by the alternative simulation method to explore various aspects of the design, thereby achieving large economies in the development of the fuse. The simulation also has particular advantages in semi-conductor fuses which are subjected to currents of unusual waveforms which can be easily accommodated in the program but cannot be implemented in a test laboratory. Simulation as an alternative to actual short circuit test has application in determining the effects of varying circuit conditions such as closing angle and power factor.

The model developed which is effectively one of third order (although more state variables are involved) has made a significant contribution to the field of fuse arc simulation under short circuit conditions and hence to the design and application of current limiting fuses in general.

Further experiments may be required with types of fuse elements other than those considered and different filler grain sizes to establish their influence on the simulation studies made. Additional parameters as necessary can be incorporated in the program to account for such factors.

Appendix 1.1

Physical Data

Silver

Thermal conductivity, K_e (200°C)	: 3.87 W.cm^{-1}. °C^{-1}
Specific heat of solid	: 0.232 W.s.g^{-1}. °C^{-1}
Specific heat of liquid (960.5°-1300°C)	: 0.288 W.s.g^{-1}. °C^{-1}
Density of solid (200°C)	: 10.0 g.cm^{-3}
Density of liquid (1000°C)	: 9.26 g.cm^{-3}
Melting Point	: 960.5° C
Boiling Point	: 2075 °C
Latent heat of fusion	: 104.2 W.s.g^{-1}
Latent heat of vaporisation	: 2356 W.s.g^{-1}
Specific resistance of solid (20°C)	: 1.62 x 10^{-6} Ω.cm
Specific resistance of solid (960.5°C)	: 8.4 x 10^{-6} Ω.cm
Specific resistance of liquid (960.5°C)	: 16.6 x 10^{-6} Ω.cm
Specific resistance of liquid just before B.P.	: 29.9 x 10^{-6} Ω.cm
Temperature coefficient of resistance	: 0.0041 °C^{-1}
Surface tension of liquid	: 1380 dyne.cm^{-1}

Filler

Type	: Redhill T fine
Mean grain size	: 0.025 cm
Density	: 1.8 g.cm^{-3}
Specific heat	: 1.18 W.s.g^{-1}. °C^{-1}
Melting Point	: 1610° C
Boiling Point	: 2230 °C
Latent heat of fusion	: 238 W.s.g^{-1}
Thermal conductivity	: 5.86 x 10^{-3} W.cm^{-1} °C^{-1}

Reference was made to (63) for the physical data in respect of silver.

Appendix 2.1

Test Circuit Elements

1. Thyristors

Type : High Power Thyristor YST 8 - 01S

On state current, r.m.s. value	: 1,100 A
Peak reverse and off-state voltages, maximum	: 1,800 V
Surge non-repetitive on-state current, maximum	: 14,000 A
I^2t for fusing related to 10ms sinusoidal surge non-repetitive on-state current ($T_j = 125°C$)	: 970,000 A^2s
On-state threshold voltage ($T_j = 125°C$)	: 0.89 V
Virtual junction temperature, T_j	: -40 to +125°C
Thermal resistance DC	: 0.04 °/W
Gate controlled turn-on time (typical value)	: 5µs

2. Coaxial Shunt

Resistance	: 1 m Ω ± 2%
Rated current	: 100 A
Short time rating	
(i) peak current	: 10 kA
(ii) I^2t	: 30,000 A^2s
Time constant	: 1.2 ns
Limiting frequency	: 100 MHz
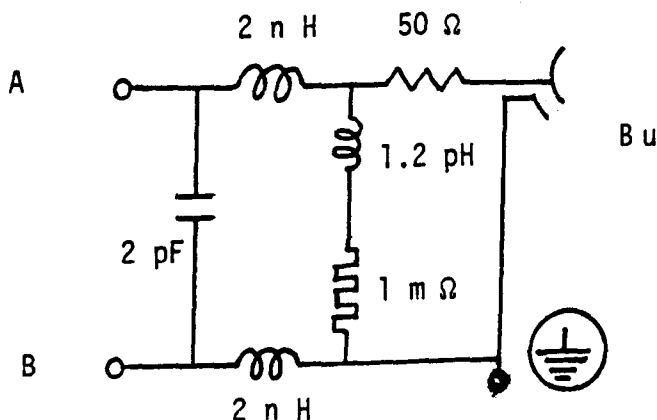
EQUIVALENT CIRCUIT OF COAXIAL SHUNT

Appendix 2.2

Control and Display Equipment

1. Delay Control Unit

The circuit diagram of the DC Unit is given in Fig. A 2.2. The unit comprises basically two modules, both being actuated by the signal output of POW2. Module 1 gives a single rectangular pulse of short duration at the instant of actuation, to trigger the main thyristor and Module 2 gives another pulse of short duration at the end of a pre-set time delay (t_c), to actuate the crowbar thyristor.

Module 1 : The module incorporates a dual monostable 74221 and two NAND gates (using 7400). The input to the Module was initially 0 V (low). When POW2 was actuated (by the firing of POW1, as described in Section 2.3.2(a)) the input increased to 17V DC. The 3V7 zener diode clipped the module input voltage to 3.7V (High). At the same time the B input to monostable 1 went from low to high. Since the A input was kept permanently low (0V), a single shot appeared at the output terminal 13 of monostable 1. The width of the shot, $t = C_1 R_1 \ln 2$

$$= 0.15 \text{ ms}$$

The monostable 2 in the same chip and the 2 NAND gates provided necessary inhibition against any inadvertant operation of monostable 1.

The output of monostable 1 triggered the NPN transistor BC 108 (100mA type) which in turn triggered the NPN transistor BD 131 (3A type). That enabled the main thyristor to be fired with a pulse of the same width and the fuse current was initiated.

Module 2 : When the 17V DC output of POW2 was applied to this module,
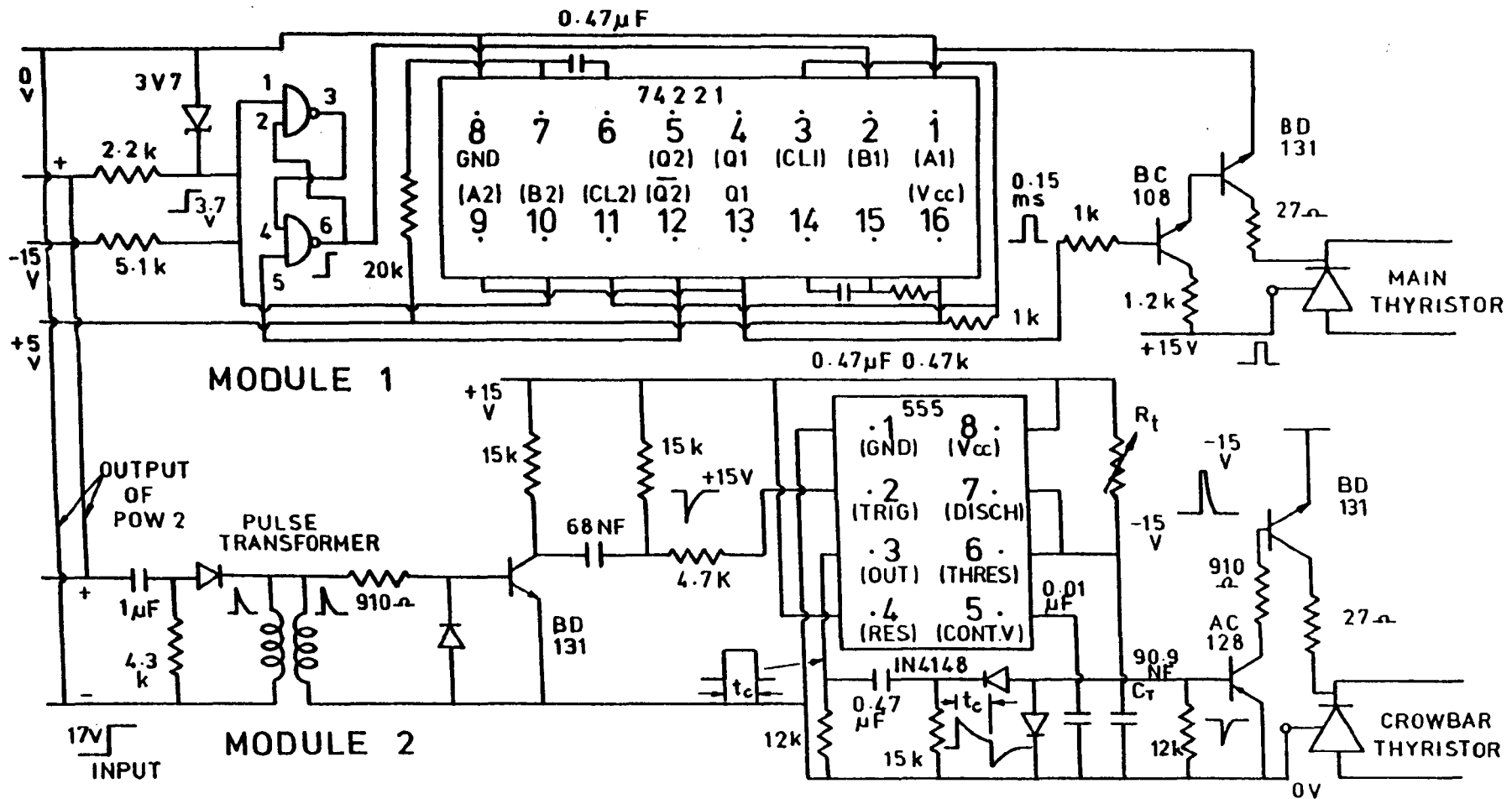
FIG. A 2.2. CIRCUIT DIAGRAM OF DELAY CONTROL UNIT

the differentiator arrangement in the primary side of the pulse transformer enabled a pulse to be formed across the transformer as indicated in the diagram. The pulse transformer used had the following characteristics :

Turns ratio : 1:1

Primary Impedance : 800 Ω

Secondary Impedance : 800 Ω

The pulse transformer had to be incorporated to provide necessary isolation between the main and crowbar thyristors lest there would have been a short circuit path for the 245V AC circuit. For the same reason, individual encapsulated power supply units had to be used for the modules, each with:

input voltage   210-250V AC

output voltage $\pm$ 15V $\pm$ 2%

output current   200 mA per rail

The + 5V DC supply required in Module 1 was obtained from its + 15V supply using a suitable power regulator.

The pulse from the secondary of the pulse transformer triggered the NPN transistor BD 131 (general purpose - medium power type). The signal from the transistor was differentiated, thus giving a negative going pulse of short duration (1 ms), which was applied to pin 2 of the timer 555. The timer was thus triggered and a single shot (monostable) was output at pin 3, the width of the shot t_c was given by :

$$t_c = 1.1 \, R_t \, C_t$$

C_t was kept at 90.9 nF (- exact value obtained by using small trimmer capacitors in series/parallel). A thumbwheel edge type decade resistance box with 4 decades was used to vary R_t. The lowest (right hand) decade, switched increments of 100 Ω resistance and therefore varied the time from zero to 0.09 ms in steps of 0.01 ms. Subsequent decades switched 1 k Ω, 10 k Ω and 100 k Ω resistances repectively and completed the time variation from 0 to 99.99 ms. This calibration hence enabled the decade resistance box setting to give directly the time t_c in milliseconds.

The rectangular shot from the output of the timer was differentiated by the network shown in the diagram to produce two pulses, one positive going at the start of the shot and the other negative going at the end of the shot. The two fast acting diodes 1N 4148 helped to block the first pulse and allow the second pulse which triggered the PNP transistor AC 128. This in turn triggered the NPN transistor BD 131, which actuated the firing of the crowbar thyristor. Thus the crowbar thyristor was switched on at the end of t_c from the instant of initiation of the fuse current.

2. Transient Recorders

Type : DL 901/2D manufactured by Datalab.

General : The DL 901/2D Transient recorder is a digital instrument designed to capture single shot or low repetitive events and present them for continuous display on an oscilloscope and read out to a Y/t plotter.

One of the main applications of the DL 901 is to record unique signals. Once the waveform has been digitised and stored in the memory using single shot mode, it will remain there permanently unless the operator instructs the unit to take a fresh record, or power is removed from the instrument.

In the studies made, a Telequipment Cathode Ray Oscilloscope type No. DM63 was used to display the stored records of the Transient Recorders.

Two Transient Recorders were used and were designated Transient Recorder (Master) and Transient Recorder (Slave) respectively. The Recorders were interconnected by a cable which conveyed synchronising signals between them. There was also display synchronisation between them so that data from both recorders may be viewed coherently on the 2 channel, single X oscilloscope. The 'Master' unit provided X and Z drive to the CRO as well as one channel of recorded data (Y1 channel). The 'Slave' unit provided the second channel of data (Y2 channel). The details of the interconnections between the Recorders and the CRO are given in the Operating Manual for the Recorders.

The following settings were generally used :

Transient Recorder (Master)
SWEEP TIME   : 20 ms

> If the CRO time setting was 0.1 ms/cm then the 20 ms sweep occupied 10 cm of the CRO screen.
>
> (In the cases involving short duration transients,

better sensitivity was obtained by selecting SWEEP
TIME of 10 ms or 5 ms as the case may be. In either
case, the sweep occupied 10 cm of the CRO screen,
provided the CRO time setting was 0.1 ms/cm).

SWEEP MODE   : PRE TRIGGER MODE. DELAY - 0.9.

About 10% of the SWEEP corresponded to the recordings
before the Trigger and the balance after the Trigger
for this setting of DELAY.

TRIG MODE   : SINGLE

TRIG COUPLING   : DC

TRIG SOURCE   : EXT +

The Recorder was triggered externally by the 17V DC
output of POW1 by connecting same to the EXT TRIG
socket.

TRIG LEVEL   : Near mid range

INPUT COUPLING   : DC

INPUT   : To CT of Test Circuit (Fig.2.4) to facilitate the
fuse current measurement.

VOLTS FULL SCALE : 2V

This determined the full scale sensitivity of the
input amplifier. The vertical display of the CRO
was calibrated as given in the Operating Manual with
the channel setting of 0.2V/cm in the CRO. The
following calibration was obtained :

$$\text{VOLTS PER CM} = \frac{\text{VOLTS FULL SCALE}}{4.8}$$

150

(In the case of higher fuse current measurement, the VOLTS FULL SCALE setting was changed to 5V).

OFFSET   : Dial turned about 20° anticlockwise from the mid range position.

The OFFSET generally allows a DC level to be added or subtracted from the input signal so that by turning anticlockwise as above, effectively, a higher input recording can be achieved on the positive side without the signal being 'clipped'.

Transient Recorder (Slave)

SWEEP TIME   :)
)
SWEEP MODE   :)
) Same as in the Transient Recorder (Master)
TRIG MODE   :)
)
TRIG COUPLING   :)

TRIG SOURCE   : EXT +

                    No connection was made to the EXT TRIG socket.

TRIG LEVEL   : Dial turned fully anticlockwise.

INPUT COUPLING   : Same as in the Transient Recorder (Master)

INPUT   : To fuse terminals via a 10:1 probe to facilitate fuse voltage measurement.

VOLTS FULL SCALE : 50V

                    With a channel setting of 0.2 V/cm in the CRO,

$$\text{VOLTS PER CM} = \frac{\text{VOLTS FULL SCALE}}{4.8}$$

OFFSET   : Dial turned about 15° anticlockwise from the mid range position.

As the TRIG MODE control was set to SINGLE in each Recorder they 'freezed' one sweep in their memory and retained the respective records until they were armed. Arming was achieved by depressing the respective TRIG MODE controls briefly and letting them to return to their 'SINGLE' points. The 'Arm' lamp lit when the unit was armed to accept a new trigger.

Horizontal Mounting of Fuse - Results

Element : $\frac{1}{8}$ " x 0.003" (RL2) Peak Value of Prospective Current : 1270A
(r.m.s. value : 890A)

t_c (ms)	i (A)	x_c (cm)	x_a (cm)	x (cm)	dx/dt (cm.s^{-1})	dv/dt (cm^3.s^{-1})
2.5	684	-	-	0.078	-	-
2.6	701	0.055	0.055	0.110	-	-
3.0	739	0.156	0.160	0.316	520	1.258
4.0	787	0.424	0.427	0.851	570	1.379
5.0	587	0.738	0.640	1.378	375	0.907
6.0	465	0.829	0.872	1.701	270	0.653
7.0	167	0.951	0.948	1.899	68	0.164
8.0	67	1.025	1.042	2.067	20	0.048
9.0	0	1.032	0.936	1.968	0	0

Element : $\frac{1}{8}$ " x 0.003" (RL2) Peak Value of Prospective Current : 1270A
(r.m.s. value : 890A)

t_c (ms)	i (A)	x_c (cm)	x_a (cm)	x (cm)	dx/dt (cm.s^{-1})	dv/dt (cm^3.s^{-1})
2.5	676	-	-	0.078	-	-
2.8	709	0.089	0.096	0.185	-	-
3.0	716	0.178	0.163	0.341	500	1.210
4.0	798	0.437	0.420	0.857	580	1.403
4.5	799	0.428	0.545	0.973	-	-
5.0	617	0.721	0.625	1.346	400	0.968
6.0	482	0.863	0.837	1.700	280	0.677
7.0	353	0.948	1.138	2.086	200	0.484
17.0	0	0.967	0.908	1.875	0	0

Element : ⅛" x 0.003" (RL2) Peak Value of Prospective Current : 1270A
(r.m.s. value : 890A)

t_c (ms)	i (A)	x_c (cm)	x_a (cm)	x (cm)	dx/dt (cm.s^{-1})	dv/dt (cm^3.s^{-1})
2.5	671	-	-	0.080	-	-
2.8	706	0.125	0.124	0.249	-	-
3.5	764	0.355	0.280	0.655	540	1.306
4.5	655	0.585	0.590	1.175	-	-
5.0	652	0.676	0.710	1.386	430	1.040
5.5	361	0.663	0.794	1.457	-	-
6.0	333	0.803	0.838	1.641	170	0.411
7.0	187	0.865	0.875	1.740	80	0.193
8.0	36	0.882	0.761	1.643	10	0.024
9.0	0	0.942	0.774	1.816	0	0
15.0	0	0.976	0.933	1.909	0	0

Element : ⅛" x 0.003" (RL2) Peak Value of Prospective Current : 2900A
(r.m.s. value : 2030A)

t_c (ms)	i (A)	x_c (cm)	x_a (cm)	x (cm)	dx/dt (cm.s^{-1})	dv/dt (cm^3.s^{-1})
1.2	729	-	-	0.070	-	-
1.4	866	0.074	0.064	0.138	-	-
1.4	834	0.061	0.056	0.117	-	-
2.0	983	0.278	0.235	0.513	780	1.887
3.0	924	0.587	0.592	1.179	710	1.718
3.5	546	0.691	0.705	1.396	-	-
4.0	573	0.923	0.904	1.827	360	0.871
5.0	236	0.982	1.012	1.994	110	0.266
6.0	156	1.109	0.959	2.068	60	0.145
7.0	33	0.952	0.934	1.886	-	-
8.0	0	0.926	0.843	1.769	0	0

Element : $\frac{1}{8}$" x 0.003" (RL2) Peak Value of Prospective Current : 2900A
(r.m.s. value : 2030A)

t_c (ms)	i (A)	x_c (cm)	x_a (cm)	x (cm)	dx/dt (cm.s^{-1})	dv/dt (cm^3.s^{-1})
1.2	733	-	-	0.080	-	-
1.3	792	0.052	0.046	0.098	-	-
1.4	838	0.061	0.065	0.126	-	-
2.0	1004	0.257	0.276	0.533	810	1.960
3.0	755	0.581	0.597	1.178	530	1.282
3.5	497	0.673	0.644	1.317	-	-
4.0	408	0.741	0.738	1.479	230	0.556
5.0	241	0.885	0.788	1.673	110	0.266
6.0	145	1.000	0.840	1.840	70	0.169
7.0	30	1.010	0.890	1.900	-	-
8.0	0	0.878	0.912	1.789	0	0

Element : $\frac{1}{8}$" x 0.003" (RL2) Peak Value of Prospective Current: 10,000A
(Fig.2.9 (a)) (POW2: 60°) (r.m.s. value : 7700A)

t_c (ms)	i (A)	x_c (cm)	x_a (cm)	x (cm)	dx/dt (cm.s^{-1})	dv/dt (cm^3.s^{-1})
1.2	1292	0.398	0.384	0.782	1180	2.855
1.5	1270	0.602	0.546	1.148	1160	2.806
2.0	745	0.801	0.766	1.567	520	1.258
3.0	296	0.939	0.694	1.633	144	0.348
3.5	220	1.108	0.745	1.853	100	0.242
4.5	32	1.050	0.981	2.031	10	0.024
26.0	0	1.042	0.961	2.003	0	0

155

Element : ⅛" x 0.003" (RL2) Peak Value of Prospective Current : 11,000A

(POW2: 80°)   (r.m.s. value : 7700A)

t_c (ms)	i (A)	x_c (cm)	x_a (cm)	x (cm)	dx/dt (cm.s^{-1})	dv/dt (cm^3.s^{-1})
0.5	879	0.070	0.076	0.146	-	-
0.8	1251	0.200	0.220	0.420	-	-
1.0	1417	0.327	0.331	0.658	1320	3.193
1.2	1433	0.423	0.410	0.833	-	-
1.4	1415	0.491	0.535	1.026	-	-
1.6	1190	0.638	0.669	1.307	920	2.226
1.8	1238	0.700	0.720	1.420	-	-
2.0	904	0.841	0.770	1.610	640	1.548
2.5	574	0.870	0.810	1.680	280	0.677
3.0	225	0.900	0.840	1.740	50	0.121
4.0	41	1.000	0.812	1.812	-	-
6.0	0	0.877	0.965	1.842	0	0
14.2	0	0.830	0.943	1.773	0	0

Element : ⅛" x 0.006" (RL2) Peak Value of Prospective Current : 1270A

(r.m.s. value : 890A)

t_c (ms)	i (A)	x_c (cm)	x_a (cm)	x (cm)	dx/dt (cm.s^{-1})	dv/dt (cm^3.s^{-1})
4.4	917	0.154	0.200	0.354	350	1.693
5.0	927	0.290	0.335	0.625	370	1.790
6.0	725	0.470	0.457	0.927	250	1.210
7.0	566	0.520	0.550	1.070	170	0.823
8.0	347	0.576	0.640	1.216	80	0.387
9.0	90	0.635	0.612	1.247	15	0.073
10.0	0	0.525	0.676	1.201	0	0
16.0	0	0.551	0.653	1.204	0	0

Element : ⅛" x 0.006" (RL2) Peak Value of Prospective Current : 2900A
(r.m.s. value : 2030A)

t_c (ms)	i (A)	x_c (cm)	x_a (cm)	x (cm)	dx/dt (cm.s^{-1})	dv/dt (cm^3.s^{-1})
2.4	1316	0.150	0.150	0.300	610	2.952
2.8	1333	0.269	0.299	0.568	620	3.000
4.0	1263	0.607	0.484	1.091	320	1.548
5.0	1171	0.706	0.593	1.299	260	1.258
6.0	710	0.740	0.755	1.495	210	1.016
7.0	194	0.891	0.858	1.749	60	0.290
8.0	0	0.841	0.856	1.697	0	0
14.0	0	0.810	0.888	1.698	0	0

Element : ⅛" x 0.006" (RL2) Peak Value of Prospective Current: 11,000A
(POW2: 80°) (r.m.s. value : 7700A)

t_c (ms)	i (A)	x_c (cm)	x_a (cm)	x (cm)	dx/dt (cm.s^{-1})	dv/dt (cm^3.s^{-1})
1.0	1642	0.180	0.177	0.357	-	-
1.5	1863	0.316	0.350	0.666	960	4.645
2.0	1885	0.480	0.536	1.016	840	4.064
2.5	1646	0.570	0.697	1.267	500	2.419
3.0	1191	0.650	0.773	1.423	200	0.968
4.0	455	0.720	0.777	1.497	40	0.193
5.0	0	0.759	0.758	1.517	0	0
10.0	0	0.769	0.852	1.621	0	0

Element : $\frac{1}{8}$" x 0.010" (RL2) Peak Value of Prospective Current : 1270A (r.m.s. value : 890A)

t_c (ms)	i (A)	x_c (cm)	x_a (cm)	x (cm)	dx/dt (cm.s^{-1})	dv/dt (cm^3.s^{-1})
5.6	1065	0.111	0.090	0.201	-	-
6.0	1024	0.190	0.186	0.376	255	2.056
6.5	955	0.282	0.282	0.564	230	1.855
7.0	894	0.380	0.390	0.770	210	1.693
7.5	760	0.406	0.402	0.808	-	-
8.0	566	0.400	0.390	0.790	110	0.887
8.5	480	0.420	0.420	0.840	-	-
9.0	297	0.404	0.351	0.755	42	0.339
9.5	123	0.478	0.442	0.920	15	0.121
11.0	0	0.432	0.390	0.822	0	0

Element : $\frac{1}{8}$" x 0.010" (RL2) Peak Value of Prospective Current: 2900A (r.m.s. value : 2030A)

t_c (ms)	i (A)	x_c (cm)	x_a (cm)	x (cm)	dx/dt (cm.s^{-1})	dv/dt (cm^3.s^{-1})
2.8	1531	0.168	0.148	0.316	-	-
3.2	1604	0.224	0.246	0.470	480	3.871
4.0	1582	0.390	0.392	0.782	480	3.871
4.5	1391	0.489	0.477	0.966	250	2.016
5.0	1432	0.525	0.524	1.049	210	1.693
5.5	1180	0.618	0.573	1.191	-	-
6.0	1036	0.659	0.569	1.228	150	1.210
7.0	676	0.731	0.664	1.395	110	0.887
8.0	226	0.769	0.715	1.484	35	0.282
8.5	60	0.730	0.835	1.565	-	-
9.0	0	0.700	0.772	1.472	0	0

Element : ⅛" x 0.010" (RL2) Peak Value of Prospective Current: 11,000A
(POW2: 80°) (r.m.s. value : 7700A)

t_c (ms)	i (A)	x_c (cm)	x_a (cm)	x (cm)	dx/dt (cm.s^{-1})	dv/dt (cm^3.s^{-1})
1.2	1944	0.173	0.135	0.308	-	-
1.5	2103	0.242	0.246	0.488	700	5.645
1.7	2219	0.331	0.295	0.626	-	-
2.0	2169	0.372	0.383	0.755	500	4.032
2.5	2077	0.442	0.437	0.879	420	3.387
3.0	1839	0.544	0.556	1.100	380	3.064
3.5	1378	0.588	0.613	1.201	240	1.935
4.0	908	0.639	0.645	1.284	150	1.210
4.5	671	0.704	0.666	1.370	90	0.726
5.0	221	0.702	0.709	1.411	-	-
7.0	0	0.646	0.645	1.291	0	0

Element : $\frac{1}{16}$" x 0.003" (RL1) Peak Value of Prospective Current : 1270A
(r.m.s. value : 890A)

t_c (ms)	i (A)	x_c (cm)	x_a (cm)	x (cm)	dx/dt (cm.s^{-1})	dv/dt (cm^3.s^{-1})
2.8	604	0.173	0.209	0.382	-	-
3.0	615	0.272	0.271	0.543	800	0.968
3.5	602	0.394	0.499	0.893	-	-
4.0	545	0.680	0.755	1.430	720	0.871
4.5	479	0.859	0.876	1.735	680	0.823
5.0	238	1.043	1.018	2.061	380	0.460
6.0	98	0.947	1.331	2.278	80	0.097
7.0	12	1.198	1.056	2.254	-	-
8.0	0	1.268	1.277	2.545	0	0
12.0	0	1.085	1.147	2.232	0	0

Element : $\frac{1}{16}$ " x 0.003" (RL1)   Peak Value of Prospective Current : 2900A
(r.m.s. value : 2030A)

t_c (ms)	i (A)	x_c (cm)	x_a (cm)	x (cm)	dx/dt (cm.s^{-1})	dv/dt (cm^3.s^{-1})
1.6	750	0.213	0.236	0.449	-	-
2.0	771	0.419	0.449	0.868	1100	1.331
2.5	679	0.630	0.645	1.275	920	-
2.8	474	0.769	0.646	1.415	-	-
3.0	361	0.730	0.860	1.590	440	1.113
4.0	142	0.910	1.072	1.982	140	0.169
5.0	96	1.031	1.031	2.062	50	0.060
6.0	47	1.149	1.398	2.547	-	-
7.0	0	1.090	1.090	2.180	0	0
10.0	0	0.928	1.237	2.165	0	0

Element : $\frac{1}{16}$ " x 0.003" (RL1)   Peak Value of Prospective Current: 11,000A
(POW2: 80°)   (r.m.s. value : 7700A)

t_c (ms)	i (A)	x_c (cm)	x_a (cm)	x (cm)	dx/dt (cm.s^{-1})	dv/dt (cm^3.s^{-1})
0.5	803	0.110	0.113	0.223	1200	1.452
0.6	1050	0.198	0.198	0.396	1610	1.948
0.7	1139	0.254	0.268	0.522	1800	2.177
0.8	1204	0.381	0.342	0.723	2000	2.419
0.9	1242	0.420	0.460	0.880	2100	2.540
1.0	1304	0.500	0.551	1.051	2400	2.903
1.1	1304	0.695	0.703	1.398	-	-
1.15	408	0.653	0.867	1.520	-	-
1.3	0	0.639	0.807	1.446	0	0
8.0	0	0.775	0.790	1.565	0	0

Element : ¼" x 0.003" (RL4) Peak Value of Prospective Current : 1270A
(r.m.s. value : 890A)

t_c (ms)	i (A)	x_c (cm)	x_a (cm)	x (cm)	dx/dt (cm.s^{-1})	dv/dt (cm^3.s^{-1})
2.8	589	0.150	0.139	0.289	-	-
3.0	621	0.200	0.197	0.397	220	1.064
4.0	733	0.301	0.307	0.608	280	1.355
4.5	741	0.436	0.391	0.827	-	-
5.0	675	0.509	0.509	1.018	240	1.161
7.0	335	0.710	0.732	1.442	110	0.532
8.0	167	0.799	0.774	1.573	50	0.242
10.0	0	0.771	0.730	1.501	0	0

Element : ¼" x 0.003" (RL4) Peak Value of Prospective Current : 2900A
(r.m.s. value : 2030A)

t_c (ms)	i (A)	x_c (cm)	x_a (cm)	x (cm)	dx/dt (cm.s^{-1})	dv/dt (cm^3.s^{-1})
1.5	725	0.110	0.111	0.221	-	-
2.0	890	0.187	0.186	0.373	340	1.645
2.5	1040	0.302	0.325	0.627	420	2.032
3.0	1090	0.460	0.481	0.941	480	2.323
3.5	973	0.640	0.572	1.212	380	1.839
4.0	818	0.635	0.713	1.348	320	1.548
5.0	533	0.804	0.810	1.614	170	0.823
6.0	406	0.976	0.976	1.952	100	0.484
7.2	108	0.901	0.887	1.788	-	-
8.0	0	0.900	0.900	1.800	0	0
12.0	0	0.904	0.903	1.807	0	0

Element : ¼" x 0.003" (RL4) Peak Value of Prospective Current: 11,000A
(POW2: 80°)   (r.m.s. value : 7700A)

t_c (ms)	i (A)	x_c (cm)	x_a (cm)	x (cm)	dx/dt (cm.s⁻¹)	dv/dt (cm³.s⁻¹)
0.6	979	0.100	0.102	0.202	-	-
1.0	1480	0.237	0.237	0.474	680	3.290
1.5	1701	0.395	0.394	0.789	820	3.968
2.0	1600	0.516	0.606	1.172	760	3.677
2.5	1098	0.702	0.729	1.431	520	2.516
3.0	673	0.850	0.850	1.700	240	1.161
4.0	202	0.881	0.894	1.775	-	-
4.5	0	0.796	0.929	1.725	0	0
7.0	0	0.820	0.835	1.655	0	0

Element : ½" x 0.003" (RL5) Peak Value of Prospective Current : 1270A
(Fig.2.9 (b))   (r.m.s. value : 890A)

t_c (ms)	i (A)	x_c (cm)	x_a (cm)	x (cm)	dx/dt (cm.s⁻¹)	dv/dt (cm³.s⁻¹)
2.8	581	0.100	0.100	0.200	90	0.871
3.0	602	0.110	0.115	0.225	100	0.968
4.0	761	0.150	0.168	0.318	130	1.258
5.0	717	0.276	0.272	0.548	180	1.742
6.0	750	0.400	0.360	0.760	-	-
7.0	651	0.440	0.430	0.870	125	1.210
8.0	439	0.500	0.416	0.916	60	0.581
9.0	207	0.495	0.461	0.956	25	0.242
9.5	0	0.540	0.463	1.003	0	0
10.0	0	0.560	0.470	1.030	0	0

Element : ½" x 0.003" (RL5) Peak Value of Prospective Current : 2900A
(r.m.s. value : 2030A)

t_c (ms)	i (A)	x_c (cm)	x_a (cm)	x (cm)	dx/dt (cm.s^{-1})	dv/dt (cm^3.s^{-1})
1.6	755	0.092	0.095	0.187	-	-
2.0	880	0.142	0.150	0.292	170	1.645
2.5	959	0.198	0.222	0.420	190	1.839
3.0	1127	0.250	0.255	0.505	240	2.323
4.0	1321	0.410	0.400	0.810	310	3.000
5.0	1229	0.620	0.602	1.222	280	2.710
6.0	800	0.700	0.710	1.410	150	1.452
7.0	493	0.735	0.751	1.486	70	0.677
8.0	75	0.758	0.753	1.511	-	-
8.5	0	0.810	0.780	1.590	0	0
10.0	0	0.780	0.763	1.543	0	0

Element : ½" x 0.003" (RL5) Peak Value of Prospective Current: 11,000A
(POW2: 80°) (r.m.s. value : 7700A)

t_c (ms)	i (A)	x_c (cm)	x_a (cm)	x (cm)	dx/dt_1 (cm.s^{-1})	dv/dt_1 (cm^3.s^{-1})
0.5	820	0.060	0.064	0.124	160	1.548
1.0	1475	0.140	0.129	0.269	360	3.484
1.5	1786	0.300	0.268	0.568	480	4.645
1.8	1833	0.360	0.380	0.740	500	4.839
2.0	1805	0.402	0.403	0.805	470	4.548
2.5	1863	0.573	0.515	1.088	-	-
3.0	1340	0.630	0.630	1.260	320	3.097
3.5	974	0.677	0.700	1.377	200	1.935
4.0	989	0.800	0.680	1.480	-	-
5.0	0	0.761	0.739	1.500	0	0
9.0	0	0.818	0.656	1.474	0	0

Appendix 2.3 (b)

i (A)	$\frac{1}{8}$" x 0.003"		$\frac{1}{8}$" x 0.006"		$\frac{1}{8}$" x 0.010"	
	$\frac{dx}{dt}$ $(cm.s^{-1})$	$\frac{dx}{dt}/j$ $(10^{-4}cm^3.A^{-1}.s^{-1})$	$\frac{dx}{dt}$ $(cm.s^{-1})$	$\frac{dx}{dt}/j$ $(10^{-4}cm^3.A^{-1}.s^{-1})$	$\frac{dx}{dt}$ $(cm.s^{-1})$	$\frac{dx}{dt}/j$ $(10^{-4}cm^3.A^{-1}.s^{-1})$
20	5	6.05	-	-	-	-
50	15	7.26	-	-	-	-
100	35	8.47	15	7.26	10	8.06
200	86	10.40	40	9.68	22	8.87
400	216	13.06	90	10.89	56	11.29
600	384	15.48	155	12.50	100	13.44
800	580	17.54	225	13.61	140	14.11
1000	800	19.35	315	15.24	198	15.97
1200	1060	21.37	415	16.73	252	16.93
1400	1320	22.81	538	18.59	320	18.43
1600	-	-	695	21.02	410	20.66
1800	-	-	882	23.71	505	22.62
2000	-	-	-	-	615	24.80

Appendix 2.3 (b) continued

i (A)	$\frac{1}{16}$" x 0.003"		$\frac{1}{4}$" x 0.003"		$\frac{1}{2}$" x 0.003"	
	$\frac{dx}{dt}$ (cm.s^{-1})	$\frac{dx}{dt}/j$ (10^{-4} cm^3.A^{-1}.s^{-1})	$\frac{dx}{dt}$ (cm.s^{-1})	$\frac{dx}{dt}/j$ (10^{-4} cm^3.A^{-1}.s^{-1})	$\frac{dx}{dt}$ (cm.s^{-1})	$\frac{dx}{dt}/j$ (10^{-4} cm^3.A^{-1}.s^{-1})
20	10	6.05	-	-	-	-
50	30	7.26	-	-	-	-
100	70	8.47	17	8.22	10	9.68
200	188	11.37	48	11.61	21	10.16
400	464	14.03	110	13.31	50	12.10
600	784	15.81	195	15.72	92	14.84
800	1152	17.42	295	17.84	146	17.66
1000	1530	18.51	405	19.60	200	19.35
1200	2020	20.36	525	21.17	260	20.97
1400	-	-	645	22.29	330	22.81
1600	-	-	770	23.29	402	24.31
1800	-	-	-	-	480	25.81
2000	-	-	-	-	-	-

i (A)	$\log i$	$\frac{dx}{dt}/j$ $(10^{-4} cm^3.A^{-1}.s^{-1})$	$\frac{dx}{dt}/j - a$	$\log [\frac{dx}{dt}/j - a]$
100	2.000	8.3	3.7	0.568
200	2.301	10.0	5.4	0.732
400	2.602	12.5	7.9	0.898
600	2.778	14.5	9.9	0.995
800	2.903	16.4	11.8	1.072
1000	3.000	18.1	13.5	1.130
1200	3.079	19.9	15.3	1.185
1400	3.146	21.5	16.9	1.228
1600	3.204	23.0	18.4	1.265
1800	3.255	24.2	19.6	1.292
2000	3.301	25.4	20.8	1.318

Appendix 2.4

Vertical Mounting of Fuse - Results

Element : ⅛" x 0.003" (RL2)

Approximate Peak Value of Prospective Current (A)	TOTAL BURNBACK									
	Horizontal Mounting					Vertical Mounting Anode on Top				
	Arcing Time (ms)	x_c (cm)	x_a (cm)	x (cm)	x_c/x_a	Arcing Time (ms)	x_c (cm)	x_a (cm)	x (cm)	x_c/x_a
1270	5.6	1.03	0.94	1.97	1.096	5.6	1.01	0.93	1.94	1.086
1270	5.6	0.94	0.78	1.72	1.205	5.5	0.92	0.76	1.68	1.211
2900	5.6	1.10	1.00	2.10	1.100	5.6	1.10	1.00	2.10	1.100
2900	5.7	0.88	0.91	1.79	0.967	5.6	0.95	0.88	1.83	1.080
10,000 (POW2 : 60°)	3.3	1.04	0.96	2.00	1.083	3.5	1.10	1.00	2.100	1.100
10,000 (POW2 : 60°)	-	-	-	-	-	3.5	1.10	1.00	2.100	1.100
11,000 (POW2 : 80°)	3.4	0.88	0.96	1.84	0.917	3.5	0.90	0.90	1.800	1.000
11,000 (POW2 : 80°)	-	-	-	-	-	3.5	0.95	0.85	1.800	1.118

Appendix 3.1

High Power Constricted Plasma Discharge Column having Rectangular Section with Infinite Width

Let us consider 1 cm width of the thin rectangular arc (plasma) having constant thickness, 2R.

Electric Field

The energy balance between the electric power generated and the power lost by thermal conduction can be written in the general form:

$$- \text{div} (K \text{ grad } T) = GE^2 \tag{1}$$

where K = thermal conductivity,

G = electrical conductivity,

E = electric field,

T = temperature, of the plasma
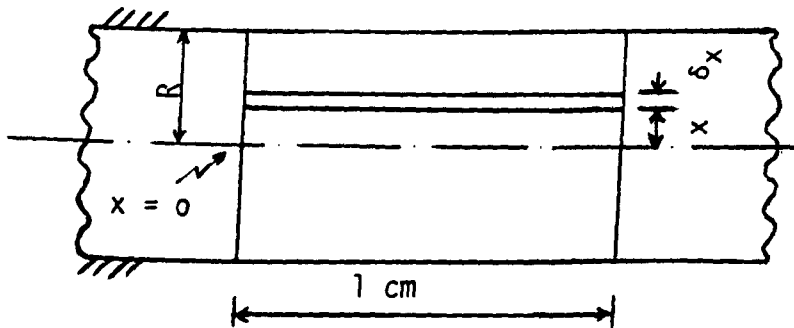
Energy loss by radiation is neglected. E is considered purely axial and uniform along the cross section and hence constant. For the case considered (1 cm width of the column), since only the dimension x is involved, Eqn (1) reduces to the simplified form,

$$- \frac{d}{dx} \left(K \frac{dT}{dx} \right) = GE^2 \tag{2}$$

The degree of ionisation in the plasma is high and hence the conductivities K and G are determined by the free electron motion and assume the values appropriate to a Lorentz gas at the temperature T as proposed by Wheeler for the high-power constricted cylindrical plasma discharge column (19)

$$K = K_0 T^{5/2} \qquad\qquad G = G_0 T^{3/2} \qquad\qquad (3)$$

The solution of Eqn (2) is simplified by replacing T by the 'heat flow potential' S

$$d S = K(T)dT \qquad\qquad\qquad (4)$$

$$S = \int_{T_0}^{T} K(T)dT$$

$$= \int_{T_0}^{T} K_0 T^{5/2} \, dT \qquad\qquad \text{(from Eqn (3))}$$

$$= K_0 \left[\tfrac{2}{7} T^{7/2} \right]_{T_0}^{T}$$

$$\simeq \tfrac{2}{7} K_0 T^{7/2} \qquad\qquad\qquad (5)$$

where T_0 = boundary temperature

which is very small compared to T and hence neglected

From Eqn (4)

$$\frac{dS}{dx} = K \frac{dT}{dx}$$

and
$$\frac{d^2S}{dx^2} = \frac{d}{dx}\left(K\,\frac{dT}{dx}\right) \tag{6}$$

From Eqns (3), (5) and (6)

$$-\frac{d^2S}{dx^2} = G_0\left(\frac{7}{2K_0}\right)^{3/7} E^2\, S^{3/7} \tag{7}$$

Multiplying Eqn (7) by $2\dfrac{dS}{dx}$ and integrating

$$\left(\frac{dS}{dx}\right)^2 = -2\,C_1 \times \frac{7}{10}\, S^{10/7} + d$$

$$= -\frac{7}{5}\,C_1\, S^{10/7} + d \tag{8}$$

where
$$C_1 = G_0\, E^2\left(\frac{7}{2K_0}\right)^{3/7} \tag{9}$$

$$d = \text{arbitrary constant}$$

It is assumed that at the axis (i.e. where $x = 0$)

$$\frac{dT}{dx} = 0$$

i.e.
$$\frac{dS}{dx} = 0$$

and
$$S = S_h$$

$$= \frac{2}{7}\,K_0\, T_h^{7/2} \qquad \text{from Eqn (5)}$$

which is a constant (10)

where T_h = axial temperature

Hence substituting in Eqn (8)

$$d = \frac{7}{5} C_1 S_h^{10/7}$$

and Eqn (8) becomes

$$\left(\frac{dS}{dx}\right)^2 = \frac{7}{5} C_1 \left(S_h^{10/7} - S^{10/7}\right)$$

i.e.

$$\left(\frac{dS}{dx}\right) = -\sqrt{\frac{7 C_1 S_h^{10/7}}{5}} \quad \frac{1}{\left[1 - \left(\frac{S}{S_h}\right)^{10/7}\right]^{-\frac{1}{2}}} \tag{11}$$

The negative sign is used in the above Eqn since $\frac{dS}{dx}$ should be negative.

Writing $\frac{S}{S_h} = m$ $\tag{12}$

where $m \leqslant 1$

and writing the series for $\left[1 - m^{10/7}\right]^{-\frac{1}{2}}$:

$$\left[1 - m^{10/7}\right]^{-\frac{1}{2}} = \left[1 + 0.5 \, m^{10/7} + 0.375 \, m^{20/7}\right.$$

$$+ 0.3125 \, m^{30/7} + 0.27344 \, m^{40/7}$$

$$\left. + 0.24609 \, m^{50/7} + \ldots \right] \tag{13}$$

The general r^{th} term is

$$\frac{-\frac{1}{2} C_r}{L_r} \, (-1)^r \, (m^{10/7})^r$$

171

where r is 0, 1, 2, ... etc.

From Eqn (12) $dS = S_h \, dm$ (14)

Using Eqns (13) and (14), Eqn (11) can be rewritten as:

$$- \sqrt{\frac{7 \, C_1 \, S_h{}^{10/7}}{5}} \;\; dx = S_h \, [1 - m^{10/7}]^{\frac{1}{2}} \, dm$$

$$= S_h \, [1 + 0.5 \, m^{10/7} + 0.375 \, m^{20/7}$$

$$\ldots .] \; dm \qquad (15)$$

Integrating both sides

$$- \sqrt{\frac{7 \, C_1 \, S_h{}^{10/7}}{5}} \;\; x + \gamma = S_h \, [m + 0.20588 \, m^{17/7}$$

$$+ 0.09722 \, m^{27/7} + \ldots .] \qquad (16)$$

The r.h.s. is a converging series with the general r^{th} term having the coefficient

$$\frac{-\frac{1}{2} \, C_r \, (-1)^r}{\lfloor r . (\frac{10r}{7} + 1)}$$

$$\gamma = \text{an arbitrary constant}$$

At the boundary (i.e. where $x = R$)

$$T = T_0$$
$$\simeq 0$$

172

so that $\quad S = S_0$

$\qquad\qquad \simeq 0$

and $\qquad m \simeq 0$

$$\therefore \qquad \gamma = R \sqrt{\frac{7\, C_1\, S_h^{10/7}}{5}} \qquad R \qquad\qquad (17)$$

Substituting Eqn (17) in Eqn (16) we get,

$$\sqrt{\frac{7\, C_1\, S_h^{10/7}}{5}} \quad (R - x) = S_h \,[m + 0.20588\, m^{17/7}$$

$$+ 0.09722\, m^{27/7} + \ldots] \qquad (18)$$

when $x = 0$, $\quad S = S_h \quad$ and $m = 1$

Hence Eqn (18) gives:

$$\sqrt{\frac{7\, C_1\, S_h^{10/7}}{5}} \quad R \simeq S_h \times 1.78$$

Substituting for C_1 from Eqn (9) and S_h from Eqn (10) in the above:

$$T_h = RE \left[\frac{49}{10}\, \frac{G_0}{K_0}\right]^{\frac{1}{2}} \quad \frac{1}{1.78} \qquad (19)$$

The values of K_0 and G_0 for a Lorentz gas are given by Spitzer (1956) as:

$$K_0 = \frac{7.81 \times 10^{-12}}{Z \ln \Lambda} \qquad (J\ s^{-1} K^{-1} cm^{-1})$$

$$G_0 = \frac{2.63 \times 10^{-4}}{Z \ln \Lambda} \qquad (\Omega^{-1} cm^{-1}) \qquad (20)$$

where Z is the charge on the plasma ions and Λ is the Coulomb cut-off.

Substituting these values in Eqn (19)

$$T_h \simeq 7.22 \times 10^3 \text{ RE} \tag{21}$$

(c.f. $T_h = 5.04 \times 10^3$ RE

for cylindrical plasma column (19))

Current

Again considering 1 cm width of the column,

$$
\begin{aligned}
J(x) &= GE \\
&= G_0 \, T(x)^{3/2} \, E \quad \text{(from Eqn (3))} \\
&= \text{current density at distance x from the axis (A.cm}^{-1})
\end{aligned}
$$

$$i = 2 \int_0^R J(x) \, dx$$

$$= 2 \int_0^R G_0 \, E \, T(x)^{3/2} \, dx \quad \text{(A)} \tag{22}$$

where i = current per cm width of the column

From Eqns (5) and (12) it can be shown:

$$T(x)^{3/2} = m^{3/7} \, T_h^{3/2} \tag{23}$$

174

Rewriting Eqn (15)

$$- \sqrt{\frac{7 \, C_i \, S_h^{10/7}}{5}} \cdot dx = S_h \, (1 - m^{10/7})^{\frac{1}{2}} \, dm$$

Substituting for C_i from Eqn (9) and S_h using Eqn (10) in the above,

$$dx = - \sqrt{\frac{10 \, K_0}{G_0}} \; \frac{T_h}{7E} \, (1 - m^{10/7})^{\frac{1}{2}} \, dm \qquad (24)$$

Substituting Eqns (23) and (24) in Eqn (22)

$$i = -2 \int_{1}^{0} G_0 \, E \, (m^{3/7} \, T_h^{3/2}) \; \frac{10 \, K_0}{G_0} \cdot \frac{T_h}{7E} \, (1 - m^{10/7})^{\frac{1}{2}} \, dm$$

$$= \frac{2}{7} \sqrt{10 \, G_0 \, K_0} \; T_h^{5/2} \, [\frac{7}{5} \, (1 - m^{10/7})^{\frac{1}{2}}]_{1}^{0}$$

$$= 2 \sqrt{\frac{2 \, G_0 \, K_0}{5}} \; T_h^{5/2} \qquad \text{(A)} \qquad (25)$$

Thus $$T_h^{5/2} = \frac{1}{2} \sqrt{\frac{5}{2 \, G_0 \, K_0}} \; i$$

$$= 1.744 \times 10^7 (Z \ln \Lambda) \, i \qquad (26)$$

(c.f. $T_h^{5/2} = 0.900 \times 10^7 (Z \ln \Lambda) \, R^{-1} \, i$

for cylindrical plasma column (19))

Eliminating T_h from Eqns (21) and (26)

$$E = 0.109 \, (Z \ln \Lambda)^{2/5} \, R^{-1} \, i^{2/5} \qquad (V.cm^{-1}) \qquad (27)$$

175

(c.f. $E = 0.120 \ (Z \ \ln \Lambda)^{2/5} \ R^{-7/5} \ i^{2/5}$ $(V.cm^{-1})$

for cylindrical plasma column (19)).

Appendix 3.2

Pinch Pressure in a Conducting Column having a Rectangular Cross Section

A current i(A) flows through the column having a rectangular cross section   2a x 2b   (m x m)

j, the current density $= i/4ab$ $(A.m^{-2})$
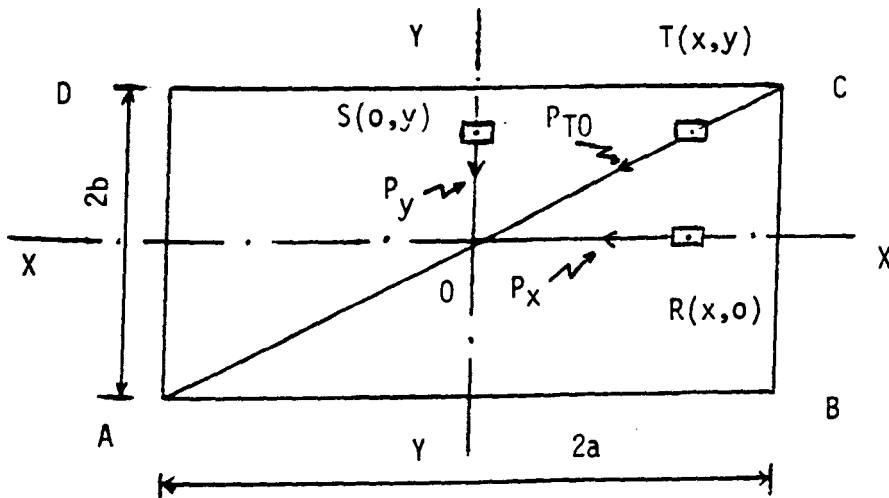
Pinch pressure at R in XX

At $R(x,o)$, flux density along XX, $B_x = o$

Flux density along a direction parallel to YY, B_y is worked out as outlined by Hague (24).

Force on element $(\Delta x \; x \; \Delta y)$ at R

$\qquad = \Delta F$

$\qquad = B_y.j.(\Delta x.\Delta y)$ per unit length

and acts along $\overrightarrow{RO}$ on an area of $(\Delta y \; x \; 1)$

∴ The pressure on the element acting towards the centre o = ΔP_x

$$= B_y.j.\Delta x$$

The total pressure acting at R

$$= \sum_{x=x}^{a} \Delta P_x$$

∴ $P_x = \int_{x}^{a} B_y.j.dx.$ (1)

Substituting the value of B_y and integrating, it can be shown:

$$P_x = \frac{i^2}{8a^2b^2} \times 10^{-7} \left[(4a^2-b^2) \cot^{-1} \frac{2a}{b} + \{b^2-(a+x)^2\} \cot^{-1} \frac{a+x}{b} \right.$$

$$+ \{b^2 -(a-x)^2\} \cot^{-1} \frac{a-x}{b} + 2ab \log (4a^2+b^2)$$

$$- b(a+x) \log \{(a+x)^2 + b^2\} -b(a-x) \log \{(a-x)^2+b^2\}$$

$$\left. - b^2\pi/2 -(a^2-x^2) \pi \right] \qquad N.m^{-2} \qquad\qquad (2)$$

(i) At the surface of the column on the x axis x = a.

Substituting this value in Eqn (2):

$P_x = o.$

(ii) At the centre o, x = o and P_x is a maximum. From Eqn (2):

$$P_{x(o)} = \frac{i^2}{8a^2b^2} \times 10^{-7} \left[(4a^2-b^2) \cot^{-1} \frac{2a}{b} + 2(b^2-a^2) \cot^{-1} \frac{a}{b} \right.$$

$$- b^2\pi/2 + 2ab \log \left(\frac{4a^2+b^2}{a^2+b^2}\right) - a^2\pi] \qquad (3)$$

Pinch pressure at S in YY

At $S(o,y)$, flux density along YY, $B_y = o$

B_x is worked out as outlined by Hague (24)

The force on the element $(\Delta x.\Delta y)$ at S can be shown to be acting along YY towards the origin o, giving rise to a pinch pressure along SO.

$$\delta F = B_y.j.(\Delta x.\Delta y) \text{ per unit length.}$$

As done for the pinch pressure in the XX axis, the pinch pressure at S can be shown to be:

$$P_y = \int_y^b B_x.j.dy$$

$$= \frac{i^2}{8a^2b^2} \times 10^{-7} [4b^2-a^2) \cot^{-1} \frac{2b}{a} + \{a^2-(b+y)^2\} \cot^{-1} \frac{b+y}{a}$$

$$+ \{a^2-(b-y)^2\} \cot^{-1} \frac{b-y}{a} + 2ab \ lot \ (4b^2+a^2)$$

$$- a(b+y) \log \{(b+y)^2 + a^2\} - a(b-y) \log \{(b-y)^2 + a^2\}$$

$$- a^2\pi/2 - (b^2-y^2) \ \pi] \qquad (N.m^{-2}) \qquad (4)$$

(a) At the surface of the column on the Y axis, $y = b$.

Substituting this value in Eqn. (4):

$$P_y = o$$

(b) At the centre 0, $y = o$ and P_y is a maximum.

From Eqn (4):

$$P_{y(o)} = \frac{i^2}{8a^2b^2} \times 10^{-7}[(4b^2-a^2)\ cot^{-1}\ \frac{2b}{a} + 2(a^2-b^2)\ cot^{-1}\ \frac{b}{a}$$

$$- a^2\pi/2 + 2ab\ log\ (\frac{4b^2+a^2}{b^2+a^2}) - b^2\pi] \qquad (5)$$

Pinch pressure at T in diagonal AC

At T(x,y), flux density comprises two components:

　　　(1) B_x in a direction parallel to XX

　　　(2) B_y in a direction parallel to YY

Analysis as for the above two is carried out. In general there would be two components for the pressure acting at T one along TO and the other (a smaller one) at right angles.

The pressure at the origin along CO is worked out to be:

$$P_d = \frac{i^2}{16a^2b^2} \times 10^{-7}[\frac{ab}{(a^2+b^2)^2}\ (3a^4+3b^4+2a^2b^2)\ log\ 4$$

$$+ (a^2\ cot^{-1}\ \frac{a}{b} + b^2\ cot^{-1}\ \frac{b}{a})$$

$$+ (\frac{a^2-b^2}{2})\ (cot^{-1}\ \frac{a}{b} - 2\ cot^{-1}\ (\frac{a^2-b^2}{2ab}) + cot^{-1}\ (-\frac{b}{a}))$$

$$- \frac{\pi}{4}\ (a^2+b^2) - \pi(a^2+b^2)] \qquad (6)$$

The following rectangular sections are considered to illustrate the difference between the values of the pinch pressures at the centre along the principal axes and the diagonals, by using the above expressions:

(1) Rectangular section with a = 2b

      (a) $P_{x(o)} = (\frac{i^2}{s} \times 10^{-7}) \times (2.087)$ $(N.m^{-2})$

      (b) $P_{y(o)} = (\frac{i^2}{s} \times 10^{-7}) \times (0.226)$ $(N.m^{-2})$

      (c) $P_d = (\frac{i^2}{s} \times 10^{-7}) \times (2.323)$ $(N.m^{-2})$

      (diagonal)

      where   s =   area of section in m^2

(2) Rectangular section with a = 4b

      (a) $P_{x(o)} = (\frac{i^2}{s} \times 10^{-7}) \times (5.078)$ $(N.m^{-2})$

      (b) $P_{y(o)} = (\frac{i^2}{s} \times 10^{-7}) \times (0.059)$ $(N.m^{-2})$

      (c) $P_d = (\frac{i^2}{s} \times 10^{-7}) \times (5.320)$ $(N.m^{-2})$

      (diagonal)

(3) Square section with a = b

      (a) $P_{x(o)} = P_{y(o)}$

          $= (\frac{i^2}{s} \times 10^{-7}) \times (0.744)$ $(N.m^{-2})$

      compare with circular section having radius a   (m)

$$P_{(o)} = (\frac{i^2}{s} \times 10^{-7}) \times (1) \qquad (N.m^{-2})$$

where   s = area of the section in m^2

Appendix 3.3

Constant Length (1 cm) Fuse Arc Experiments - Results

$$A_{obs} = 0.9 \frac{i^{0.47}}{E^{1.18}} \quad (cm^2)$$

$$\frac{dA}{dt} = \{0.08 + 0.55 (1 - e^{-\frac{t}{10}})\} \frac{E\,i}{3800} \quad (cm^2.s^{-1})$$

where t is time in ms from the commencement of arc

$$A_{calc}(t' + \Delta t_1) = A_{calc}(t') + \frac{dA}{dt}(t') \times \Delta t_1$$

where t' is time in ms from the initiation of fuse current

Test 1 :   Element - $\frac{1}{16}$" x 0.003" (RL1)

Inductor Tap No.1   POW2 : 18°

Time to commencement of arc, t_1' = 2.2 ms

t' (ms)	E (V.cm^{-1})	i (A)	dA/dt (cm^2.s^{-1})	A_{calc} (cm^2)	A_{obs} (cm^2)
2.2	440	792	7.34	0.0157	0.0157
2.3	360	500	4.05	0.0165	0.0161
2.8	262	329	2.54	0.0185	0.0192
3.2	241	325	2.73	0.0195	0.0211
3.6	232	329	3.05	0.0206	0.0222
4.0	228	367	3.76	0.0218	0.0238
4.4	224	379	4.21	0.0233	0.0247
4.8	222	383	4.61	0.0250	0.0251
5.2	219	396	5.08	0.0268	0.0259
5.6	213	388	5.19	0.0289	0.0265
6.0	200	375	5.01	0.0309	0.0281
6.4	184	329	4.28	0.0329	0.0292
6.8	167	288	3.58	0.0347	0.0307
7.2	143	213	2.38	0.0361	0.0320
8.0	96	104	0.85	0.0380	0.0366
8.5	78	0	0	0.0384	-

From Fulgurite Measurement: A $\simeq$ 0.04 (cm^2)

Test 2 :   Element - $\frac{1}{16}$" x 0.003" (RL1)

Inductor Tap No.1   POW2 : 18°

Tiem to commencement of arc, t_1' = 2.2 ms

t' (ms)	E (V.cm^{-1})	i (A)	dA/dt (cm^2.s^{-1})	A_{calc} (cm^2)	A_{obs} (cm^2)
2.2	449	833	7.87	0.0157	0.0157
2.3	359	500	4.04	0.0165	0.0161
2.8	257	279	2.11	0.0186	0.0182
3.2	244	276	2.34	0.0194	0.0193
4.0	240	281	3.03	0.0213	0.0198
5.2	224	333	4.37	0.0249	0.0232
6.0	209	328	4.58	0.0284	0.0251
6.4	190	297	3.99	0.0302	0.0268
6.8	169	250	3.18	0.0318	0.0283
7.2	145	182	2.06	0.0331	0.0293
8.0	99	83	0.70	0.0347	0.0317
8.4	86	0	0	0.0350	-

Test 3 : Element - $\frac{1}{16}$ " x 0.003" (RL1)

Inductor Tap No.1   POW2 : 5°

Time to commencement of arc, t_1' = 2.6 ms

t' (ms)	E (V.cm^{-1})	i (A)	dA/dt (cm^2.s^{-1})	A_{calc} (cm^2)	A_{obs} (cm^2)
2.6	404	859	7.31	0.0181	0.0181
2.8	328	547	4.29	0.0196	0.0187
3.2	249	391	2.87	0.0213	0.0221
3.6	239	385	3.20	0.0224	0.0231
4.0	229	411	3.76	0.0237	0.0250
4.4	229	458	4.71	0.0252	0.0263
4.8	229	479	5.44	0.0271	0.0269
5.2	219	505	5.99	0.0293	0.0290
6.0	211	531	7.03	0.0341	0.0311
6.4	201	521	7.00	0.0369	0.0326
7.2	179	422	5.62	0.0425	0.0339
8.0	140	260	2.96	0.0470	0.0360
8.4	120	208	2.11	0.0481	0.0389
9.1	74	0	0	0.0496	-

Test 4 :   Element - $\frac{1}{16}$" x 0.003" (RL1)

Inductor Tap No.1   POW2 : 80^0

Time to commencement of arc, $t_1' = 1.1$ ms

t' (ms)	E (V.cm^{-1})	i (A)	dA/dt (cm^2.s^{-1})	A_{calc} (cm^2)	A_{obs} (cm^2)
1.1	406	1380	11.80	0.0225	0.0225
1.2	344	1042	8.06	0.0237	0.0240
1.4	282	937	6.69	0.0253	0.0288
1.8	251	781	6.04	0.0280	0.0303
2.0	238	755	6.02	0.0292	0.0318
2.4	225	677	5.89	0.0316	0.0323
3.0	196	547	4.94	0.0351	0.0344
4.0	145	338	2.82	0.0401	0.0391
5.0	82	104	0.58	0.0429	0.0440
5.3	72	0	0	0.0431	-

From Fulgurite Measurement: A $\simeq$ 0.04 (cm^2)

Test 5 :   Element - $\frac{1}{16}$" x 0.003" (RL1)

Inductor Tap No.6   POW2 : 18^0

Time to commencement of arc, t_1' = 3.9 ms

t' (ms)	E (V.cm^{-1})	i (A)	dA/dt (cm^2.s^{-1})	A_{calc} (cm^2)	A_{obs} (cm^2)
3.9	426	646	5.79	0.0149	0.0149
4.0	396	583	5.19	0.0154	0.0154
4.2	344	504	4.39	0.0165	0.0170
4.6	272	396	3.32	0.0183	0.0201
5.0	242	354	3.10	0.0196	0.0218
5.8	209	292	2.81	0.0221	0.0237
7.0	157	196	1.83	0.0254	0.0276
7.8	122	121	1.00	0.0269	0.0296
8.2	100	75	0.54	0.0273	0.0300
8.6	72	37	0.20	0.0275	0.0316
9.0	53	17	0.07	0.0276	0.0315
9.2	42	0	0	0.0276	-

Test 6 : Element - $\frac{1}{16}$" x 0.003" (RL1)

No Inductor   POW2 : 80°

Time to commencement of arc, t_1' = 1.0 ms

t' (ms)	E (V.cm^{-1})	i (A)	dA/dt (cm^2.s^{-1})	A_{calc} (cm^2)	A_{obs} (cm^2)
1.0	449	1354	12.80	0.0198	0.0198
1.1	376	958	8.10	0.0211	0.0207
1.2	344	917	7.54	0.0219	0.0226
1.4	313	812	6.79	0.0234	0.0238
1.6	282	729	6.06	0.0248	0.0256
2.0	249	667	5.78	0.0272	0.0284
2.4	235	646	6.07	0.0295	0.0300
3.0	209	542	5.36	0.0331	0.0317
3.4	186	490	4.73	0.0353	0.0347
4.0	149	333	2.91	0.0381	0.0376
4.4	126	250	1.98	0.0393	0.0401
5.0	77	83	0.44	0.0405	0.0427
5.2	58	42	0.17	0.0405	0.0433
5.26	58	0	0	0.0406	-

189

Test 7 : Element - $\frac{1}{8}$ " x 0.003" (RL2)

Inductor Tap No.1   POW2 : 18°

Time to commencement of arc, t_1' = 3.4 ms

t' (ms)	E (V.cm^{-1})	i (A)	dA/dt (cm^2.s^{-1})	A_{calc} (cm^2)	A_{obs} (cm^2)
3.4	412	1562	13.55	0.0234	0.0234
3.6	334	1159	9.26	0.0261	0.0261
3.8	303	1042	8.44	0.0280	0.0278
4.2	256	885	7.29	0.0314	0.0314
4.6	235	838	7.37	0.0343	0.0339
5.0	222	786	7.41	0.0372	0.0352
5.4	209	768	7.59	0.0402	0.0374
5.8	190	734	7.39	0.0432	0.0409
6.2	182	677	6.95	0.0462	0.0415
6.6	167	625	6.33	0.0490	0.0442
7.0	146	521	4.93	0.0515	0.0476
7.4	132	422	3.83	0.0535	0.0485
7.8	122	365	3.23	0.0550	0.0497
8.2	94	214	1.53	0.0563	0.0526
8.6	67	99	0.53	0.0569	0.0546
8.8	55	0	0	0.0570	-

Test 8 :   Element - $\frac{1}{8}$" x 0.003" (RL2)

Inductor Tap No.1   POW2 : 18°

Time to commencement of arc, $t_1' = 3.4$ ms

t' (ms)	E (V.cm^{-1})	i (A)	dA/dt (cm^2.s^{-1})	A_{calc} (cm^2)	A_{obs} (cm^2)
3.4	455	1406	13.47	0.0198	0.0198
3.6	390	1172	10.93	0.0225	0.0218
4.0	296	854	7.45	0.0269	0.0261
4.8	234	755	7.06	0.0328	0.0325
5.2	217	729	7.10	0.0357	0.0349
6.0	188	667	6.80	0.0413	0.0396
6.8	159	542	5.41	0.0468	0.0438
7.2	144	437	4.20	0.0489	0.0445
8.0	103	250	1.92	0.0523	0.0508
8.4	84	156	1.02	0.0531	0.0518
8.8	45	0	0	0.0535	-

From Fulgurite Measurement: $A \simeq 0.07 (cm^2)$

Test 9 : Element - $\frac{1}{8}$" x 0.003" (RL2)

No Inductor POW2 : 80^0

Time to commencement of arc, t_1' = 1.7 ms

t' (ms)	E (V.cm^{-1})	i (A)	dA/dt (cm^2.s^{-1})	A_{calc} (cm^2)	A_{obs} (cm^2)
1.7	428	2083	18.77	0.0256	0.0256
1.8	370	1615	13.44	0.0275	0.0270
1.9	353	1593	13.45	0.0289	0.0284
2.0	318	1500	12.08	0.0302	0.0312
2.4	263	1229	10.00	0.0350	0.0355
3.0	219	990	8.39	0.0410	0.0399
3.4	188	854	7.01	0.0444	0.0445
4.0	151	604	4.63	0.0486	0.0490
4.4	128	469	3.32	0.0504	0.0529
5.0	87	250	1.34	0.0524	0.0620
5.4	59	94	0.36	0.0530	0.0619
5.6	40	0	0	0.0530	-

From Fulgurite Measurement: A ≃ 0.08 (cm^2)

Test 10 :   Element - ⅛" x 0.006" (RL2)

Inductor Tap No.1   POW2 : 18°

Time to commencement of arc, t_1' = 6.0 ms

t' (ms)	E (V.cm^{-1})	i (A)	dA/dt (cm^2.s^{-1})	A_{calc} (cm^2)	A_{obs} (cm^2)
6.0	377	1354	10.75	0.0243	0.0243
6.1	344	1187	9.18	0.0254	0.0255
6.4	287	969	7.43	0.0291	0.0287
6.8	230	729	5.40	0.0320	0.0326
7.2	199	563	4.19	0.0342	0.0342
7.6	157	396	2.64	0.0359	0.0384
8.0	126	260	1.55	0.0369	0.0408
8.4	108	208	1.17	0.0376	0.0441
8.9	69	0	0	0.0381	-

From Fulgurite Measurement: $A \simeq 0.05 (cm^2)$

Test 11 : Element - $\frac{1}{8}$" x 0.006" (RL2)

No Inductor POW2 : 80°

Time to commencement of arc, t_1' = 3.3 ms

t'	E	i	dA/dt	A_{calc}	A_{obs}
(ms)	$(V.cm^{-1})$	(A)	$(cm^2.s^{-1})$	(cm^2)	(cm^2)
3.3	415	2083	18.20	0.0266	0.0266
3.4	365	1719	14.11	0.0284	0.0283
3.5	334	1562	12.48	0.0298	0.0300
3.6	313	1447	11.47	0.0311	0.0312
3.8	266	1135	8.49	0.0334	0.0338
4.0	238	989	7.26	0.0351	0.0361
4.2	204	859	5.87	0.0365	0.0405
4.4	183	703	4.65	0.0377	0.0419
4.6	162	521	3.27	0.0386	0.0421
4.8	144	417	2.47	0.0393	0.0435
5.0	121	312	2.12	0.0398	0.0466
5.2	108	234	1.16	0.0402	0.0466
5.4	89	146	0.63	0.0404	0.0469
5.6	68	62	0.21	0.0405	0.0431
5.72	54	0	0	0.0406	-

Test 12 : Element - ¼" x 0.003" (RL4)

Inductor Tap No.1   POW2 : 18°

Time to commencement of arc, $t_1' = 6.1$ ms

t' (ms)	E (V.cm^{-1})	i (A)	dA/dt (cm^2.s^{-1})	A_{calc} (cm^2)	A_{obs} (cm^2)
6.1	383	1354	10.92	0.0239	0.0239
6.2	360	1250	10.12	0.0250	0.0247
6.4	315	1052	8.39	0.0270	0.0267
6.8	244	781	5.88	0.0303	0.0314
7.2	209	573	4.33	0.0327	0.0326
7.6	167	354	2.44	0.0344	0.0338
8.0	147	271	1.84	0.0354	0.0347
8.4	113	187	1.07	0.0361	0.0397
8.6	105	135	0.75	0.0363	0.0372
8.8	65	0	0	0.0365	-

From Fulgurite Measurement: $A \simeq 0.05$(cm^2)

Test 13 : Element - $\frac{1}{4}$" x 0.003" (RL4)

No Inductor   POW2 : 80°

Time to commencement of arc, t_1' = 3.2 ms

t' (ms)	E (V.cm^{-1})	i (A)	dA/dt (cm^2.s^{-1})	A_{calc} (cm^2)	A_{obs} (cm^2)
3.2	457	2187	21.04	0.0243	0.0243
3.3	407	1823	16.69	0.0264	0.0256
3.5	344	1531	13.34	0.0297	0.0287
3.6	313	1344	11.24	0.0310	0.0302
3.8	261	1083	8.33	0.0333	0.0338
4.0	246	1010	8.00	0.0350	0.0351
4.2	211	833	6.12	0.0366	0.0384
4.4	188	677	4.76	0.0378	0.0399
4.6	167	521	3.48	0.0387	0.0406
4.8	147	385	2.40	0.0394	0.0409
5.0	134	313	1.88	0.0399	0.0414
5.2	126	260	1.55	0.0403	0.0408
5.4	110	146	0.80	0.0406	0.0365
5.56	86	0	0	0.0407	-

Appendix 3.4

Voltage Gradient vs Current for Two of the Constant Length Fuse Arc

Experiments

Test 1 :   Element - $\frac{1}{16}$" x 0.003" (RL1)

Inductor Tap No. 1   POW2 : 18°

Time to commencement of arc, t_1' = 2.2 ms

t'	i	E_{obs}	dA/dt	A_{calc}	E_{calc}
(ms)	(A)	$(V.cm^{-1})$	$(cm^2.s^{-1})$	(cm^2)	$(V.cm^{-1})$
2.2	792	440	7.34	0.0157	440
2.3	500	360	4.05	0.0165	360
2.8	329	262	2.54	0.0185	276
3.2	325	241	2.73	0.0195	262
3.6	329	232	3.05	0.0206	252
4.0	367	228	3.76	0.0218	251
4.4	379	224	4.21	0.0233	240
4.8	383	222	4.61	0.0250	227
5.2	396	219	5.08	0.0268	217
5.6	388	213	5.19	0.0289	202
6.0	375	200	5.01	0.0309	188
6.4	329	184	4.28	0.0329	169
6.8	288	167	3.58	0.0347	153
7.2	213	143	2.38	0.0361	131
8.0	104	96	0.85	0.0380	94
8.5	0	78	0	0.0384	-

Test 13 :   Element - ¼" x 0.003" (RL4)

No Inductor   POW2 : 80°

Time to commencement of arc, t_1' = 3.2 ms

t'	i	E_{obs}	dA/dt	A_{calc}	E_{calc}
(ms)	(A)	$(V.cm^{-1})$	$(cm^2.s^{-1})$	(cm^2)	$(V.cm^{-1})$
3.2	2187	457	21.04	0.0243	457
3.3	1823	407	16.69	0.0264	405
3.5	1531	344	13.34	0.0297	341
3.6	1344	313	11.24	0.0310	312
3.8	1083	261	8.33	0.0333	270
4.0	1010	246	8.00	0.0350	251
4.2	833	211	6.12	0.0366	224
4.4	677	188	4.76	0.0378	200
4.6	521	167	3.48	0.0387	177
4.8	385	147	2.40	0.0394	154
5.0	313	134	1.88	0.0399	141
5.2	260	126	1.55	0.0403	129
5.4	146	110	0.80	0.0406	102
5.56	0	86	0	0.0407	-

Appendix 3.5

Stored Energy of Fuse Arc Column

PV

Used experimental results of 1 cm (constant length) arc test (Test 7 of Appendix 3.3)

Element : $\frac{1}{8}$" x 0.003" (RL2)

Inductor Tap No.1   POW2 : 18°

t' (ms)	i (A)	E i (10^3 W.cm^{-1})	A_{obs} (cm^2)	Pressure (10^4 .N.m^{-1})	p Δ V (10^{-3} J)
3.4	1562	643.5	0.0234	10.43 k	2.44 k
3.8	1042	315.7	0.0278	3.91 k	3.15 k
4.2	885	226.6	0.0314	2.49 k	1.15 k
4.6	838	196.9	0.0339	2.07 k	0.57 k
5.0	786	174.5	0.0352	1.76 k	0.25 k
5.4	768	160.5	0.0374	1.58 k	0.37 k
5.8	734	139.5	0.0409	1.32 k	0.51 k
6.2	677	123.2	0.0415	1.10 k	0.07 k
6.6	625	104.4	0.0442	0.88 k	0.27 k
7.0	521	76.1	0.0476	0.57 k	0.25 k
7.4	422	55.7	0.0485	0.37 k	0.04 k
7.8	365	44.5	0.0497	0.27 k	0.04 k
8.2	214	20.1	0.0526	0.08 k	0.05 k
8.6	99	6.6	0.0546	0.01 k	0.01 k
8.8	0	0	-	0	0

t' = time in ms from the initiation of fuse current

i = instantaneous value of arc current (A)

$E i$ = instantaneous power in column $(W.cm^{-1})$

A_{obs} = area of lumen section using expression in Eqn (3.44) (cm^2)

Pinch pressure, $p = k \dfrac{i^2}{A_{obs}} \times 10^{-3}$ $(N.m^{-2})$

k = a factor to account for the shape of the lumen section ($k = 1$ for a circular section and 0.744 for a square section if pressure along the principal axes is considered)

ΔV = change in volume of lumen in any discrete time interval considered

Pinch pressure is a maximum at the centre and reduces to zero at the boundary of the lumen section at any time. Lumen pressure, should be generally higher than the pinch pressure for the lumen to expand. Both pressures collapse at arc extinction. For the purpose of estimating PV during the arcing period, the average lumen pressure, P at any instant is considered equal to the pinch pressure, p at the centre with $k = 1$.

Hence $PV = \sum p \Delta V$ (in the arcing period)

$\qquad\qquad = 0.009$ J   (1)

Column input energy in the arcing period

$\qquad\qquad = \sum E i \Delta t$

$\qquad\qquad = 915$ J   (2)

Specific Enthalpy

From the tables for Nitrogen plasma (33) the following parameters were obtained:

For temperature of $10,000^{O}$ K,

Density, $\rho = 16.7 \times 10^{-6}$ $g.cm^{-3}$

Specific enthalpy $= 12.78$ k cal.g^{-1}

$\therefore$ Enthalpy $= 16.7 \times 10^{-6} \times 12.78 \times 10^3 \times 4.2$ J.cm^{-3}

                 $= 0.9$ J.cm^{-3}

$\therefore$ Enthalpy in 1 cm plasma. (with $A \simeq 0.06 \, (cm^2)$)

                 $= 0.06 \times 0.9$ J

                 $= 0.054$ J   (3)

The same value is assumed for the fuse arc plasma as it could be of the same order although the fuse arc plasma comprises vapours of silver and silica.

Internal energy $=$ Enthalpy $-$ PV

In Eqn (1) PV has been shown to be neglibgibly small and is neglected.

$\therefore$ Internal Energy $=$ Enthalpy

                 $= 0.054$ J

Hence $\dfrac{\text{Internal Energy}}{\text{Total column input energy}} = \dfrac{0.054}{915}$

                             $= 0.006\%$

Comparison between Electrode Fall Voltages Observed (U_B(obs)) and Calculated (U_B(calc))

$$U_B \text{ (calc)} = 15.0 + i^{0.39} \qquad (V)$$

i (A)	U_B (obs)	U_B (calc)
617	21	27
584	21	27
751	22	28
792	24	29
625	21	27
1835	32	34
2208	31	35

Appendix 4.2

Comparison between Ignition Voltages Observed (U_0(obs)) and Calculated (U_0(calc)).

$$U(\text{calc}) = 0.4 \; 1' \sqrt{\frac{i_0}{s_z}} + n_s \, (15.0 + i_0^{0.39}) \; V.$$

i_0 (A)	s_z ($10^{-4} \times cm^2$)	$1'$ (cm)*	U_B(calc) (V)	E_0(calc) ($V.cm^{-1}$)	U_0(calc) (V)	U_0(obs) (V)
808	9.144	0.306	28.6	376	172	169
800	9.144	0.313	28.6	374	174	167
1000	9.144	0.301	29.8	418	186	187
1450	9.144	0.314	32.1	504	222	235
1567	9.144	0.316	32.6	524	231	239
1750	18.290	0.243	33,4	391	162	156
1292	18.290	0.182 (1)	31.3	336	93	106
1333	14.310	0.185 (1)	31.5	386	103	118
1750	14.310	0.120 (1)	33.4	442	87	100
2604	23.930	0.222	36.5	417	166	167
2604	23.930	0.228	36.5	417	168	165
435	5.080	0.10 (1)	25.7	370	63	52
710	5.080	0.10 (1)	27.9	473	75	85
704	5.810	0.08 (1)	30.4	440	63	62

* In column for $1'$, (1) refers to where there was 1 notch considered (i.e. $n_s = 1$).

Appendix 5.1

Effect of Varying Time step, XL and XXL on Arcing - Results of Arc Simulation Program

Element parameters
Element : $\frac{1}{8}$" x 0.003" (RL2)
Notch length : 0.08 cm
Notch width : 0.08 cm
Single notched element

Circuit conditions
RMS voltage : 240 V
Z : 0.271 Ω
ϕ : 27.6°
θ : 18°

A_e : 0.017 cm^2
Prearcing time : 2.5 ms
Current at disruption : 750 A

XL (cm)	XXL (cm)	Arcing Time (ms)	Arc Length (cm)	Arcing i^2t (A^{2}s)	Arcing Energy (J)
Time step : 0.10 ms					
0.25	7.80	5.81	1.492	1318	508
1.00	7.80	5.79	1.494	1315	509
2.00	7.80	5.80	1.498	1312	508
0.25	1.25	5.97	1.250	1351	521
1.00	1.40	5.90	1.40	1317	511
Time step : 0.20 ms					
0.25	7.8	6.71	1.498	1344	507
Time step : 0.05 ms					
0.25	7.8	5.96	1.494	1309	511

Observed values
arc length $\simeq$ 1.75 cm
arcing time $\simeq$ 5.9 ms

References

1. Wilkins, R.

(1977) "Semiempirical models of arcing in current-limiting fuses" 3rd Int. Symp. on Switching Arc Phenomena, Lodz, Poland, pp 338 - 342

2. Kroemer, H.

(1942) "Der Lichtbogen an Schmelzleitern in Sand" Archiv für Elektrotechnik, 36, p 455

3. Schonholzer, E.T.

(1972) "Fuse protection for power thyristors" IEEE Transations on Industry Applications, 1A - 8, No.3, p 301

4. Oliver, R.

(1976) "The behaviour of d.c. overcurrent arcs in cartridge fuselinks" Int. Conf. on Electric Fuses and their applications, Liverpool Polytechnic, p 101

5. Wright, A. and Beaumont, K.J.

(1976) "Analysis of high-breaking - capacity fuselink arcing phenomena" Proc. IEE, 123, p 252

6. Danders, M.

(1977) "Gleichungsansatz für den zeitlichen Verlauf der Schaltspannung von schmelzsicherungen zur Simulation von Störungsfallen in Halbleiter - Stromrichteranlagen"

		Wiss. Ber. AEG - TELEFUNKEN, 50, p 32
7.	Ossowicki, J.	(1973) Second Int. Symp. Switching Arc Phenomena, Lodz, Poland, Part II : Post Conference Materials pp 178-180
8.	Turner, H.W. and Turner, C.	(1977) "Calculation of the burnback rate of a fuse element and its relation to contact erosion" 3rd Int. Symp. on Switching Arc Phenomena, Lodz, Poland, p 334
9.	Dolegowski, M.	(1976) "Calculation of the course of the current and voltage of a current-limiting fuse" Int. Conf. on Electric Fuses and their applications, Liverpool Polytechnic, p 218
10.	Guile, A.E.	(1971) "Arc-electrode Phenomena" Proc. IEE, IEE Reviews, 118, No.9R, p 1131
11.	Onuphrienko, Y.I.	(1977) "On researches of the arcing process in fuses with filler (sand filled fuses)" 3rd Int. Symp. on Switching Arc Phenomena, Lodz, Poland
12.	Wheeler, C.B.	(1976) Int. Conf. on Electric fuses and their applications, Liverpool Polytechnic (Discussion contribution, p 3.6)

13. Lowke, J.   (1977) 3rd Int. Symp. on Switching
                                        Arc Phenomena, Lodz, Poland,
                                        Part II : Postconference Materials

14. Carslaw, H.S. and
    Jaeger, J.C.   (1959) "Conduction of heat in solids"
                                        Oxford University press, second
                                        Edition, p 293

15. Oliver, R.
    Lakshminarasimha, C.S.
    and Barrault, M.R.   (1977) "Influence of filler on the
                                        properties of arcs in cartridge
                                        fuselinks"
                                        3rd Int. Symp. on Switching Arc
                                        Phenomena, Lodz, Poland, p 315

16. Huhn, P.   (1971) "Ueber das Verhalten eines
                                        durch Draht explosion eingeleiteten
                                        Lichtbogens im körnigen Medium"
                                        Dissertation. Techn. Universität
                                        Hannover, Figs 17 and 21

17. Maecker, H.   (1964) "Theory of thermal plasma and
                                        application to observed phenomena"
                                        Chapter 18 of book: 'An introduction
                                        to Discharge and Plasma Physics' ed
                                        by Haydon, S.C. - Dept. of Univ.
                                        Extension, The Univ. of New England,
                                        ARMIDALE

18. Fraser, S.G.   (1964) "Extinguishing an arc"
                                        Chapter 23 of the same book as
                                        referred to in (17)

19. Wheeler, C.B. (1970) "The high-power constricted plasma discharge column

I. Theoretical analysis"

J. Phys. D : Appl. Phys., 3, pp 1374-80

20. Wheeler, C.B. (1971) "The high-power constricted plasma discharge column

II. Experimental investigation"

J. Phys. D : Appl. Phys., 4, pp 400-407

21. Hibner, J. (1976) "The calculation of over-voltage characteristics of H.R.C. fuses"

Int. Conf. on Electric Fuses and their applications, Liverpool Polytechnic, p 70

22. Hibner, J. (1968) "Overvoltage calculation of low voltage strip element fuses using the resistance gradient method"

Przeglad Elektrotechniczny, No.10

23. Hibner, J. (1978) "Obliczanie napiecia zaplonu tuku na prostokqtnych przewezeniach swarciowych tropika paskowego"

Przeglad Elektrotechniczny, R. Liv Z.

24. Hague, B. (1929) "The principles of Electormagnetism applied to Electical Machines"

Dover publications, Inc. New York, p 282 and p 347

208

25. Vermij, L. (1969) "Electrical behaviour of fuse elements"

Ph.D. Thesis, Technological University, Eindhoven

26. Hibner, J. (1973) "The voltage of single disrupt in a chain of arc intervals by short-circuit disintegration of strip fuse elements of fuses"

2nd Int. Symp. Switching Arc Phenomena, Lodz, Poland, p 226

27. Kleen, W. (1931) "Über den Durchgang der Elektrizität durch metallische Haardrähte"

Ann. Phys. (Germany), 11, pp 579-605

28. Baxter, H.W. (1950) "Electic fuses"

Edward Arnold & Co., London

29. Lipski, T. and Furdal, A. (1970) "New observations on the formation of unduloids on wires"

Proc. IEE, 117, No.12, p 2311

30. Arai, S. (1976) "Deformation and disruption of silver wires"

Int. Conf. on Electric Fuses and their applications, Liverpool Polytechnic, p 50

31. Plateau, J. (1873) "Statique des liquides"

(Paris)

32. Kukekov, G. (1956) "Volt-ampere characteristics of the electric arc in slit-type canal"

33. Lee, T.H.

Zh. Tek Fiz., 26, pp 2548-2552
(1975) "Physics and Engineering of
High Power Switching Devices"
The Massachusetts Institute of
Technology Press, Cambridge,
Massachusetts, and London, England,
p 111

34. Tslaf, A.

(1979) "Temperature of an electric
arc in a narrow insulating channel"
Proc. IEE, 126, No.2, pp 209-214

35. Frind, G.

(1979) Private Communication

36. Nasilowski, J.

(1965) "Badanie podzialki rozpadu
drutow topikowych"
Ph.D. Thesis, IEL, Warsaw, Poland

37. Vermij, L

(1973) Second Int. Symp. Switching
Arc Phenomena, Lodz, Poland,
Part II : Post Conference Materials,
pp 169-173

38. Turner, C.

(1973) Second Int. Symp. Switching
Arc Phenomena, Lodz, Poland,
Part II : Post Conference Materials,
pp 167-169

39. Lipski, T.

(1973) Second Int. Symp. Switching
Arc Phenomena, Lodz, Poland,
Part II : Post Conference Materials,
pp 173-175

40. Carne, E.B.

(1953) "A mechanism for the fuse
pre-arcing period"

Trans. Amer. Inst. Elect. Engrs., 72,

Pt. III, pp 593-598

41. Hibner, J.   (1973) Second Int. Symp. Switching

Arc Phenomena, Lodz, Poland,

Part II : Post Conference Materials,

pp 183-185

42. Hibner, J.   (1968) "Calculation of over-voltages

of low voltage fuses with strip fusing

elements by the resistance gradient

method (in Polish)"

Przeglad Elektrotechniczny, No.10,

pp 436-440

43. Hibner, J.   (1973) "Calculation of over-voltage

peak-values when breaking short-

circuits by means of multi-strip

fuses"

Second Int. Symp. Switching Arc

Phenomena, Lodz, Poland,

Part I : Conference Materials,

pp 269-274

Part II : Post Conference Materials,

pp 183-185

44. Hibner, J.   (1973) "Resistance gradient method

for calculating arc over-voltage peak

values generated by short circuit

current limiting (in Polish)

Dissertation T.U. Gdańsk

45. Dolegowski, M.   (1970) "Spannungsverlauf an der
                              einfachen Lichtbogenunterbrechung in
                              den Sicherungen mit Sandlöschung und
                              Einengungsschmetzstreifen"
                              Switching Arc Phenomena, SEP, Lodz,
                              Poland.

46. Lipski, T.   (1977) "Why unduloids do not always
                              appear?"
                              3rd Int. Symp. on Switching Arc
                              Phenomena, Lodz, Poland, pp 305-309

47. Frind, G.   (1960) "Uber das Abklingen von
                              Lichtbogen"
                              II, Zeit. Angew, Physik, 12, pp 515-
                              521

48. Mayr, O   (1943) "Beitrag zur Theorie der
                              Statischen und der Dynamischen
                              Lichtbogens"
                              Archiv. für Elektrotechnik, p 588

49. Cassie, A.M.   (1939) "Arc rupture and circuit
                              severity"
                              CIGRE Conference Paper 102, Paris,
                              pp 1-14

50. Butler, T.F. and
    Whittaker, D.   (1972) "A normalised moving-boundary
                              circuit breaker model in severe fault
                              circuits"
                              IEE Conference Publications, 90,
                              pp 302-303

212

51. Butler, T.F. and Whittaker, D. (1972) "Distributed moving-boundary circuit-breaker model" Proc. IEE, 119, pp 1295-1300

52. Browne, T.E. (1948) "A study of arc behaviour near current zero by means of mathematical models" Trans, Am. Inst. Elec. Eng., 67, Pt I, pp 141-153

53. Reece, M.P. (1975) "Physics of circuit breaker arcs" IEE Monograph Series 17 Power circuit breaker theory and design, ed by Flurscheim, C.H.

54. Nairne, E. (1773) "Electrical Experiments" Phil. Trans. Roy. Soc. (London)

55. Wilkins, R. and McEwan, P.M. (1975) "A.C. short-circuit performance of notched fuse elements" Proc. IEE, 122, No.3, p 289

56. Smith, G.D. (1965) "Numerical solution of partial differential equations" Oxford University Press, New York, Toronto

57. Gibson, J.W. (1941) "The high rupturing capacity cartridge fuse with special reference to short-circuit performance J. IEE, 88, Pt II, pp 2-40

58. Boehne, E.W.   (1946) "Performance criteria for current-limiting power fuses" Trans. AIEE, p 1034

59. Lipski, J. and Zimny, P.   (1972) "Ein Beitrog zur Berechnung des Jouleschen Lichtbogens - integrals und der Ausschaltarbeit von strombegrenzenden Schmelz-sicherungen" E.U.M., p 461

60. Vermij, L and Roclofs, J.B.J.   (1975) "The Joule-integral of fuses for the protection of semiconductor devices" CIRED, Paper No. 48

61. Wilkins, R.   (1975) "Generalised short-circuit characteristics for h.r.c. fuses" Proc. IEE, p 1289

62. Hirose, A.   (1976) "Mathematical analysis of breaking performance of current-limiting fuses" Int. Conf. on Electric Fuses and their applications, Liverpool Polytechnic, p 182

63. Butts, A.   (1967) "Silver, Economics, Metallurgy and Use" D.Van Norstrand Company, Inc. Princeton, Newjersey

The Author

The author followed a four year under-graduate course in Engineering in the University of Ceylon and passed B.Sc.(Eng) with Honours. He then worked for one year as an Instructor in Electrical Engineering in the University.

The author then joined the Department of Government Electrical Undertakings of Sri Lanka and served in the various branches of the utility which controlled the generation, transmission, distribution and retailing of electricity in the island.

In 1969 he went to Canada to work for one year with the Engineering Consultants, M/S Surveyer, Nenniger and Chenevert and Canadian General Electric Co., on the design, manufacture and testing of electrical plant and machinery.

The author then returned to Sri Lanka and served as Chief Engineer on the design, supervision of construction and commissioning of a hydro power station in the country. He was also a visiting lecturer for Engineering undergraduate students in the University of Ceylon, Katubedde Campus.

In October 1975, the author embarked upon a one year M.Sc. course in Power Systems Engineering by examination and dissertation at UMIST. After obtaining the M.Sc. in October 1976, he joined Liverpool Polytechnic as a Research Assistant under the supervision of Dr. R. Wilkins.

Acknowledgements

The author thanks Dr. R. Wilkins for providing the facilities at Liverpool Polytechnic for the research project and for his personal supervision, advice and guidance throughout the work presented in this thesis. He also wishes to thank Dr. B.H. Swanick for the encouragement and assessment of the overall work.

Most sincere thanks are also due to all the technical staff who helped in the project work.

The author wishes to thank GEC Fusegear Limited for the financial support and also the Liverpool Polytechnic Computer Services for the computing facilities provided.

The author is also very thankful to Donna Girling for the efficient and accurate typing of his manuscripts.

Finally he is very grateful to his wife who has been the continuous source of inspiration.

```
      MASTER GNANALINGAM
      DIMENSION C(45,44),T(45,44),TNEW(45,44),DUM(45,44),IREF(45,44),
     1LIMIT(44),PT(45,44)
      LOGICAL MELT
      REAL L,ISQT
      COMMON/B1/M,N,MM,NN,N1
      COMMON/B2/A1,AA1,CONV1,LIMIT1
      COMMON/B3/A2,AA2,CONV2,LIMIT2
      COMMON/B4/A3,AA3,CONV3,LIMIT3,TMELT
      COMMON/B5/BETA,TAMB,RHOZ
      COMMON/B6/DELX,DELT
      COMMON/B7/SN,NE
      COMMON/B8/AK,BK,CK
      COMMON/B9/ALPHA,TKS
      COMMON/B10/ERMS,Z,PHI,THETA
  999 CONTINUE
      CALL INPUT(H)
      SET INITIAL CONDITIONS
      MELT=.FALSE.
      CALL INITIAL(C,DUM,T,TNEW,LIMIT,IREF,W,ITER,ITERT,TIME,NSTEP,ISQT
      PROSPC=ERMS/Z
      R=Z*COS(PHI*W/18000.0)
      XL=Z*SIN(PHI*W/18000.0)
      L=XL/W
      WRITE(2,1002) ERMS,Z,PHI,R,XL,L,THETA
 1002 FORMAT(1H1,5X,'CIRCUIT PARAMETERS',//6X,'ERMS',3X,E10.4/6X,'Z',6X
     1E10.4/6X,'PHI',4X,E10.4/6X,'R',6X,E10.4/6X,'XL',5X,E10.4/6X,
     2'L',5X,E10.4/6X,'THETA',2X,E10.4//)
      WRITE(2,1003) PROSPC
 1003 FORMAT(1H0,5X,'RMS PROSPECTIVE CURRENT =',F10.3,'AMPS')
      CONVERT ANGLES TO RADIANS
      PHI=PHI*W/18000.0
      THETA=THETA*W/18000.0
      EM=ERMS*SQRT(2.0)
      WRITE(2,108)
  108 FORMAT(1H0,3X,'TIME',5X,'I(PROSP)',2X,'I(ACTUAL)',3X,'T(1,1)',1X,
     1'T(MM,1)',1X,'T(MM,NN)',1X,'T(1,N)',2X,'ITER',2X,'ITERT',4X,'RF',
     29X,'ISQT',9X,'PISQT'/)
    9 CONTINUE
      IF(NSTEP.GT.0) GO TO 10
      SET INITIAL CURRENT
      CUR=0.001
      CUR=CUR/NE
      CALL SCURF1(C,LIMIT,IREF,0.5*CUR/H,ITER)
      CALL RESIS(C,T,0.5*CUR,RF)
      RF=SN*RF
      ISQT=0.5*DELT*CUR*CUR
      PISQT=NE**2*ISQT
      THIS NEXT STATEMENT DEPENDS UPON THE CIRCUIT L/R
      IF(L.EQ.0.0) GO TO 30
      PROSPC=(EM/Z)*(SIN(W*TIME*THETA-PHI)-SIN(THETA-PHI)*
     1EXP(-R*TIME/L))
      GO TO 31
   30 PROSPC=(EM/Z)*SIN(W*TIME+THETA)
   31 CONTINUE
      WRITE(2,109) TIME,PROSPC,CUR,T(1,1),T(MM,1),T(MM,NN),T(1,N),
     1ITER,ITERT,RF,ISQT,PISQT
      GO TO 11
   10 CALL SCURF2(C,T,LIMIT,IREF,0.5*CUR/H,ITER)
      CALL RESIS(C,T,0.5*CUR,RF1)
```

```
      RF1=SN*RF1
      IF(L.EQ.0.0) GO TO 32
      FK1=(EM*SIN(W*TIME+THETA)-CUR*(NE*R+RF))/L
      FK2=(EM*SIN(W*(TIME+DELT/2.)+THETA)-(CUR+FK1*DELT/(2.*NE))*
     1(NE*R+0.5*(RF+RF1)))/L
      FK3=(EM*SIN(W*(TIME+DELT/2.)+THETA)-(CUR+FK2*DELT/(2.*NE))*
     1(NE*R+0.5*(RF+RF1)))/L
      FK4=(EM*SIN(W*(TIME+DELT)+THETA)-(CUR+FK3*DELT/NE)*
     1(NE*R+RF1)))/L
      CUR=CUR+(FK1+2*FK2+2*FK3+FK4)*DELT/(6.0*NE)
      GO TO 33
   32 RAV=R+0.5*(RF+RF1)/NE
      CUR=EM*SIN(W*(TIME+DELT)+THETA)/RAV
   33 CONTINUE
      RF=RF1
      WRITE(2,301)RF
  301 FORMAT(40X,'RF=',E10.4/40X,13(1H*))
      TIME=TIME+DELT
      IF(L.EQ.0.0) GO TO 34
      ISQT=ISQT+DELT*CUR*CUR
      PISQT=NE**2*ISQT
      PROSPC=(EM/Z)*(SIN(W*TIME+THETA-PHI)-SIN(THETA-PHI)*
     1EXP(-R*TIME/L))
      FK1=(EM*SIN(W*TIME+THETA)-CUR*(NE*R+RF))/L
      FK2=(EM*SIN(W*(TIME+DELT/4.)+THETA)-(CUR+FK1*DELT/(4.*NE))*
     1(NE*R+RF))/L
      FK3=(EM*SIN(W*(TIME+DELT/4.)+THETA)-(CUR+FK2*DELT/(4.*NE))*
     1(NE*R+RF))/L
      FK4=(EM*SIN(W*(TIME+DELT/2.)+THETA)-(CUR+FK3*DELT/(2.*NE))*
     1(NE*R+RF))/L
      CURN=CUR+(FK1+2.*FK2+2.*FK3+FK4)*DELT/(12.*NE)
      WRITE(2,65)CURN
   65 FORMAT(///,30X,'CURN=',E10.4)
      GO TO 35
   34 PROSPC=(EM/Z)*SIN(W*TIME+THETA)
   35 CONTINUE
      WRITE(2,109) TIME,PROSPC,CUR,T(1,1),T(MM,1),T(MM,NN),T(1,N),
     1ITER,ITERT,RF,ISQT,PISQT
  109 FORMAT(1X,F10.8,2(1X,E10.3),4(2X,F6.2),I5,I6,2X,E10.3,2X,F10.3,
     13X,E11.4)
      CALL SCURF2(C,T,LIMIT,IREF,0.5*CURN/H,ITER)
   11 CONTINUE
      CALL CALJSQ(C,IREF,DUM)
      CALL NEWTON(T,TNEW,DUM,IREF,ITERT,MELT,I,J,PT)
      IF(MELT) GO TO 12
      NSTEP=NSTEP+1
      IF(TIME.GT.0.01) STOP
      GO TO 9
   12 WRITE(2,110) I,J
  110 FORMAT(1H0,5X,'MELTING OCCURS AT I=',I3,'AND J=',I3)
      PAT=TIME+DELT*(TMELT-T(I,J))/(TNEW(I,J)-T(I,J))
      WRITE(2,111) PAT
  111 FORMAT(1H0,5X,'PREARCING TIME=',F10.8,'SEC')
      ISQT=ISQT+CUR*CUR*(PAT-TIME-0.5*DELT)
      PISQT=NE**2*ISQT
      WRITE(2,112)ISQT,PISQT
  112 FORMAT(1H0,5X,'LET-THROUGH ISQT=',E10.3//5X,'PRE-ARCING ISQT=',
     1E11.4/)
      GO TO 999
      STOP
      END
```

218

```
      SUBROUTINE INPUT(H)
      COMMON/B1/M,N,MM,NN,N1
      COMMON/B2/A1,AA1,CONV1,LIMIT1
      COMMON/B3/A2,AA2,CONV2,LIMIT2
      COMMON/B4/A3,AA3,CONV3,LIMIT3,TMELT
      COMMON/B5/BETA,TAMB,RHOZ
      COMMON/B6/DELX,DELT
      COMMON/B7/SN,NE
      COMMON/B9/ALPHA,TKS
      COMMON/B10/ERMS,Z,PHI,THETA
      READ(1,1000) ERMS,Z,PHI,THETA
 1000 FORMAT(4F11.4)
      IF(ERMS.LT.1.0) STOP
      READ(1,100) M,N,MM,NN,H,DELX
      READ(1,101) A1,CONV1,LIMIT1
      READ(1,101) A2,CONV2,LIMIT2
      READ(1,101) A3,CONV3,LIMIT3
      READ(1,102) ALPHA,TKS,SPHS,RHOZ,BETA,TAMB
  100 FORMAT(4I5,2E10.4)
  101 FORMAT(2F10.6,I5)
  102 FORMAT(6E10.4)
      WRITE(2,103)
  103 FORMAT(1H0,////42H          FUSE GEOMETRY          PHYSICAL CONSTANTS,3X,
     121H NUMERICAL PARAMETERS/)
      WRITE(2,104) M,ALPHA,A1,N,TKS,CONV1,MM,SPHS,LIMIT1,NN,RHOZ,A2,H,
     1BETA,CONV2,DELX,TAMB,LIMIT2,A3,CONV3,LIMIT3
  104 FORMAT(6X,1HM,4X,I5,8X,5HALPHA,2X,E10.4,5X,2HA1,6X,F6.3/
     16X,1HN,4X,I5,8X,3HTKS,4X,E10.4,5X,5HCONV1,3X,F6.4/
     26X,2HMM,3X,I5,8X,4HSPHS,3X,E10.4,5X,6HLIMIT1,2X,I6/
     36X,2HNN,3X,I5,8X,4HRHOZ,3X,E10.4,5X,2HA2,6X,F6.3/
     46X,1HH,4X,E10.4,3X,4HBETA,3X,E10.4,5X,5HCONV2,3X,F6.4/
     56X,4HDELX,1X,E10.4,3X,4HTAMB,3X,E10.4,5X,6HLIMIT2,2X,I6/
     644X,2HA3,6X,F6.3/46X,5HCONV3,3X,F6.4/46X,6HLIMIT3,2X,I6)
      READ(1,105) TNT
  105 FORMAT(F5.3)
      DELT=(DELX**2)/(4.0*ALPHA)
      WRITE(2,106) DELT
  106 FORMAT(1H0,5X,41HLIMITING TIME STEP FOR EXPLICIT METHOD = ,F10.8,
     14H SEC/)
      DELT=TNT*DELT
      WRITE(2,107) TNT,DELT
  107 FORMAT(6X,26HIN THIS PROGRAM A STEP OF ,F5.1,
     125H TIMES THIS IS USED (I.E. ,F10.8,5H SEC)/////)
      READ(1,200) SN,TMELT,NE
  200 FORMAT(2F8.2,I3)
      WRITE(2,201) SN,NE,TMELT
  201 FORMAT(////////10X,31HNUMBER OF NOTCHES PER ELEMENT = ,F8.2/10X,
     125HNUMBER OF FUSE ELEMENTS = ,I3/10X,21HMELTING TEMPERATURE = ,
     2F8.2/)
      RETURN
      END


LENGTH   256, NAME  INPUT
```

```
      SUBROUTINE INITIAL(C,DUM,T,TNEW,LIMIT,IREF,W,ITER,ITERT,TIME,
     1NSTEP,ISQT)
      DIMENSION C(M,N),DUM(M,N),T(M,N),TNEW(M,N),LIMIT(N),IREF(M,N)
      COMMON/B1/M,N,MM,NN,N1
      COMMON/B2/A1,AA1,CONV1,LIMIT1
      COMMON/B3/A2,AA2,CONV2,LIMIT2
      COMMON/B4/A3,AA3,CONV3,LIMIT3,TMELT
      COMMON/B5/BETA,TAMB,RHOZ
      COMMON/B6/DELX,DELT
      COMMON/B8/AK,BK,CK
      COMMON/B9/ALPHA,TKS
      PRELIMINARY ASSIGNMENTS
      AMOD=(DELX**2)/(ALPHA*DELT)
      AK=0.5/(AMOD+2.0)
      BK=(AMOD-2.0)/(AMOD+2.0)
      CK=AMOD/(AMOD+2.0)
      CK=CK*ALPHA*DELT*RHOZ/TKS
      M1=M-1
      N1=N-1
      MM1=MM-1
      NN1=NN-1
      NN2=NN+1
      MM2=MM+1
      AA1=A1-1.0
      AA2=A2-1.0
      AA3=A3-1.0
      W=314.15927
      DO 20 I=1,M
      DO 20 J=1,N
      C(I,J)=0.0
      DUM(I,J)=0.0
      T(I,J)=TAMB
   20 TNEW(I,J)=TAMB
      C(1,1)=1.0
      DO1 J=1,NN
    1 LIMIT(J)=MM1
      DO2 J=NN2,N
    2 LIMIT(J)=M1
      DO3 I=1,M
      DO3 J=1,N
    3 IREF(I,J)=0
      DO4 J=1,NN
      IREF(1,J)=1
    4 IREF(MM,J)=1
      DO5 J=NN,N
      IREF(1,J)=1
    5 IREF(M,J)=1
      DO6 I=1,MM
      IREF(I,1)=1
    6 IREF(I,N)=1
      DO7 I=MM,M
      IREF(I,NN)=1
    7 IREF(I,N)=1
      DO8 I=MM2,M
      DO8 J=1,NN1
    8 IREF(I,J)=-1
      ITER=0
      ITERT=0
      TIME=0.0
      NSTEP=0
```

```
      ISQT=0.)
      WRITE(2,21)AK,BK,CK
21    FORMAT(6X,3HAK=,F8.5/6X,3HBK=,F8.5/6X,3HCK=,E10.4/)
      RETURN
      END
```

LENGTH   421, NAME INITIAL

```
      SUBROUTINE SCURF1(C,LIMIT,IREF,CUR,IT)
      DIMENSION C(M,N),IREF(M,N),LIMIT(N)
      COMMON/B1/M,N,MM,NN,N1
      COMMON/B2/A1,AA1,CONV1,LIMIT1
      SF=CUR/C(1,1)
      DO 10 J=1,N
   10 C(1,J)=CUR
      DO11 J=1,N
      L=LIMIT(J)
      DO11 I=2,L
   11 C(I,J)=SF*C(I,J)
      IT=0
    1 IT=IT+1
      BIG=0.0
      DO4 J=1,N
      L=LIMIT(J)
      DO4 I=2,L
      IF(IREF(I,J).EQ.1) GO TO 2
      CGS=0.25*(C(I-1,J)+C(I,J+1)+C(I+1,J)+C(I,J-1))
      GO TO 3
    2 CALL BOUND(C,C1,C2,C3,C4,I,J)
      CGS=0.25*(C1+C2+C3+C4)
    3 DELC=CGS-C(I,J)
      C(I,J)=CGS+AA1*DELC
      IF(ABS(DELC).GT.BIG) BIG=ABS(DELC)
    4 CONTINUE
      IF(BIG.LT.ABS(CONV1*CUR)) GO TO 5
      IF(IT.GT.LIMIT1) GO TO 6
      GO TO 1
    5 RETURN
    6 WRITE(2,100)
  100 FORMAT(1X,25HSCURF1 FAILED TO CONVERGE)
      RETURN
      END
```

LENGTH   253, NAME   SCURF1

```
      SUBROUTINE SCURF2(C,T,LIMIT,IREF,CUR,IT)
      DIMENSION C(M,N),T(M,N),IREF(M,N),LIMIT(N)
      COMMON/B1/M,N,MM,NN,N1
      COMMON/B3/A2,AA2,CONV2,LIMIT2
      COMMON/B5/BETA,TAMB,RHO2
      WRITE(2,43)CUR,T(1,1)
   43 FORMAT(/16X,5H2CUR=,E10.4,16X,7HT(1,1)=,F9.5/)
      SF=CUR/C(1,1)
      DO 10 J=1,N
   10 C(1,J)=CUR
      DO11 J=1,N
      L=LIMIT(J)
      DO11 I=2,L
   11 C(I,J)=SF*C(I,J)
      IT=0
    1 IT=IT+1
      BIG=0.0
      DO4 J=1,N
      L=LIMIT(J)
      DO4 I=2,L
      IF(IREF(I,J).EQ.1) GO TO 2
      RA=1.0+BETA*(0.5*(T(I-1,J)+T(I,J))-TAMB)
      RB=1.0+BETA*(0.5*(T(I,J+1)+T(I,J))-TAMB)
      RC=1.0+BETA*(0.5*(T(I+1,J)+T(I,J))-TAMB)
      RD=1.0+BETA*(0.5*(T(I,J-1)+T(I,J))-TAMB)
      R=RA+RB+RC+RD
      CGS=(RA*C(I-1,J)+RB*C(I,J+1)+RC*C(I+1,J)+RD*C(I,J-1))/R
      GO TO 3
    2 CALL BOUND(C,C1,C2,C3,C4,I,J)
      CALL BOUND(T,T1,T2,T3,T4,I,J)
      RA=1.0+BETA*(0.5*(T1+T(I,J))-TAMB)
      RB=1.0+BETA*(0.5*(T2+T(I,J))-TAMB)
      RC=1.0+BETA*(0.5*(T3+T(I,J))-TAMB)
      RD=1.0+BETA*(0.5*(T4+T(I,J))-TAMB)
      R=RA+RB+RC+RD
      CGS=(RA*C1+RB*C2+RC*C3+RD*C4)/R
    3 DELC=CGS-C(I,J)
      C(I,J)=CGS+AA2*DELC
      IF(ABS(DELC).GT.BIG) BIG=ABS(DELC)
    4 CONTINUE
      IF(BIG.LT.ABS(CONV2*CUR)) GO TO 5
      IF(IT.GT.LIMIT2) GO TO 6
      GO TO 1
    5 RETURN
    6 WRITE(2,100)
  100 FORMAT(1X,25HSCURF2 FAILED TO CONVERGE)
      RETURN
      END


LENGTH   457, NAME   SCURF2
```

223

```
      SUBROUTINE RESIS(C,T,CUR,R1)
      DIMENSION C(M,N),T(M,N)
      COMMON/B1/M,N,MM,NN,N1
      COMMON/B5/BETA,TAMB,RHOZ
      COMMON/B7/SN,NE
      IF(MM.LT.4) GO TO 2
      WRITE(2,71)R1
71    FORMAT(/18X,5HR1=,E10.4/)
      V12=0.0
      V12=(1.0+BETA*(T(1,1)-TAMB))*(-11*C(1,1)+18*C(2,1)-9*C(3,1)+2*C(
     11))+(1.0+BETA*(T(1,N)-TAMB))*(-11*C(1,N)+18*C(2,N)-9*C(3,N)
     2+2*C(4,N))
      V12=0.5*V12
      DO1 J=2,N1
1     V12=V12+
     1(1.0+BETA*(T(1,J)-TAMB))*(-11*C(1,J)+18*C(2,J)-9*C(3,J)+2*C(4,J))
      V12=RHOZ*V12/6.0
      R1=-(V12/CUR)
      WRITE(2,81)R1
81    FORMAT(28X,'VALUE OF R1 OUTPUTTED=',E10.4/28X,32(1H-))
      RETURN
2     WRITE(2,100)
100   FORMAT(1X,51HSUBR.RESIS WILL NOT ACCEPT VALUES OF MM LESS THAN 4)
      STOP
      END


LENGTH   248, NAME   RESIS
```

```fortran
      SUBROUTINE CALJSQ(C,IREF,JSQ)
      DIMENSION C(M,N),JSQ(M,N),IREF(M,N)
      COMMON/B1/M,N,MM,NN,N1
      COMMON/B6/DELX,DELT
      REAL JX,JY,JSQ
      DO4 I=1,M
      DO4 J=1,N
      IF(IREF(I,J)) 4,1,2
    1 JX=0.5*(C(I+1,J)-C(I-1,J))
      JY=-0.5*(C(I,J+1)-C(I,J-1))
      GO TO 3
    2 IF(I.EQ.1) GO TO 50
      IF(I.EQ.MM.AND.J.EQ.NN) GO TO 51
      IF(I.EQ.M.AND.J.EQ.NN) GO TO 53
      IF(I.EQ.MM.OR.I.EQ.M) GO TO 52
      IF(J.EQ.NN) GO TO 54
      JX=0.5*(C(I+1,J)-C(I-1,J))
      JY=0.0
      GO TO 3
   50 JX=(-11*C(1,J)+18*C(2,J)-9*C(3,J)+2*C(4,J))/6.0
      JY=0.0
      GO TO 3
   51 JX= (11*C(MM,NN)-18*C(MM-1,NN)+9*C(MM-2,NN)-2*C(MM-3,NN))/6.0
      JY=(11*C(MM,NN)-18*C(MM,NN+1)+9*C(MM,NN+2)-2*C(MM,NN+3))/6.0
      GO TO 3
   52 JX=(11*C(I,J)-18*C(I-1,J)+9*C(I-2,J)-2*C(I-3,J))/6.0
      JY=0.0
      GO TO 3
   53 JX=0.0
      JY=0.0
      GO TO 3
   54 JX=0.0
      JY=(11*C(I,NN)-18*C(I,NN+1)+9*C(I,NN+2)-2*C(I,NN+3))/6.0
    3 JSQ(I,J)=(JX**2+JY**2)/(DELX**2)
    4 CONTINUE
      WRITE(2,31)JSQ(1,1)
   31 FORMAT(10X,9HJSQ(1,1)=,E10.4/)
      RETURN
      END


LENGTH   500, NAME   CALJSQ
```

225

```
      SUBROUTINE NEWTCN(T,TNEW,ST,IREF,IT,MELT,I,J,PT)
      DIMENSION T(M,N),TNEW(M,N),ST(M,N),IREF(M,N),PT(M,N)
      COMMON/B1/M,N,MM,NN,V1
      COMMON/B4/A3,AA3,CONV3,LIMIT3,TMELT
      COMMON/B5/BETA,TAMB,RHOZ
      COMMON/B8/AK,BK,CK
      LOGICAL MELT
C     SET CONSTANT TERM (A PRIOR CALC OF JSQ MUST HAVE BEEN MADE)
      DO1 I=1,M
      DO1 J=1,N
      IF(IREF(I,J)) 1,2,3
    2 PT(I,J)=AK*(T(I+1,J)+T(I-1,J)+T(I,J+1)+T(I,J-1))+BK*T(I,J)
     1+CK*ST(I,J)*(1.+BETA*(0.5*T(I,J)-TAMB))
      GO TO 1
    3 CALL BOUND(T,T1,T2,T3,T4,I,J)
      PT(I,J)=AK*(T1+T2+T3+T4)+BK*T(I,J)
     1+CK*ST(I,J)*(1.+BETA*(0.5*T(I,J)-TAMB))
    1 CONTINUE
C     ITERATIVE SOLUTION FOR NEW TEMPERATURES
      IT=0
   20 IT=IT+1
      BIG=0.0
      DO10 I=1,M
      DO10 J=1,N
      IF(IREF(I,J)) 10,11,12
   11 TGS=AK*(TNEW(I+1,J)+TNEW(I-1,J)+TNEW(I,J+1)+TNEW(I,J-1))+PT(I,J)
     1+CK*ST(I,J)*(1.+BETA*(0.5*TNEW(I,J)-TAMB))
      GO TO 100
   12 CALL BOUND(TNEW,T1,T2,T3,T4,I,J)
      TGS=AK*(T1+T2+T3+T4)+PT(I,J)
     1+CK*ST(I,J)*(1.+BETA*(0.5*TNEW(I,J)-TAMB))
  100 DT=TGS-TNEW(I,J)
      TNEW(I,J)=TGS+AA3*DT
      IF(ABS(DT).GT.BIG) BIG=ABS(DT)
   10 CONTINUE
      IF(BIG.LT.(CONV3*T(1,1))) GO TO 21
      IF(IT.GT.LIMIT3) GO TO 22
      GO TO 20
   22 WRITE(2,99)
   99 FORMAT(1H0,25HNEWTCN FAILED TO CONVERGE)
   21 DO13 I=1,M
      DO13 J=1,N
      IF(TNEW(I,J).GE.TMELT) GO TO 14
   13 CONTINUE
      DO15 I=1,M
      DO15 J=1,N
   15 T(I,J)=TNEW(I,J)
      RETURN
   14 MELT=.TRUE.
      RETURN
      END


LENGTH    511, NAME   NEWTCN
```

226

```fortran
      SUBROUTINE BOUND(V,V1,V2,V3,V4,I,J)
      DIMENSION V(M,N)
      COMMON/B1/M,N,MM,NN,N1
      IF(I.EQ.1.AND.J.GT.1.AND.J.LT.N) GO TO 1
      IF(J.EQ.N.AND.I.GT.1.AND.I.LT.M) GO TO 2
      IF((I.EQ.MM.AND.J.GT.1.AND.J.LT.NN).OR.(I.EQ.M.AND.J.GT.NN.AND.
     1J.LT.N)) GO TO 3
      IF((J.EQ.1.AND.I.GT.1.AND.I.LT.MM).OR.(J.EQ.NN.AND.I.GT.MM.AND.
     1I.LT.M)) GO TO 4
      IF((I.EQ.MM.AND.J.EQ.1).OR.(J.EQ.NN.AND.I.EQ.M)) GO TO 5
      IF(I.EQ.1.AND.J.EQ.1) GO TO 6
      IF(I.EQ.1.AND.J.EQ.N) GO TO 7
      IF(I.EQ.M.AND.J.EQ.N) GO TO 8
      IF(I.EQ.MM.AND.J.EQ.NN) GO TO 9
    1 V2=V(I,J+1)
      V3=V(I+1,J)
      V4=V(I,J-1)
      V1=V3
      GO TO 99
    2 V1=V(I-1,J)
      V3=V(I+1,J)
      V4=V(I,J-1)
      V2=V4
      GO TO 99
    3 V1=V(I-1,J)
      V2=V(I,J+1)
      V3=V1
      V4=V(I,J-1)
      GO TO 99
    4 V1=V(I-1,J)
      V2=V(I,J+1)
      V3=V(I+1,J)
      V4=V2
      GO TO 99
    5 V1=V(I-1,J)
      V2=V(I,J+1)
      V3=V1
      V4=V2
      GO TO 99
    6 V2=V(I,J+1)
      V3=V(I+1,J)
      V1=V3
      V4=V2
      GO TO 99
    7 V4=V(I,J-1)
      V3=V(I+1,J)
      V1=V3
      V2=V4
      GO TO 99
    8 V4=V(I,J-1)
      V1=V(I-1,J)
      V3=V1
      V2=V4
      GO TO 99
    9 V1=(4.0/3.0)*V(I-1,J)
      V2=(4.0/3.0)*V(I,J+1)
      V3=(2.0/3.0)*V(I+1,J)
      V4=(2.0/3.0)*V(I,J-1)
   99 RETURN
      END
```

227

```
      MASTER MAIN PROGRAM
      DIMENSION Y(1000),DY(1000),P(1000),Q(1000),DX(500),DXE(500),
     1E(1000),D(500),DD(500),A(1000),X(500),XE(500)
      COMMON/BLOCK11/ERMS,R,EL,F,THETA,C1,TI1,C,XF,VARC,TI,PI,TIO
      COMMON/BLOCK12/X0,XL,XXL,AREA,AREAZ,NS,NP,ELAMDA
      COMMON/BLOCK13/DELTT,TMAX,ALPH1,ALPH2,CS,CK1,CK2
      COMMON/BLOCK14/K,K1,KE,KE1,KH,TICOR1,TICOR2,JJ3,JJ4,JJ5,E
      COMMON/BLOCK15/WID,DEP,SILDIA,AE,GAMA
      READ(1,151)JJ1,JJ2
  151 FORMAT(2I5)
      JJ3=JJ1+JJ2
      JJ4=JJ1-2
      JJ5=JJ1+2
      JJ6=JJ2+2
      M=JJ3+6
      PI=ATAN(1.0)*4
    1 CONTINUE
      CALL PREARC
      WRITE(2,251)JJ1,JJ2
  251 FORMAT(6X,'MAXIMUM POSSIBLE NUMBER OF LUMEN SEGMENTS PER ARC BEFOR
     1E ARC MERGING =',I5/6X,'MAXIMUM POSSIBLE NUMBER OF LUMEN SEGMENT E
     2XTENSIONS'/6X,'AT THE TWO OUTER ENDS OF THE FUSE AFTER ARC MERGING
     3 =',I5//////)
C     THIS PROGRAM IS FOR SIMULATION OF DYNAMIC ARC IN AN HRC FUSE
      WRITE(2,100)
  100 FORMAT(8X,'TIME',11X,'C',12X,'XF',9X,'DC/DT',8X,'DX/DT',8X,'DXE/DT
     1',7X,'VFUSE',8X,'AISQT',8X,'AENGY'//)
C     INITIALISE VARIABLES
      DO 604 J=1,3
      Y(J+1)=0.
      DY(J+1)=0.
  604 CONTINUE
      DO 601 J=1,JJ3
      E(J)=0.
      Y(J+4)=0.
      DY(J+4)=0.
  601 CONTINUE
      DO 602 J=1,JJ1
      X(J)=0.
      DX(J)=0.
      D(J)=0.
  602 CONTINUE
      DO 603 J=1,JJ2
      XE(J)=0.
      DXE(J)=0.
      DD(J)=0.
  603 CONTINUE
      K=1
      K1=1
      KE=1
      KG=1
      KH=0
      KF=1
      TICOR1=0.
      TICOR2=0.
      Y(2)=C1/NP
      Y(3)=X0
      Y(4)=0.0
      X(1)=X0
      XE(1)=0.0
```

```
      XF(2)=0.0
      DX(1)=X0
      D(1)=0.25*X0
C     TI0 IS DISRUPTION TIME
      TI0=ELAMDA*AREAZ/ABS(Y(2))
      Y(1)=TI0
      E(1)=0.4*SQRT(ABS(Y(2))/AREAZ)
      Y(5)=0.9*ABS(Y(2))**0.47/E(1)**1.18
C     UB IS ELECTRODE FALL VOLTAGES.
      UB=15.0+ABS(Y(2))**0.39
      VARC=NS*(E(1)*DX(1)+UB)
      DIFCI=(VS(Y(1)-TI0/2.0)-R*Y(2)*NP-VARC*C1/ABS(C1)/2.)/(NP*EL)
      Y(2)=Y(2)+DIFCI*TI0
      C=NP*Y(2)
      Y(JJ3+5)=Y(2)**2*TI0/3.0
      Y(JJ3+6)=ABS(Y(2)*VARC*TI0/2.0)
      WRITE(2,210)UB,TI0
  210 FORMAT(/10X,'ELECTRODE FALL VOLTAGES AT THE START =',F10.2//10X,
     1'DISRUPTION TIME =',E10.4,'SEC'/)
      CALL F4RUNK(M,0,DELTT,Y,DY,P,Q)
      GO TO 19
    3 CONTINUE
      UB=15.0+ABS(Y(2))**0.39
   19 CONTINUE
      X(K)=Y(3)
      PROD11=0.0
      PROD12=0.0
      PROD21=0.0
      PROD22=0.0
      PROD31=0.0
      PROD32=0.0
      PROD41=0.0
      PROD42=0.0
      DO 10 J=1,JJ3
      A(J)=Y(J+4)
   10 CONTINUE
      IF(K.GT.JJ1)GO TO 83
      IF(TI.GT.TMAX)GO TO 5
      IF(NP*Y(2)*C1/ABS(C1).LE.CS)GO TO 9
      IF((Y(3).GE.XL).AND.(KE.EQ.1))GO TO 52
      IF((ABS(XL-Y(3)).LE..1000E-06).AND.(KE.GE.2))GO TO 54
      IF(K.EQ.1)GO TO 61
      CALL AINIT(M,Y,DY)
      DX(K)=Y(3)-X(K1)
      DO 20 J=1,K
      E(J)=0.914*ABS(Y(2))**0.4/Y(J+4)**0.85*CK2/ABS(Y(2))
      PROD11=PROD11+E(J)*DX(J)
   20 CONTINUE
      VARC=NS*(PROD11+UB)
      D(K)=0.5*Y(3)-0.25*DX(K)
   61 CONTINUE
      K=K+1
      K1=K-1
      WRITE(2,109)K,E(1),E(2),E(3),E(4),E(5),E(6)
  109 FORMAT(/2X,' K= ',I2,4X,' E(1)= ',E10.4,' E(2)= ',E10.4,' E(3)= ',
     1E10.4,' E(4)= ',E10.4,' E(5)= ',E10.4,' E(6)= ',E10.4//)
      GO TO 90
   54 CONTINUE
      IF(KE.GE.JJ6)GO TO 93
      IF(((NS*Y(3)+Y(4)).GE.XXL).AND.(KG.EQ.1))GO TO 63
      IF((ABS(XXL-XF).LE..1000E-06).AND.(KG.GE.2))GO TO 73
```

```
            KE=KE+1
            KF1=KE-1
            XF(KE)=Y(4)
            CALL AINIT(M,Y,DY)
            DXE(KE)=Y(4)-XF(KF1)
            DO 30 J=1,K
            F(J)=0.914*ABS(Y(2))**0.4/Y(J+4)**0.85+CK2/ABS(Y(2))
            PROD21=PROD21+E(J)*DX(J)
   30 CONTINUE
            WRITE(2,31)KF,Y(205),Y(206)
   31 FORMAT(//15X,' KE= ',I4,15X,' Y(205)= ',E10.4,' Y(206)= ',E10.4/)
            DO 40 J=3,KE
            E(J+JJ4)=0.914*ABS(Y(2))**0.4/Y(J+JJ5)**0.85+CK2/ABS(Y(2))
            PROD22=PROD22+E(J+JJ4)*DXE(J)
   40 CONTINUE
            VARC=NS*PROD21+PROD22+UB
            DD(KE)=0.5*(Y(3)+Y(4))-0.25*DXE(KE)
            GO TO 90
   83 WRITE(2,801)
  801 FORMAT(6X,'NUMBER OF LUMEN SEGMENTS PER ARC IS GOING TO EXCEED NUM
     1BER ALLOWED FOR'/6X,70(1H*)/)
            GOTO 7
   93 WRITE(2,901)
  901 FORMAT(6X,'THE NUMBER OF LUMEN SEGMENT EXTENSIONS AT THE TWO ENDS
     1OF'/6X,'THE FUSE AFTER ARC MERGING IS GOING TO EXCEED THE NUMBER A
     2LLOWED FOR'/6X,68(1H*)/)
            GO TO 7
   52 KE=KE+1
            CALL AINIT(M,Y,DY)
C     TICOR1 IS CORRECTION IN TIME TO DETERMINE INSTANT AT WHICH ARC
C     JUST MERGED.
            TICOR1=(Y(3)-XL)/DY(3)
            Y(1)=Y(1)-TICOR1
            Y(2)=Y(2)-DY(2)*TICOR1
            Y(3)=XL
            Y(JJ3+5)=Y(JJ3+5)-DY(JJ3+5)*TICOR1
            Y(JJ3+6)=Y(JJ3+6)-DY(JJ3+6)*TICOR1
            DX(K)=Y(3)-X(K1)
            DO 95 J=1,K1
            Y(J+4)=Y(J+4)-DY(J+4)*TICOR1
            E(J)=0.914*ABS(Y(2))**0.4/Y(J+4)**0.85+CK2/ABS(Y(2))
            PROD12=PROD12+E(J)*DX(J)
   95 CONTINUE
            F(K)=0.914*ABS(Y(2))**0.4/Y(K+4)**0.85+CK2/ABS(Y(2))
            VARC=NS*(PROD12+F(K)*DX(K))+UB
            D(K)=0.5*Y(3)-0.25*DX(K)
            CC=NP*Y(2)
            WRITE(2,700)K,Y(3)
  700 FORMAT(/16X,'ARCS HAVE JUST MERGED'/16X,21(1H*)/16X,'NUMBER OF SEG
     1MENTS IN EACH ARC =',I3/16X,'LENGTH OF EACH ARC =',E10.4,'CM'/)
            IF(NS*Y(3).GE.XXL)GO TO 201
            GO TO 90
  201 WRITE(2,720)TI,CC,XF,VARC,AISQT,AENGY
  720 FORMAT(//5X,'TIME=',E10.4,10X,'CIRCUIT CURRENT=',E10.4,10X,'TOTAL
     1ARC LENGTH=',E10.4 /5X,'ARC VOLTAGE=',E10.4,10X,'ARCING ISQT=',
     2E10.4,10X,'ARCING ENERGY=',E10.4//5X,'TOTAL ARC LENGTH AT ARC MERG
     3ING EXCEEDS END CAP SPACING AND HENCE THIS SIMULATION IS TERMINATE
     4D'/5X,95(1H*)/)
            GO TO 1
   63 CONTINUE
            KG=KG+1
```

```
      KE=KE+1
      KE1=KE-1
      CALL AINIT(M,Y,DY)
C     TICOR2 IS CORRECTION IN TIME TO DETERMINE INSTANT WHEN ARC REACHED
C     END CAPS.
      TICOR2=((NS*Y(3)+Y(4))-XXL)/DY(4)
      Y(1)=Y(1)-TICOR2
      Y(2)=Y(2)-DY(2)*TICOR2
      Y(4)=Y(4)-DY(4)*TICOR2
      Y(JJ3+5)=Y(JJ3+5)-DY(JJ3+5)*TICOR2
      Y(JJ3+6)=Y(JJ3+6)-DY(JJ3+6)*TICOR2
      XF(KF)=Y(4)
      Y(4)=XXL-NS*Y(3)
      XF=NS*Y(3)+Y(4)
      DXE(KE)=Y(4)-XE(KE1)
      DO 150 J=1,K
      Y(J+4)=Y(J+4)-DY(J+4)*TICOR2
      E(J)=0.914*ABS(Y(2))**0.4/Y(J+4)**0.85+CK2/ABS(Y(2))
      PROD31=PROD31+E(J)*DX(J)
  150 CONTINUE
      DO 155 J=3,KE1
      Y(J+JJ5)=Y(J+JJ5)-DY(J+JJ5)*TICOR2
      E(J+JJ4)=0.914*ABS(Y(2))**0.4/Y(J+JJ5)**0.85+CK2/ABS(Y(2))
      PROD32=PROD32+E(J+JJ4)*DXE(J)
  155 CONTINUE
      E(KE+JJ4)=0.914*ABS(Y(2))**0.4/Y(KE+JJ5)**0.85+CK2/ABS(Y(2))
      VARC=NS*PROD31+PROD32+E(KF+JJ4)*DXE(KE)+UR
      DD(KF)=0.5*(Y(3)+Y(4))-0.25*DXE(KE)
      WRITE(2,69)XF
   69 FORMAT(/16X,'TOTAL ARC LENGTH HAS REACHED END CAP SPACING OF',
     1F9.4,' CM '//16X,61(1H*)/16X,61(1H*)/)
      GO TO 90
   73 CONTINUE
      KH=KH+1
      DO 76 J=1,K
      E(J)=0.914*ABS(Y(2))**0.4/Y(J+4)**0.85+CK2/ABS(Y(2))
      PROD41=PROD41+E(J)*DX(J)
   76 CONTINUE
      DO 86 J=3,KF
      E(J+JJ4)=0.914*ABS(Y(2))**0.4/Y(J+JJ5)**0.85+CK2/ABS(Y(2))
      PROD42=PROD42+E(J+JJ4)*DXE(J)
   86 CONTINUE
      VARC=NS*PROD41+PROD42+UB
   90 CONTINUE
      TI=Y(1)
      C=NP*Y(2)
      XF=NS*Y(3)+Y(4)
      RRC=NP*DY(2)
      AISQT=NP**2*Y(JJ3+5)
      AENGY=NP*Y(JJ3+6)
      WRITE(2,203)Y(3),KE
  203 FORMAT(//20X,'Y(3)=',F10.3/20X,15(1H-)/20X,'KE=',I3/)
      WRITE(2,110)TI,C,XF,RRC,DY(3),DY(4),VARC,AISQT,AENGY
  110 FORMAT(5X,9(E10.4,3X))
C     TEST CURRENT VALUES OF VARIABLES HERE IF REQUIRED
      IF(Y(3).EQ.XL)DY(3)=0.0
      IF(XF.EQ.XXL)DY(4)=0.0
      CALL F4RUNK(M,1,DELTT,Y,DY,P,Q)
      WRITE(2,501)K,E(K),E(K1),DY(5),DY(6),DY(7),DY(8),DY(9)
  501 FORMAT(22X,' K= ',I5//6X,' E(K)= ',E10.5,10X,'E(K1)= ',E10.5///6X,
     1' DY(5)= ',E10.5,6X,' DY(6)= ',E10.5,6X,' DY(7)= ',E10.5,6X,
```

231

```
      2' DY(8)= ',E10.5,6X,' DY(9)= ',E10.5///)
        GO TO 3
      9 WRITE(2,200)TI,XF,AISQT,AENGY
    200 FORMAT(1H0,6X,'CIRCUIT CURRENT REACHED ASSIGNED MINIMUM VALUE'////
       16X,'TOTAL ARCING TIME =',F11.8,'  SEC  '//6X,'TOTAL ARC LENGTH =',
       2F12.5,'  CM  '//6X,'ARCING ISQT =',F12.3,'  ASQ.S  '//6X,'TOTAL AR
       3C ENERGY =',F12.3,'  J  '//)
        WRITE(2,900)TICOR1,TICOR2
    900 FORMAT(/20X,'TICOR1 =',E10.4,20X,'TICOR2 =',E10.4/)
        DO 23 J=1,K
        WRITE(2,301)J,A(J)
    301 FORMAT(/7X,'J=',I4,' A(J)= ',E11.4)
     23 CONTINUE
        DO 24 J=3,KE
        WRITE(2,302)J,A(J+JJ4)
    302 FORMAT(/17X,'J=',I4,' A(J+JJ4)= ',E11.4)
     24 CONTINUE
        WRITE(2,117)GAMA,AE
    117 FORMAT(//10X,'GAMA FACTOR=',E10.4/10X,22(1H*)//10X,
       1'INITIAL AREA OF SECTION AT ELECTRODE ENDS=',E10.4/10X,52(1H*)/)
        GO TO 7
      5 WRITE(2,300)
    300 FORMAT(6X,'ARCING TIME EXCEEDED TMAX')
      7 GO TO 1
        STOP
        END


LENGTH  2719, NAME  MAINPROGRAM
```

```
      SUBROUTINE F4DERY(M,Y,DY)
      DIMENSION Y(M),DY(M),E(1000)
      COMMON/BLOCK11/ERMS,R,EL,F,THETA,C1,TI1,C,XF,VARC,TI,PI,TIO
      COMMON/BLOCK12/XO,XL,XXL,AREA,AREAZ,NS,NP,ELAMDA
      COMMON/BLOCK13/DELTT,TMAX,ALPH1,ALPH2,CS,CK1,CK2
      COMMON/BLOCK14/K,K1,KE,KE1,KH,TICOR1,TICOR2,JJ3,JJ4,JJ5,E
      DY(2)=(VS(Y(1))-R*Y(2)*NP-VARC*C1/ABS(C1))/(NP*EL)
      VVS=VS(Y(1))
      DY(JJ3+5)=Y(2)**2
      DY(JJ3+6)=ABS(Y(2)*VARC)
      IF((ABS(XL-Y(3)).LE..1000E-06).AND.(KE.GE.2))GO TO 31
      DIF=Y(3)-XL
      IF(KE.GE.2)WRITE(2,44)Y(3),DY(3),DIF
   44 FORMAT(/15X,'Y(3)=',E12.5,15X,'DY(3)=',E12.5,15X,'(Y(3)-XL)=',
     1E12.5//20X,'IT HAS LEAKED DOWN'/)
      DY(3)=0.0001*(4.6+0.219*ABS(Y(2))**0.6)*ABS(Y(2))/AREA
      DY(4)=0.0
      DO 10 J=1,K1
      P=(K1-J)*DELTT
      ALPH=ALPH1+ALPH2*(1-EXP(-100.0*P))
      DY(J+4)=ALPH*E(J)*ABS(Y(2))/CK1
   10 CONTINUE
      GO TO 100
   31 DY(3)=0.0
      Y(3)=XL
      IF((ABS(XXL-(NS*Y(3)+Y(4))).LE..1000E-06).AND.(KE.EQ.KE))GO TO 41
      KE=KE+1
      DY(4)=0.0001*(4.6+0.219*ABS(Y(2))**0.6)*ABS(Y(2))/AREA
      GO TO 51
   41 DY(4)=0.0
      Y(4)=XXL-NS*Y(3)
   51 CONTINUE
      IF(KE.EQ.2)GO TO 61
      DO 20 J=3,KE
      P=(KE+KH-J)*DELTT-TICOR1-TICOR2
      ALPH=ALPH1+ALPH2*(1-EXP(-100.0*P))
      DY(J+JJ5)=ALPH*E(J+JJ4)*ABS(Y(2))/CK1
   20 CONTINUE
      DO 14 J=1,K
      P=(K1+KE1+KH-J)*DELTT-TICOR1-TICOR2
      DY(J+4)=(ALPH1+ALPH2*(1-EXP(-100.0*P)))*E(J)*ABS(Y(2))/CK1
   14 CONTINUE
      GO TO 100
   61 CONTINUE
      DY(JJ1+5)=0.0
      DO 12 J=1,K
      P=(K-J)*DELTT-TICOR1
      DY(J+4)=(ALPH1+ALPH2*(1-EXP(-100.0*P)))*E(J)*ABS(Y(2))/CK1
   12 CONTINUE
  100 CONTINUE
      RETURN
      END


, LENGTH   660, NAME   F4DERY
```

233

```
      SUBROUTINE AINIT(M,Y,DY)
      DIMENSION Y(M),DY(M),F(1000)
      COMMON/BLOCK11/ERMS,R,EL,F,THETA,C1,TI1,C,XF,VARC,TI,PI,TIO
      COMMON/BLOCK12/XO,XL,XXL,AREA,AREAZ,NS,NP,ELAMDA
      COMMON/BLOCK13/DELTT,TMAX,ALPH1,ALPH2,CS,CK1,CK2
      COMMON/BLOCK14/K,K1,KF,KE1,KH,TICOR1,TICOR2,JJ3,JJ4,JJ5,E
      COMMON/BLOCK15/WID,DEP,SILDIA,AE,GAMA
      IF((ABS(XL-Y(3)).LE..1000E-06).AND.(KF.GE.2))GO TO 31
C     MODEL FOR INITIAL AREA OF LUMEN SECTION
      Y(K+4)=AE
      GO TO 100
   31 IF(KF.EQ.2)GO TO 42
C     MODEL FOR INITIAL AREA OF LUMEN SECTION
      Y(KE+JJ5)=AE
      GO TO 100
   42 CONTINUE
      Y(K+4)=AE
  100 CONTINUE
      RETURN
      END


LENGTH    113, NAME   AINIT
```

234

```
      SUBROUTINE INPUTS
      COMMON/BLOCK11/ERMS,R,EL,F,THETA,C1,TI1,C,XF,VARC,TI,PI,TIO
      COMMON/BLOCK12/XO,XL,XXL,AREA,AREAZ,NS,NP,ELAMDA
      COMMON/BLOCK13/DELTT,TMAX,ALPH1,ALPH2,CS,CK1,CK2
      COMMON/BLOCK15/WID,DEP,SILDIA,AE,GAMA
      READ(1,10)XL,XXL,NS,NP
      READ(1,20)DELTT,TMAX,ALPH1,ALPH2,CS,CK1,CK2
      READ(1,40)WID,DEP,WIDZ,XO
      READ(1,50)SILDIA,ELAMDA,GAMA
   10 FORMAT(2E10.4,2I5)
   20 FORMAT(7E11.4)
   40 FORMAT(4F10.4)
   50 FORMAT(3E10.4)
C     PAGE HEADING
      AREA=WID*DEP
      AREAZ=WIDZ*DEP
      AE=WID*(DEP+0.5*SILDIA*GAMA*(2.0-PI/3.0))
      WRITE(2,100)
  100 FORMAT(1H1,///10X,'CIRCUIT PARAMETERS',20X,'ELEMENT DETAILS'//)
      WRITE(2,110)ERMS,XO,R,XL,EL,XXL,F,AREA,THETA,NS,C1,NP,TI1,AREAZ
  110 FORMAT(6X,'VOLTAGE',9X,E10.4,12X,'NOTCH LENGTH',9X,E10.4//6X,
     1'RESISTANCE',6X,E10.4,12X,'NOTCH SPACING',8X,E10.4//6X,'INDUCTANCE
     2',6X,E10.4,12X,'END CAP SPACING',6X,E10.4//6X,'FREQUENCY',7X,E10.4
     3,12X,'STRIP C.S.A.',9X,E10.4//6X,'CLOSING ANGLE',3X,E10.4,12X,'NO.
     4 IN SERIES',13X,I5//6X,'INITIAL CURRENT',1X,E10.4,12X,'ELEMENTS IN
     5 PARALLEL',6X,I5//6X,'PREARCING TIME',2X,E10.4,12X,'NOTCH C.S.A.',
     69X,E10.4/////)
      WRITE(2,200)DELTT,TMAX,ALPH1,ALPH2,CK1,CK2
  200 FORMAT(6X,'DELTT',11X,E10.4,12X,'TMAX',17X,E10.4//6X,'ALPH1',11X,
     1E10.4,12X,'ALPH2',16X,E10.4//6X,'CK1',13X,E10.4,12X,'CK2',18X,
     2E10.4////)
      WRITE(2,111)SILDIA,ELAMDA
  111 FORMAT(/6X,'MEAN GRAIN SIZE OF FILLER =',F9.3,' CM '/6X,'DISRUPTIO
     1N TIME MODEL CONSTANT = ',F9.4/)
      RETURN
      END
```

LENGTH   214, NAME INPUTS

```fortran
      FUNCTION VS(TIME)
      COMMON/BLOCK11/ERMS,R,EL,F,THETA,C1,TI1,C,XF,VARC,TI,PI,TI0
C     SOURCE VOLTAGE:AC IF F+VE,DC IF F=0,SPECIAL IF F-VE
      IF(F)1,2,3
    1 CONTINUE
C     SPECIAL WAVE FORM CAN BE INSERTED HERE
      VS=0.0
      RETURN
    2 VS=ERMS
      RETURN
C     NOTE THAT TIME IS MEASURED FROM THE START OF ARCING
    3 VS=1.4142136*ERMS*SIN(2.0*PI*F*(TIME+TI1)+(THETA*PI/180))
      RRR=VS
      RETURN
      END


LENGTH    76, NAME  VS
```

```
      SUBROUTINE PREARC
      COMMON/BLOCK11/ERMS,R,EL,F,THETA,C1,TI1,C,XF,VARC,TI,PI,TIO
      COMMON/BLOCK12/X0,XL,XXL,AREA,AREAZ,NS,NP,ELAMDA
      COMMON/BLOCK13/DELTT,TMAX,ALPH1,ALPH2,CS,CK1,CK2
      COMMON/BLOCK15/WID,DEP,SILDIA,AE,GAMA
      READ(1,10)ERMS,R,EL,F,THETA
   10 FORMAT(5E10.4)
      IF(ERMS.LE.1.0)STOP
      READ(1,20)C1,TI1
   20 FORMAT(2E10.4)
      CALL INPUTS
      RETURN
      END
```

LENGTH   65, NAME   PREARC